

Post-fire debris flows in southeast Australia: initiation, magnitude and landscape controls

Petter Nyman

Submitted in total fulfilment of the requirements of the degree of Doctor of Philosophy

March, 2013

Melbourne School of Land and Environment

The University of Melbourne

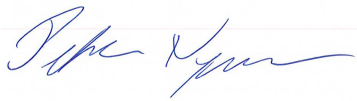
Abstract

Surface runoff and sediment availability can increase after wildfire, potentially resulting in extreme erosion, flash floods and debris flows. These hydro-geomorphic events supply large amounts of sediment to streams and can represent a hazard to water supply systems, infrastructure and communities. This thesis combines observations, measurements and models to quantify and represent the post-fire processes that result in hazardous catchment responses. The processes that constitute risk to water quality and infrastructure were identified through field surveys of burnt catchments in the eastern upland of Victoria (southeast Australia) where impacts had occurred. The survey established that the majority of high-impact events after wildfire were linked to runoff-generated debris flows, a process previously undocumented in the region. The debris flows were initiated through progressive sediment bulking, and occurred in response to short duration and high intensity rainfall events, within one year after wildfire. Debris flows were confined to dry sclerophyll forests that had been subject to crown fire. Wet forest types displayed comparatively subdued responses, a pattern attributed to the relatively high infiltration capacity in these systems. Infiltration and sediment availability were isolated as the key hillslope components that were sensitive to burning and which strongly influenced catchment processes and debris flow susceptibility. The aims of subsequent work were therefore to develop models of infiltration and sediment availability as controls on hillslope response and use these to quantify changes in key parameters during recovery from wildfire. Infiltration was modelled as function of surface storage (H), matrix flow (K_{mat}) and macropore flow (K_{mac}). Macropore flow was found to be the main parameter driving the temporal trends in infiltration capacity during recovery from wildfire. Water repellency was ubiquitous in headwater recovering from wildfire, although the strength diminished during prolonged wet weather conditions, a dependency which could be modelled as a function of monthly weather patterns. Sediment availability was highly variable with soil depth, a feature which contrasts with assumptions underlying commonly used erosion models, typically developed in agricultural systems. The majority of erosion following wildfire was found to occur in a shallow layer of highly erodible material which could be represented through d_{nc} , a parameter describing the depth of non-cohesive soil. This depth of available soil decreased exponentially during recovery. The models of sediment availability and infiltration were effective at capturing both spatial variability and recovery processes and form a basis on which to model debris flow initiation and magnitude in variable landscapes during recovery from wildfire.

Declaration

This is to certify that;

- the thesis comprises only my original work towards the PhD except where indicated in the Preface,
- due acknowledgement has been made in the text to all other material used,
- the thesis is fewer than 100 000 words in length, exclusive of tables, maps, bibliographies and appendices.



Petter Nyman,

January 2013

Preface

The thesis consists of four data chapters with an introduction and synthesis at either end. The first two data chapters are based on field surveys that were conducted opportunistically at different stages during the candidature. The data generated during the first set of surveys are reported in Chapter 2 and used to provide evidence of debris flow occurrence after wildfire in southeast Australia. This chapter is now published in *Geomorphology* and co-authored by my supervisors - Dr. Gary Sheridan, Dr Hugh Smith and Associate Professor Patrick Lane - who provided ideas and guidance along the way. Chapter 4 is written as a journal article and a manuscript has been submitted for publication in *Journal of Hydrology*, also with supervisors as co-authors. Chapter 5 is currently under review in the *Journal of Geophysical Research*. This manuscript draws partly on a dataset collected during a collaborative project with John Moody at the US Geological Survey, who is also a co-author on the manuscript. The data produced during this collaborative component was first published as a USGS scientific investigations report with John Moody and I as first and second author respectively.

Acknowledgements

The research was carried out with funding from Melbourne Water, eWater CRC and The University of Melbourne. Thank you for supporting my research and giving me the opportunity to attend conferences and carry out research with international research partners. A big thank you to my supervisors – Dr Gary Sheridan, Dr Hugh Smith and Associate Professor Patrick Lane - who were there to inspire and provide guidance throughout the PhD journey. I value, so much, what I learned from you in different stages of the project! Also, it has been fun to work alongside Philip J. Noske and Chris Sherwin at the Forest and Water Research Group. The field work (usually involving water and dirt) wouldn't have been the same without our friendship. Thank you for your help! Thank you also to John Costenaro for help tracking down debris flows and to Gabi Szegedy for her assistance in the lab. I am grateful to Peter Mercurio, Matt Richardson and Jane Cawson who were there during some of the long and hard field campaigns. I also want to acknowledge the valuable input from Ralph Barraclough, John Knocks and Russ Ritchie and helpful landowners in general for providing valuable information, video recordings and photographs relating to debris flow events and flash floods after wildfire.

Dr John Moody at the US Geological Surveys hosted my research visit to Colorado. The research collaboration was incredibly rewarding in terms of learning about science and producing research outputs, but more importantly, it helped foster new friendships and strong connections with research colleagues in another part of the world. Thank you John Moody, Deborah Martin and Brian Ebel for being incredibly welcoming and supportive hosts during my research visit! Working with you at the USGS is a major highlight. Thank you also to Dick Martin (Martin Enterprise) who was instrumental in designing and fabricating equipment used during my research visit.

Thank you mom and dad for helping me see nature and find inspiration from it. This is why I search to understand it! To my dearest Sula - you and me, always! Thank you for being unbelievably patient and supportive over the last few years. Students and friends in room 2.47 – Wim, Sina, Jane, Rachael, Ashley, Cameron - I really enjoyed sharing the PhD experience with you and I look forward to staying connected in the future as friends and colleagues. And finally to Break the Chain on PBS radio 106.7FM - Thank you for keeping my spirits up!

Table of Contents

Abstract	i
Declaration	ii
Preface	iii
Acknowledgements	iv
Table of Contents	v
List of Tables	vii
List of Figures	viii
Notation	xiii
Chapter 1 : Introduction	1
1.1 Wildfire and catchment processes.....	1
1.2 Predicting post-fire erosion – current models	3
1.3 Melbourne Water – Wildfire and Water Security research project.....	7
1.4 Extreme erosion events in burnt catchments.....	8
1.5 Research question.....	9
Chapter 2 : Evidence of debris flow occurrence after wildfire in upland catchments of south-east Australia	11
Abstract	11
2.1 Introduction.....	12
2.2 Regional Setting.....	14
2.3 Methods.....	21
2.4 Results	28
2.5 Discussion	46
2.6 Conclusion.....	54
Chapter 3 : Modelling hillslope and channel erosion during post-fire debris flows	56
Abstract	56
3.1 Introduction.....	57
3.2 Methods.....	59
3.3 Results and discussion.....	63
3.4 Conclusion.....	79
Chapter 4 : Effects of ash, water repellency and macropore flow on infiltration during recovery from wildfire	82
Abstract	82
4.1 Introduction.....	83
4.2 Methods.....	85
4.3 Results	93

4.4 Discussion	105
4.5 Conclusion.....	109
Chapter 5 : Sediment availability on burnt hillslopes	110
Abstract	110
5.1 Introduction.....	111
5.2 Methods.....	113
5.3. Results.....	122
5.5. Discussion	137
5.6 Conclusion.....	142
Chapter 6 : Sediment availability and infiltration as controls on the initiation and magnitude of runoff-generated debris flows – a synthesis	143
6.1 Introduction.....	143
6.2 Spatial and temporal variability in infiltration and sediment availability	147
6.3 Modelling response during recovery: transport equations revisited.....	151
6.4 Conclusions and future research priorities	156
References	159
Appendices	A-i

List of Tables

Table 2.1 List of regional wildfires in forested catchments of south east Australia from 2000 to 2009 and the associated post-fire erosion research that has been published in the scientific literature	15
Table 2.2 The structure and distribution of different Ecological Vegetation Classes (EVC) in the eastern uplands of Victoria.....	17
Table 2.3 List of key features used in field evaluation of extreme erosion events. See Pierson (2005) for further details on distinguishing between debris flows and floods.	23
Table 2.4 .General site characteristics for locations where high-magnitude erosion events were recorded.....	30
Table 2.5 Hillslope and channel erosion rates measured for upper, mid and lower sections of three runoff generated debris flows in northeast Victoria.	42
Table 3.1 Debris flow research sites in eastern uplands of Victoria, southeast Australia.	60
Table 3.2 Hillslope and channel erosion at debris flow research sites in eastern uplands of Victoria, southeast Australia.	68
Table 3.3 Nutrient concentrations (g kg^{-1}) and loads (kg ha^{-1}) for hillslope and channel material at debris flow sites. The concentrations were measured on soil samples from Rose River, Yarrarabula and Germantown. The average loads were calculated for sediment < 2 mm based on the average sediment load across all surveyed debris flow sites ($n = 10$).	69
Table 3.4 Rainfall and infiltration parameters at debris flow sites.....	73
Table 3.5 Observed and predicted erosion in debris flow catchments in Myrtle Creek Sunday Creek.	79
Table 4.1 The three main study sites and some their key features.	89
Table 4.2 Soil hydrological properties measured on intact cores (~8 cm deep and 5.3 cm in diameter) from Sunday Creek, Stony Creek and Ella Creek in Victoria, southeast Australia	95
Table 4.3 Summary of soil hydrological properties and initial conditions for four separate measurement campaigns to headwater catchments in southeast Australia which were recovering from wildfire impacts.	101
Table 5.1 List of research sites used in different components of the study.....	115
Table 5.2 Correlations between soil properties and erodibility at different depths. Significant correlations are in typed in bold font.	125
Table 5.3 Flow properties measured in the field flume and the associated estimates of shear stress and sediment flux parameters.	127

List of Figures

Figure 1.1 Conceptual diagram showing the interacting effects of “time since fire” and magnitude of rainfall events on catchment response to wildfire. As time since fire progresses, the rainfall event required to trigger a given catchment response increases. A catchment response of 1 is an extreme case and represents some maximum response potential of particular catchment.	3
Figure 1.2 Conceptual representation of overland flow generation and erosion in burned and unburnt systems. In an unburnt hillslope infiltration occurs readily through preferential pathways. Overland flow is transient and occurs within the litter-soil surface interface. Erosion rates by overland flow are very low. In the burnt state, hydrophobic soil is often overlaid by wettable and unconsolidated soil and ash. Overland flow is generated when high intensity rainfall exceeds the storage capacity of ash, topsoil and micro-depressions.....	9
Figure 2.1 A conceptual representation of the catchment and the layout of the field survey. Photos from the field survey are provided in Appendix B (Figures 7 to 10).	25
Figure 2.2 A map outlining the extent of recent wildfires in Victoria and the location of high magnitude events that were investigated.....	29
Figure 2.3 Images from the upper catchment showing a) eroded hillslopes with a small patch of relatively intact topsoil containing ash and rock fragments at Sunday Ck and b) channel initiation and levees of pale coloured rocks in a convergence zone with confined flow near Myrtle Ck.	32
Figure 2.4 Images from mid to lower section of the catchment showing a) channel scour and exposed bedrock at Rose River and, b) a terminal debris flow deposit at the confluence with Sunday Ck. The height of the measuring pole in a) is 1.2 m.	33
Figure 2.5 The slope distribution (a) and the burn severity (b) in debris flow affected catchments estimated for the area above the main debris flow deposit.	35
Figure 2.6 a) The location of debris flows at Yarrarabula in relation to local topography and b) the channel profile, sediment entrainment rate and channel cross-sections for a selected catchment. The error bar for sediment entrainment rate is the standard error of the mean. The horizontal length is measured as the distance from the channel initiation point. Note difference in map scale and contour intervals compared to Figure 2.7 and Figure 2.8.....	37
Figure 2.7 a) The location of debris flows at Rose River in relation to local topography and b) the channel profile, sediment entrainment rate and channel cross-sections for a selected catchment. The error bar for sediment entrainment rate is the standard error of the mean.....	38
Figure 2.8 a) The location of debris flows at Germantown in relation to local topography and b) the channel profile, sediment entrainment rate and channel cross-sections for a selected catchment. The error bar for sediment entrainment rate is the standard error of the mean.....	38
Figure 2.9 Images from erosion event at Yarrarabula showing a) the granitic foothills of Mt Buffalo in the background and sedimentary hillslopes in the foreground, b) a non-debris flow boulder deposit behind a log jam and flattened grass from flooding, c) matrix supported debris flow deposit in the adjacent sedimentary catchments, and d) channel scour and damaged roots from a debris flow.	39
Figure 2.10 a) The net soil loss and b) maximum deposited clast size from the lower-, mid- and upper catchments at Yarrarabula (n = 83), Rose River (n = 80) and Germantown (n = 91). The error bars are the standard error of the mean.....	40
Figure 2.11 a) Radar image from a debris flow generating storm cell, and the radar derived cumulative rainfall for b) Bright, c) Black Range Ck and d) Lake Buffalo where rainfall was known from tipping-bucket rain gauges.....	44

Figure 2.12 Radar derived cumulative rainfall for debris flow events in northeast Victoria. The radar derived rainfall accumulation was adjusted by the rainfall totals from rain gauge measurements at each site.	44
Figure 2.13 Field-saturated hydraulic conductivity (K_{fs}) (n = 5) and water repellency measurements (n = 20) at three depths from a 20 m x 20 m plot in three debris flow sites. Additional measurements were obtained for an unburnt site nearby (9 km) and comparable in aspect, rainfall and forest type to Germantown.....	46
Figure 3.1 a) Location of 7 debris flow research sites in southeast Australia and b) outline of a catchment that was surveyed at Rose River showing the location of channel cross-sections and hillslope transects.	59
Figure 3.2 The intensity-duration relation for debris flow triggering rainfall after wildfire in south-east Australian Eucalypt forests (storm totals in legend). The intensity-duration relation is shown for storms with return interval of 1-10 year at Myrtleford in northeast Victoria. The values for California and Colorado are obtained from Cannon <i>et al.</i> (2008) and show lower and upper thresholds for debris flow initiation in these regions.	64
Figure 3.3 a) The mean cumulative sediment yield ($t\ ha^{-1}$) with increasing particle size across all debris flow catchments. b) The hillslope and channel contribution to the total nutrient content in eroded material. Bray P is the plant available phosphorous, TC is total carbon and TN is total nitrogen. Error bars show the standard deviation of the mean for all catchments (n = 10).....	70
Figure 3.4 Erosion and deposition by debris flows 1-3 order catchment in the eastern uplands of Victoria, southeast Australia. Each data point of erosion (E_{ch}) is the average erosion within individual stream order reach (n = 60) at 8 debris flow catchments. There were 44 first order channels, 13 second order channels and 3 third order channels. Deposition (U) was measured in 8 stream order reaches (6 second order and 2 third order).	74
Figure 3.5 Debris flow initiation thresholds for headwater catchments (n = 45) across 7 sites in the eastern uplands of Victoria, southeast Australia. The threshold curve was fitted manually by adjusting the parameters in the linear function so that no data points were within the threshold curve.....	75
Figure 3.6 The relation between transport and local slope for channel initiation points in lower-, mid- and upper catchments at five post-fire debris flow sites southeast Australia.	77
Figure 3.7 Model of channel initiation, erosion depth and sediment yield in debris flow catchments at Sunday Creek (a - b) and Myrtle Creek (c - d). See Appendix C for photos of hillslope erosion, initiation points, channel scour and terminal deposits at Myrtle Creek and Sunday Creek.	78
Figure 4.1a) Storage (H), matrix flow (K_{mat}), and macropore flow (K_{mac}) as three parameters in the infiltration processes. b) A schematic representation of infiltration parameters in a water repellent soil.	86
Figure 4.2 The infiltration measurements were made on soils from three sites in uplands of eastern Victoria, southeast Australia.	88
Figure 4.3 The date, time since fire and season for three sites sampled for infiltration rates, water repellency and soil moisture during four measurement campaigns to small headwater catchment in upland areas of eastern Victoria, southeast Australia. The solid black bold horizontal lines represent different sampling campaigns.	92
Figure 4.4 The strength of water repellency (critical surface tension) at different depths at a) Sunday Creek, b) Stony Creek and c) Ella Creek in Victoria southeast Australia. Ella Creek was burnt by wildfire in January 2007 and Stony Creek and Sunday Creek were burnt in February 2009.....	94
Figure 4.5 a) Initial soil moisture (θ_i) b) matrix flow potential (K_{mat}) and c) change in soil moisture ($\Delta\theta$) during infiltration into intact soil cores from Ella Creek, Stony Creek and Sunday	

Creek (n = 9) at different stages of wetting on a tension table. All values are for $h = -15$ mm. The water uptake in c) was obtained from the mass of soil cores measured before and after each 35 minute infiltration.....	96
Figure 4.6 The normalized hydraulic conductivity (K_{mat}/K_s) and absorption rate ($\Delta\theta/\theta_s/t_{hrs}$) as a function of initial soil moisture. The data was obtained from infiltration measurements on intact cores that were sampled from Ella, Stony Creek and Sunday Creek (n = 9) at 4 different stages of wetting (Figure 4.5). The normalized flow potential was fitted with an exponential function. Once this function equals 1, the matrix flow potential K_{mat} is equal to the full flow potential of the soil K_s and there can be no further increase in K	98
Figure 4.7 Soil hydrological properties of headwater catchments in dry Eucalypt forests during recovery from wildfire. a) Initial soil moisture versus KBDI. b) Matrix flow K_{mat} and soil moisture c) Normalised water repellency (CST_{min}^+) versus KBDI. d) The change in matrix flow K_{mat} with changing water repellency (CST_{min}). Each soil moisture and water repellency (CST) data point represents the average of 27 measurements made on composite samples collected from two points ($d_s = 0-10$ cm) at 9 locations along 3 transects (80 m) at Sunday Creek, Stony Creek and Ella Creek (n = 27). Each matrix flow K_{mat} data point is the average of 4 mini-disc measurement point in quadrats (1 x 1 m) at 3 locations along each of three sampling transects (total n = 36).....	100
Figure 4.8 a) Scaled a) macropore flow and b) storage as a function of time since fire. The changes in macropore flow during recovery was analysed using infiltration data from Sunday Creek South (n = 24) and East Kiewa (Nyman <i>et al.</i> 2010) in addition to data from the three main study site at Ella Creek, Sunday Creek and Stony Creek.....	103
Figure 4.9 a) The infiltration rate for tension infiltrometer measurements (n = 12) and rainfall simulation plots (2 x 1.5 m; n = 3) at Sunday Creek in March 2010. A storage based infiltration equation (4.1) was fitted to all 12 replicate tension infiltrometer measurements and shown as a single function representing the average infiltration for the three plots. b) The runoff from rainfall simulation plots (data points) and the modelled hydrograph using the parameters from the fitted function in a).....	105
Figure 5.1 A conceptual representation of fire-effects on sediment availability in forest soils.	113
Figure 5.2 Map showing the location of research sites in a) southeast Australia (Sunday Creek, Stony Creek and Ella Creek) and b) western US (Fourmile Canyon in Colorado and Pozo in California).....	114
Figure 5.3 Upper section a) shows the location for collecting cluster samples (A, B, and C) along transects (T1, T2, and T3) from one site called Fourmile Canyon South. b) Lower section shows the details of the method of collecting subsamples of the soil core. See Appendix E (Figure 1) for photo of sampling technique.	116
Figure 5.4 The components of the a) tilting flume, b) the core attachment and extruding device and the c) water supply system. Additional flume specification available in (Moody and Nyman 2012).	118
Figure 5.5 Changes in mean erodibility of burnt near surface soil at a) Fourmile Canyon North, b) Fourmile Canyon South and c) Pozo South. Three burnt clusters and one unburnt cluster are plotted for each site. Each point is the average erodibility obtained from four detachment experiments on four different cores in each cluster. The surface erodibility of four burnt soil cores at FMC North ranged from 8.37×10^{-4} to 38.8×10^{-4} . At FMC South the corresponding values were 19.4×10^{-4} and 122×10^{-4} and at Pozo they were 15.3×10^{-4} and 61.6×10^{-4}	124
Figure 5.6 The observed and predicted erodibility, k_d ($s\ m^{-1}$), from a general linear model with depth, d_s (cm), and root density, RD ($g\ cm^{-3}$), as fixed effects. The analysis was performed on \log_{10} transformed erodibility values.	126

Figure 5.7 The mean change in sediment flux (q_s) with time (t) for sequentially increasing levels of shear stress (τ_f) in field flumes (4m long and 0.15 m wide) on a burnt hillslope at Sunday Creek (southeast Australia)	129
Figure 5.8 a) Median particle diameter (D_{50}) of eroded sediment for different flow rates applied sequentially to a confined test area on steep slopes (36-38 %) burnt at high severity. b) The particle size distribution as a function of sequentially increasing shear stress (τ_f) shown using the median (D_{50}), upper (D_{75}), and lower (D_{25}) quartiles of the distribution.....	130
Figure 5.9 The cumulative availability of sediment as a function of shear stress (τ_f) and the non-dimensional ratio, h_w/d_{nc} (i.e. flow depth relative to the depth of available material). The plots are generated from i) measurements of total erosion (kg m^{-1}) and ii) modelled erosion from the fitted sediment flux functions (Equation 2; Figure 5.7).	132
Figure 5.10 Mean vane shear strength (τ_v) and standard deviation (SD) as a function of soil depth (d_s) for 15 sample points along the outside edge of the flume experiment test area at Sunday Creek. The depth of highly erodible soil, d_{nc} , was used to define the point (+) of transition from non-cohesive to cohesive material.....	133
Figure 5.11 Changes in shear strength (τ_v) with depth (d_s) at two time steps (September 2009 and March 2009) at a) Stony Creek (n = 27) b) Sunday Creek (n = 50) and c) Ella Creek (n = 27), systems in different stages of recovery from wildfire. The shear strength at 0.5 yrs since fire was measured on non-eroded sections of the hillslope and therefore represents the surface properties without depletion effects that may have taken place between the initial fire impact and the sampling campaign (i.e. taken to represent conditions immediately following the burn). At Stony Creek and Sunday Creek the number of sampling points was about 10 % lower for d_s at 6.5 and 10 cm, due to the rock and gravel encountered during sampling.	135
Figure 5.12 a) The percentage non-cohesive soil plotted as function of depth (d_s) by applying a vane shear strength (τ_v) threshold of 5 kPa. The threshold was defined based on the average depth of soil removed from the flume bed in sediment flux experiments at Sunday Creek (Figure 5.10). b) A cumulative density function was fitted to the data in a) and presented as a probability density function (pdf). c) The expected depth $E[d_s]$ of the pdf in b) as a measure of the average depth of non-cohesive soil, d_{nc} , (cm) as function time (years) since fire (t_{sf}).....	136
Figure 5.13 Conceptual models of sediment availability on burnt hillslopes in systems with a) low and b) high background erodibility. The low and high background erodibility scenarios represent hillslopes from Sunday Creek, southeast Australia (clay loam soil) and Arroyo Seco, California (sandy soil) (see Kean <i>et al.</i> 2011). The fire-effect in the conceptual models is equal for both systems in terms of the depth of non-cohesive soil produced during burning. The impact on sediment availability however is different due to contrasting background (fire-independent) soil properties.	141
Figure 6.1 Conceptual representation of hillslope controls on debris flow initiation after a high severity fire. The responses at different sites are based on observation and data from Chapter 2. Sediment availability and infiltration excess are affected by fire but differ in different landscape units resulting in debris flows susceptibility which varies depending on geology and forest ecosystems. Landscape units such as exposed bedrock, shallow soil (dry forest) and deep soils (wet forest) are represented as red bars positioned in hypothetical locations along the two axes. The fractions above and below each bar are hypothetical storm return intervals. The bars shift around on the two depending on the severity of the fire and subsequent recovery. The site names are from post-fire erosion surveys in Chapter 2.	146
Figure 6.2 Model of infiltration capacity, K_p , as a function of time since fire (t_{sf}) in wet and dry forest ecosystems (EVC) at different levels of dryness ($KBDI$) in eastern uplands of Victoria, southeast Australia. The infiltration capacity is a function of macropore availability (θ_{mac}), matrix flow potential (K_{mat}) and its dependency on temporal dynamics in water repellency	

(CST_{min}). The model is restricted to conditions where $t_{sf} \leq 1$ yr, because there not sufficient data to support the model for wet and dry EVCs beyond this point. 149

Figure 6.3 Mass of non-cohesive soils on burnt hillslopes in of wet and dry forest ecosystems (EVCs) in Eastern Uplands of Victoria, southeast Australia. 151

Figure 6.4 Exponential probability distribution function, $g(K_p)$, of infiltration capacity (K_p) measured at a) Ella Creek in July 2009 ($K_p = 161 \text{ mm h}^{-1}$), b) Sunday Creek in Sept 2010 (mean $K_p = 143 \text{ mm h}^{-1}$), and c) Stony Creek in December 2009 (mean $K_p = 31 \text{ mm h}^{-1}$). The distributions were exponential for all time-steps at all other sites. d) The envelope curves for the apparent infiltration rate as a function of rainfall intensity. In this example the mean infiltration capacity (K_p) is 17.5 mm h^{-1} , representative of hillslopes in dry *Eucalypt* with 15% rock content two months after fire. 152

Figure 6.5 a) Depth of channel erosion and deposition and b) channel initiation as a function of contributing infiltration excess and local slope. 153

Figure 6.6. a) Hillslope erosion as function of rainfall excess (Q_{t5}) and local slope (S). Each site represents erosion at different stages of recovery so the sediment availability parameter k_b varies from site to site. b) Changes in sediment availability, k_e , with time since fire, t_{sf} 154

Notation

K_{fs}	Field-saturated hydraulic conductivity	[L T ⁻¹]
K_p	Ponded hydraulic conductivity (Infiltration capacity)	[L T ⁻¹]
h	Hydraulic head	[L]
D	Particle diameter	[L]
ΔZ	Debris flow relief	[L]
L	Debris flow length	[L]
Q	Rainfall excess	[L ³ T ⁻¹]
I	Rainfall intensity	L T ⁻¹
S	Slope	non-dimensional
A	Area	[L ²]
Y	Sediment yield	[L ³]
E	Erosion depth	[L]
E_{hs}	Erosion depth (hillslope)	[L]
E_{ch}	Erosion depth (channel)	[L]
U	Deposition depth (channel)	[L]
k_u, k_e	Erosion and deposition parameters	[T L ⁻²]
m, n, β	Transport parameters (fitted)	-
H	Surface storage potential	[L]
K_{mat}	Matrix flow potential (h = -15 mm)	[L T ⁻¹]
K_{mac}	Macropore flow potential (-15 mm < h ≤ 5 mm)	[L T ⁻¹]
K_{ash}	Hydraulic conductivity of ash	[L T ⁻¹]
θ	Soil moisture	[L ³ L ⁻³]
θ_i	Initial soil moisture	[L ³ L ⁻³]
θ_s	Soil moisture at saturation	[L ³ L ⁻³]
θ_f	Final soil moisture	[L ³ L ⁻³]
t	Time	[T]
t_p	Time to ponding	[T]
R	Water supply rate	[L T ⁻¹]
V	Surface storage	[L ³]
CST	Critical surface tension	[M T ⁻² L ⁻¹]
d_s	Soil depth	[L]
u, v	Fitted water repellency parameters (fitted)	-
CST_{min}	Maximum water repellency	[M L ⁻¹ T ⁻²]
d_{max}	Depth of maximum water repellency	[L]
P	Daily precipitation	[L]
T_{max}	Daily maximum temperature	-
P_{yrs}	Average annual precipitation	[L]
r	Soil pore radius	[L]
ρ	Density of water	[M L ⁻²]
g	Standard gravity	[LT ⁻²]
α	Contact angle	non-dimensional
K_s	Saturated hydraulic conductivity	[L T ⁻¹]
h_w	Water depth	[L]
S_f	Friction slope	non-dimensional
v	Flow velocity	[LT ⁻¹]
C_r	Resistance factor	[L ^{0.5} T ⁻¹]
t_{sf}	Time since fire	[T]
q_s	Sediment flux	[M L ⁻¹ T ⁻¹]
q	Flow rate	[L ³ T ⁻¹]
D_c	Detachment capacity	[M L ⁻² T ⁻¹]
T_c	Transport capacity	[M L ⁻¹ T ⁻¹]
k_d	Erodibility	[T L ⁻¹]
τ_f	Flow shear stress	[M L ⁻¹ T ⁻²]
τ_v	Shear vane strength	[M L ⁻¹ T ⁻²]
d_{nc}	Depth of non-cohesive soil	[L]
RD	Root density	[M L ⁻³]
RLD	Root length density	[L L ⁻³]
a, b	Sediment depletion parameters (fitted)	-
f, p	Shear strength parameters (fitted)	-

Chapter 1: Introduction

1.1 Wildfire and catchment processes

Wildfire impacts on the hydrological and geomorphic processes in forested catchments through the removal of vegetation and changes to soil properties (DeBano *et al.* 2005; Ice *et al.* 2004; Moody and Martin 2009b; Shakesby and Doerr 2006). Impacts can result in increased susceptibility to erosion and increased probability of floods, debris flows and landslides (Cannon 2001; Lane *et al.* 2006b; Moody and Martin 2001b; Wondzell and King 2003). The responses have been attributed to a number of factors relating to both erodibility of source material and the hydrological mechanisms by which material is mobilized and redistributed (Shakesby and Doerr 2006).

The effect of fire on hillslope hydrology is related to both infiltration and runoff processes. Low vegetation cover, lack of woody debris and hydraulic smoothing by eroded ash, can result in low rainfall interception and high runoff velocity (Lavee *et al.* 1995). At the same time infiltration is reduced through fire induced water repellency (Doerr *et al.* 2004; Doerr *et al.* 2006), breakdown of soil structure (Giovannini and Lucchesi 1983; Neary *et al.* 1999) and sealing of macropores by ash and eroded soil (Gabet and Sternberg 2008; Leavesley *et al.* 1989; Onda *et al.* 2008). The interacting and synergistic effects of these factors generate a system with properties and processes that deviate from what is typically observed in the unburned state. During recovery to pre-fire conditions, the temporal changes in these properties result in a transitional system where properties and dominant processes are likely to change markedly with time (Moody and Martin 2009b).

Empirical studies on runoff and erosion response in burned catchments show that there is large variability in how catchments respond to wildfire (Moody and Martin 2009a; Sheridan *et al.* 2007b). This variability can be attributed to three main factors.

- i. First, there are large functional differences between catchments in different geological settings and forest ecosystems, both at local (<5km), regional (500km) and global scales (Gartner *et al.* 2008; Lane *et al.* 2006b; Larsen *et al.* 2006; Moody *et al.* 2008a; Tomkins *et al.* 2008). Site specific characteristics such as geology, topography, vegetation type, soil type and structure result in

different levels of sensitivity to burn impacts and variability in the overall susceptibility to erosion. The result is i) variation in the magnitude and type of response to rainfall, and ii) different recovery rates (Lane *et al.* 2011; Larsen *et al.* 2006; Moody and Martin 2001b; Shakesby and Doerr 2006; Wondzell and King 2003).

- ii. Second, post-fire catchment responses are highly dependent on local rainfall regimes and associated random variability in post-fire rainfall events during the recovery period known as the 'window of disturbance' (Figure 1.1) (Istanbulluoglu *et al.* 2004; Moody and Martin 2009a; Prosser and Williams 1998; Smith *et al.* 2009).
- iii. Third, each fire event represents a different impact in terms of the size (area), severity and pattern of burn with large implications for how catchment processes are impacted (Cawson *et al.* 2012; Hyde *et al.* 2007; Moody *et al.* 2008b).

The interacting effects of intrinsic catchment properties, fire severity and randomness in rainfall combine to generate both deterministic and random variability in the catchment responses to wildfire. Understanding how these sources of variability operate in different landscapes is important when modelling hydro- geomorphic responses and their potential impacts on water resources and other assets (Benda and Dunne 1997; Cannon *et al.* 2010; Gartner *et al.* 2008; Istanbulluoglu *et al.* 2004; Lane *et al.* 2011; Moody 2012; Robichaud *et al.* 2007; Smith *et al.* 2011c).

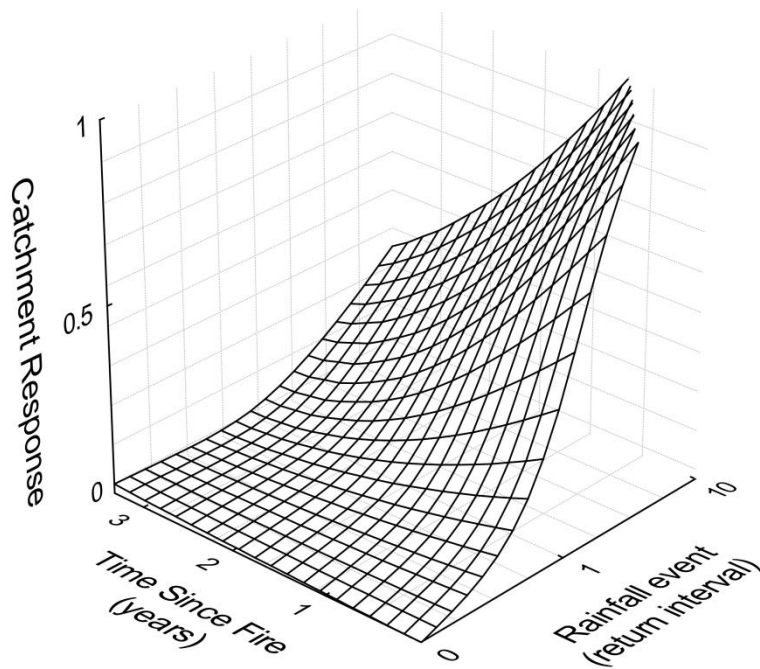


Figure 1.1 Conceptual diagram showing the interacting effects of “time since fire” and magnitude of rainfall events on catchment response to wildfire. As time since fire progresses, the rainfall event required to trigger a given catchment response increases. A catchment response of 1 is an extreme case and represents some maximum response potential of particular catchment.

1.2 Predicting post-fire erosion – current models

1.2.1 Purpose of prediction

Predictions of post-fire erosion help inform land managers of the impacts that wildfire may have on catchment processes (Robichaud and Ashmun 2012). Predictive tools can be used to:

- i. Prioritize resources in post-fire rehabilitation programmes.
- ii. Map hydrological hazards and high risk areas.
- iii. Quantify the magnitude of risk in water supply catchments.

Different management questions require different predictions. Sometimes a relative measure of erosion susceptibility provides sufficient information to support decision making. A relative measure of susceptibility may be sufficient for instance when a limited amount of resources for post-fire rehabilitation are to be prioritised across a large burnt area (e.g. Myronidis *et al.* 2010). In other scenarios, a land manager may want to compare the effectiveness of one rehabilitation strategy versus another,

demanding more accurate models of actual erosion rates including the underlying processes (e.g. Robichaud *et al.* 2007). In hazard predictions the modelling is targeted on specific assets, requiring information on magnitude and frequency of response, but not necessarily the processes driving the response (e.g. Cannon *et al.* 2010). The following subsections provide a brief overview of some modelling tools that have been used in by to support land management decisions in relation to hydrologic and geomorphic impacts from wildfire.

1.2.2 Annual hillslope erosion.

The Revised Universal Soil Loss Equation (RUSLE) model (Renard *et al.* 1991) was designed to predict annual soil loss ($\text{Mg ha}^{-1} \text{y}^{-1}$) from hillslopes due to erosion from rainfall and runoff. It was originally developed for agricultural land but its use is now widespread across different land-uses and natural environments including burnt landscapes in different fire prone regions (Fernández *et al.* 2010; Larsen and MacDonald 2007; Miller *et al.* 2003b; Myronidis *et al.* 2010). The model estimates mean annual soil loss as the product of rainfall erosivity, soil erodibility, and non-dimensional factors to account for topography, land-use and crop management. In absolute terms the hazard reflects an average response and not designed to consider the magnitude of event-based hazards. In terms of initiating events it is therefore not suited for determining the magnitude of risk in systems where sediment concentration is a risk factor.

RUSLE represents some basic topographic and soil information and is therefore effective at distinguishing between areas of high and low risk, despite the lack of accuracy in absolute terms. As such it can be a useful tool for prioritizing post-fire rehabilitation efforts (Fernández *et al.* 2010; Myronidis *et al.* 2010) and assessing the effectiveness of erosion control strategies (Miller *et al.* 2003b). RUSLE and other similar models are readily coupled with GIS and remotely sensed data on fire severity to produce landscape scale assessments of post-fire erosion hazard (Chafer 2008; Miller *et al.* 2003b; Sheridan *et al.* 2009; Vafeidis *et al.* 2007). These types of assessments can produce a realistic representation of the relative erosion hazard across burn areas.

1.2.3 Event based hillslope erosion.

The Erosion Risk Management Tool (ERMiT) is a distributed and event-based hydrological model which uses the Water Erosion Prediction Project (WEPP) to model

runoff and erosion response for individual storms after a fire (Elliot *et al.* 2001; Flanagan *et al.* 2007; Robichaud *et al.* 2007). WEPP was initially developed in an agricultural context but has later been developed further to better represent systems which are more variable in time and space (Elliot *et al.* 2001). ERMiT was specifically designed to help land managers assess the risk of damaging runoff and erosion events after fire without and without mitigation treatments such as seeding, straw mulch and erosion barriers. The model is more realistic than RUSLE in its representation of fire impact on erosion processes which also means that more detailed parameters are required to parameterise it (Larsen and MacDonald 2007).

In ERMiT the WEPP structure was modified to account for parameters which are influenced by high levels of spatial variability and the transient nature of fire-effects (Elliot *et al.* 2001). Fire effects on soil properties were modelled as three burn severity classes with parameters obtained through rainfall simulations and overland flow experiments (Robichaud *et al.* 2007; Robichaud *et al.* 2010). Random spatial variability due to variable fire-effects was introduced by simulating the response while varying the spatial configurations of homogenous tiles or overland flow elements along the hillslope. Recovery was incorporated through yearly adjustments to the soil parameters and the configuration of burn severity overland flow elements.

ERMiT combines event-based WEPP response models with storm outputs from a daily climate generator (CLINGEN) to simulate the full range of potential post-fire erosion outcomes for a sequence of yearly post-fire increments. This means that the predictions capture the event-based nature of the hazard whilst incorporating the variability due to random rainfall events. The distribution of possible erosion outcomes in the post-fire period were presented as erosion exceedance probabilities for events within individual years during the recovery from fire disturbance.

1.2.4 Event based channel and gully erosion.

Fire-Enhanced Runoff and Gully Initiation Model (FERGI) combines a stochastic climate generator and a deterministic geomorphology model to estimate the probability of post-fire rainfall excess, runoff generation and gully initiation position in catchments with and without contour felled logged barriers (Istanbulluoglu *et al.* 2003). The coupling of response model with a random rainfall component is similar to ERMiT despite the processes and scale is being different. FERGI calculates the water balance

for the wettable soil/ash layer overlying water repellent soils incorporating the depth of wettable soil, infiltration, precipitation, evaporation, runoff and stochastic climate inputs. It routes runoff along homogenous rectangular hillslope units using the kinematic wave equation.

The outputs from FERGI include hillslope runoff ($\text{m}^3 \text{s}^{-1} \text{m}^{-1}$) and gully length (m) and the effectiveness of log barriers in preventing gully erosion as a function of storm return periods. The log barrier treatment is represented in the model by adjustments to the water storage potential on the hillslope and the fractional area that is water repellent. The model does not provide direct estimates of erosion but assumes that once a gully has been initiated, the sediment transport rate is at transport capacity (Istanbulluoglu *et al.* 2003).

1.2.5 Event based debris flow hazard model

Debris flows contain high concentrations of sediment resulting in rheology and flow processes that are different from stream flow and clear-water floods (Julien and Lan 1991). Debris flows represent an extreme post-fire catchment response and pose a threat through direct impact on people and infrastructure (Cannon and Gartner 2005). The degree of damage that can be caused is linked to the area that is inundated or impacted by the debris flow at the catchment outlet and on the fan. The large amount of sediment generated during debris flow events also means that downstream impacts on water quality can be large (Smith *et al.* 2011c).

Cannon *et al.* (2010) at the US Geological Surveys (USGS) describe a model of debris flow hazard by predicting the probability of occurrence as well as the magnitude of debris flow events from burned areas. Using volume estimates from debris flows in 55 recently burned catchments in the intermountain western US (Utah, Colorado and California), Gartner *et al.* (2008) fitted a multiple linear regression model for the log-transformed mean volume (m^3) of material at the catchment outlet using information on the area with high slopes $> 30\%$, the area which was burned at high or moderate severity and the total storm rainfall. The probability of debris flow occurrence (%) was determined by fitting binary occurrence data with a logistic regression model using information on topography, burn impact, rainfall intensity and soil properties. The average rainfall intensity parameter in the model was linked to design storm by extracting intensity values for $< 1\text{hr}$ storms with recurrence intervals between 2 and 10

years. This debris flow model is used routinely by the USGS to characterise debris flow hazards after wildfire in the western US.

1.2.6 Current models- summary

The modelling tools outlined above have been developed to address different management objectives and therefore vary in terms of outputs and process representation. A major distinction between models such as RUSLE and ERMiT and the USGS debris flow models is temporal scale at which erosion models. RUSLE is designed to provide measures of the mean annual load from burnt hillslopes while ERMiT and the USGS debris flow model characterise erosion during individual events. The different timescales of these models can have large implications for how outputs can be used to inform land and water managers on the hazards associated with post-fire erosion. In water supply systems for instance the main concern is often linked to concentration of constituents in supply reservoirs and its effects in treatability (Emelko 2011; Smith *et al.* 2011c). The probability of exceeding these thresholds requires a model which predicts impacts on event-based timescales.

1.3 Melbourne Water – Wildfire and Water Security research project

The negative impacts on water quality resulting from wildfire disturbance have been highlighted in previous research (Bisson *et al.* 2003; Lane *et al.* 2006b; Rhoades *et al.* 2011; Smith *et al.* 2011a; Smith *et al.* 2011c; Wilkinson *et al.* 2007). Increased siltation, turbidity, and elevated nutrient levels as well as the introduction of toxic chemicals released during burning of biomass, can have implications for aquatic ecosystems and water supply (Bisson *et al.* 2003; Emelko 2011; Smith *et al.* 2011c) (see Appendix A for photos of rivers in Victoria, southeast Australia, that were impacted by post-fire erosion after wildfires in 2007 and 2009) The processes, impacts and challenges regarding wildfire and water quality impacts are addressed specifically in a series of conference proceeding from the International Association of Hydrological Sciences in 2012 (Stone *et al.* 2012).

Water supply catchments in fire-prone landscapes are at risk of contamination due to post-fire erosion (Emelko 2011; Smith *et al.* 2011c; White *et al.* 2006). In Melbourne in southeast Australia (population ~ 5 million), the water supply system (managed by Melbourne Water) is based primarily on water from forested catchments. Large wildfires in the region in the decade leading up to 2010 highlighted a strong need to

develop a quantitative basis on which to evaluate the actual water quality risk associated with post-fire erosion in Melbourne Water supply catchments. The need for research in this area was reinforced by the large impacts on Canberra's water supply system after wildfire in 2003 (Wasson *et al.* 2003; White *et al.* 2006).

In 2009 Melbourne Water and The University of Melbourne therefore initiated a research programme aiming to develop and parameterise a probabilistic model of the frequency and magnitude of water quality impacts due to wildfire in critical Melbourne Water supply catchments. The modelling approach was based on three key areas of research:

- i. Conceptual development of a probabilistic wildfire pollutant risk model
- ii. Conceptual development of a post-fire pollutant risk model
- iii. Parameter estimation for erosion and nutrient models in Melbourne Water catchments

The aim was to develop a model which integrates a probabilistic wildfire component with post-fire hydro-geomorphic models that account for the key erosion processes that constitute risk to water quality.

1.4 Extreme erosion events in burnt catchments

The majority of sediment transport and hydrological risk associated with post-fire hydrology is often embedded in large and relatively infrequent erosion events (Cannon and Gartner 2005; Istanbuluoglu *et al.* 2004; Smith *et al.* 2011c) which in upland catchments can occur as flash floods and debris flows (Cannon 2001; Jordan *et al.* 2004; Leitch *et al.* 1984; Moody 2012; Wondzell and King 2003). These types of events are difficult to capture in monitoring studies due to logistical constraints and the relatively infrequent occurrence, hence the opportunistic nature of research into these processes (Cannon 2001; Gartner *et al.* 2008; Jordan *et al.* 2004; Meyer *et al.* 2001; Wohl and Pearthree 1991).

Runoff generated debris flows in particular have been identified as an important erosion process leading to high magnitude events following wildfire (Cannon *et al.* 2001a; Cannon *et al.* 2008; Cannon *et al.* 2001b; Elliott *et al.* 2004; Gabet and Bookter 2008; García-Ruiz *et al.* 2012; Jordan *et al.* 2004). This type of debris flows are initiated by high intensity rainfall events resulting in large volumes of runoff and progressive sediment bulking. This is a process where runoff develops into debris flows due to the

rapid accumulation of sediment in the steep upper slopes of a catchment (Figure 1.2). The erosion response to large wildfires in Victoria and Australian Capital Territory in 2003 and 2007 indicate that this process can represent an important source of risk to water quality (Smith *et al.* 2011c; Worthy and Wasson 2004), yet very little is known about the processes and controls that determine their frequency and magnitude.

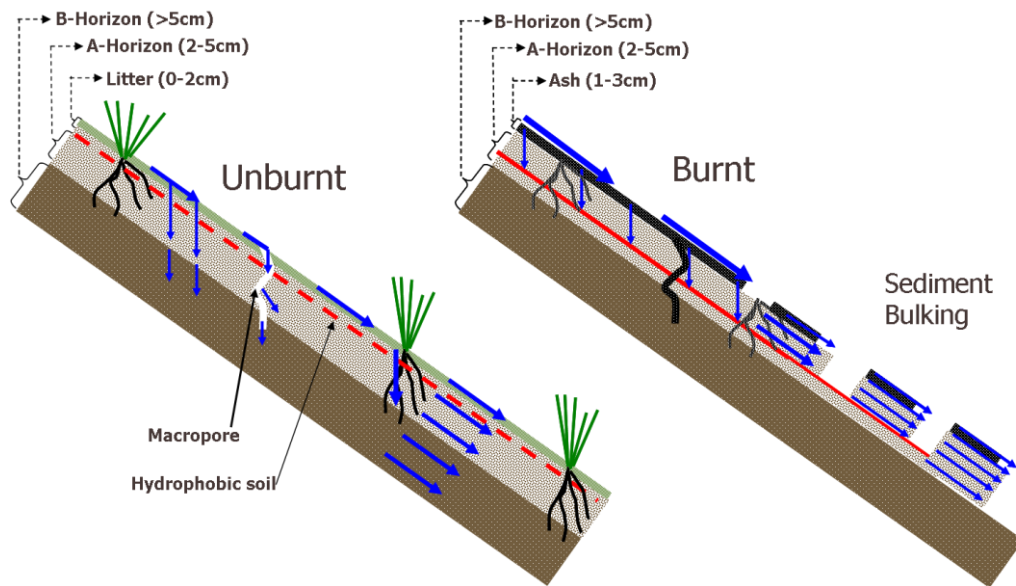


Figure 1.2 Conceptual representation of overland flow generation and erosion in burned and unburnt systems. In an unburnt hillslope infiltration occurs readily through preferential pathways. Overland flow is transient and occurs within the litter-soil surface interface. Erosion rates by overland flow are very low. In the burnt state, hydrophobic soil is often overlaid by wettable and unconsolidated soil and ash. Overland flow is generated when high intensity rainfall exceeds the storage capacity of ash, topsoil and micro-depressions.

1.5 Research question

The lack of research on high magnitude erosion events in southeast Australia is a major shortcoming in the current capacity of land managers to evaluate the risks associated with post-fire erosion. Large events do occur after fire in the southeast Australian region, but it is unclear how they occur, where they occur and how wildfire may act as a control in the underlying processes driving the events. The overall objective of this thesis is to address some of these knowledge gaps. The study uses a combination of erosion surveys and intensive measurements of hillslope properties in order to identify the key hydrological processes involved in debris flow initiation and develop

meaningful ways of quantifying the relevant parameters during the recovery to pre-fire condition. This will help link variation in observed responses with the soil properties that drive the variability in response across variable landscapes. While the work focuses on sites in the eastern uplands of Victoria, the outcomes of the research should provide generic knowledge relevant to processes and responses in other systems. More specifically the aims were to:

- i. Identify the dominant processes leading to post-fire debris flows and how these processes operate across variable landscapes.
- ii. Quantify the magnitude of erosion and develop a model to predict the initiation and magnitude of post-fire debris flows.
- iii. Measure changes in sediment availability and infiltration during recovery and use these to explore how hillslope controls change in time and space in landscapes with variable soil properties.

The thesis consists of four main data chapters. The first data chapter (Chapter 2) describes the regional setting and the processes leading to observed debris flow responses after wildfire. Chapter 3 provides an in-depth analysis of source contributions and magnitude of erosion during debris flow events. Chapter 4 is about infiltration in burnt soils and the role of macropore flow, ash and water repellency as controls on runoff generation. Chapter 5 is concerned with sediment availability on burnt hillslopes and aims to develop new ways of quantifying fire-effects on erodibility. The last chapter (Chapter 6) is a synthesis in which hillslope parameters are linked to debris flow processes as a way to explore the effects of landscape variability and recovery on debris flow initiation.

Chapter 2: Evidence of debris flow occurrence after wildfire in upland catchments of south-east Australia

Paper published in *Geomorphology*: Nyman, P., G. J. Sheridan, H. G. Smith, and P. N. J. Lane (2011), Evidence of debris flow occurrence after wildfire in upland catchments of south-east Australia, *Geomorphology*, 125(3), 383-401.

Abstract

Numerous reports of “flash floods”, “mud torrents” and “landslides” in burnt landscapes of south-east Australia were only recently linked to debris flows and recognised as a significant process that warrant more detailed investigation. This paper provides a systematic documentation of high-magnitude erosion events after wildfire in south-east Australia, focusing on small (<5 km²), upland catchments in eastern Victoria that were burnt by wildfire between 2003 and 2009. The aims of the study were to i) collect and show evidence of debris flow occurrence after wildfire; ii) quantify erosion rates from debris flows and; iii) identify rainfall thresholds and key hydrological properties. Runoff generated debris flows were the main process underlying 13 out of the 16 recorded high-magnitude erosion events. These occurred in dry eucalypt forests burnt at high or very high severity in steep headwater catchments throughout the eastern uplands of Victoria. The debris flows were triggered by intense, short duration rainfall events ($35 \text{ mm h}^{-1} < I_{30} < 59 \text{ mm h}^{-1}$) with annual exceedance probability in the order of 20%. This is the first paper to document the occurrence of post-fire runoff generated debris flows in Australia, so the discussion draws on literature from the western USA, where a large body of research has been dedicated to evaluating the risk posed by post-fire debris flows and their role in landscape processes. Typical features common to both systems include low infiltration capacity of burnt catchments; widespread sheet erosion and levee lined rills on steep upper hillslopes; and severe channel erosion initiated in response to convergent flow in previously un-scoured drainage lines. The depth of sheet erosion on surveyed slopes in the upper catchments ($18.4 \text{ mm} \pm 2.7 \text{ SE}$ to $4.6 \text{ mm} \pm 0.96 \text{ SE}$) indicates that hillslope material provides an important source of sediment. The average channel entrainment rate of three debris flows ranged from $0.6 \text{ m}^3 \text{ m}^{-1}$ to $1.4 \text{ m}^3 \text{ m}^{-1}$. Runoff generated debris flows were not recorded in wet or damp forest types where infiltration rates are higher, suggesting that this process is less likely to operate in these forest environments. The outcome of the study indicates that runoff generated debris flows are an important process to be considered during post-fire risk assessment of hydrological hazards.

2.1 Introduction

South-eastern Australia was affected by several large regional wildfires in the period 2003-2009. The burnt areas (~4 million hectares) encompass a range of climates, geologic units and forest types that collectively make up the Great Dividing Range of south-east Australia. While the region is naturally prone to wildfire, the years from 2003 to 2009 were associated with an increase in wildfire activity due to drought conditions with above average temperatures and below average rainfall. The increase in fire activity instigated several field based research projects aimed at quantifying the hydrological effects of fire and the associated impacts on erosion processes and water quality (eg. Lane *et al.* 2006b; Tomkins *et al.* 2008). Earlier post-fire erosion research from the region (Brown 1972; Chessman 1986; Leitch *et al.* 1984; Prosser and Williams 1998) combined with these studies from recently burned areas (Blake *et al.* 2009; Lane *et al.* 2006b; Sheridan *et al.* 2007b; Smith and Dragovich 2008; Tomkins *et al.* 2008) show clearly that the hydro-geomorphic response of burned upland regions in south-east Australia is highly variable and dependent on a range of factors including i) the fire severity, ii) the timing and properties of post-fire rainfall events, as well as iii) the inherent geomorphic and hydrological characteristics of fire affected catchments. It is noteworthy that much of the research from the region has focused on study sites in gauged catchments (Brown 1972; Lane *et al.* 2006b; Tomkins *et al.* 2008; White *et al.* 2006) where catchment monitoring has been coupled with experiments and process based research (Blake *et al.* 2009; Doerr *et al.* 2006; Sheridan *et al.* 2007a) to provide valuable insights into the processes and controls that influence the post-fire erosion responses in different systems within the region. However, the limitation in conducting research in a fixed and predetermined geographic setting is the low likelihood of capturing data on high magnitude or extreme events.

While high-magnitude erosion events are relatively infrequent, they are important both in a geomorphic context and in a water supply and management context where the aim could be to predict whether a value of interest will exceed a critical threshold (Kantz *et al.* 2006). In the western United States, wildfire and high-magnitude erosion events are closely linked, and there is body of ongoing research that focuses on the underlying hydrological processes (Cannon *et al.* 2001b; Gabet and Sternberg 2008; Jordan *et al.* 2004; Moody *et al.* 2008a; Wells 1987; Wondzell and King 2003), the magnitude of events (Cannon *et al.* 2008; Santi *et al.* 2008), the risk of occurrence (Cannon *et al.* 2010; Istanbuluoglu *et al.* 2004) and their significance for longer-term erosion rates and

landform development (Jackson and Roering 2009; Kirchner *et al.* 2001; Meyer *et al.* 1992; Wohl and Pearthree 1991). Studies indicate that the occurrence of high magnitude and fire related events such as landslides and debris flows is influenced by both landscape heterogeneity and stochastic rainfall, both of which contribute towards “episodic patches of activity” (Miller *et al.* 2003a). When attempting to predict occurrence and magnitude of high magnitude erosion events such as debris flows across the landscape, it is therefore important to clearly distinguish between randomness in rainfall as well as elements of landscape heterogeneity (e.g. topography, vegetation and soil) as sources of spatial variability (or patchiness) in the observed erosion response.

The literature reveals only a few studies that have focused specifically on aspects relating to high-magnitude erosion events following fire in south-east Australia. In early work, Brown (1972) showed that peak discharge in a recently burnt catchment in the Snowy Mountains, New South Wales, was ~30 times higher than the unburnt catchment given two comparable rainfall events. The highest observed sediment concentration ($143\,000\text{ mg l}^{-1}$) after wildfire increased by up to three orders of magnitude relative to the pre-fire data. Leitch *et al.* (1984) showed how an intense convective storm following a wildfire near Warburton, Victoria 1983 triggered a “mud torrent” from severe erosion where up to 22 t h^{-1} of material was removed from the burnt hillslope. More recently following wildfires in 2003 and 2007, debris flows were found to be the main source of sediment leading to water quality issues in both the Buckland River and the Upper Goulburn River, in northeast and central regions of Victoria (Ferguson *et al.* 2004; Lyon and O'Connor 2008; Tennant and Turner 2009; Tryhorn *et al.* 2008). Large erosion events with significant water quality impacts also occurred in the Cotter River catchments near Canberra after intense wildfire in 2003 (Worthy 2006). While they were not specifically identified as debris flows, the images of deposits and scoured channels reveal a number of characteristics that are typical of debris flow processes.

There are also a number of newspaper reports from Victoria following wildfires in 2003, 2007 and 2009 that indicate large erosion events do occur with major impacts: -“A flash flood swept their 4WD off a bridge into a creek...a fire fighter was washed away in a two-metre wall of water” (Berry and Bradley 2003)

- “A severe storm has brought flash flooding to the Gippsland town of Licola, knocking a house off its foundations and damaging seven others, weeks after bushfire” (Houghton 2007)

-“Road left covered in sludge...25mm of rain fell in about 15 minutes...caused a torrent of water and debris to rush down from the fire affected areas” (Dulhunty 2009). (see Appendix B, Figure 1 to 4, for examples of some of these events):

These reports and the limited available literature show that that the impacts from fire-related erosion processes on water resources, infrastructure and humans can often be linked to discrete high magnitude events. However, there seems to be a substantial knowledge gap when it comes to understanding the circumstances under which these ‘large’ erosion events occur after wildfire in the south-east Australian region, the processes involved, the volumes of material exported and the associated risks to water quality and other assets. This paper summarises recent efforts to document and investigate the occurrence of high-magnitude erosion events after wildfire in south-east Australia and aims to i) collect and show evidence of debris flow occurrence after wildfire in south-east Australia; ii) identify rainfall thresholds and key hydrological properties; and iii) present data on erosion rates from selected debris flows. The work focuses on small, first to third order upland catchments within Victoria that were burnt by wildfires in 2003, 2006/07 and 2009.

2.2 Regional Setting

2.2.1 Recent wildfires

In Victoria alone, nearly three million hectares of mostly forested public land were burnt by three large wildfire events between 2002 and 2009 (Table 2.1). The Eastern Victorian Alpine Fires of 2003 (~1 million Ha) and the Great Divide Fire Complex of 2006/07 (~1 million Ha) were caused by lightning strikes and both burnt through mountainous forested landscape over the course of two months. The intensity of the fires ranged from low to very high (Department of Sustainability and Environment 2009) with the variability in intensity known to be driven by local topography, fuel loads and the climatic conditions during the passage of the fire fronts (Bradstock *et al.* 2010). During the Black Saturday bushfires of February 2009 (~0.5 million Ha), four separate wildfires burnt through central, eastern and north-eastern parts of Victoria. Drought conditions, strong winds ($> 100 \text{ km h}^{-1}$) and temperatures exceeding $40 \text{ }^{\circ}\text{C}$

resulted in extremely high fire intensity ($> 70\,000\text{ kW m}^{-1}$) on 7th February 2009 during which more than 50% of the total area was burnt (Teague *et al.* 2010).

Table 2.1 List of regional wildfires in forested catchments of south east Australia from 2000 to 2009 and the associated post-fire erosion research that has been published in the scientific literature

Date & Location	Cause	Burn Area	Peer-reviewed research publications
New South Wales, Dec - Jan 2001/02 Black Christmas Bushfires	Arson & Lightning	6500 km ²	<i>Nattai Catchments</i> (Blake <i>et al.</i> 2009; Doerr <i>et al.</i> 2004; Tomkins <i>et al.</i> 2008; Tomkins <i>et al.</i> 2007)
Victoria/New South Wales Jan - Feb 2003 Alpine Fires	Lightning	15000 km ²	<i>Kiewa Catchments</i> (Lane <i>et al.</i> 2006b; Lane <i>et al.</i> 2008; Noske <i>et al.</i> 2010; Nyman <i>et al.</i> 2010; Sheridan <i>et al.</i> 2007a) <i>Snowy Mountains</i> (Smith and Dragovich 2008)
Australian Capital Territory, Jan 2003 Canberra Bushfires	Lightning	1650 km ²	<i>Cotter Catchments</i> (White <i>et al.</i> 2006)
Victoria, Dec - Jan 2006/07 Great Divide Fire Complex	Lightning	10500 km ²	-
Victoria, Feb 2009 Black Saturday	Powerlines & Arson	4500 km ²	-

2.2.2 Geology and landform

The wildfires burned through the east Victorian uplands which forms part of the Great Dividing Range, and described by Jenkins (1991) as a belt of “ridges, plateaus and corridors”. The range was formed during a series of uplifts and mountain building phases in the middle Palaeozoic. Today, the elevation ranges from 200 meters above sea level (m.s.l) in foothills to 2000 m.s.l in the alpine regions along ridges and on upland plateaus. A large majority of the bedrock is of Palaeozoic origin and consists of marine sedimentary rocks (mudstone, shales and sandstone) which in the eastern part of the state have been formed into a belt of metamorphic rocks (schist and gneisses). There is a distinct region of fluvial sedimentary rocks in the central part of the eastern uplands (mudstone, sandstone and conglomerates). Acid plutonic outcrops (granite and granodiorite) occur in patches throughout the region. Dissected uplands is the main

landform which is typically characterised by mountains with long steep slopes, narrow valleys and ridges and spurs with narrow crests (Jenkins 1991). Upland plateaus and high plains are found in regions underlain by more resistant rock formations and often associated with granitic or volcanic geologies. Headwater catchments ranging in size from 20 Ha to 400 Ha are steep with a relative relief ranging from 200m to 800m.

2.2.3 Climate

Victoria has a temperate Mediterranean type climate with hot, dry summers and cool, wet winters. The region experiences large annual variability in temperature and rainfall due to ENSO (El Nino-Southern Oscillation) effects and positive Indian Ocean Dipole (pIOD) events both of which have been linked to the recent drought in Victoria and the increase in wildfire activity (Cai *et al.* 2009). In Melbourne on the coast, the January (summer) and July (winter) average maximum temperatures are 25.8 °C and 13.4°C, respectively. Summer temperatures are typically 2 to 4 degrees hotter in inland regions. At Falls Creek, northeast Victoria (1765 m.s.l.) the average maximum temperatures are 17.6 °C and -1.1°C for January and July, respectively. The average annual precipitation in the eastern uplands ranges from 600 mm to 2500 mm. The majority of precipitation in Victoria is generated from cold fronts during winter (May – September) when easterly moving continental high pressure systems are interspersed with easterly or north-easterly moving low pressure systems that originate in the southern ocean. When the moist air masses reach the central and eastern uplands, the mountainous terrain and the prevailing north easterly moving pressure systems result in high variability in precipitation across short geographic distances.

In general, precipitation increases with altitude and tends to be higher on the south and south westerly slopes of the dividing ranges. Pronounced rain shadow effects are common on north and easterly facing slopes. In winter, precipitation often falls as snow at elevations greater than 1200m. The eastern part of the state (East Gippsland) is less influenced by the south-westerly moving air masses and instead receives rainfall from large easterly moving low pressure systems that form off the south east coast of Australia. Summer rainfall (December – March) is less frequent but often occurs as high intensity storms due to strong convection and high moisture content of warm air. Remnant tropical low pressure systems can occasionally affect Victorian weather patterns in summer by supplying large masses of warm and moist air from the north, which can potentially result in heavy and widespread rainfall.

2.2.5 Vegetation and wildfire

The eastern Victorian upland region encompasses a wide range of *Eucalyptus* dominated forest types which vary greatly in structure depending on the interplay between spatial variability in climate, topography and fire. The Ecological Vegetation Class (EVC) is widely used as landscape scale classification scheme for vegetation types in Victoria. The scheme, developed by the Victorian Department of Sustainability and Environment (DSE), is available as a state-wide dataset for use in a geographic information system (GIS). The distribution of EVC's across a landscape is largely driven by variability in effective rainfall (precipitation *minus* evaporation) and in this paper we consider three broad categories: dry, damp and wet forests (Table 2.2). The EVC is a useful indicator of the effects of aspect, elevation, and rainfall patterns on the distribution of vegetation structure and associated soil types, with implications for examining landscape-scale variability in soil hydrological properties under different moisture regimes.

Table 2.2 The structure and distribution of different Ecological Vegetation Classes (EVC) in the eastern uplands of Victoria.

Rainfall (mm)	Ecological Vegetation Class (EVC)	Vegetation Structure (Specht 1972)	Tree height (m)	Tree density (stems/ha)	Canopy cover (%)	Ground cover (%)	Area ¹ (%)
200-1000	Shrubby dry forest						
	Heathy dry forest	Open forest	<30	~20	20-40	50-80	43
	Grassy dry forest						
800-1200	Damp forest	Tall open forest	30-50	~20	30-50	100	15
	Damp montane forest						
>1200	Wet forest	Tall open forest	75-100	20-50	40-80	100	7
	Wet montane forest						

¹The area (in percent) occupied by the respective EVC groupings at elevation above 200 m in the forested region of the east Victorian uplands (~4.4 million Ha).

In broad terms, the vegetation at the wet end of the spectrum (annual rainfall > 1200 mm yr⁻¹) in sheltered valleys and on southerly aspects at elevations between 200 and 900 m.s.l. is dominated by pure stands of tall Mountain ash forest (*Eucalyptus regnans*). Montane tall open Alpine ash (*E. delegatensis*) forests also fall in the wet forest category and dominate at higher elevations from 900 to 1500 m.s.l., above which the vegetation shifts towards sub-alpine low open forest. The understorey in wet forest is

dense and consists of smaller trees, dense shrubs and ferns with grasses becoming increasingly dominant at higher elevations. The other end of the spectrum ($600 \text{ mm yr}^{-1} < \text{annual rainfall} < 800 \text{ mm yr}^{-1}$) at moderate elevations (200-1000 m.s.l) is dominated by dry open forest consisting of various combinations of Broad-leaved Peppermint (*E. dives*), stringybark (*E. macrorhyncha*) and box-type eucalypts (e.g. *E. polyanthemos*). The understorey is generally of an open structure and dominated by shrubs in moist areas and graminoids in drier areas on ridges and steep northerly facing slopes. For intermediate rainfall zones ($800 \text{ mm yr}^{-1} < \text{annual rainfall} < 1200$) the vegetation is strongly affected by aspect. On northerly facing slopes the vegetation resembles a dry open forest category as described above. On southerly facing slopes where the evaporative loss is considerably lower, the vegetation shifts towards a damp open or tall open-forest structure which typically consists of Messmate (*E. obliqua*), Narrow-leaved Peppermint (*E. radiata*), some Candlebark (*E. rubida*) and various species of gum (e.g. *E. globulus* and *E. cypellocarpa*, *E. viminalis*).

Fire plays a central role in maintaining vegetation communities in the Myrtaceae (family) dominated forests of south-east Australia and so wildfires are considered a natural part of the ecosystem (Bradstock 2008). The history of fire in the region is a product of the complex interaction between climate change, vegetation change and anthropogenic factors. The limited available evidence from charcoal records in south-eastern Australia indicate that there has been a general increase in fire activity during the Holocene most likely due to the combination of a warming climate and increasing population density (Kernshaw *et al.* 2002). Studies further indicate that there was a peak in fire activity during the immediate post-European settlement phase followed by a subsequent decline in the latter part of the 20th century (Kernshaw *et al.* 2002). However, the lack of historical data on fire occurrence in the region makes it difficult to determine what constitutes a natural fire regime (see Bradstock (2008) for a discussion on contemporary vs historical fire regimes).

Life history strategies of fire adapted plants are closely linked to fire with fire-return intervals acting to maintain the vegetation communities that currently occupy the region (Kennedy and Jamieson 2007). The current distribution of vegetation communities can therefore provide clues to the lower and upper bounds on 'natural' fire recurrence intervals for areas where data on long term fire history is unavailable. Using this approach, Kennedy and Jamieson (2007) found that the EVC comprising dry forests

(fire dependent) has a minimum and maximum fire return interval of 5 and 60 years respectively (average: 20-30 yrs). The corresponding minimum and maximum figures for wet forest (fire sensitive) are 25 and 150 years (average: 70 yrs). Wet forests burn only under exceptionally dry circumstances, but the high fuel loads (up to 50 t ha⁻¹) in these systems tend to result in extreme fire conditions (McCarthy *et al.* 1999). More frequent fire and lower productivity of dry forests mean that the fuel loads are relatively low (surface fuels > 6mm = 10-15 t ha⁻¹) compared to wet forests, however steep terrain and low fuel moisture can also result in high intensity fires in these dry forests (Gould *et al.* 2007; Sharples 2009; Tolhurst and Kelly 2003; Turner and Romme 1994).

2.2.5 Soils and erosion

The majority of the marine sedimentary or metamorphic geologic units in the eastern Victorian uplands produce clay loam textured Red or Brown Dermosols or Leptopodsol (Isbell 1996) with considerable variability in depth and structure depending in particular on local moisture regimes. In wet forests, the total soil depth ranges from 1 to more than 3 m and consists of a deep (10-30 cm), granular and highly structured brown to black loamy A-horizon overlaying a light clay loam B-horizon with low stoniness (< 10%). The soil is often mantled by deep (~10 cm) accumulations of litter and surface organic matter. The soils in these systems are macroporous and capable of rapid infiltration due to the high saturated hydraulic conductivity (100-2000 mm h⁻¹) (Davis *et al.* 1999; Nyman *et al.* 2010).

In dry forest the soils are generally less developed with a weakly structured, shallow (< 5 cm) and stony dark or light brown loam to clay loam surface soil over a clearly distinguishable yellow or red clay loam A2-horizon which extends to a depth of < 15 cm. The B-horizon is generally stony (25-30 %) with a medium to strong structure. Granitic geologies produce sandier soils. The litter layer is thin (1-3 cm) and on steep slopes often patchy with litter, soil and gravel accumulations interspaced by sections of exposed mineral soil. Soil depths are shallow (0.2 -1 m) on hillslopes, although the depth can be much greater in convergence zones and alongside the drainage network where alluvial and colluvial sediment accumulates. Exposed bedrock is often apparent on upper hillslopes and along ridgelines. Under dry conditions in very steep (> 35 degrees) sections of the catchments, the surface soils become increasingly skeletal and tend towards Lithosols which are shallow, stony and lack structure.

Undisturbed forest environments in the region display relatively low susceptibility to erosion by rainsplash and overland flow due to dense vegetation, high ground cover and often high infiltration rates. Using the fallout radionuclide Caesium – 137, Loughran *et al.* (2004) estimated a soil loss of $< 1 \text{ t ha}^{-1} \text{ yr}^{-1}$ from forested hillslopes and pastures in south-east Australia which is similar to the measured pre-fire sediment yield from small mountain catchments in northeast Victoria (Lane *et al.* 2006b). These estimates correspond with modelled values obtained using the Revised Universal Soil Loss Equation (RUSLE) to forested catchments on either side of the Dividing Ranges (Hancock *et al.* 2007; Lu *et al.* 2003). Hillslope erosion occurs primarily in summer in response to high intensity rainfall events. However, the short event durations relative to the travel time of entrained sediment often results in deposition on hillslopes or in ephemeral first and second order drainage lines, ultimately resulting in low sediment delivery ratio at larger catchment scales (Hancock *et al.* 2007; Lu *et al.* 2003). This pattern becomes increasingly prevalent for coarser sediments. Lower ground cover, lower soil organic matter and lower infiltration rates in dry forest environments mean that they are more susceptible to hillslope erosion than soils in wet forests (Rees 1982). Soils in eucalypt forests display strong water repellency under low soil moisture conditions in summer and autumn, which increases runoff, and exacerbates the erosion response to summer storms. This pattern is more pronounced in dry forest soils where macroporosity and background infiltration capacity are low compared to wet forest soils (Burch *et al.* 1989; Nyman *et al.* 2010; Rees 1982).

Mass wasting such as slides and slumps are relatively rare in the eastern Victorian uplands. This is mainly due to the shortage of rainfall as indicated by the higher frequency of landslides in high rainfall regions south of the dividing ranges and the marked increase in landslide activity during exceptionally wet years (Cecil 1981; Evans and Joyce 1974; Rutherford *et al.* 1994). The distribution of landslide activity as documented over the last century indicates that sedimentary and volcanic rocks are more susceptible to mass failure than metamorphic and igneous rock types (Evans and Joyce 1974). Rutherford *et al.* (1994) documented the occurrence of more than 30 debris flows in dry Eucalypt forest that were triggered by mass failures in colluvial hollows and on steep planar hillslopes following a large 50-year rainfall event (250 mm in 24 hrs) in 1993 in north east Victoria. The failures occurred predominantly in acid volcanic and granitic geologies and were less common on areas underlain by sedimentary rocks such as greywacke and sandstone. While the study concluded that the debris flows

represented a rare event in northeast Victoria, they were considered to be an important geomorphic process in that they transferred coarse colluvial material to larger streams where they are made available for further reworking (Rutherford *et al.* 1994).

2.3 Methods

2.3.1 Post-fire erosion events in eastern Victoria

The occurrence of high-magnitude post-fire erosion events was detected through information provided by regional catchment management authorities, landowners and news reports. Reported events were followed up with site visits and/or examination of events through aerial photographs, satellite imagery and written documents relating the conditions under which the events occurred. The aim was to build a record of significant post-fire erosion events and provide a set of sites that could be selected for detailed field surveys. The method of detecting erosion events meant that the sample was restricted to those events that impacted communities, landowners or catchment managers through flooding, damage to private property and road infrastructure and/or through ongoing water quality issues. Recorded events were therefore considered to represent a sample of high risk scenarios associated with hydrological and geomorphic processes in upland catchments after wildfire. Large widespread events such as the floods in Gippsland in June 2007 caused by synoptic rainfall were not considered in this study since the key erosion and sediment transfer processes operate at scales larger than first- to third- order upland catchments which are the focus of the paper.

Spatial data on geology, fire severity and vegetation type were obtained for each recorded event. The fire severity was determined from severity maps generated from the Normalised Burn Ratio using Landsat (30m resolution) and SPOT (10m resolution) imagery. The severity was then categorised according to the classification scheme used by the Victoria Department of Sustainability and Environment (DSE) (Department of Sustainability and Environment 2009). Very high severity is assigned to areas with intense overstorey burn, with 70-100% crown burnt and 100% understorey burnt. High severity is an intense understorey fire with 60-100% crown scorch. Moderate severity is a variable intensity fire ranging from a warm ground burn with no crown scorch to an intense understorey fire with 60-100% crown scorch of most eucalypt.

Field examination of each event was carried out with the aim of distinguishing between floods and debris flows as manifested by the different flow mechanisms underlying the

two event types. In debris flows, the flow dynamics are determined by both solid and fluid forces whereas in sediment laden floods the flow is determined by fluid forces alone. The transition from flood through to hyper-concentrated flood to debris flow is represented by a continuum and a single event is often associated with several flow pulses that have different characteristics (Costa 1988; Pierson 2005). Furthermore, the flow properties can vary along the course of the channel with the lower channel reaches often exhibiting flood characteristics due to increased sediment deposition as well as dilution from increased water content relative to the sediment entrainment rate (Hungr *et al.* 2001; Hungr *et al.* 1984; Meyer and Wells 1997). During field evaluation it was therefore important to consider all the available evidence along the entire channel where the event occurred. The majority of evidence of debris flow processes is found in depositional features and the damage caused to vegetation (Hungr *et al.* 2001). See Appendix B (Figures 5 and 6) for typical features used to identify debris flow processes.

The event characteristics at different positions within the catchment were systematically assessed based on the key features listed in Table 2.3. Those events that were classified as debris flows were inspected in more detail in order to determine if they were generated from mass failure or surface runoff and progressive sediment entrainment (Cannon *et al.* 2001a). For erosion events that were recorded following the 2003 wildfires, the information obtained was subject to the availability of data from reports, catchments managers or landowners.

Table 2.3 List of key features used in field evaluation of extreme erosion events. See Pierson (2005) for further details on distinguishing between debris flows and floods.

Features	Flood	Debris Flow
Deposit Margins and Surfaces	<ul style="list-style-type: none"> -Horizontal stratification, cross bedding. Dunes and ripples -Deposits occur as bars, fans and sheets. No levees. -Vertical stratification. Course clasts may be imbricated. -Voids common between larger clasts. Deposits are loose and friable. -Logjams occur but are not associated with localised deposits. -Deposits are mainly confined to channel bed. 	<ul style="list-style-type: none"> -Unstratified. No dunes or ripples. -Deposits occur as marginal levees or fronts/snouts of very course material. Deposits often exhibit convex surface morphology. Snout is lobate and steep. -Normal and/or inverse grading common in vertical sections. No imbrication. Coarse clast more concentrated at margins -Matrix filling voids between large clasts within deposit. Deposits typically are compact and difficult to dig out. -Debris flow deposits often occur behind logjams or boulder clusters. -Consolidated sediments often packed into cavities in rocks and vegetation.
Damage to Vegetation	<ul style="list-style-type: none"> -Moderate to light scaring on upstream side of tree trunks. Scaring is usually irregular and concentrated near the stream bed. -Branches and roots bend but not broken or stripped. 	<ul style="list-style-type: none"> -Severe scaring on upstream side of tree trunks. Scaring is evenly distributed up to the maximum stage/height of the debris flow event. -Branches and roots broken and tapered by erosion
Channel	<ul style="list-style-type: none"> -Channel have large width to depth ratio 	<ul style="list-style-type: none"> -Severely eroded channel, often U shaped and eroded to bedrock

Three debris flows (Germantown, Yarrarabula and Rose River) in northeast Victoria were selected as sites for detailed surveys and measurement of soil hydrological properties due their accessibility and the availability of rainfall data. The field survey was conducted between December 2007 and March 2008, approximately one year after the fire and up to five months following the debris flow events. The survey was designed to provide i) detailed description of the selected debris flow events; ii) rainfall intensity and duration and iii) data on the hydrological properties of the affected catchments.

2.3.2 Intensive field survey

The sites were first mapped in order to identify the catchments where debris flows occurred and map the drainage lines that were scoured to bedrock. A combination of methods were utilised for mapping debris flows including ground based surveys and aerial surveys using a Trimble Differential GPS (DGPS) device and a laser rangefinder (Contour™ XLR) to locate and map scoured channels. Once the debris flows within the respective sites were mapped, the data was imported into ArcGIS along with a digital elevation model (10 m resolution) and data on fire severity, vegetation and geology.

Soil loss as a result of the debris flow events was measured on hillslopes and in channels within one catchment in each of the three selected sites (Figure 2.1). Hillslope erosion was measured in quadrats along transects that were laid out perpendicular to the contours. The extent and severity of hillslope erosion appeared to be much higher in the upper part of the catchment. The locations of transects were therefore stratified according to the lower, mid and upper sections. These sections were each defined as contributing to a third of the channel length between the debris flow initiation point and the main deposit or debris flow fan. The initiation point was defined as the location along the drainage line where the maximum depth of scour first exceeded 0.2 meters and where depositional features were consistent with the debris flow type characteristics listed in Table 2.2. A scour depth of 0.2 m was considered an appropriate cut-off point because it represented a point from which the channel scour increased progressively in magnitude as opposed to the discontinuous nature of shallower rills. Since the lower-, mid- and upper hillslope transects were situated within equal proportions of the main channel length, we could assume that the hillslope length of the three sections was directly proportional to the area of each section relative to the area of the entire

catchment. While this assumption requires a simplified representation of the catchment shape, it provides a way of partitioning sediment sources to the different sections of the catchment.

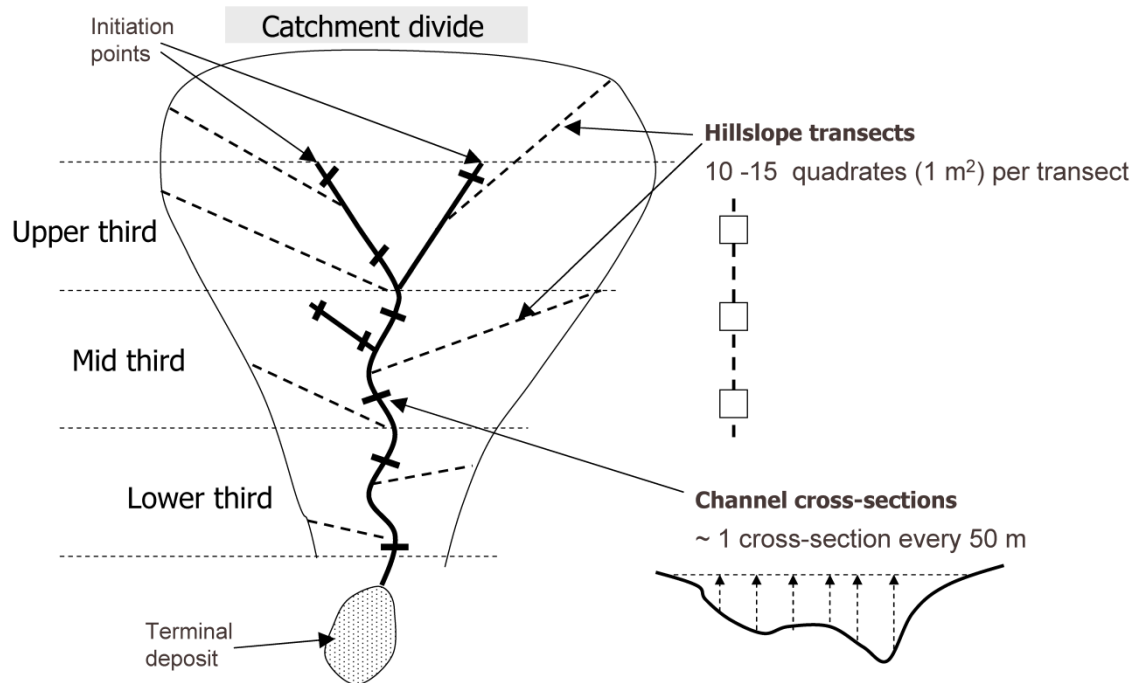


Figure 2.1 A conceptual representation of the catchment and the layout of the field survey. Photos from the field survey are provided in Appendix B (Figures 7 to 10).

Erosion depth was measured in 10-15 quadrats (1 m^2) evenly spaced along three transects in the upper section and two transects in the mid and lower sections of the catchment. The soil loss from quadrats was estimated based on indicators that provided a reference from which the pre-existing soil surface could be extrapolated. Typical indicators included pedestals capped by stones and roots, sections of unburnt stem from grasses and shrubs pre-dating the fire, and distinct burn marks on rocks. The proportion of eroded and non eroded surfaces was recorded alongside the measures of erosion depth. An estimate of the mean erosion depth within the eroded section of the quadrat was based on three to six separate measures of ground surface change. In cases where there were no indicators within the quadrat, a surface lowering of zero was assumed, unless there was clear evidence to suggest that there had been significant erosion across the entire quadrat in which case the quadrat was excluded due to the absence of measureable features. The area within the quadrat where deposition occurred was recorded as being non-eroded. The presence or absence of rills was recorded at each

quadrat and a note was made as to whether there was evidence of widespread sheet erosion.

Channel erosion was measured through cross-sectional surveys of all scoured channels contributing to the debris flow. Cross sections were measured by suspending a horizontal string across the channel and measuring the height at 50 cm and 25 cm intervals for channels wider or less than 2 m, respectively. The spacing between cross-sections along the channel was determined by the variability in magnitude of channel scour and channel morphology. The maximum distance between two cross sections was 190 m and the average spacing was 50 m. The cross sections were set up so that they extended into the non-eroded segments of the banks leading into the channel. These non-eroded banks were then used to project the pre-existing channel form using the same procedure as outlined in Gartner et al. (2008). The volume of eroded material was calculated by averaging between segments along the channel, each represented by one cross section at either end.

The standard error of soil erosion depth within the lower-, mid and upper catchments sections was the main source of estimation error for hillslope erosion estimates. There was also an error associated with the proportional area that comprises the lower-, mid- and upper catchment sections given that the proportion was estimated based on the mean length of hillslope transects. Both the standard error of erosion depth and standard error in the area estimation were propagated through the volume computation and reported alongside the final volume estimate. For channel erosion, the error of the erosion estimates was calculated from the standard error of the mean channel entrainment rate ($\text{m}^3 \text{m}^{-1}$) within the lower-, mid- and upper sections of the catchments. The estimation error within catchment sections (lower, mid or upper) was then obtained by multiplying the error of the mean entrainment rate with the total channel length for which the volume of material was calculated. The estimation error for channel erosion is likely to be an overestimate given that the downslope increasing trend in erosion (which is accounted for in the volume estimates) provides a major source of variability when the channel entrainment rate is averaged across the entire catchment section. The additional errors associated the mean proportion of rock > 30 mm and the mean bulk density of hillslope material, channel material and rock were accounted for and propagated in the volume to mass conversion.

2.3.3 Rainfall properties

The total rainfall was measured in manual rain gauges by landowners in the vicinity (< 0.5 km) of the selected debris flow events. The cumulative rainfall data at 10 min resolution was available from weather stations located between 5 and 10 km from the debris flow sites. The rainfall intensity and duration of the debris flow generating events was obtained by coupling the known total rainfall with radar data from the Australian Bureau of Meteorology which provides radar reflectivity (dBz) scans at a 10 min temporal resolution. The rainfall accumulation at a point was then estimated based on the known total rainfall and the distribution of radar derived intensities for the duration of the event. The continuous intensity at debris flow locations was obtained by first estimating the direction and tracking velocity of storm cells, then extracting the radar derived intensity values for a transect of pixels (0.5 km x 0.5 km) within each 10 minute data frame covering the duration of the rainfall event. The length and the orientation of the transect was determined by the velocity and direction in which the storm was travelling, and these measures were obtained by manually tracking the position of at least three separate storm cells during a 30 min sequence of radar images that included the storm cell for which the rainfall accumulation was extracted. The rainfall accumulation curve was then obtained by adjusting the extracted relative intensity values to the known total rainfall from each site. The representativeness of the extracted intensity was tested for each event at the sites where the 10 min rainfall accumulation was known from tipping bucket rain gauges.

2.3.4 Soil hydraulic properties

Ponded hydraulic conductivity or infiltration capacity (K_p) was measured in February 2008 using a 5mm constant head custom build infiltrometer with a disc diameter of 50 mm. The infiltrometer was manufactured in accordance with the design outlined in Perroux and White (1988). Steady state infiltration measurements were obtained in the upper region of the catchment where the surface soil was intact and non-eroded. Infiltration was measured at five random locations within a 20 m x 20 m plot. The sampling locations were prepared by carefully driving a thin walled steel cylinder into the soil to depth of 5 cm. Vaseline was applied to the inside of the cylinder in order to prevent preferential flow along the perimeter of the sample. At all the surveyed sites, there was a discrete transition from shallow (1-3 cm) dark organic rich topsoil to a pale and gravelly subsurface soil. Measurements were obtained first on the surface of the intact soil then repeated at 3 cm and 5 cm depths in the same location after carefully

removing the overlying soils. The ponded steady state infiltration rate was converted to field saturated hydraulic conductivity (K_{fs}) using the correction proposed by (Reynolds 1993).

Water repellency was measured at three depths (surface, 1-3 cm, and 5 cm) at 20 random locations within the plot using a modification of the water drop penetration time (WDPT) (Letey 1969), including additional measurements of 2M ethanol (MacDonald *et al.* 1990). If water was absorbed in 10s or less, the soil was classified as hydrophilic. If water was absorbed in >10 s while 2M ethanol absorbed in < 10 s, the soil was classified as water repellent. If it took > 10 s for 2M ethanol to absorb the soil was classified as strongly water repellent. For one of the surveyed events, hydraulic conductivity and water repellency were measured in a nearby unburnt catchment. This allowed for a direct comparison between a burnt and unburnt system.

2.4 Results

2.4.1 Post-fire erosion events in eastern Victoria

High magnitude erosion events were reported in steep catchments throughout the burnt regions of the eastern uplands of Victoria (Figure 2.2). The events listed in Table 2.4 do not represent an exhaustive record of all significant events that have occurred in the region, but a set of events in upland catchments that have had large known impacts on water quality and/or infrastructure. A full record of events would require aerial imagery of all burnt areas combined with state-wide field surveys which would not be feasible given i) the large burn area, ii) the inaccessible terrain, and iii) rapid recovery of the overstorey vegetation resulting in poor visibility in aerial photographs within the first year after wildfire.

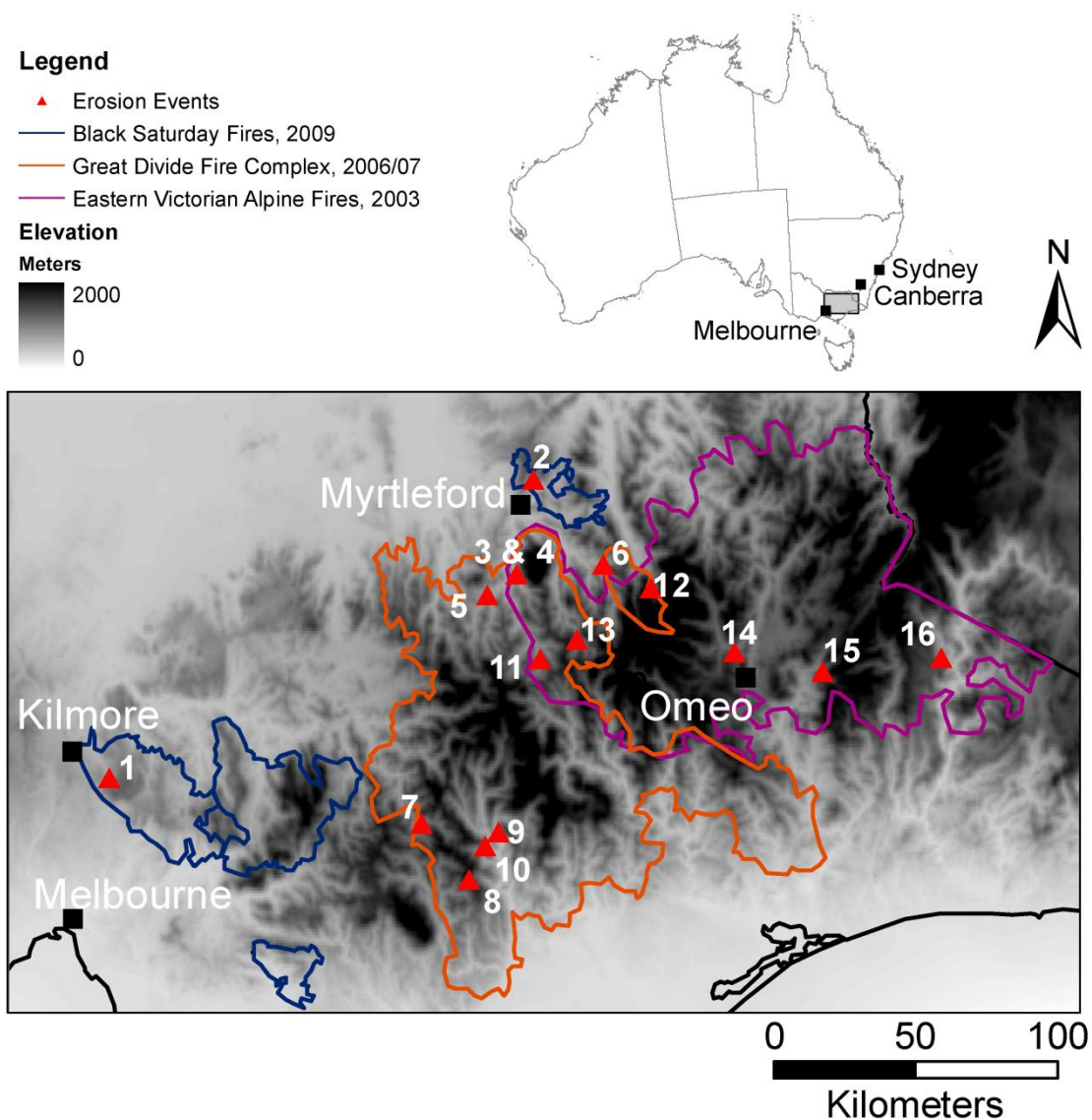


Figure 2.2 A map outlining the extent of recent wildfires in Victoria and the location of high magnitude events that were investigated.

The large majority of the listed events in Table 2.4 (13 out of 16) occurred as debris flows triggered by infiltration-excess runoff and erosion as a result of localised convective rainfall events. Runoff generated debris flows occurred in steep (30% - 70% of slopes > 25°) and northerly facing catchments in heathy-, grassy- and shrubby dry eucalypt forest which was burnt at high or very high severity (Table 2.4). All the debris flow events occurred within the first 12 months of the wildfire and were recorded throughout the Victorian uplands in metamorphic and sedimentary geologies as well as in mixed geologies such as the Big River event (# 14 in Table 2.4) which occurred in catchments consisting of igneous granite and sedimentary sand- and siltstone.

Table 2.4 .General site characteristics for locations where high-magnitude erosion events were recorded.

#	Site and Event Date	Location	Catchment size (ha)	Elevation (m)	Slope (degrees)	Fire Severity ^b	Annual Rainfall (mm)	Geology	Ecological vegetation class (EVC)	Event type	Run-out length (L/ ΔZ)
1	Sunday Ck, March 2009	N 5861774 E 334100	8-18	400-600	30% $\geq 25^\circ$ 9% $\geq 30^\circ$	100% ≥ 2	800-1000	-Sedimentary (marine) mudstone & sandstone -Metamorphic derivatives	Grassy dry	Runoff generated debris flow	3.4
2	Myrtle Ck, March, 2009	N 5963909 E 479045	10-25	450-800	55% $\geq 25^\circ$ 25% $\geq 30^\circ$	100% ≥ 2	1000-1200	-Sedimentary (marine) mudstone & siltstone -Metamorphic derivatives	Heathy dry	Runoff generated debris flow	2.8
3	Yarrarabula 1 Oct, 2007	N 5931411 E 473200	10-90	300-800	54% $\geq 25^\circ$ 25% $\geq 30^\circ$	95% $\geq 2^c$	1000-1200	-Sedimentary (marine) mudstone & siltstone -Metamorphic derivatives	Heathy dry	Runoff generated debris flow	3.4
4	Yarrarabula 2 Oct, 2007	N 5931411 E 473200	90-200	300-1400	41% $\geq 25^\circ$ 24% $\geq 30^\circ$	98% $\geq 2^c$	1000-2000	-Igneous granite	Heathy dry ^a	Flash flood	n/a
5	Rose River Dec, 2007	N 5925691 E 464878	30-90	350-650	48% $\geq 25^\circ$ 24% $\geq 30^\circ$	95% ≥ 2	1000-1200	-Sedimentary (marine) mudstone & siltstone	Heathy dry	Runoff generated debris flow	3.9
6	Germantown Oct, 2007	N 5935095 E 502684	30-100	450-1000	74% $\geq 25^\circ$ 45% $\geq 30^\circ$	73% ≥ 2	1000-1200	-Sedimentary (marine) mudstone & siltstone	Heathy dry	Runoff generated debris flow	3.4
7	Black River Unknown, 2007	N 5846104 E 440702	10-140	500-900	64% $\geq 25^\circ$ 37% $\geq 30^\circ$	100% ≥ 2	1200-1500	-Sedimentary (marine) mudstone & siltstone	Shrubby dry	Runoff generated debris flow	-
8	Aberfeldy Unknown, 2007	N 5826790 E 456970	-	1300	13% $\geq 25^\circ$ 3% $\geq 30^\circ$	99% ≥ 2	1200-1600	-Sedimentary (marine) mudstone & siltstone	Montane wet	Mass-failure	-
9	Mt Tamboritha Feb, 2007	N 5843139 E 467165	70-350	250-1000	52% $\geq 25^\circ$ 29% $\geq 30^\circ$	100% ≥ 2	800-1000	-Sedimentary (marine and fluvial) mudstone & sandstone	Heathy dry	Runoff generated debris flow	3.0
10	Target Creek Feb, 2007	N 5838539 E 462910	100-350	350-850	36% $\geq 25^\circ$ 10% $\geq 30^\circ$	100% ≥ 2	800-1000	-Sedimentary (marine) mudstone & siltstone	Shrubby dry	Runoff generated debris flow	3.3
11	Abbeyard, June, 2007	N 5902168 E 481366	-	500-900	62% $\geq 25^\circ$ 25% $\geq 30^\circ$	99% ≥ 2	1000-1200	-Sedimentary (marine) mudstone & siltstone	Heathy dry	Runoff generated debris flow	-
12	East Kiewa January 2004	N 5926579 S 519300	130 - 250	650-1400	31% $\geq 25^\circ$ 11% $\geq 30^\circ$	60% ≥ 2	1600-1800	- Metamorphic derivatives of sedimentary rock -Igneous grandiorite	Montane wet	Flood event	n/a
13	Dingo Ck , Feb, 2003	N 5909223 E 493698	350-400	600-1200	76% $\geq 25^\circ$ 48% $\geq 30^\circ$	96% ≥ 2	1200-1400	-Sedimentary (marine) mudstone & siltstone	Heathy dry	Runoff generated debris flow	3.8
14	Big River (Omeo), 2003	N 5904544 E 548026	~60	700-1000	42% $\geq 25^\circ$ 15% $\geq 30^\circ$	100% ≥ 2	800-1000	- Sedimentary (fluvial) sandstone & siltstone - Igneous granite & grandiorite	Heathy dry	Runoff generated debris flow	-
15 ^d	Blueys Ck, 2003	N 5898006 E 577947	20-50	700-1000	70% $\geq 25^\circ$ 37% $\geq 30^\circ$	96% ≥ 2	800-1000	- Sedimentary (marine) siltstone	Shrubby dry	Runoff generated debris flow	-
16 ^d	Suggan Buggan, 2003	N 5903000 E 618653	80-110	600-900	39% $\geq 25^\circ$ 25% $\geq 30^\circ$	43% ≥ 2	600-800	- Sedimentary (marine) mudstone & sandstone - Igneous granite	Shrubby dry	Runoff generated debris flow	-

^a Vegetation changes towards Wet Montane forest at elevation > 1000m.

^b Fire severity presented as the proportion of catchment with severity class of 1 or 2 according to the Classification of Remotely Sensed Imagery into Fire Severity maps (DSE, 2009): **1** = (very high severity) an intense overstorey burn with widespread crown removal with 100% understory burnt, **2** = (high severity) an intense understory fire with complete crown scorch of most eucalypt, **3** = (moderate severity) a variable intensity of fire ranging from a warm ground burn with no crown scorch to an intense understory fire with complete crown scorch of most eucalypt.

^c Yarrarabula was burnt in both 2003 (light to moderate severity) and in 2007 (high to very high severity)

^d Debris flow events first reported in (Harman and Stewardson 2007).

Each of the listed debris flow events represents a cluster of flows that covered an area ranging from 0.22 km² (two small terminal deposits at Sunday Ck) to 18 km² (seven large terminal deposits at Mt Tamboritha Rd). The catchment size for individual debris flows ranged from 8 ha (relief = 200 m) at Sunday Ck (# 1 in Table 4) to 350 ha (relief = 750m) at Mt Tamboritha Rd (# 9 in Table 2.4). Figure 2.3 and 2.4 show some key features typical of the runoff generated debris flows that were examined. In the upper third of the catchment where hillslopes are relatively long (100 m to 250 m) and steep (25° to 35°), there were signs of widespread sheetwash erosion where the slope in most cases was completely stripped bare of ash and topsoil exposing a paler and less organic subsurface soil (Figure 2.3a). Unburnt and freshly exposed roots across the entire width of the upper hillslopes and deposited material containing large clasts (up to 150 cm α -axis) provided a clear indication of the severity of the erosion and the large volume of overland flow generated during the events. Rills on planar hillslope sections were generally shallow (< 5 cm) and only apparent where sheetwash was less widespread. Rills extending to depths > 5 cm and beyond the depth of the unconsolidated and burnt topsoil were only observed in a short section (< 20 m) on converging hillslopes before they merged into a single eroded channel which defined the point of debris flow initiation. Damaged, ripped and/or tapered roots were typically first observed in convergence zones within 100 m of the catchment divide. A typical debris flow initiation point is depicted in Figure 2.3b. It is noteworthy that the initiation point is arbitrarily defined and that flow levees along rills on hillslopes and the presence of matrix supported coarse deposits behind logs and trees on hillslopes indicate that the runoff attained debris flow characteristics on hillslopes prior to entering confined flow in drainage lines.

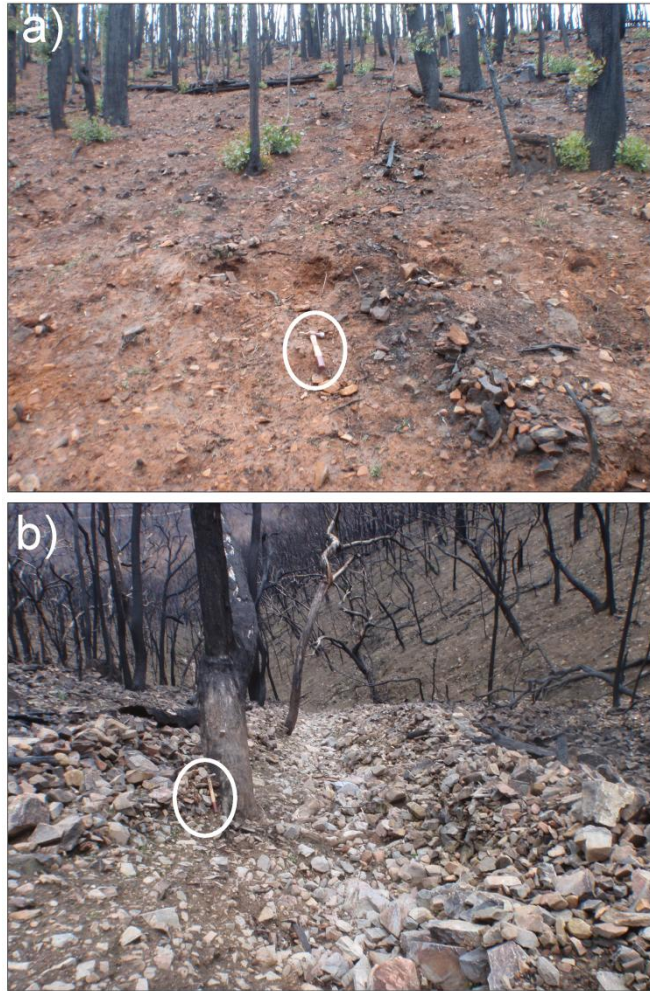


Figure 2.3 Images from the upper catchment showing a) eroded hillslopes with a small patch of relatively intact topsoil containing ash and rock fragments at Sunday Ck and b) channel initiation and levees of pale coloured rocks in a convergence zone with confined flow near Myrtle Ck.

Confined flow in convergence zones and pre-existing drainage lines resulted in rapid channel development where bedrock eventually set the lower limit of scour depth. Colluvial hollows and the intersections between drainage lines were often rich in material available for entrainment and scoured channels in these channel sections were bounded by vertical walls of up to 4 m in height (Figure 2.4a). Depositional features were often absent from these steep and severely scoured sections of the debris flow unless there were obstructions to flow within the channel. Terminal debris flow deposits were observed either at the intersection with permanent streams/rivers or at a point within the debris flow catchment after which the channel gradient decreased to below 10° (Figure 2.4b). The debris flow run-out length ($L/\Delta Z$) in Table 2.4 is given as the ratio of the horizontal travel distance (L) to the change in elevation (ΔZ) from the point

of initiation to the start of the terminal deposit. The average $L/\Delta Z$ values within eight debris flow sites ranged from 2.8 to 3.9, with an overall mean of 3.4 (std dev = 0.35). Below the main deposit, the amount of coarse debris in the diminished, clasts were no longer supported by a matrix of fine material and there was reduced channel incision. The channels below the main deposits were often associated with decreased channel definition and a wider flow path over which coarse material was continually deposited.

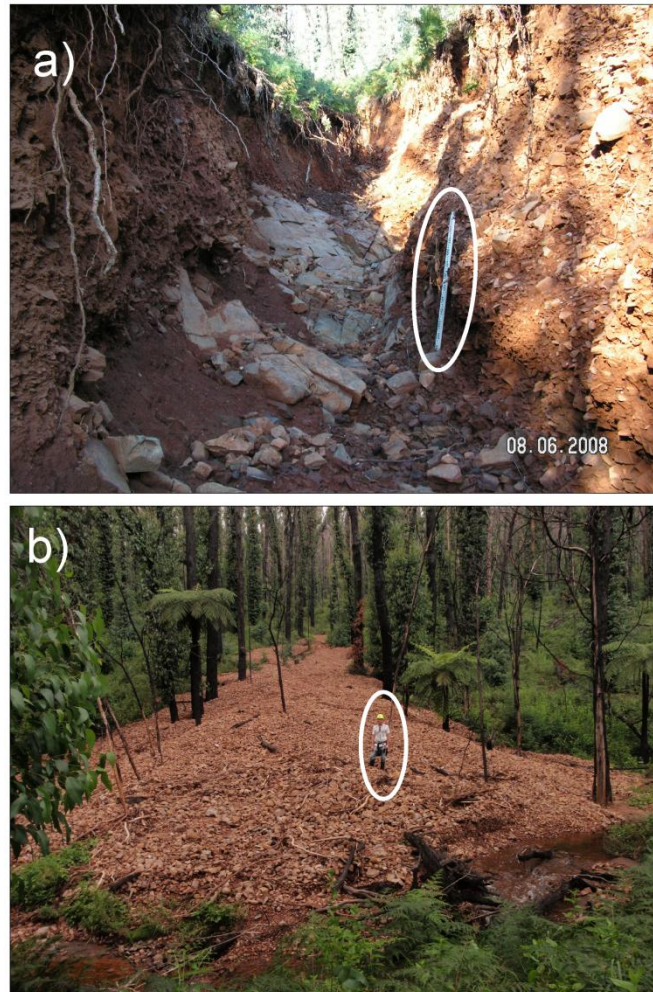


Figure 2.4 Images from mid to lower section of the catchment showing a) channel scour and exposed bedrock at Rose River and, b) a terminal debris flow deposit at the confluence with Sunday Ck. The height of the measuring pole in a) is 1.2 m.

The site at Aberfeldy (# 8 in Table 2.4) was inspected after reports from the local ranger of severe flooding and damage to roads, bridges and properties in the upper catchment after a synoptic scale rainfall event in June 2007, where approximately 150 mm of rain fell in 24 hours ($I_{30} = 12 \text{ mm h}^{-1}$ and $I_{10} = 19 \text{ mm h}^{-1}$). The catchments in the upper Aberfeldy are typical of the region in terms of both geology and topography and contain

both dry and wet eucalypt forests and therefore provided a suitable site for examining the response of severely burnt catchments to a very large rainfall event. The rainfall event with an estimated recurrence interval of 100 years occurred 6 months after the wildfire and there were fresh signs of widespread hillslope, gully and riverbank erosion. While the overland flow had resulted in shallow rills and stripping of ash and topsoil particularly on northerly facing slopes in dry eucalypt forests, there were no signs of runoff generated debris flows. However, one debris flow was detected in a first to second order drainage line and traced back to a small (16 m^3) soil slip in a steep ($\sim 30^\circ$) portion of a hillslope convergence zone. This isolated event occurred at a high elevation (1300 m.s.l.) in wet montane (Alpine Ash) forest which was burnt at very high severity.

The East Kiewa event in January 2004 (#12) was included as a case in Table 2.4 because it represents the highest recorded erosion event in a catchment monitoring study by (Lane *et al.* 2006b) in burnt wet eucalypt forest where the rainfall properties and topography were comparable to events that were recorded in nearby dry eucalypt forests. A high intensity convective rainfall event where 45 mm fell in < 2 hours ($I_{30} = 47 \text{ mm h}^{-1}$ and $I_{15} = 66 \text{ mm h}^{-1}$) resulted in a suspended sediment yield of 127 tonnes which accounted for 45 % of the total sediment yield in the first year after fire. The catchment was inspected and there were no signs of debris flows or mass failure.

2.4.2 Intensive field survey

An intensive field survey was carried out at Yarrarabula (# 3 & 4 in Table 2.4), Rose River (# 5 in Table 2.4) and Germantown (# 6 in Table 2.4) in northeast Victoria. Rose River and Germantown were both situated on Ordovician marine sedimentary geology while at Yarrarabula there were catchments on both igneous granite and on Ordovician marine sedimentary rocks with some sections of metamorphic derivatives. The catchments near Germantown were steeper ($45 \% \geq 30^\circ$) than the two other sites which were both similar in terms of the slope distribution ($24 \% \geq 30^\circ$). (Figure 2.5a). The majority (67 – 89 %) of the debris flow affected catchments were burnt at high severity (Figure 2.5b). At Germantown, the lower section of the catchments was burnt at moderate severity as part of a back-burning operation and did not result in high or very high severity caused by the wildfire in the upper sections.

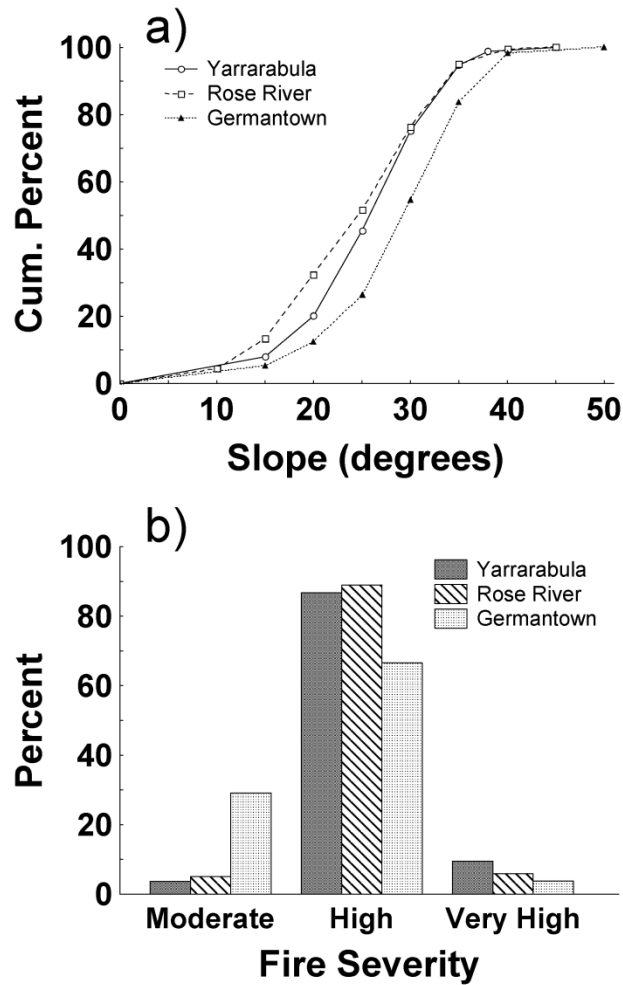


Figure 2.5 The slope distribution (a) and the burn severity (b) in debris flow affected catchments estimated for the area above the main debris flow deposit.

Figure 2.6-2.8 show the extent of debris flow affected catchments within each site, the channel profile and results from cross-section measurements for sampled debris flows. At Yarrarabula (Figure 2.6) the map clearly shows the absence of debris flows in the granitic foothills of Mt Buffalo where the valley floor east of the Yarrarabula River is slightly wider than the valley formed by the surrounding sedimentary geology. The catchments that were situated on the granitic intrusion consist of large areas of exposed bedrock devoid of soil and vegetation (Figure 2.9a). These relatively large catchments (< 200 ha) produced flash floods carrying rounded boulders (α -axis up to 1.5 m) and large volumes of woody debris, rocks and sand (Figure 2.9b), but the event did not display features consistent with the debris flow characteristics listed in Table 2.3. Channel scour occurred in some areas but it was discontinuous, there were no terminal deposits, the sediment deposited along banks and in low energy zones was well sorted with fine material absent from boulder deposits higher up in the catchments (Figure

2.9b). The smaller (< 100 ha) soil mantled catchments on mixed sedimentary and metamorphic rock on either side of the granitic intrusion produced several debris flows with features typical of other debris flows recorded and surveyed after fire Figure 2.9 (c and d). The survey focused on these latter events since they were debris flows and thus comparable to the other surveyed sites.

At Yarrarabula, a total of ~9 km of channel in 9 separate catchments (< 100 ha) was scoured down to bedrock by debris flows (Figure 2.6a). The sediment entrainment in the channel (m^3 of material per every m of channel length) increased gradually from < 0.5 $\text{m}^3 \text{m}^{-1}$ at 50 m towards a peak of 1.75 $\text{m}^3 \text{m}^{-1}$ between 400 m and 500 m at a point which coincides with the maximum rate of decrease in the channel slope (Figure 2.6b). The terminal deposits occurred at intersections with higher order streams or directly onto the gently sloping (7.5° - 10°) valley floor (pediment) where the flow was no longer confined to pre-existing channels. When the terminal debris flow deposits intersected with larger non-debris flow producing catchments, the material was redistributed by flooding water with much of the fine sediment absent from the coarse deposits suggesting that it had been transported further to the Yarrarabula River.

At Rose River (Figure 2.7a), ~8 km of channel was scoured by debris flows which occurred in 10 separate catchments (each < 100 ha) along the northern face of a ridgeline separating the Rose River from Dandongadale River. The south facing catchments on the opposite side of the ridge which were burnt at lower severity did not produce debris flows. These catchments consist of the more fertile herb-rich foothill forest typical of gullies and lower slopes on southern and eastern aspects in this region as opposed to the sparser shrubby dry forest on north-facing debris flow producing catchments which have a drier moisture regime. The debris flows at Rose River resulted in deep U-shaped channel scour in the upper to mid-sections of the catchment where up to 7 m^3 was entrained for every meter of channel between 200 m and 350 m (Figure 2.7b). The high magnitude of channel erosion at Rose River compared to the other sites was due to the large volumes of colluvial and alluvial material stored in the mid to upper sections of the channel. Scour depths of up to four meters occurred within 50 m of the debris flow initiation point. Similarly to Yarrarabula, the peak in channel erosion coincided with the point at which the rate of change in channel slope was highest. Beyond 400 m, the lower limit of scour depth was still set by the bedrock and so the decrease in entrainment rate was due to less available material within the channel and

not due to changes in the shear stress exerted by the debris flow. Two of the debris flows at Rose River reached the river itself, where the terminal deposits resulted in the formation of large pools above a section of riffle created by deposited coarse material. In most cases however, the terminal deposits occurred within ephemeral channels (gradient $< 10^\circ$) of the debris flow catchment.

At Germantown (Figure 2.8a), debris flows occurred in 5 north-facing catchments (each < 100 ha) situated along a spur which extends down from the Tawonga Gap. Nearly 11 km of channel was scoured to bedrock by debris flows. Channel erosion measurements show a different pattern to Rose River and Yarrarabula. The entrainment rate increases towards $\sim 1 \text{ m}^3 \text{ m}^{-1}$, and then decreases before increasing again to a peak of $\sim 2.5 \text{ m}^3 \text{ m}^{-1}$ just prior to the start of deposition. The slight decrease in entrainment between 400 m and 600 m occurred in a section of channel with low slope (11°) and relatively wide flow path where the bedrock within channel had not been exposed. While some deposition occurred in this region, the flow seemed to have been maintained by the inputs from three debris flows entering from small sub catchments into the main channel. A second peak in entrainment occurred in a section with a small step in the channel profile. The terminal deposit was laid down within the ephemeral valley floor once there was no further input from small tributary debris flow. Of the five debris flows at Germantown, only one terminal deposit intersected with German Ck.

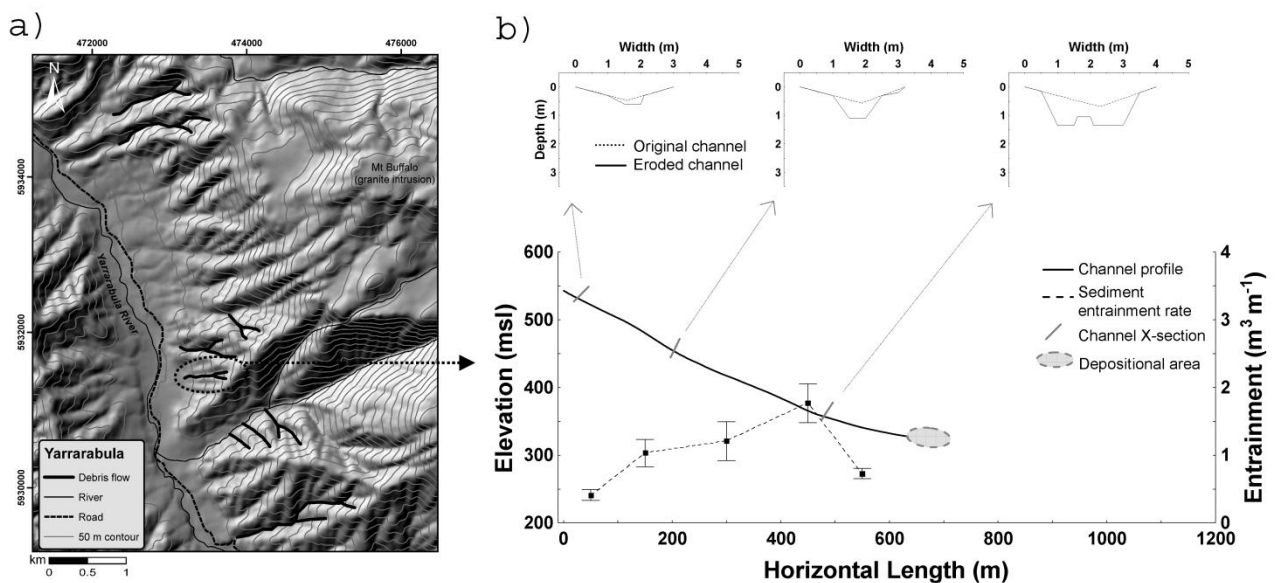


Figure 2.6 a) The location of debris flows at Yarrarabula in relation to local topography and b) the channel profile, sediment entrainment rate and channel cross-sections for a selected catchment. The error bar for sediment entrainment rate is the standard error of

the mean. The horizontal length is measured as the distance from the channel initiation point. Note difference in map scale and contour intervals compared to Figure 2.7 and Figure 2.8.

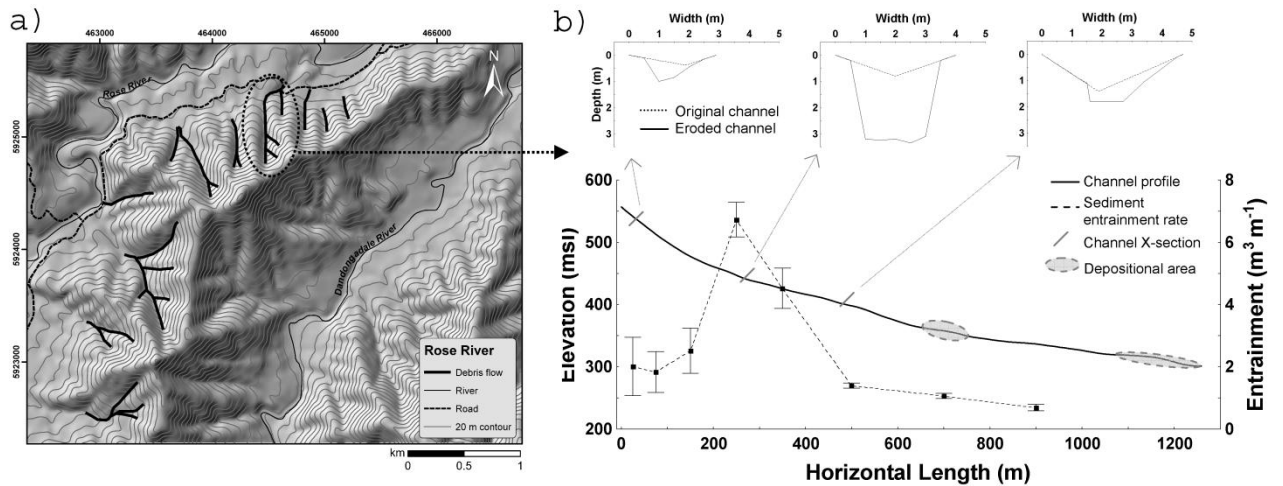


Figure 2.7 a) The location of debris flows at Rose River in relation to local topography and b) the channel profile, sediment entrainment rate and channel cross-sections for a selected catchment. The error bar for sediment entrainment rate is the standard error of the mean.

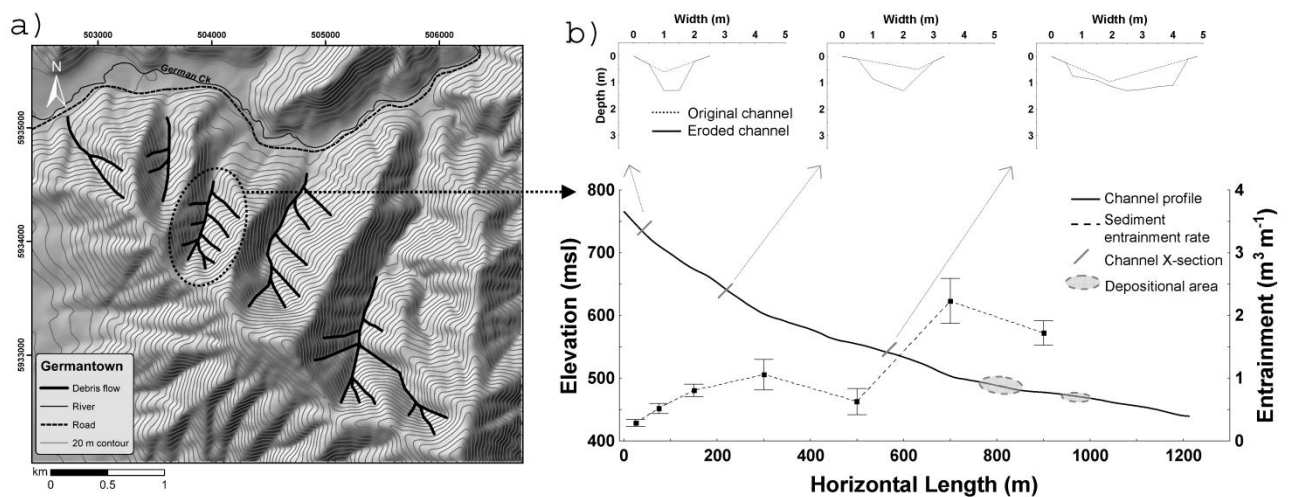


Figure 2.8 a) The location of debris flows at Germantown in relation to local topography and b) the channel profile, sediment entrainment rate and channel cross-sections for a selected catchment. The error bar for sediment entrainment rate is the standard error of the mean.

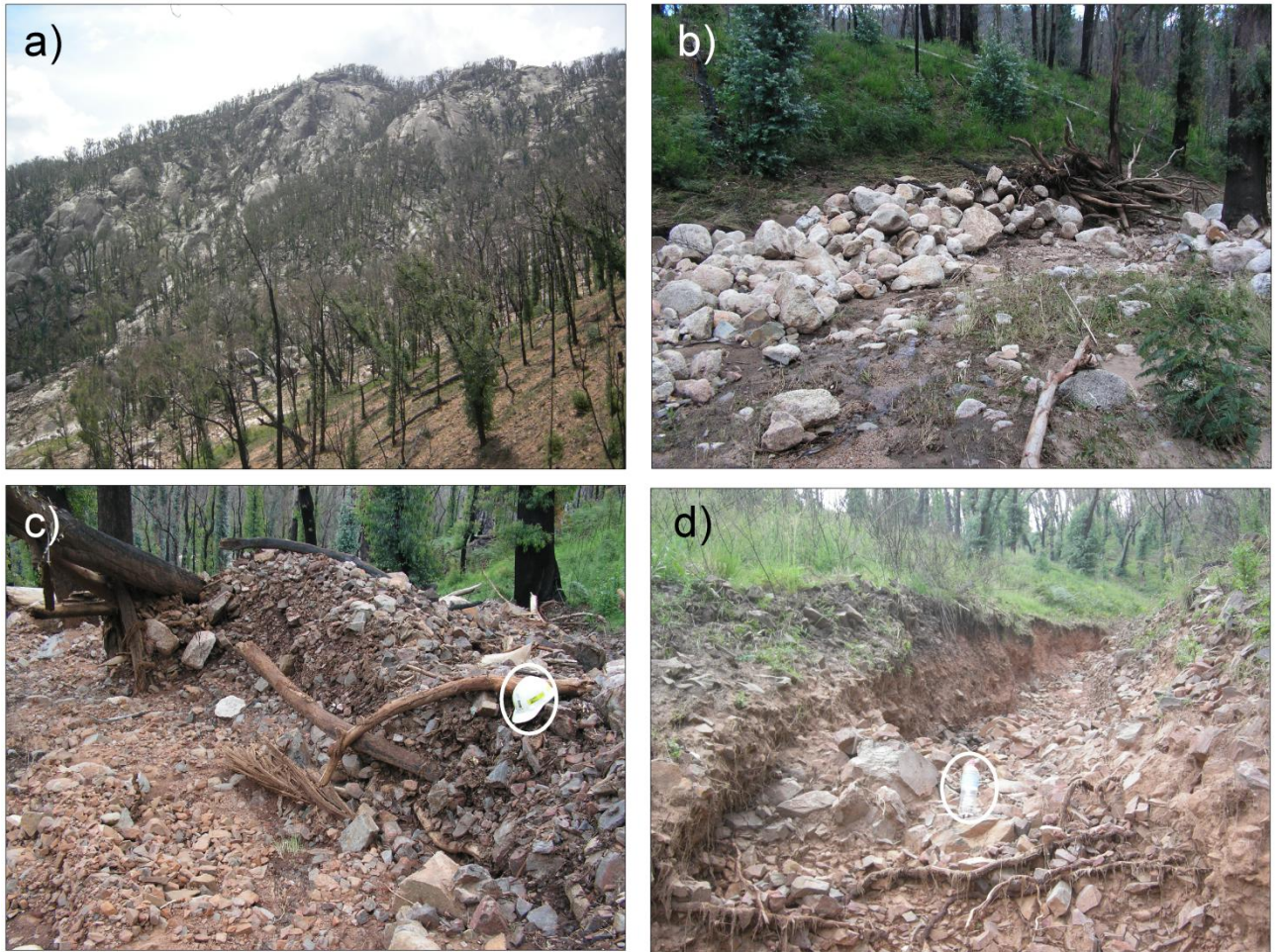


Figure 2.9 Images from erosion event at Yarrarabula showing a) the granitic foothills of Mt Buffalo in the background and sedimentary hillslopes in the foreground, b) a non-debris flow boulder deposit behind a log jam and flattened grass from flooding, c) matrix supported debris flow deposit in the adjacent sedimentary catchments, and d) channel scour and damaged roots from a debris flow.

Erosion measurements on hillslopes showed a strong increasing trend in the depth of erosion and the size of mobilized clasts going from lower to upper sections of the catchments (Figure 2.10). The mean hillslope erosion depth was higher at Yarrarabula across all catchment locations, particularly in the upper sections where the erosion depth ($18.4 \text{ mm} \pm 2.7 \text{ SE}$) was four times higher than that measured at Rose River ($4.6 \text{ mm} \pm 0.96 \text{ S.E}$) (Figure 2.10a). At Yarrarabula, there was a more constant increase in the erosion depth from lower to upper section as opposed to the other sites which display a sharp increase in hillslope erosion towards the top of the catchment. The soil surface was eroded in 68 %, 71 %, and 72 % of the upper catchment at Yarrarabula, Rose River and Germantown, respectively, which then decreased linearly to 51 %, 35 % and 45 % in the lower sections of the same catchments. The maximum clast size displays a similar

pattern to erosion depth with Yarrarabula showing more of a linear increase than the two other catchments (Figure 2.10b). Large clasts (up to 150 mm) had been dislodged and carried by gravity and overland flow before depositing behind trees, logs or other rocks. The steep slopes in the upper catchment means once a large rock is dislodged and set into motion by overland flow, the force of gravity alone will result in increased momentum.

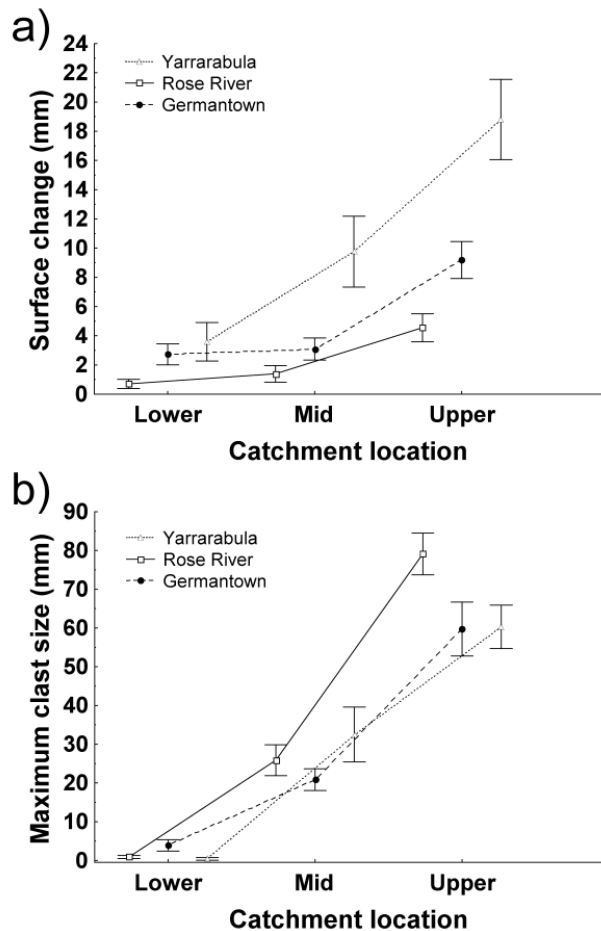


Figure 2.10 a) The net soil loss and b) maximum deposited clast size from the lower-, mid- and upper catchments at Yarrarabula (n = 83), Rose River (n = 80) and Germantown (n = 91). The error bars are the standard error of the mean.

The patterns in Figure 2.10 are closely related to the difference in the average slope and slope length between the lower-, mid- and upper sections of the catchment which are presented for each site in Table 2.5 and show that upper slopes are steeper and longer than slopes in the lower section of the catchments. Based on the channel and hillslope erosion measurement, the total volume of debris flow material from hillslopes and channels ranged from $2\,300\text{ m}^3 \pm 220\text{ SE}$ to $5\,990\text{ m}^3 \pm 970\text{ SE}$ (Table 2.5). These

values represent the volume of in situ soils, sediments and rocks that was eroded and mobilised during the event.

The volumetric contribution of hillslopes and channels to total sediment entrainment is not proportional to the mass of sediment entrained, due to different properties of the material. For instance, rocks greater than 30 mm made up 32-40 % and 4-10 % of channel and hillslope material, respectively. The published bulk density value for sandstone (2.22 g cm^{-3}) was used in the volume to mass conversion of the rock fraction. Soil samples from hillslopes and channels, respectively, contained by mass an average of 37.5 % (std dev = 8) and 52.5 % (std dev = 10) of gravel between 30 mm and 2 mm. The bulk density of eight 16 cm^3 cores (including gravel between 2mm and 30mm) at 0 - 5cm on hillslopes did not differ between six burnt sites in dry *Eucalypt* forest and the overall average of 48 cores was 1.3 g cm^{-3} (std dev = 0.19). Due to the higher gravel content, bulk density of channel material, which was measured from 6 cores at Rose River, was higher (1.8 g cm^{-3} , std dev = 0.14) than the hillslope material.

Table 2.5 Hillslope and channel erosion rates measured for upper, mid and lower sections of three runoff generated debris flows in northeast Victoria.

	Germantown (70 ha)			Yarrarabula (12 ha)			Rose River (30 ha)		
Hillslope	Mean gradient (degrees)	Mean hillslope length ^a (m)	Eroded Volume ± SE (m ³)	Mean gradient (degrees)	Mean hillslope length ^a (m)	Eroded Volume ± SE (m ³)	Mean Gradient (degrees)	Mean hillslope length ^a (m)	Eroded Volume ± SE (m ³)
Upper	31.8	187 (48)	3 240 ± 900	29.3	151 (45)	1 040 ± 180	31.1	167 (52)	780 ± 300
Mid	29.2	150 (39)	880 ± 220	25.4	105 (31)	370 ± 90	27.5	105 (33)	150 ± 60
Lower	21.5	50 (13)	260 ± 90	19.6	78 (23)	100 ± 40	20.7	50 (16)	40 ± 20
Hillslope volume			4 280 ± 940			1 510 ± 210			970 ± 310
Channel	Mean gradient (degrees)	Channel length ^b (m)	Eroded Volume ± SE (m ³)	Mean gradient (degrees)	Channel length ^b (m) (m)	Eroded Volume ± SE (m ³)	Mean gradient (degrees)	Channel length ^b (m)	Eroded Volume ± SE (m ³)
Upper	30.2	1 412 (8)	770 ± 140	25.5	551 (4)	340 ± 60	27.8	665 (3)	1 560 ± 280
Mid	24.9	1099 (5)	170 ± 170	16.2	151 (1)	300 ± 20	15.1	380 (2)	340 ± 280
Lower	7.1	412 (1)	680 ± 100	8.6	145 (1)	160 ± 11	8.6	390 (1)	50 ± 50
Channel volume			1 620 ± 250			800 ± 70			1 950 ± 400
Total volume (m ³)			5 990 ± 970			2300 ± 220			2920 ± 500
t ha ^{-1c}			120 ± 20			270 ± 40			150 ± 40

^a The value in the brackets for hillslope length is the percentage of catchment made up of the respective hillslope units.

^b Value in the brackets for channel length is the number of tributary channels contributing to the total channel length.

^c A bulk density of 1.3 g cm⁻³ and 1.8 g cm⁻³ was used for hillslope and channel material. Rocks > 30 mm were converted to mass using published bulk density values for sandstone (2.22 g cm⁻³) (Carmichael 1989)

2.4.3 Rainfall properties

The debris flows at Yarrarabula and Germantown were triggered by different storm cells from the same rainfall event on 28th October 2007 and at Rose River one rainfall event occurred on 3rd December and then another smaller event on 22nd December. The available video footage from Rose River indicates that both rainfall events resulted in debris flows and that the initial debris flow on 3rd December was much larger in magnitude. The average size of storm cells was 110 km² (SD = 52) and the rainfall events were tracking in a south-easterly (130° – 160°) direction at speeds of 80 -110 km h⁻¹. Ten minute or 15 minute rainfall data from rain gauges (pluvio) was available at locations < 15 km from the debris flow sites. These data were plotted along with the radar derived rainfall intensity which had been calibrated against the total rainfall recorded for the event at the location of the rain gauge (Figure 2.11). The calibrated radar derived rainfall accumulation fitted well with the observed data (refer to section 2.3.3 for methods of calibration). When compared to a fitted constant intensity for the duration of the event (i.e. linear fit), the radar-derived rainfall accumulation provided a 40 % improved representation of the actual measured rainfall at Bright (Figure 2.11b) and Lake Buffalo (Figure 2.11d). The rainfall intensity at Black Range Ck (Figure 2.11c) was relatively uniform throughout the rainfall event and as a result the radar-derived intensity provided a lower improvement (25 %) relative to a linear fit but a good overall fit ($R^2 = 0.99$). The peak 3-minute, 10-minute and 30-minute rainfall intensity (I_3 , I_{30} & I_{10}) could therefore be extrapolated from the radar data with high confidence at the debris flow locations where only the rainfall total for the event was known (Figure 2.12). The smaller debris flow event at Rose River on the 22nd December was caused by a rainfall event (20 mm in 4 hrs) with I_{10} and I_{30} of 42 mm h⁻¹ and 14 mm h⁻¹, respectively. The peak in intensity occurred after a 3 hour period with 10 mm of rainfall.

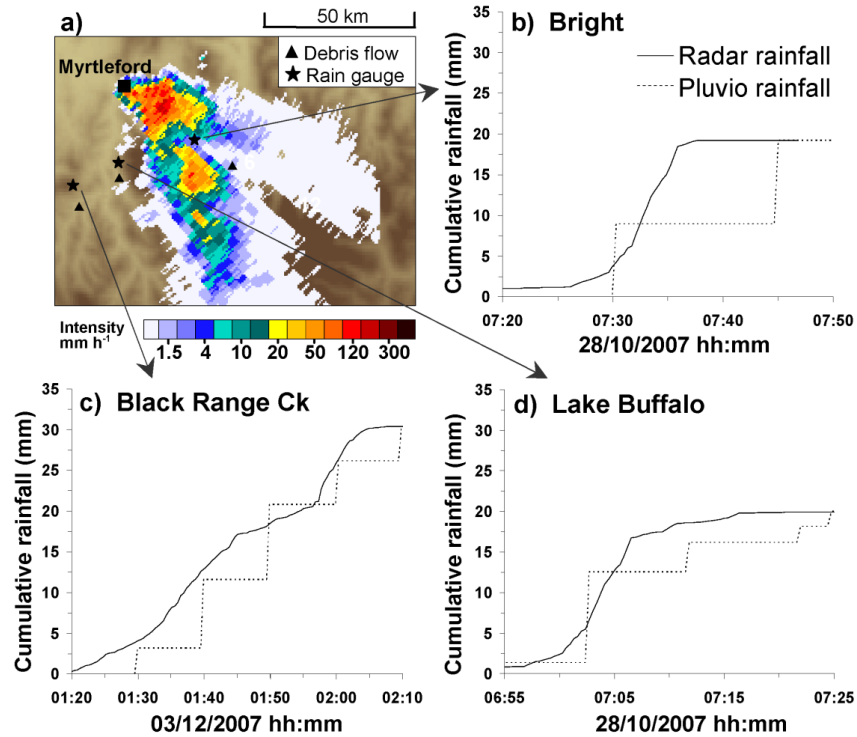


Figure 2.11 a) Radar image from a debris flow generating storm cell, and the radar derived cumulative rainfall for b) Bright, c) Black Range Ck and d) Lake Buffalo where rainfall was known from tipping-bucket rain gauges.

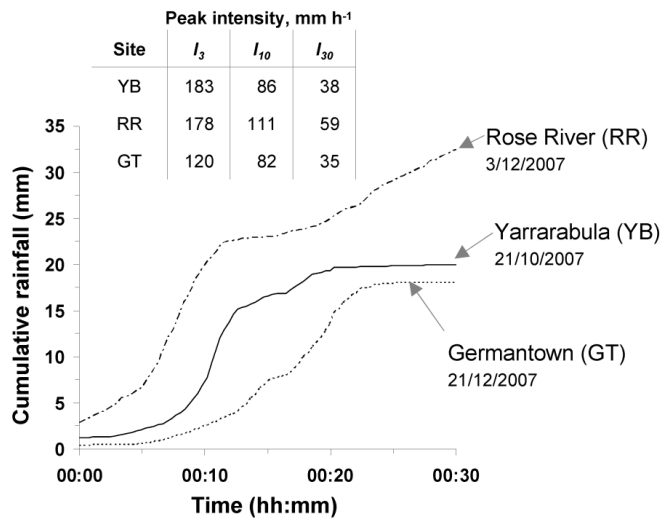


Figure 2.12 Radar derived cumulative rainfall for debris flow events in northeast Victoria. The radar derived rainfall accumulation was adjusted by the rainfall totals from rain gauge measurements at each site.

2.4.4 Soil hydraulic properties

Some trends can be seen in the vertical distribution of water repellency (Figure 2.13). At all burnt sites there was little or no water repellency at the soil surface. Water repellency appeared to be concentrated at soil depths between 2 and 5 cm. The soil at Yarrarabula stands out with a strongly water repellent soil at depths greater than 2-5 cm. The unburnt soil has a larger proportion of soil that is moderately repellent. The high levels of water repellency mean that the soil infiltration measurements reflect the field saturated conductivity (K_{fs}) rather than true saturated hydraulic conductivity of the soil. While sample size of K_{fs} was small and insufficient for parameterisation, the results show some consistent patterns in relation to the flow potential within the top 5 cm of the soil. In theory, the vertical infiltration potential of the soil is restricted by the layer at which K_{fs} is the lowest. The soil layer with lowest K_{fs} acts as a throttle for infiltration and this minimum is therefore representative of the actual K_{fs} of the hillslope. At Yarrarabula, Rose River and Germantown the minimum K_{fs} was 28 mm h^{-1} , 36 mm h^{-1} and 31 mm h^{-1} , respectively (Figure 2.13). At the unburnt site near Germantown the lowest K_{fs} was 43 mm h^{-1} .

For all sites the lowest K_{fs} was measured at the surface except for Yarrarabula where stronger water repellency at depth resulted in the lowest K_{fs} at a depth of 2-5 cm. The high K_{fs} for surface soils at Yarrarabula was a surprising result given that the K_{fs} should have been restricted by low flow potential within the soil profile. Lateral flow within the wettable surface material could have influenced the measurement because rocks and large gravel embedded within the soil profile at Yarrarabula made it difficult to insert the retention ring to a sufficient depth without disturbing the soil. It is noticeable that Germantown has very high K_{fs} for non-repellent subsurface soils (239 mm h^{-1}). While the mean K_{fs} at the burnt site at Germantown did not differ significantly from the unburnt site ($p > 0.05$), the lower levels of water repellency at the unburnt site seems to have resulted in higher maximum K_{fs} values and a more skewed distribution within the repellent and flow-restricting soil layer. The measurements were only conducted at few sample sites at one point in time and therefore did not allow detection of fire-induced changes to temporal trends and spatial variability in water repellency and hydraulic conductivity.

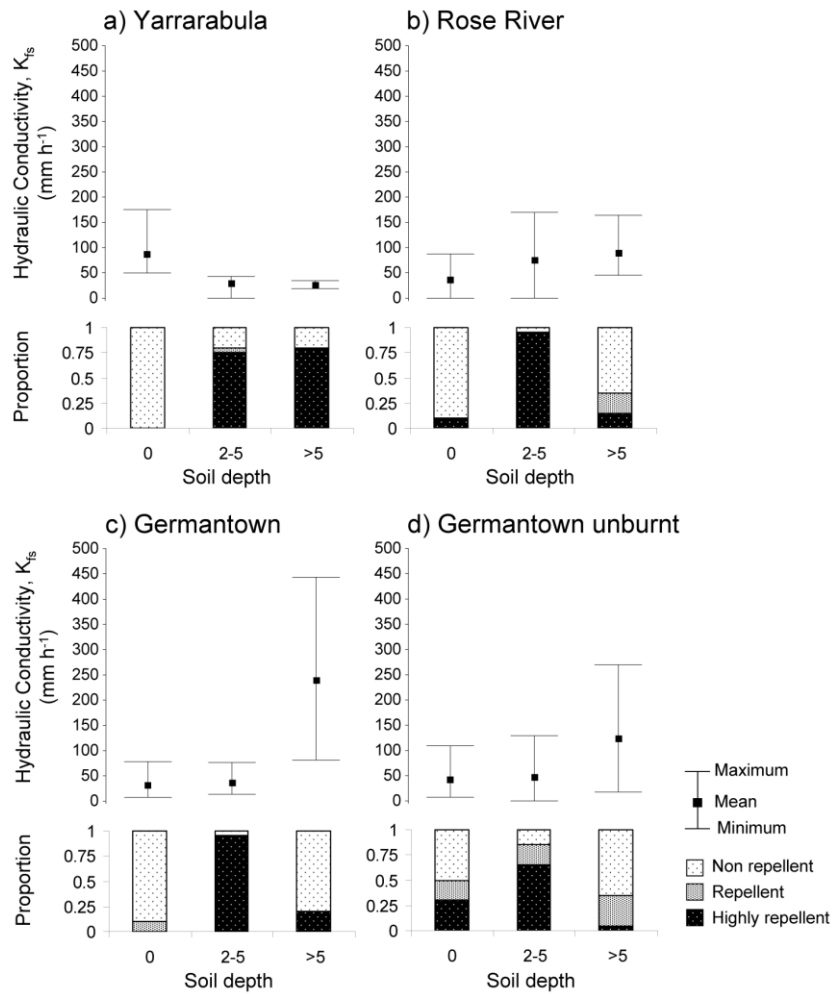


Figure 2.13 Field-saturated hydraulic conductivity (K_{fs}) ($n = 5$) and water repellency measurements ($n = 20$) at three depths from a 20 m x 20 m plot in three debris flow sites. Additional measurements were obtained for an unburnt site nearby (9 km) and comparable in aspect, rainfall and forest type to Germantown.

2.5 Discussion

2.5.1 Post-fire debris flows in Victoria, south-east Australia

At least 13 debris flows occurred in response to high intensity and short duration rainfall events in different geographic settings and on both metamorphic and sedimentary geologies after recent (2003-2009) wildfires in Victoria, south-east Australia. These debris flows were initiated from hillslope runoff and progressive sediment entrainment (Meyer and

Wells 1997) and/or thin hillslope failures (Wells 1987) and display similar characteristics to runoff generated debris flows reported from the western USA and Canada after wildfire (Cannon *et al.* 2001a; Gabet and Bookter 2008; Meyer *et al.* 2001; VanDine *et al.* 2005; Wohl and Pearthree 1991). Levees and matrix supported coarse deposits indicate that the flow attained debris flow characteristics prior to initiating channel scour in previously un-channelized portions of the upper drainage network. Most rills were shallow (<5cm) and formed between patches of un-eroded ash and burned top soil, and only in convergent zones did the rills penetrate into the consolidated B-horizon. All the events occurred on northerly aspects (270°– 90°), on shallow and poorly developed soils in response to surface runoff from short intense rainfall events, primarily in first and second order catchments with slopes > 25° in at least 30 % of the catchment . All runoff generated debris flows occurred in dry eucalypt forests that were burnt by wildfire at high or very high severity with >75 % of crowns burned.

While both sedimentary and metamorphic geologies were susceptible to runoff generated debris flows, the fluvial sand deposits and apparent flash-flood type response in the granitic catchments at Yarrarabula shows that geological factors influence landscape susceptibility. Similarly, in a field survey of the debris flows in Upper Tambo, Victoria, Harman and Stewardson (2007) found that sub-catchments with granitic geologies were less likely to produce post-fire debris flows than the catchment underlain by sedimentary and volcanic rocks. Granitic catchments are more resistant to weathering and erosion, and on the foothills of Mt Buffalo the catchments are larger in size than adjacent sedimentary catchments and display a different morphology with steep cliffs and large sections of exposed and un-vegetated granite in the upper sections of drainage area. The different response in sedimentary and granitic geologies maybe linked to lower sediment availability in the more resistant granitic geology and the different sediment source properties with sedimentary catchments being more clay and silt dominated than the sand and gravel dominated granitic catchments. In turn, these would result in a lower sediment to water ratio and a lower proportion of fine material, both of which could be important precursors to progressively bulked debris flows (Gabet and Sternberg 2008). These findings are similar to the processes observed in the Green River Canyon of Utah where Larsen et al.

(2006) found that weathering limited systems were less susceptible to fire related debris flows than the transport limited systems on soil mantled hillslopes. Several debris flows have occurred on the granitic slopes and cliffs of Mt Buffalo in the past century but these were not necessarily fire-related and all known events were associated with mass failure from exceptional rainfall events (return interval, $RI > 50$ yrs) (Ritchie 2009; Rutherford *et al.* 1994).

The surveyed debris flows in north east Victoria were triggered by intense and localised rainfall from south-easterly moving storm cells which were associated with regional frontal systems. The rainfall intensity and duration for debris flow triggering rainfall events was successfully extracted from 10-min radar images. The annual exceedance probability (AEP) of the debris flow generating rainfall events ($35 < I_{30} < 59$) ranged from 0.2 to 0.4 (2-5yr return interval). However, the AEP is only a point measurement, and the overall probability of a rainfall event occurring within a debris flow susceptible catchment is a function of the area of susceptible landscape, the AEP, as well as the scale of spatial correlation in rainfall intensities. For instance, an intense storm cell with an AEP of 20 % which on average covers an area of 100 km^2 , has a probability of 90 % of occurring at least once somewhere within a debris flow susceptible area of 1000 km^2 . The lowest debris flow triggering rainfall event which was recorded at Germantown ($I_{30} = 35 \text{ mm h}^{-1}$ & $I_{10} = 82 \text{ mm h}^{-1}$) corresponds to an AEP for I_{30} and I_{10} of 50 % (2yr ARI) and 20 % (5yr ARI), respectively. This rainfall event is similar to the debris flow threshold reported from New Mexico ($I_{30} = 30 \text{ mm h}^{-1}$, AEP = 50 %) (Cannon *et al.* 2001a), but higher than the reported rainfall events ($12 \text{ mm h}^{-1} < I_{15} < 30 \text{ mm h}^{-1}$) in southern California (Wells 1987) and the thresholds derived for post-fire debris flows and floods in Colorado ($I_{30} = 10.6$ & 15.5 mm h^{-1}) California ($I_{30} = 16.5 \text{ mm h}^{-1}$) (AEP = 50 -100 %) (Cannon *et al.* 2008). In terms of the various rainfall regimes identified for regions in western US (Moody and Martin 2009a), the rainfall measured in northeast Victoria falls in the upper end of intensity spectrum along with Arizona where the 2 year I_{30} ranged from $\sim 35 - 58 \text{ mm h}^{-1}$.

All the recorded debris flows occurred within twelve months of wildfires suggesting that susceptibility is closely linked to fire and diminishes quickly during recovery of the

catchments. Reduced debris flow susceptibility with time since fire may be linked to the depletion of fine sediments (Meyer and Wells 1997; Reneau *et al.* 2007) and reduced runoff rates and peak flows due to combined effects of increased infiltration capacity of recovering hillslopes and the increased hydraulic roughness from regrowing vegetation (Brown 1972; Moody and Martin 2001a). Unburnt conditions would require much larger rainfall events to trigger the same runoff response and even then, the response would be likely to produce flash floods rather than debris flows given the intact soil and lack of available material. According to a retired district officer for the former Forest Commission, ‘gravel flows’ in north-east Victoria had previously been observed in association with wildfires in 1939 or more recent post-logging slash burns, but never in the absence of fire (Ritchie 2009). Deposits from previous debris flows were observed in catchments in West Gippsland near Mt Tamboritha, and photographs from local residents confirmed that these occurred in catchments burnt at high severity during the Caledonia wildfire in 1998 when up to 25 mm of rain fell in 30 minutes immediately following the fire. Old debris flow deposits were also observed at Myrtle Ck, northeast Victoria, and charcoal fragments within levees indicated that this past event may also have been linked to fire. With fire seemingly a key control on the occurrence of these events in both Victoria and western USA, the resemblance in the observed processes must be due to the similar properties of burned catchments which typically display i) reduced resistance to erosion and increased sediment/ash availability (Cannon *et al.* 2001a; Gabet 2003), ii) increased runoff rates (Cannon *et al.* 2001b; Meyer *et al.* 2001) and iii) enhanced sediment transport capacity of ash slurries (Gabet and Sternberg 2008).

Water repellency has been identified as an important fire related property of soils in debris flow susceptible catchments in the western USA (VanDine *et al.* 2005; Wells 1987). Water repellency reduces the infiltration capacity of the soil (Doerr *et al.* 2006) and the presence of wettable and unconsolidated material overlaying an otherwise water repellent soil is a precondition for thin hillslope failures to occur (Gabet 2003). Soils in dry eucalypt forests in south-east Australia, however, display strong background levels of water repellency in the absence of fire (Burch *et al.* 1989; Crockford *et al.* 1991; Doerr *et al.* 2004). While the study did not include enough sampling locations to detect significant differences between

burn and unburnt soil in terms of water repellency and hydraulic conductivity, the results show that hydraulic conductivity in both burnt and unburnt soils was limited by water repellency at soil depths of 2-5 cm. The data also indicate that water repellency is less widespread at the soil surface after fire. This might be linked to the addition of wettable ash to the hillslopes (Leitch *et al.* 1984; Woods and Balfour 2008) and reduced water repellency at the soil surface due to high burn temperatures (Doerr *et al.* 2004), both of which result in a layer of wettable soil which could be important in providing the material required to generate debris flow slurries. The range of hydraulic conductivity K_{fs} values measured in dry eucalypt forest are low ($28 \text{ mm h}^{-1} < K_{fs} < 31 \text{ mm h}^{-1}$) compared to wet eucalypt forest where the K_{fs} immediately following fire was $> 100 \text{ mm h}^{-1}$ (Nyman *et al.* 2010).

The study detected no runoff generated debris flows following wildfire in the wet forests of the region, and no debris flow occurred in severely burned wet forests at East Kiewa (Table 2.4, # 12) despite the intense rainfall event ($I_{30} = 47 \text{ mm h}^{-1}$) that exceeded the apparent rainfall thresholds for debris flow initiation in the dry eucalypt forest. The study therefore indicates that runoff generated debris flow events are probably less likely to occur in wet eucalypt forest than dry eucalypt forests. A large volume of surface runoff is an important precursor for debris flow generation (Cannon *et al.* 2001b; Wondzell and King 2003). At East Kiewa, there was little evidence of widespread overland flow following the event and it is likely that most of the runoff and sediment was generated from within meters of the drainage lines even during intense rainfall events (Sheridan *et al.* 2007a). The highly structured and loamy soils in wet forest result in high saturated hydraulic conductivity ($> 100 \text{ mm h}^{-1}$) and transient surface runoff on hillslopes even if water repellency is widespread (Nyman *et al.* 2010; Sheridan *et al.* 2007a). The difference in soil structure between forest types is evident from the measured bulk density of surface soils (0-10 cm) at East Kiewa and other wet forest in Victoria ($0.6 - 0.8 \text{ g cm}^{-3}$) (Lane *et al.* 2006b) which contrast with the 1.3 g cm^{-3} measured for six dry forest sites in this study. Furthermore, the rapid vegetation recovery of wet forests results in a shorter duration over which the catchment is susceptible to surface runoff and hillslope erosion (Lane *et al.* 2006b; Sheridan *et al.* 2007a). Both the high infiltration capacity and rapid vegetation recovery

would act to promote high effective infiltration rates at the hillslope scale and result in low connectivity between overland flow on hillslopes and the drainage networks even during intense rainfall events.

One debris flow occurred in wet eucalypt forest following a slip in a convergent headwater basin (Table 2.4, # 8). This debris flow represents an isolated case that occurred in response to an exceptional rainfall event and therefore the role of the fire in generating this event remains unclear. However, mass failure generated debris flows were also visible in aerial photographs from 1941 of catchments in wet forests near Graceburn Ck which were burnt by wildfires in 1939 (Cecil 1981). Landslides and slips have previously been linked to wildfire through tree mortality and subsequent reduction in root strength (Meyer *et al.* 2001; Wondzell and King 2003). Alpine Ash and Mountain Ash forest which dominate wet forest environments are serotinous, so the trees are killed by intense wildfire and the forest regenerates from seeds. While there was extensive tree mortality of Alpine Ash at the mass failure site in Aberfeldy, it is unlikely that this mechanism was instrumental in triggering this debris flow, given that the event occurred less than one year following the fire and not allowing for the effect of declining root strength to set in. It can also be speculated that the fire can prompt slope-failure through short term reduction in evapotranspiration (Lane *et al.* 2010), leading to increased levels of saturation and higher pore pressures in slopes with convergent topography.

2.5.2 Sediment sources and entrainment rates

The volume of available material in channels would depend on i) the timing of last channel evacuation or ii) channel accumulation rates which could differ depending on catchment morphology and long term erosion processes. For three debris flows in north east Victoria the volume of eroded and mobilized material from channels ranged from $800 \text{ m}^3 \pm 190 \text{ SE}$ (Yarrarabula, 0.12 km^2) to $1950 \text{ m}^3 \pm 630 \text{ SE}$ (Rose River, 0.33 km^2). In comparison, the average volume scoured from channels in 45 debris flows across Utah, Colorado and California was estimated at $6\,274 \text{ m}^3$ and ranged from 170 m^3 to $59\,000 \text{ m}^3$ for catchments between 0.01 km^2 and 27.9 km^2 (Gartner *et al.* 2008; Santi *et al.* 2008). The study shows that sediment entrainment rate along the length of the scoured drainage line peaks at the

point of maximum rate of decrease in channel slope where large volumes of available material had accumulated. This accumulation zone occurred in a concave portion of the channel where the potential stream power and shear stress decrease rapidly downstream, and could represent a threshold where channel deposition exceeds channel erosion for average runoff events in these small systems (channel length < 500 m) which are dominated by surface hydrology. This process of longer term sediment accumulation and periodic evacuation by debris flow is something which could be modelled using a combination geomorphic response models and stochastic forcing by rainfall and fire. For downstream channel reaches, the larger catchment scales result in increased runoff from surface and subsurface processes which means that the channel is exposed more frequently to larger flow events, hence limiting the accumulation of channel material. When averaging across the length of all channels contributing to the measured debris flows in northeast Victoria, the entrainment rate ranged from $0.55 \text{ m}^3 \text{ m}^{-1}$ (Germantown) to $1.36 \text{ m}^3 \text{ m}^{-1}$ (Rose River) and falls within the lower end of distribution of entrainment rates (range: $0.3 \text{ m}^3 \text{ m}^{-1}$ - $9.93 \text{ m}^3 \text{ m}^{-1}$, median: $1.86 \text{ m}^3 \text{ m}^{-1}$, mean: $2.47 \text{ m}^3 \text{ m}^{-1}$) reported by Santi et al. (2008). Given that that channels were eroded to bedrock at all sites, the large difference in channel entrainments rates between Germantown and Rose River could be due to i) differences in available channel material and/or ii) widening of the channel at Rose River during a smaller debris flow which occurred three weeks after the major event on 3rd December.

The depth of hillslope erosion averaged across the catchments range from $3.2 \text{ mm} \pm 0.8 \text{ SE}$ at Rose River to $12.6 \text{ mm} \pm 2.3 \text{ SE}$ at Yarrarabula and falls within range of values summarized for yearly erosion rates in burned sites elsewhere (Moody and Martin 2001a). This means that hillslopes represent an important sediment source of debris with 25 % to 65 % of sediment entrainment occurring on hillslopes. Hillslopes in the upper- and mid-section of the catchments were mostly convex so little or no deposition was observed at the base of hillslopes prior to the confluence with the channel network. Furthermore, the large volumes of overland flow and the uniform, steep ($50 \% > 25^\circ$) and hydrologically smooth hillslopes resulted in low deposition rates and high sediment delivery rate from hillslope to channels during the event. When standardised by catchment size and assuming 50 % deposition as per (Leitch *et al.* 1984), the magnitude of hillslope erosion at Germantown ($41 \pm 7 \text{ t ha}^{-1}$)

and Rose River ($20 \pm 8 \text{ t ha}^{-1}$) are similar to or higher than the hillslope erosion estimates (22 t ha^{-1}) from a mud torrent after wildfire and a subsequent storm event (total rainfall = 17 mm) in 1983 (Leitch *et al.* 1984). Yarrarabula stands out from the other two sites with a very high hillslope erosion rate despite the relatively small difference between sites in terms of rainfall. Having been burnt in both 2003 (low severity) and again in 2007 (high severity) the hillslopes at Yarrarabula could have had larger volumes of readily available sediment than the other sites. There were no signs of previous debris flows in the catchment and the relatively low severity of the fire in 2003 would have promoted lower erosion rates with most material being retained on the hillslopes. Secondly, the debris flows at Yarrarabula occurred adjacent to a large granitic intrusion, which resulted in a metamorphic geology which is different to the regional Ordovician sedimentary rocks which underlie the catchments at Rose River and Germantown.

2.5.3 Hazards from post-fire debris flows

Debris flows play an important role in the delivery of large volumes of material to mountain streams and rivers where sediment transport is usually supply limited (Benda and Dunne 1997; Istanbuluoglu *et al.* 2004; Rutherford *et al.* 1994). In a review of impacts on water quality resulting from recent wildfires in south-east Australia, it is evident that the debris flows provide an injection of fine sediment, nutrients and other contaminants that may be transferred large distances downstream in subsequent flow events (Smith *et al.* 2011c). The increased sediment availability can result in high turbidity and high nutrient levels which are detrimental to aquatic ecosystems and problematic in the supply of clean drinking water to several regional townships (Lyon and O'Connor 2008; Smith *et al.* 2011c). Fish kills were reported in rivers downstream of debris flow affected catchments in northeast Victoria and East Gippsland (Department of Primary Industries 2009; Lyon and O'Connor 2008). Following debris flows in the Upper Goulburn in central Victoria, the communities along the river were unable to divert river water for domestic purposes and the area suffered reduced tourism as a result of the poor condition of the river (Tennant and Turner 2009).

In addition to water quality impacts, recent events also highlight the role of debris flows as a direct risk to human life and infrastructure. A debris flow at Dingo Ck in northeast Victoria resulted in loss of life with the death of a fire fighter who was caught by the event when trying to cross a riverbed as part of a post fire reconnaissance (Berry and Bradley 2003). While this particular event was the result of extremely unfortunate circumstances, the tragedy helps emphasize how rapid and destructive these events can be and the need for accurate information to inform forest workers, landowners and recreational visitors of the potential risk. There are several instances where roads and private property have been severely damaged through the direct impact from debris flows. The cost associated with the damage is difficult to obtain but again, the events support the need for more research which will allow land managers and engineers to account for these high-magnitude events in the planning and design of new infrastructure projects.

2.6 Conclusion

A complex mosaic of geological units and different climates across the south-east Australian region result in a landscape with a wide range of landforms, soils, and vegetation communities which has important implications for the susceptibility of the landscape to high magnitude post-fire erosion events. In this paper we have shown that high magnitude erosion events with impacts on water quality and other assets in the eastern Victorian uplands usually occur as runoff-generated debris flows which display processes that are similar to what has been reported from research in burnt systems in western US. As a post-fire hydrological hazard and as a geomorphic process within first to third order drainage systems, debris flows represent an important erosion response to wildfire in the Victorian uplands and probably in other regions within SE Australia such as the Snowy Mountains (Brown 1972) and the mountains in Namadgi National Park near Canberra (White *et al.* 2006). While the events occur at relatively small temporal scales (minutes) and small spatial scales ($< 20 \text{ km}^2$), the impacts on aquatic systems have been detected well beyond the scale at which the debris flow processes typically operate (Lyon and O'Connor 2008).

The occurrence and distribution of debris flows across the landscape is a function of the spatial extent of debris flow susceptible catchments in relation to the spatial distribution of

rainfall events that exceed a rainfall threshold during the post-fire period of susceptibility. In Victoria, all runoff generated debris flows occurred in dry eucalypt forests as opposed to wet eucalypt forests where high infiltration rates result in low surface runoff response, even after fire. The study indicates that the more resistant granitic geologies are less likely to generate debris flows, probably due to low sediment availability on exposed granitic hillslopes. The large spatial extent of dry eucalypt forests in Victoria, the high susceptibility to wildfire of these ecosystems and the seemingly low rainfall thresholds for debris flow initiation, suggest that debris are a regular erosion process after fire. The likelihood of future events is high, especially given the current climate change projections for south-east Australia which indicate that the region is moving towards increased risk of fire due to warmer and drier conditions during an increasing proportion of the year (Hennessy *et al.* 2005; Pitman *et al.* 2007) and higher frequency of convective storms and extreme rainfall events (Alexander *et al.* 2007; Nicholls 1995; Whetton *et al.* 1993).

The study provides an important foundation on which to pursue further research relating to landscape responses to wildfire in the south-east Australian region. Future studies should aim to i) develop erosion models which include key processes and landscape controls in the context of climate change and forest management, ii) quantify and develop predictive models relating to the frequency and magnitude of post-fire debris flow events, and iii) establish the role of fire related erosion events as a geomorphic agent in these systems over time. From a practical perspective the work will allow i) much better prediction of post-fire water quality risk, ii) much better understanding of the role of fire as a geomorphic agent in the south-east Australian landscape and iii) more insight into the links between forest ecosystem and resilience to the impacts of fire on erosion.

Chapter 3: Modelling hillslope and channel erosion during post-fire debris flows

Abstract

Post-fire debris flows are extreme erosion events and can dominate the long term supply of sediment from headwaters to streams in upland catchments and they represent a hazard to infrastructure, lives and water quality. Predicting the location, frequency and magnitude of debris flows is therefore important for i) understanding sediment dynamics in upland catchments and ii) as a basis on which to manage hydro-geomorphic risk in burnt areas. The infrequent and destructive nature of debris flows however means that field monitoring and catchment instrumentation are often ineffective at capturing processes and event magnitudes. In this study we use field surveys of 10 post-fire debris flow events in southeast Australia with aims to i) identify rainfall conditions underlying the debris flow response and to ii) quantify erosion and deposition rates in order to estimate the delivery of sediment and water quality constituents to receiving waterways. Rainfall conditions that triggered debris flows had an annual exceedance probability ranging from 0.1 to 0.6 and 30-minute intensities, I_{30} , ranging from 17-60 mm h⁻¹. The magnitude of debris flows (100-200 t ha⁻¹) is similar to that which has been reported for the same type of events in the western US and Spain. In terms of eroded volume, there was on average an equal contribution from hillslopes and channels to debris flows. When evaluating the potential impacts on water quality however the hillslopes had much higher concentration of constituents such as fines clay and silt, plant available phosphorous and total carbon. The erosion data was used to parameterise equations for hillslope erosion, channel initiation and sediment transport in channels during debris flow events. The equations represent erosion rates as function of contributing area (A), local slope (S), rainfall intensity (I) and fire sensitive properties such as infiltration capacity and sediment availability. The modelling approach provided an integrated approach for representing debris flow initiation and magnitude and allowed for explicit representation of key hillslope properties which are affected by fire. The equations were used effectively to predict the initiation and magnitude of debris flow at two sites which were used as independent tests of model performance.

3.1 Introduction

Runoff generated debris flows after fire can be an important process by which sediment and debris is eroded and transported from hillslopes and headwaters to streams and valley bottoms in wildfire-prone landscapes (Cannon *et al.* 2003; Gabet and Bookter 2008; García-Ruiz *et al.* 2012; Kean *et al.* 2011; Meyer *et al.* 2001; Nyman *et al.* 2011; Wohl and Pearthree 1991; Wondzell and King 2003). In landscapes where wildfire acts as an important control on runoff and sediment supply, it is the extreme erosion events that result from the intersection of burnt headwaters and storms which can drive the long term erosion rates in headwater systems (Istanbulluoglu *et al.* 2004; Pierce *et al.* 2004; Smith *et al.* 2012). While the debris flow processes generally operate at relatively small spatial and temporal scales (< 10 km² and minutes) they are important for long term sediment and ecosystem dynamics at larger scales (Benda *et al.* 2003; Miller *et al.* 2003a; Rutherford *et al.* 1994; Smith *et al.* 2011c).

The physical processes contributing to the initiation and propagation of runoff generated debris flows are difficult to model (e.g. Welcker 2011). The initiation process includes a combination of i) runoff generation (Cannon *et al.* 2001a; Kean *et al.* 2011), ii) hillslope erosion (Cannon *et al.* 2001a), iii) thin hillslope failures (Gabet 2003), iv) channel incision in converging zero-order headwaters (Cannon *et al.* 2001b; Gabet and Bookter 2008) and v) subsequent debris flow propagation within the channel (Kean *et al.* 2011). The propagation and persistence of debris flow processes in downstream channels is a function of local slope, channel configuration as well as changes in flow rheology due to runoff accumulation, sediment entrainment and deposition within channels (Cannon *et al.* 2003; Iverson 1997). The processes controlling debris flow dynamics within channels have been modelled using physical principles (Iverson 1997; O'Brien *et al.* 1993) although there are few cases where these modelling approaches have been applied specifically to post-fire debris flows (Elliott *et al.* 2004).

Wildfire contributes to runoff generated (or progressively bulked) debris flows by reducing infiltration and increasing sediment availability (Cannon *et al.* 2001a; Gabet and Sternberg 2008; Wells 1987). The threshold for initiation of post-fire runoff-generated debris flows is

essentially a function of runoff and sediment generation from contributing hillslopes (Cannon *et al.* 2001b; Gabet and Bookter 2008; Wohl and Pearthree 1991). The subsequent magnitude of erosion by debris flows is a function of the sediment availability and transport capacity in channels and on hillslopes which contribute to the debris flow process (Cannon 2001; Gabet 2003; Gartner *et al.* 2008; Santi *et al.* 2008). Statistical models of initiation and magnitude of debris flows are typically used to predict the event based-hazard associated with debris flows from recently burnt basins (Cannon *et al.* 2010; Gartner *et al.* 2008; Pak and Lee 2008). These statistical models were developed in the context of hazard at the catchment outlet, and therefore rely on arbitrarily defined catchment boundaries. The transition from debris flow processes to flood require separate models that represent the downstream reduction in debris flow potential (Miller and Burnett 2008; Prochaska *et al.* 2008). Over time, the delivery to stream channels from debris flows has been modelled using stochastic models which focus more on capturing the episodic nature of events in headwater systems and less on variability in event magnitude (Benda and Dunne 1997). Istanbulluoglu *et al.* (2004) developed a numerical modelling approach which represents both magnitude and frequency of events in forested systems prone to wildfire disturbance.

In this study we develop a model of debris flow magnitude which is coupled with the factors that determine the hydrological thresholds for debris flow initiation. The aim was to provide a modelling approach which represents topographic controls as well as properties which are affected by fires. Both hillslopes and channels contribute to sediment during runoff generated debris flows. These sediment sources display different properties in terms of particles size distribution and nutrient content and should therefore be treated explicitly as separate inputs to downstream channels environments. The study was designed with three main objectives:

1. Use field surveys of a sampled of post-fire debris flows to quantify magnitude of erosion, the properties of source material and the triggering storm conditions.
2. Parameterise geomorphic transport equations as predictive models of hillslope erosion, channel erosion and deposition.
3. Use the equation to independently predict the debris flow initiation and magnitude of debris flows

3.2 Methods

3.2.1 Regional context and site characteristics

Debris flow surveys were carried out in 10 catchments at 7 sites in the eastern uplands of Victoria, southeast Australia (Figure 3.1). The geomorphology of the region is described in Jenkins (1991) and the overall setting in terms of post-fire erosion processes is provided in Chapter 2, section 2.2 (or see Nyman *et al.* 2011). The sites were selected because of access to the debris flow catchments and availability of rainfall data from nearby rain gauges.

Hillslope and channel erosion measurements at Rose River, Yarrarabula and Germantown (data presented in Chapter 2) were made in two replicate catchments whereas measurements at Target Creek, Mt Tamboritha, Myrtle Creek and Sunday Creek were made in a single catchment. Catchments were defined above the upstream end of the main fan.

All debris flows terminated at the intersection with higher order streams apart from a debris fan at Yarrarabula 1 and Germantown 2 which deposited within the catchments, above the small flood plains that bordered the main creeks. Catchment properties are summarised in Table 3.1.

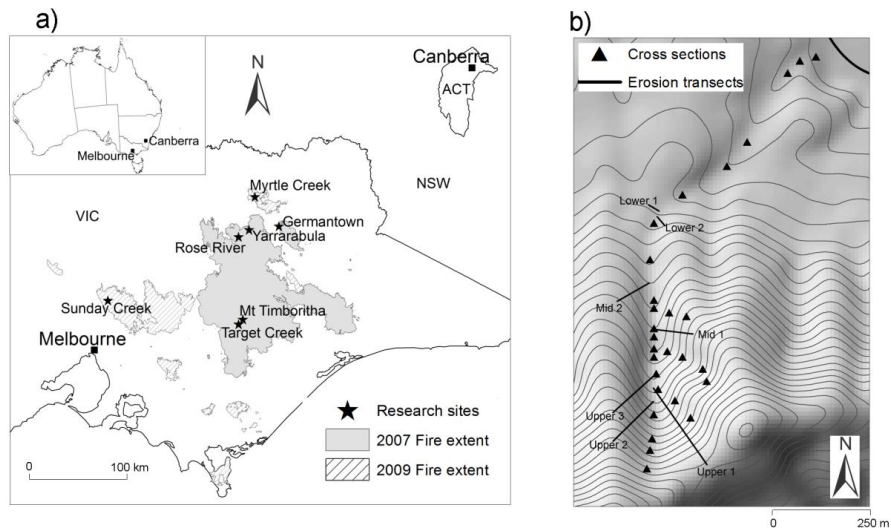


Figure 3.1 a) Location of 7 debris flow research sites in southeast Australia and b) outline of a catchment that was surveyed at Rose River showing the location of channel cross-sections and hillslope transects.

Table 3.1 Debris flow research sites in eastern uplands of Victoria, southeast Australia.

Site	Size ^a km ²	Relief ^b m	Burn severity % > 2	Bulk density (0-10 cm) kg m ⁻³	Particle size (hillslope) (0 - 2 cm depth)				Rock content (D > 30 mm)	
					gravel (2-30 mm) %	sand (< 2 mm) %	silt (< 0.075 mm) %	clay (< 0.0075 mm) %	Hillslope %	Channel %
Rose River 1 ^c	0.33	260	89 % ≥ 2	1.18	48	15	21	16	4	43
Rose River 2	0.72	237	86 % ≥ 2	1.24	34	35	21	10	6	41
Germantown 1 ^c	0.65	310	71 % ≥ 2	1.21	33	34	23	10	4	42
Germantown 2	0.36	302	66 % ≥ 2	1.27	34	29	27	11	7	36
Yarrarabula 1	1.00	421	84 % ≥ 2	1.41	52	23	17	9	15	50
Yarrarabula 2 ^c	0.12	217	87 % ≥ 2	1.24	31	33	25	10	28	53
Target Creek	1.20	322	100 % ≥ 2	1.28	54	18	18	10	23	41
Mt Tamboritha	2.20	613	100 % ≥ 2							
Myrtle Creek	0.23	209	100 % ≥ 2							
Sunday Creek	0.08	76	100 % ≥ 2							

^a Values represent the area above the fan

^b Relief calculated as the height from channel initiation point to the start of terminal deposit

^c Catchments used in analysis of hillslope and channel erosion in Chapter 2.

3.2.2 Rainfall

Rainfall intensity was measured using a combination of rain gauge measurements and radar data from Australian Bureau of Meteorology (The method is described briefly here, however, see Chapter 2, section 2.3.3 or Nyman *et al.* (2011) for more details on method). The sequence of intensity above each debris flow catchment was extracted from a sequence of 10 min radar images covering the debris-flow initiating storms cells. The continuous intensity at debris flow locations was obtained by first estimating the direction and tracking velocity of storm cells, then extracting the radar-derived intensity values for a transect of pixels (0.5 x 0.5 km) within each 10 min data frame covering the duration of the rainfall event. The length and the orientation of the vector were determined by the velocity and direction in which the storm was travelling which was measured by manually tracking the position of at least three separate storm cells during a 30-60 min sequence of radar images. The rainfall intensity in radar images was extracted for a vector of pixels and represented along with time (minutes), where min/pixel = total pixels/10. The product of intensity and time intervals was then used to calculate a cumulative rainfall distribution. This distribution

was finally calibrated with the known ground-based total rainfall. This approach was found to yield realistic intensity measured at < 30 min timescales (Nyman *et al.* 2011). This extrapolation procedure was required because the duration of high intensity rainfall was short relative to the 10 minute temporal resolution of the radar data. This means that characterising the rainfall for single pixel above the site at for each 10 min image would often result the actual storm cells not being captured.

3.2.3 Channel Erosion

Channel erosion was measured in cross sections (m^2) along all channels above the terminal debris flow fan. On average 30 cross-sections were measured per catchment at an average interval of 55 m. The cross sections were measured at shorter intervals in regions of large absolute variability in channel erosion. In depositional areas, the cross sections were made at higher intervals because of large variability in the width of channel deposit. The locations of each cross section and the initiation points were measured at < 10 m accuracy using differential GPS. Initiation points were defined as the location along the drainage line where the maximum depth of scour first exceeded 0.2 m and where depositional features along the channel banks were consistent with the debris flow type. A scour depth of 0.2 m was considered an appropriate cut-off point because it represented a point from which the channel scour increased progressively in magnitude as opposed to the discontinuous nature of shallower rills. The cross sectional area of erosion at each survey point was calculated by assuming that the pre-existing channel could be extrapolated from the side slopes leading into the channels. This method is consistent with previous studies that quantify post-fire debris flow volumes (Gartner *et al.* 2008; Nyman *et al.* 2011; Santi *et al.* 2008). The side slopes were also used to estimate the cross sectional area of deposits. While consistent with other studies, this makes for a large error. This error can be quantified when the exact channel form prior to the debris flow event is known. In our study we did not have this information so the actual magnitude of the error is unknown. The proportion of clasts > 30 mm within the eroded and exposed channel banks was recorded as a proportion at each cross section.

3.2.4 Hillslope Erosion

Hillslope erosion was measured from surface lowering using pedestals, scour around embedded rocks and intact sections of soil/ash. These indicators were used to extrapolate the pre-existing surface height (for more detailed description see Chapter 2, section 2.3.2 or Nyman *et al.* (2011)). The measurements were made in 1 m x 1 m quadrats along transects from channel to ridge top (perpendicular to the contours). The location of transects were stratified according to lower, mid and upper hillslope regions with a total of 2-4 transects for each catchment region. The proportion of eroded and non-eroded surfaces was recorded for each transect alongside the measures of erosion depth within eroded sections. An estimate of the mean erosion depth within the eroded section of the quadrat was based on three to six separate measures of ground surface change. The proportion of area covered with rocks > 30 mm in diameter was recorded for each quadrat.

3.2.5 Soil sampling and analysis

Bulk density was sampled in cores (4.7 cm in diameter and 10 cm deep) at 10 locations on hillslopes and in channel banks at each site. The hillslopes cores were extruded so that bulk density could be measured from the dry weight at different depth intervals (0-2, 2-5 and 5-10 cm). A separate and more extensive sampling campaign was carried out on hillslopes and channels in order to measure particle size distribution and nutrient content of debris-flow source material. About 50 g of soil was collected at 10 points distributed along erosion transects in the upper, mid and lower sections of one catchment at Rose River, Germantown and Yarrarabula (10 samples x 5 transects = a total of 50 sample points per site). Surface soil (0-2 cm) was collected from non-eroded section of the hillslopes. Subsurface soil (2-5 cm) was sampled after removing the surface material. Samples from surface and subsurface soil were composited separately, mixed and then sub-sampled into 500 g bags, two for each depth interval. One sub-sample was used for nutrient analyses and the other was used for particle size analysis. Channel material was sampled across the full bank profile that had been exposed by the erosion from the debris flow. The soil was sampled at each channel cross-section, composited into upper and lower channel regions, and then sub-sampled into 500 g soil bags (two from each channel region).

The particle size analysis of channel and hillslope material at all sites was performed on 50 g of soil < 2 mm after ultrasonic dispersion and digestion of organic matter with hydrogen peroxide (Bowman and Hutka 2002). Gravel content (2 mm > D < 30 mm) was estimated from sieving the composite sample (> 2 kg) that remained after sub-sampling for nutrient and particle size analysis. The proportion of large clast ($D > 30$ mm) was measured volumetrically during the erosion survey and converted to mass using bulk density values of sandstone (2220 kg m⁻³). Nutrient analysis was performed on sediment < 2 mm from Rose River, Germantown and Yarrarabula. Total nitrogen (TN) and total carbon (TC) was measured by the Dumas combustion procedure using a Leco CNS 2000 analyser (McGeehan and Naylor 1988). Total phosphorous (TP) measured from nitric perchloric acid digest and plant available phosphorous (Bray-P) was analysed through extraction by dilute acid fluoride (Bray and Kurtz 1945). The method for soil nutrient analysis is described in detail by (Noske *et al.* 2010).

3.3 Results and discussion

3.3.1 Rainfall

The average intensity (I) of debris flow triggering rainfall events ranged from 17 - 60 mm h⁻¹ and 35 – 85 mm h⁻¹ for 30-minute (I_{30}) and 15-minute (I_{15}) rainfall respectively (Figure 3.2). The average annual exceedance probability (AEP) of I_{30} was between 0.6 and 0.3 for 5 out of 7 events. The AEP for I_{30} and I_{15} at Rose River (maximum) and Myrtle Creek (minimum) was 0.1 and 0.6 respectively. A power law equation explained 60 - 99 % of variation in average intensity (I) with duration (t_{hrs}). The total rainfall for debris flow triggering storm events ranged from 16 mm to 34 mm. The range of 15 minute peak intensities (I_{15} : 35-85 mm h⁻¹) were higher than the minimum intensities reported by (Kean *et al.* 2011) for post-fire debris flows in the San Gabriel Mountains, California ($I_{15} = 12$ mm h⁻¹) but lower in some cases than the I_{15} which triggered debris flows in the Santa Ynez site ($I_{15} = 56$ mm h⁻¹). The minimum intensity - duration relation for debris flow triggering rainfall could be represented by the power law relation, $I = 11t_{hrs}^{-0.8}$. This does not represent a threshold, but the value is indicative of the rainfall conditions under which debris flows could be expected to occur. The intensity-duration relation are above the range

of thresholds reported for post-fire debris flow in Colorado and California (Cannon *et al.* 2008) (Figure 3.2).

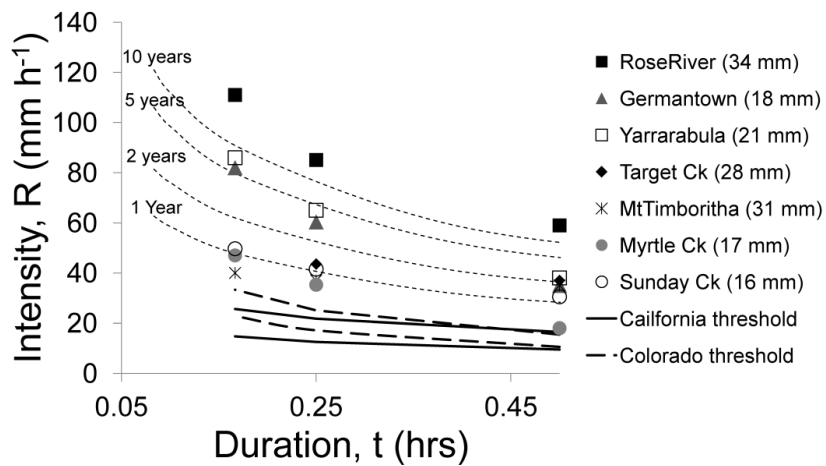


Figure 3.2 The intensity-duration relation for debris flow triggering rainfall after wildfire in south-east Australian Eucalypt forests (storm totals in legend). The intensity-duration relation is shown for storms with return interval of 1-10 year at Myrtleford in northeast Victoria. The values for California and Colorado are obtained from Cannon *et al.* (2008) and show lower and upper thresholds for debris flow initiation in these regions.

3.3.2 Debris flow magnitude

Channel and hillslope contributions were estimated within the lower, mid and upper sections of the catchments (see Chapter 2, Figure 2.1). The mean and standard error (SE) of hillslope erosion was calculated within region by treating each transect as a sample ($n = 2$ to 4 transects per region). Channel erosion was calculated in segments and accumulated within regions. The average cross-sectional area (m^2) (also referred to as channel yield rate (m^3/m) (Santi *et al.* 2008)) was then obtained by dividing the total volume by total channel length for that catchment region. The standard error of the eroded channel volume was measured from the variability in average channel yield rate between all segments within each region. Total channel erosion within each region was calculated from the sum of all eroded channel segments. The erosion depth with the upper-, mid- and lower regions was used to estimate total hillslope erosion by assuming that each region comprised an area which was proportional to the average transect length. The proportional split between

catchment regions was consistent across all sites with the upper-, mid- and lower-catchment regions, respectively, making up $50 \pm 4 \%$, $35 \pm 3 \%$ and $15 \pm 2 \%$ of the total catchment area. Total channel erosion and associated error estimate was obtained by adding the volumetric erosion measurements from all regions.

The bulk density of hillslope soil (0-2 cm) across all sites ($1270 \text{ kg m}^{-3} \pm 33 \text{ SE}$) was on average 12 % lower than bulk density of sediment within channel banks ($1610 \text{ kg m}^{-3} \pm 69 \text{ SE}$). The volumetric contribution from hillslopes to debris flows was therefore adjusted to correspond with bulk density in channels. The bulk density of surface and channel material at all sites was combined into a single measure since there were no significant differences between sites. The uncertainty in bulk density values, size of catchment regions, and the estimated volume within regions was propagated through to the final estimate of debris flow volume. Volume was converted to mass treating soil $< 30 \text{ mm}$ and rocks $> 30 \text{ mm}$ separately. The volume of rocks $> 30 \text{ mm}$ (measured for source material in channels and hillslopes during the erosion survey) was converted to mass using a bulk density of sandstone (2220 kg m^{-3}) (Carmichael 1989). Material $< 30 \text{ mm}$ was converted to mass using the separate bulk density values for channel and hillslope material.

In terms of mass the average debris flow yield, Y , was $195 \text{ t ha}^{-1} \pm 68 \text{ SD}$. In terms of volume the yield was $113 \text{ m}^3 \text{ ha}^{-1} \pm 40 \text{ SD}$. These values are lower than what was reported for post-fire debris flows in the Ibirena Ranges, Spain (García-Ruiz *et al.* 2012) but correspond well with the mass of material produced from debris flows in the Idaho batholith ($140 - 440 \text{ t ha}^{-1}$) (Meyer *et al.* 2001) and the volume the erosion reported for debris flow elsewhere in the intermountain western US (Gartner *et al.* 2008; Santi *et al.* 2008). In terms of volume, $V (\text{m}^3)$, the debris flow magnitude and could be predicted reliably by the empirical post-fire debris flow model that has been calibrated and tested for that region (Gartner *et al.* 2008):

$$\ln(V) = 7.2 + 0.6 \ln(S_{th}) + 0.7B^{0.5} + 0.2R_{tot}^{0.5} \quad 3.1$$

Where S_{th} is the area with slope $> 30\%$ and B is the area with burn severity > 2 , R_{tot} is the total storm rainfall. The coefficient of determination (R^2) of the observed versus predicted volumes was 0.92. On average our study found that there was an equal contribution from hillslopes (52 %) and channels (48 %) but with a relatively wide range of hillslope contributions (26-88 %) across the 12 debris flow events (Figure 3.3 and Table 3.2). The hillslope source dominance is consistent with large post-fire erosion events reported previously from the region (Smith *et al.* 2012; Wasson *et al.* 2003; White *et al.* 2006). After wildfire in Cotter catchments, Australian Capital Territory, 48-100 % of the fine sediment ($< 4 \mu\text{m}$) delivered to the water supply reservoirs was sourced from burnt topsoil (Wasson *et al.* 2003). Similarly in post-fire debris flow deposits hillslopes have been found to contribute somewhere between 22 % and 75 % of fine ($< 10 \mu\text{m}$) sediment (Smith *et al.* 2012).

The hillslope source contribution reported in Table 3.2 assumes negligible hillslope deposition and is therefore an overestimate. Some deposition was observed where flow obstacles such as tree stems or in-situ rocks acted as physical barriers. However, the steep slopes ($> 25^\circ$) and strong coupling between hillslopes and channels in the intensively eroded upper- and mid- sections of the catchment meant that deposition was low. For similar burn forest Leitch *et al.* (1984) found that depositional areas occupied 4 % of the overall hillslope area. In this study, the effect of assuming zero hillslope deposition could be explored by comparing hillslope source contribution at Myrtle Creek and Sunday Creek with values obtained for the same events using radionuclide tracers (Smith *et al.* 2012).

In the present study, the hillslope source contribution of fines ($< 10 \mu\text{m}$) was 80 % and 83 % at Myrtle Creek and Sunday Creek, respectively, which (as expected) is higher compared to range of values obtained in Smith *et al.* (2012) using fallout radionuclide tracers.

Radionuclide tracers indicated that hillslope deposition ranged from 22-69 % and 32-75 % at Myrtle Creek and Sunday Creek, respectively (Smith *et al.* 2012). If the mean of all radionuclide samples in Smith *et al.* (2012) is used as a measure of the minimum hillslope contribution, then hillslopes comprised a minimum of 47% and 51% of debris flow material at Myrtle Creek and Sunday Creek, respectively. These average measures represent a

maximum deposition because the hillslope contribution is underestimated due to the large proportion of debris flow material exported during peak flow when hillslope material contribution is higher (69-75 %) (Smith *et al.* 2012). When coupled with our erosion depth measurements, the results of Smith *et al.* (2012) indicate that no more than 33 % of eroded hillslope material was depositing within the hillslope before reaching the channel.

Table 3.2 Hillslope and channel erosion at debris flow research sites in eastern uplands of Victoria, southeast Australia.

Site	Size km ²	# initiation points	Max stream order	Run-out length ^a (L/ΔZ)	Average hillslope (HS) erosion depth			Average channel (CH) erosion x-section			Deposit volume ^b m ³	Debris flow volume			Mass t ha ⁻¹
					m (*10 ³)			m ²				m ³	m ³ ha ⁻¹	HS prop ^c	
					lower	mid	upper	lower	mid	upper					
Rose River 1	0.33	9	2	4.5	0.7 ± 0.3	1.39 ± 0.8	4.6 ± 1.9	0.73 ± 0.11	1.84 ± 0.57	2.77 ± 0.53	789	3328 ± 835	91 ± 23	0.26	156 ± 30
Rose River 2	0.72	4	3	3.3	0.7 ± 0.3	1.39 ± 0.8	4.6 ± 1.9	1.80 ± 0.36	2.73 ± 0.34	1.73 ± 0.26	671	5714 ± 1096	79 ± 15	0.29	141 ± 19
Germantown 1	0.65	9	3	3.0	2.7 ± 0.5	3.1 ± 0.8	9.2 ± 1.5	1.89 ± 0.37	0.78 ± 0.17	0.79 ± 0.10	975	5160 ± 826	79 ± 13	0.62	133 ± 23
Germantown 2	0.36	3	2	3.8	2.7 ± 0.5	3.1 ± 0.8	9.2 ± 1.5	1.29 ± 0.48	1.20 ± 0.13	0.39 ± 0.19	20	2800 ± 477	78 ± 13	0.68	135 ± 24
Yarrarabula 1	1.0	2	2	2.8	3.6 ± 1.9	9.8 ± 0.5	19.2 ± 4.4	1.4 ± 0.19	0.63 ± 0.30	3.93 ± 0.66	1528	13696 ± 3158	137 ± 32	0.79	229 ± 51
Yarrarabula 2	0.12	4	2	4.1	3.6 ± 1.9	9.8 ± 0.5	19.2 ± 4.4	1.00 ± 0.27	1.18 ± 0.29	0.63 ± 0.12	45	2094 ± 390	174 ± 32	0.62	300 ± 52
Target Creek	1.2	7	3	3.3	2.1 ± 0.3	5.6 ± 1.1	9.6 ± 1.5	3.22 ± 1.02	1.72 ± 0.21	1.07 ± 0.24	750	11968 ± 1616	99 ± 13	0.58	171 ± 21
Mt Tamboritha	2.2	11	3	3.0	4.2 ± 0.9	14.9 ± 2.4	8.9 ± 4.0	8.53 ± 4.03	10.21 ± 1.42	1.47 ± 0.61	1512	38463 ± 8693	177 ± 40	0.47	325 ± 52
Myrtle Creek	0.23	3	2	2.8	6.8 ± 1.1	10.4 ± 1.9	10.9 ± 1.2	0.76 ± 0.19	0.94 ± 0.15	0.39 ± 0.04	386	2267 ± 348	97 ± 15	0.83	181 ± 19
Sunday Creek	0.08	1	1	3.4	5.0 ± 1.9	8.3 ± 2.9	14.0 ± 1.0	0.16 ± 0.04	0.32 ± 0.06	0.49 ± 0.06	32	732 ± 134	98 ± 18	0.88	181 ± 24

^a This is the ratio of horizontal to vertical travel distance between the highest initiation point and the terminal deposit

^b The values represent the measured volumes within debris flow affected channels prior to terminal deposits and intersection with higher order streams

^c This is the volumetric proportion of sediment that is sourced from hillslopes assuming no hillslope deposition

There were significant differences between the nutrient concentration of hillslope and channel source material at the debris flow sites (Table 3.3). The production of nitrogen (TN) in hillslopes (233 kg ha^{-1}) is similar to the 225 kg ha^{-1} measured using similar method after a debris torrent following a wildfire near Warburton, SE Australia in 1983 (Leitch *et al.* 1984). The relatively low rock content and high nutrient content of hillslope material compared to channels means that hillslopes contributed disproportionately to the production of fine sediment (72 %) and nutrients (95 %, 65 %, 91 % and 90 % for Bray P, Na, TC and TN, respectively) (Figure 3.3). Organic matter (TC) made up 6 % of the total mass within the $< 2 \text{ mm}$ fraction which is similar to the ratio of sediment to organic matter reported for large post-fire erosion events (including debris flows) that lead to water quality impacts in the Cotter catchments (White *et al.* 2006). Overall, these results indicate that hillslope erosion and channel erosion should be weighted differently when evaluating potential impacts on aquatic ecosystems or water supply reservoirs.

Table 3.3 Nutrient concentrations (g kg^{-1}) and loads (kg ha^{-1}) for hillslope and channel material at debris flow sites. The concentrations were measured on soil samples from Rose River, Yarrarabula and Germantown. The average loads were calculated for sediment $< 2 \text{ mm}$ based on the average sediment load across all surveyed debris flow sites ($n = 10$).

Constituent	Channel		Hillslope surface (0-2 cm)		Total kg ha ⁻¹
	g kg ⁻¹	kg ha ⁻¹	g kg ⁻¹	kg ha ⁻¹	
Bray-P	0.010 ± 0.011	0.26 ± 0.12	0.074 ±0.031	4.2 ±2.3	4.46 ±2.3
Na	0.315 ± 0.074	8.2 ± 3.4	0.230 ±0.036	13.1 ±6.9	21.3 ±7.4
TC	19.9 ± 9.83	519 ± 238	82.4 ±16.7	4690 ±2576	5210 ±2516
TN	1.13 ± 0.46	53.5 ± 30	4.06 ±0.80	233 ±128	287 ±158

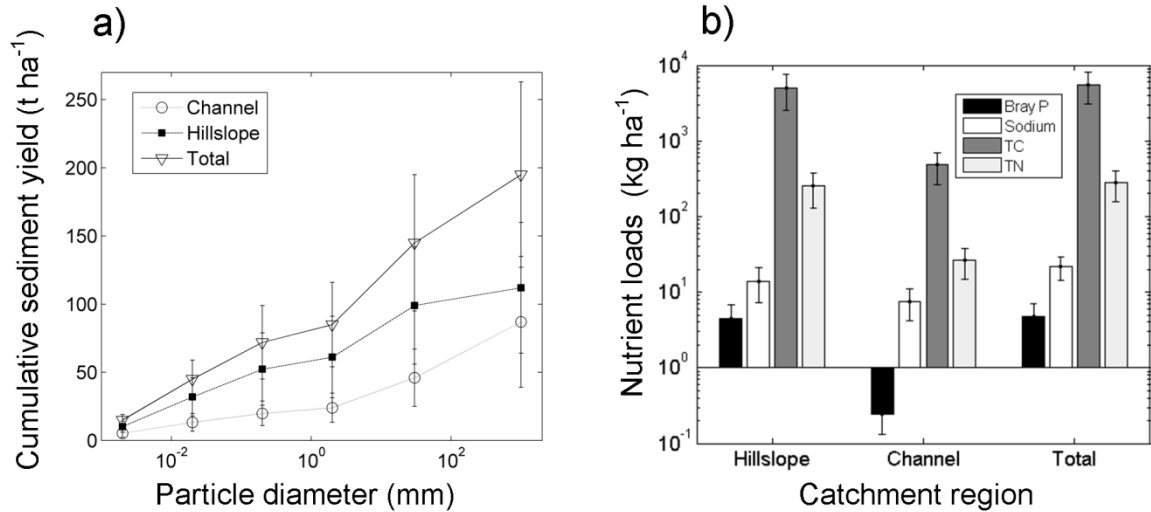


Figure 3.3 a) The mean cumulative sediment yield (t ha⁻¹) with increasing particle size across all debris flow catchments. b) The hillslope and channel contribution to the total nutrient content in eroded material. Bray P is the plant available phosphorous, TC is total carbon and TN is total nitrogen. Error bars show the standard deviation of the mean for all catchments (n = 10).

3.3.3 Equations for erosion a debris flow initiation and magnitude

In this section the aim is to parameterise a model that represents rainfall, infiltration capacity and sediment availability as the key variables that drive variability in the initiation thresholds and magnitude of debris flows in catchments that are impacted by wildfire. The sediment yield, (Y , m³) from the debris flow process at any point (x , y) within the catchment is represented as the sum of point-based erosion depth, E (m), and channel deposition, U (m), above that point in a flow accumulation grid where A is the contributing area:

$$Y(x, y, A) = \left(\sum_{A' < A} E(x, y, A') - \sum_{A' < A} U(x, y, A') \right) * cellsize \quad 3.2$$

The sum of erosion depths in pixels is multiplied by the cell size because this converts depth of erosion in m to volume of erosion in m³. Point-based measurements of erosion depth, E (m), within the debris flow affected catchments were modelled as a function of catchment position and runoff potential using the variables of local slope (S), contributing

area (A), rainfall intensity (I) and the infiltration capacity (K_p) using the geomorphic transport equation:

$$E = k_e Q^m S^n \quad 3.3$$

where k , m and n are fitted parameters and Q is the rainfall excess ($\text{m}^3 \text{h}^{-1}$);

$$Q = (I - K_p) * A \quad 3.4$$

The equation (3.4) for rainfall excess (Q) does not represent the transfer of surface water from one point to another and equation (3.4) is therefore not a physical representation of the shear strength or transport capacity of the flow. When k_e , m and n are parameterised using erosion measurements from field surveys, the erosion equation (3.3) is essentially an empirical relation between erosion depth (E) and the explanatory variables (S , A , I and K_p) underlying landscape variation in sediment transport during rain storms.

The depth of erosion at each measurement location was calculated as the average depth across DEM pixels which were 10 m wide. For channel erosion this meant that each channel cross-section (m^2) was divided by 10 m to get erosion depth (E) in metres. The parameters (k_e , m and n) were calibrated separately for hillslope and channel erosion (E_{hs} and E_{ch} , respectively) since the erosion processes differ between the two. The proportionality constant, k_e , has units of h m^{-2} and can be interpreted as sediment availability (i.e. the depth of erosion per unit of $Q^m S^n$).

The first step in the analysis was to extract values for S and A that corresponded with each geo-referenced measurements of E_{hs} and E_{ch} that were collected as part of the debris flow survey (data shown in Table 3.2). The local slope (S) and contributing area (A) were obtained at each measurement location from a 10 m DEM. The values of S and A were calculated as the average of 3 channel pixels centred on the location of each erosion measurement. The spatial averaging of slope was necessary to remove the variability which may be an artefact of the DEM and the limits in the accuracy (1-10 m) of the GPS (< 10 m) used to locate each cross section.

Both hillslope and channel erosion was highly variable at small scales. Some of this variability was caused by factors other than those represented in the model and therefore somewhat random with respect to the proposed model. For instance the channel shape, bedrock exposure and rill erosion on hillslope can result high spatial variability that is not related to the local slope, contributing area or runoff generation. The values of E_{hs} , E_{ch} , S and A were therefore averaged within sampling units. For hillslopes, the point values were averaged within upper, mid and lower sections as per Table 3.2. For channel segments, the measurements were averaged within stream orders. First-order streams originated at each channel initiation point below zero order headwater. Second order stream originate from joining of two first order stream and a third order stream is produced by joining two 2nd order streams (Strahler 1957).

The steady state infiltration capacity (K_p) was calculated as the geometric mean of ponded infiltration rate on burnt soil at Rose River, Yarrarabula and Germantown, using measurements from field surveys described in Chapter 2 ($K_p = 30 \text{ mm h}^{-1}$; $n = 15$). The geometric mean was used because it is a better measure of central tendency when the distribution of K_p is lognormal (Reynolds *et al.* 2000; Sharma *et al.* 1980) (Lee *et al.* 1985). The infiltration measurements were made on soil, not rock, and are therefore an overestimate of the actual infiltration capacity of the hillslope given that up to 28 % of the surface consisted of exposed rocks > 30 mm (see Table 3.2 for the rock data which was measured in 1 m² quadrats during the hillslope erosion surveys). The steady state infiltration capacity was therefore adjusted accordingly by setting K_p to 0 in the proportion of hillslope covered by rocks. All events occurred within the first year of the fire and it is assumed that recovery of the soil did not take effect within this period (i.e. K_p was kept constant during the first year after fire). The rainfall excess, Q , in the equation (3.4) was calculated using rainfall intensity values at 15- and 30-minute temporal sales (I_{15} and I_{30} , respectively) to give rainfall excess (Q) at two temporal scales of (Q_{15} and Q_{30} , respectively).

Table 3.4 Rainfall and infiltration parameters at debris flow sites.

Site	K_p	I_{15}	I_{30}	$I_{15} K_p$	$I_{30} K_p$
	m h^{-1}	m h^{-1}	m h^{-1}	m h^{-1}	m h^{-1}
	$\times 10^3$	$\times 10^3$	$\times 10^3$	$\times 10^3$	$\times 10^3$
Rose River	27	85	59	58	32
Germantown	26	60	35	34	9
Yarrarabula	27	65	38	38	11
Target Creek	25	44	37	19	12
Mt Tamboritha	19	37	35	18	16
Myrtle Ck	11	35	18	24	7
Sunday Ck	12	42	30	30	18

The best fit for channel erosion (E_{ch}) was obtained using infiltration excess from 30-minute rainfall (Q_{30}) and parameter values of 0.09, 0.5 and 0.7 for k_e , m and n respectively ($R^2 = 0.4$) (Figure 3.4). The parameters were optimised in Matlab using the Gauss-Newton non-linear least squares algorithm. A large proportion of the variability in E_{ch} was unaccounted for, something that was expected given i) the strong dependency between sediment availability and time since last channel evacuation and ii) a strong random component in the exact location of sediment accumulation in channels. However, the calibration of equation (3.4) incorporates data from multiple sites across a large geographic region and the parameters are therefore considered to represent the average channel response if catchments were sampled randomly from the landscape.

The depth of deposition in channels (U) was very low in upper parts of the catchment and was not measured. Lower regions however began storing large amounts of material once the channel slope was $< 10^\circ$. Within some reaches of the channel, the storage of material exceeded the volume of eroded material. This meant that the deposition rate was higher than the erosion rate, and that debris flow conditions could no longer be sustained unless there was a contribution from incoming tributaries or a change in overall channel properties (steepness or confinement). The channel deposition depth was modelled as a power function of slope (S) and 30-minute rainfall excess (Q_{30}) in equation (3.4) with parameters m and n which had been calibrated for channel erosion:

$$U = k_e(Q_{30}^{0.5}S^{0.7})^\beta \quad 3.5$$

where k_e and β are fitted parameters. The depth of channel deposition U was calculated from the debris flow survey data as the average depth within stream orders. The equation was fitted using deposition data (U) from 2 and 3 order channels representing 8 out of the 10 debris flow events reported in Table 3.2. The best fit ($R^2 = 0.47$) was obtained with parameter values of 0.0003 and 1.7 for k_e and β , respectively. Channel deposition U is initially very low but increases exponentially and equals E_{ch} when $Q_{30}^{0.5}S^{0.7} = 118$. The debris flow conditions persists while $U < E_{ch}$. The shift from an eroding debris flow region ($U < E_{ch}$) to a non-eroding region ($U > E_{ch}$) can occur gradually within valley bottoms or abruptly in a terminal deposit at the confluence with trunk stream or larger catchment.

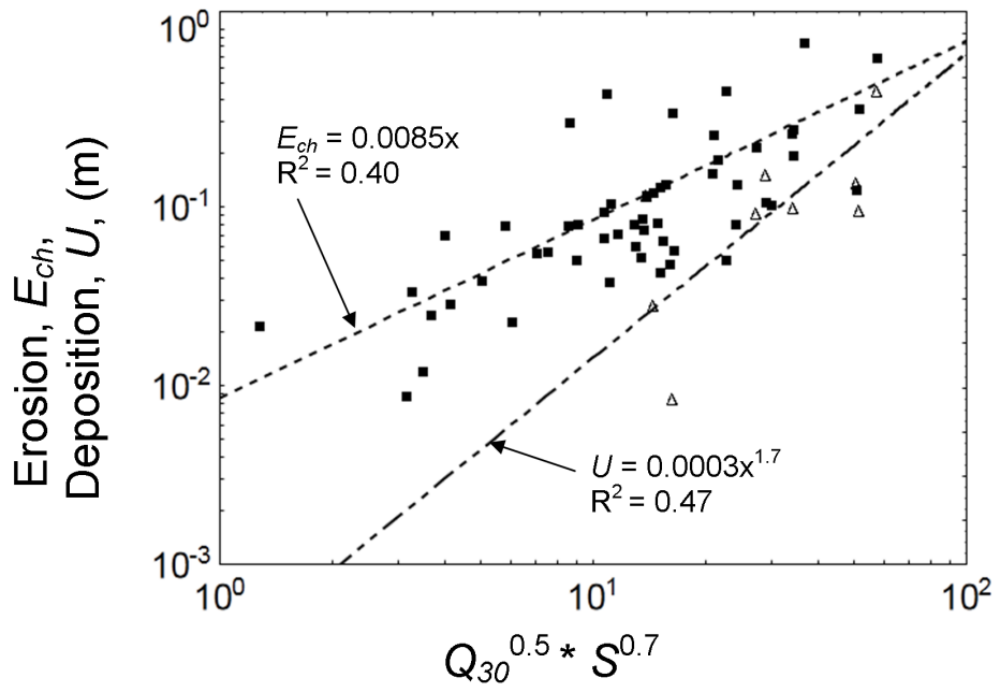


Figure 3.4 Erosion and deposition by debris flows 1-3 order catchment in the eastern uplands of Victoria, southeast Australia. Each data point of erosion (E_{ch}) is the average erosion within individual stream order reach ($n = 60$) at 8 debris flow catchments. There were 44 first order channels, 13 second order channels and 3 third order channels. Deposition (U) was measured in 8 stream order reaches (6 second order and 2 third order).

The parameters m and n which were parameterised for E_{ch} were assumed to be representative of the processes contributing to channel initiation. The threshold for channel initiation during debris flow events was represented as a function of the 30-minute rainfall excess (Q_{30}) and the local slope (S) (Figure 3.5). Essentially, this means that the channel initiation points (CIP) during the debris flow is a function of the local slope and the rainfall excess Q_{30} contributing to at that point. The critical Q_{30} was a linear function of S when m and n were carried across from the fitting procedure for channel erosion.

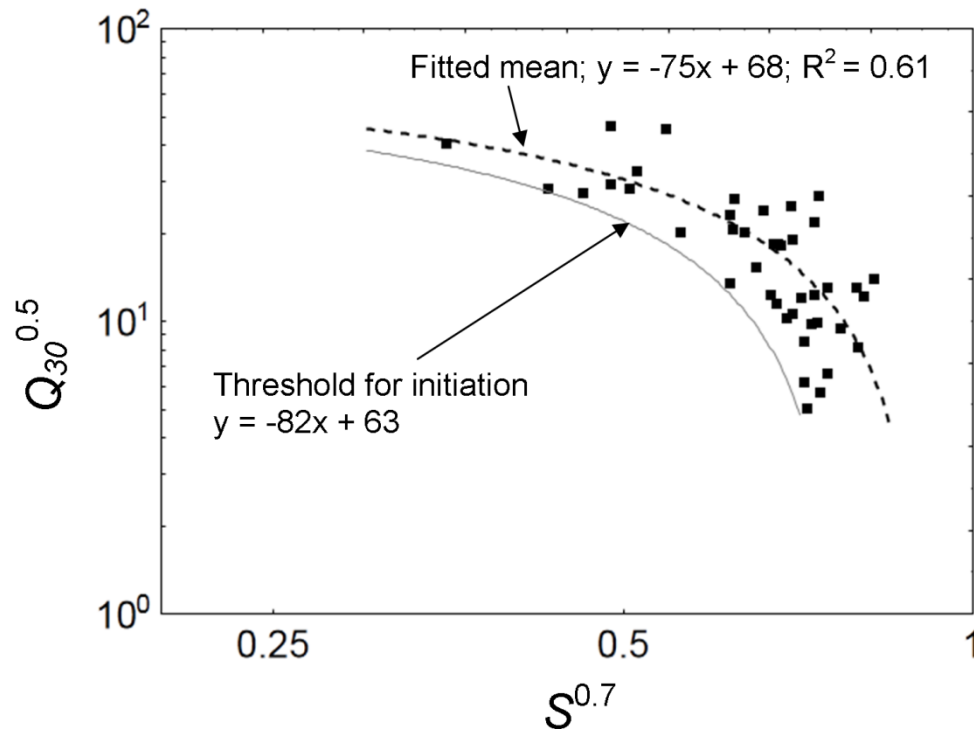


Figure 3.5 Debris flow initiation thresholds for headwater catchments ($n = 45$) across 7 sites in the eastern uplands of Victoria, southeast Australia. The threshold curve was fitted manually by adjusting the parameters in the linear function so that no data points were within the threshold curve.

The fitted mean line represent an average relation whereas the minimum fit represents a more conservative measure of the initiation threshold. The fitted line for debris flow initiation thresholds is only valid within the region of the data. This means that the region in which debris flows can initiate is bounded on either end by some minimum value for q_{30} and some S . The channel initiation points (CIP) can be predicted by applying the channel threshold function and locating the position where the threshold for initiation is exceeded.

There should be no initiation when $Q_{30} = 0$, hence $S^{0.68}$ must be greater than 0.72. This results in the following conditions for channel initiation:

$$\frac{(Q_{30}^{0.52} - 63)}{S^{0.68}} > -82 \quad 3.6$$

$$S^{0.68} < 0.72$$

All points in the landscape that satisfy both of these conditions can be considered channels. The channel initiation points are defined at the end points in the upper headwaters where the conditions shift from false to true.

The hillslope erosion (E_{hs}) was modelled in similar way to channels erosion, using equation (3.3) to relate rainfall excess (Q) and local slope (S) to erosion depth (E_{hs}), although the parameters k_e , m and n were parameterised separately to the channel component since the transport behaviour is different. The best fit between E_{hs} , q and S was obtained using the 15-minute rainfall excess, Q_{15} , as opposed to Q_{30} which was the best predictor of channel erosion. This difference in rainfall dependency is reasonable given that the travel time on hillslopes is shorter and the erosion processes are more responsive to short burst of rainfall. The fitted parameters, m and n , were 0.8 and 1.6, respectively. The value of n for hillslopes indicates that hillslope erosion was more sensitive to slope than channel erosion.

The debris flows at Rose River and Germantown displayed much lower hillslope erosion than all other sites and represents a different population to the other sites. The proportionality constant (k_e) (representing sediment availability) for these two sites was 0.0005 as opposed 0.0027 for the other sites (Mt Tamboritha, Target Ck, Yarrarabula). One possible explanation for this difference is that the debris flows at Rose River and Germantown occurred 10 – 12 months after the burn and the low k_e may represent a recovery signal. However, the same time period had lapsed between the wildfire and debris flow event at Yarrarabula and this site did not display such a low k_e . Although it is noteworthy that the catchment at Yarrarabula was burnt twice (once in 2003 and then again in 2007), making it a unique case. At all other sites the debris flows occurred within 2 months of the fire.

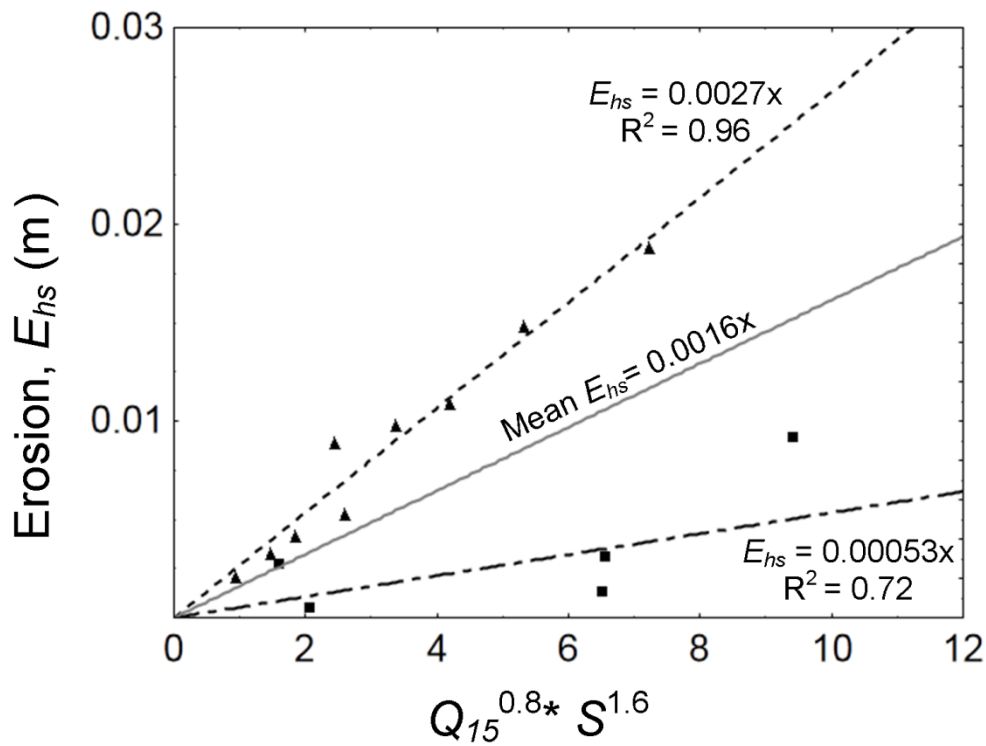


Figure 3.6 The relation between transport and local slope for channel initiation points in lower-, mid- and upper catchments at five post-fire debris flow sites southeast Australia.

3.3.4 Modelling debris flow initiation and magnitude - testing

In this section we used the calibrated transport equations to model erosion during debris flows at Sunday Creek and Myrtle Creek. The survey data from these two sites were not used in the previous parameterisation of m , n and k_e which means that the erosion measurements from these sites are independent data. The volumetric rock content at Myrtle Creek and Sunday Creek was similar (28 % and 23%, respectively), therefore giving similar infiltration rates ($K_p = 11$ and 12 mm h^{-1} for Myrtle and Sunday Creek, respectively). The I_{30} and I_{15} (in mm h^{-1}) were 18 and 35 and 30 and 42 for Myrtle Creek and Sunday Creek, respectively. Infiltration and rainfall variables are shown in Table 3.4.

The first step in the model application was to calculate slope (S) and the 30-minute infiltration excess (Q_{30}) at Myrtle Creek and Sunday Creek in a 10 m DEM. Channels and hillslopes could then be differentiated based on the conditional statements for channel initiation in equation (3.5). Deposition (U) and erosion (E_{ch}) in channels (depth in meters) was then calculated at each pixel using the equation (3.2) and the parameter values (k_e , m ,

n , k_d and β) obtained as part of the fitting procedure shown in Figure 3.4. The hillslope erosion depth (E_{hs}) was calculated at all non-channel pixels using the mean E_{hs} function in Figure 3.6 ($k_e = 0.0016$). The yield, Y (m^3), at each pixel was obtained as the sum of erosion depths minus the sum of deposition, then multiplied by the area of each pixel (m^2), as per equation (3.1). The location of the terminal deposit emerged once $U > E_{ch}$. The modelled erosion depth (m) and sediment yield (m^3) at Myrtle Creek and Sunday Creek are shown in Figure 3.7.

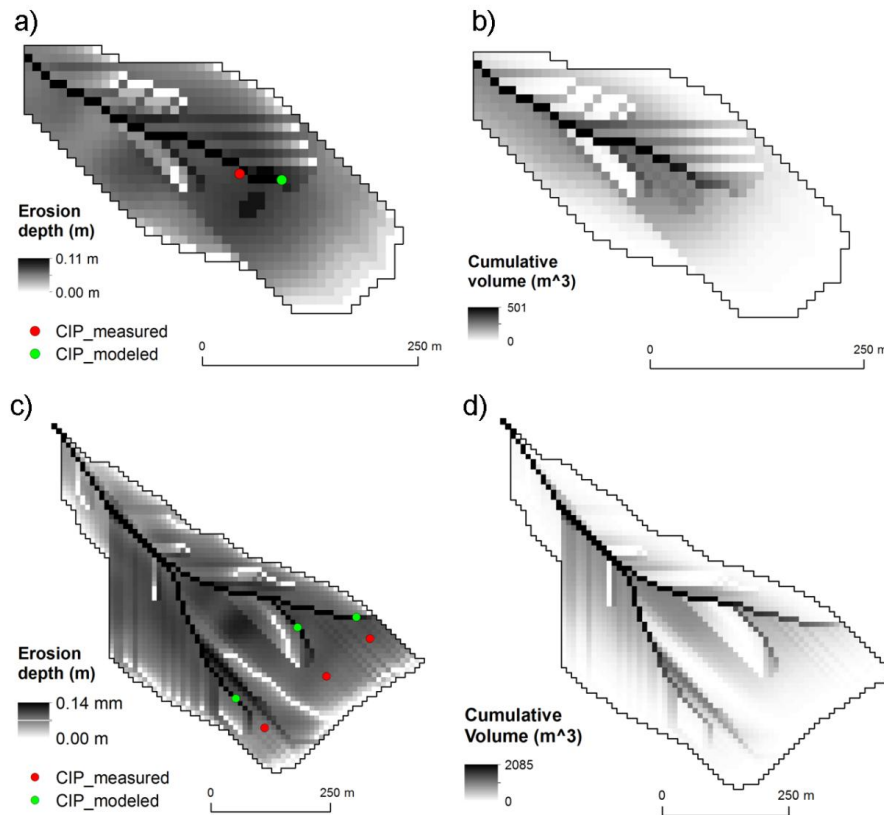


Figure 3.7 Model of channel initiation, erosion depth and sediment yield in debris flow catchments at Sunday Creek (a - b) and Myrtle Creek (c - d). See Appendix C for photos of hillslope erosion, initiation points, channel scour and terminal deposits at Myrtle Creek and Sunday Creek.

Table 3.5 compares the modelled values with values obtained from erosion calculations in Table 3.2. The model was able to reproduce key feature of the debris flow at the two sites in terms of i) the location of initiation points, ii) channel sediment contribution (m^3), iii)

hillslope sediment contribution (m^3), and iv) the location of the terminal deposit. Using the mean value for the sediment availability parameter ($k_e = 0.0016$) (Figure 3.6) meant that the predicted hillslope contribution is lower than observed values, thus resulting in slightly lower overall volume. Using the upper value ($k_e = 0.0027$) resulted in better predictions with hillslope contributions of $2092 m^3$ and $583 m^3$ for Myrtle Creek and Sunday Creek respectively.

Table 3.5 Observed and predicted erosion in debris flow catchments in Myrtle Creek Sunday Creek.

	Myrtle Creek		Sunday Creek	
	Predicted m^3	Observed m^3	Predicted m^3	Observed m^3
Hillslope	1240	1886	346	640
Channel	1045	767	225	123
Deposit	200	386	70	32
Total	2085	2267	501	732

3.4 Conclusion

Post-fire debris flows in southeast Australia produce similar sediment yield rates ($m^3 ha^{-1}$) to debris flows that have been reported in other fire-prone regions indicating that key processes are similar and that predictive models are transferrable across different regions. This meant that predictions of debris flow magnitude from the USGS model (Gartner *et al.* 2008) corresponded well with the observed responses in southeast Australia. Overall the actual magnitude of events is on average lower in the southeast Australia than what has been reported for post-fire debris flows in the intermountain west of the US (Gartner *et al.* 2008; Meyer *et al.* 2001). This difference in magnitude is due to the smaller debris flow producing basins and the relatively low relief in the upland catchments of southeast Australia when compared to those of the western US (Cannon 2001; Santi *et al.* 2008; Wohl and Pearthree 1991).

The effectiveness of the USGS models in predicting debris flow volumes in catchments of western US, southeast Australia and Mediterranean (García-Ruiz *et al.* 2012) indicate that the model captures the key properties underlying debris flow response and that it is universally applicable for predicting debris flow volumes from runoff generated debris

flows in burnt landscapes. This makes it an attractive option for modelling the magnitude of debris flows. Disadvantages with the USGS model include i) the need for arbitrarily defining debris flow catchment boundaries, ii) the absence of soil infiltration properties, fire severity and recovery as independent predictor variables, and iii) the lack of integration between debris flow initiation (probability of occurrence) and the magnitude of events.

One of the aims in this chapter was to develop an alternative modelling approach where hillslope and channel erosion by debris flows could be represented separately and modelled as a function of landscape position and the hydrological variables that are directly affected by fire. The results in Table 3.5 indicate that the variables of local slope, the contributing area, and infiltration excess can be effective at capturing variability in erosion and deposition during post-fire debris flows. The model was tested on two debris flow events only, and further work is therefore required to provide a more rigorous test of this modelling approach. The potential advantages of the proposed approach over the existing USGS model include i) better linkage between initiation processes and debris flow magnitude, ii) partitioning of hillslope and channel source contribution and iii) explicit representation of deposition and debris flow termination. These features make the model more suitable for landscape scale application at event scales but also for longer temporal scales under the influence of randomly occurring fires and storms.

In terms of initiation and magnitude of debris flows, the property (other than topography) driving variability in susceptibility, is infiltration and sediment availability. In upland catchments of southeast Australia, the infiltration characteristics of different forest ecosystems seem to be particularly important as controls on debris flow initiation. This was established in Chapter 2 as part of the landscape scale survey of debris flow responses. Predicting landscape scale variability in infiltration properties may therefore allow for better characterisation of debris flow probability across landscapes with variable soil properties. Similarly by quantifying changes in infiltration properties during recovery it is possible to explore the change in debris flow probability as a function of time since fire. Furthermore, the strong sensitivity of the predicted volumes to the sediment availability parameter (k_e) on hillslopes means that more experimental work is required to quantify how this property varies between systems and how it changes during recovery. In the following

chapters we therefore aim to develop models that capture the spatial and temporal variability in infiltration capacity and sediment availability on burnt hillslopes.

Chapter 4: Effects of ash, water repellency and macropore flow on infiltration during recovery from wildfire

Paper submitted to *Journal of Hydrology*:

Nyman, P., G. J. Sheridan, H. G. Smith (2011), Effects of ash, water repellency and macropore flow on infiltration during recovery from wildfire. *Submitted April 2013*.

Abstract

Wildfires produce ash and can cause i) extreme soil drying, ii) increased water repellency and iii) reduced soil structure, thereby reducing infiltration into the soil. High severity wildfire often results in a non-repellent layer of ash, charcoal and burnt soil overlying a water repellent soil matrix. In these conditions the hydraulic parameters can vary across discrete layers in the soil profile, making the infiltration process difficult to measure and model. The difficulty is often exacerbated by the discrepancy between actual infiltration processes and the assumptions that underlie commonly used infiltration models, which often stem from agricultural environments where soils are homogenous and typically less variable in space and time. In this study we use a simple two-layered infiltration model consisting of surface storage (H), macropore flow (K_{mac}) and matrix flow (K_{mat}) in order to identify and analyse spatial-temporal infiltration patterns in soils recovering wildfire. Infiltration in intact soil cores showed that the soil contained a region of strong water repellency that was hydrologically inactive, slow to take on water, ultimately restricting flow through the matrix. The resistance of wetting in the near surface soil was represented by the minimum critical surface tension (CST_{min}) within the soil profile. Under field conditions, the soils remained water repellent in small headwater catchments throughout a 3.5-year recovery period, but the strength diminished exponentially during wet conditions, resulting in some temporal changes in infiltration capacity (K_p). An increase in macropore availability during recovery, however, was the main source of temporal variability in K_p , confirming the common observation that macroporosity dominates infiltration processes in forest soils. Surface storage was initially high (4 mm) after wildfire, then declined exponentially. Overall the study shows that the two layered soil can be represented and parameterized by partitioning the infiltration process into surface storage and flow through a partially saturated and restrictive soil layer. Ash, water repellency and macropore flow are key characteristics of burnt forest soils in general and the proposed model may therefore be a useful tool for characterizing fire impact and recovery in other systems.

4.1 Introduction

Fire can increase overland flow by reducing interception, infiltration and surface roughness (Cawson *et al.* 2012; Martin and Moody 2001; Robichaud 2000; Shakesby and Doerr 2006; Sheridan *et al.* 2007a). Increased production of overland flow can in turn lead to increased erosion rates and increased frequency of threshold driven responses such as flash floods and debris flows (Cannon 2001; Lane *et al.* 2006b; Moody and Martin 2001b; Nyman *et al.* 2011; Robichaud *et al.* 2008b; Wondzell and King 2003). High severity fire removes vegetation, burns the topsoil and deposits ash on hillslopes. Under these condition the surface roughness and rates of interception are low and (relatively) homogenous across hillslopes, irrespective of the catchment conditions prior to burning (Johansen *et al.* 2001). Infiltration however can be highly variable due to a strong dependency on pre-fire soil conditions. Properties such as porosity, pore distribution, macroporosity and water repellency are therefore important controls on variation in hydrological responses across burnt landscapes (Larsen *et al.* 2009; Nyman *et al.* 2011; Robichaud *et al.* 2007; Shakesby and Doerr 2006).

Infiltration models use theory of flow in porous media to estimate the rate at which water enters the soil. Essentially the infiltration rate is modelled as a function of i) the pore size distribution of the soil matrix, ii) the initial soil moisture and iii) the rate at which water is supplied at the surface (Green and Ampt 1911; Philip 1957). Hydraulic conductivity (mm h^{-1}), sorbtivity ($\text{mm h}^{-0.5}$), or the suction at the wetting front (mm) are infiltration parameters that reflect the combined effects of these properties on flow and retention of water within the soil (Smith 2002). The parameters can be obtained from laboratory studies, field experiments or pedotransfer functions (Cook 2007; Moody *et al.* 2009; Rawls *et al.* 1983; Risse *et al.* 1994; Robichaud 2000).

The effect of burning on infiltration rates is well documented in the literature. Fire impacts on infiltration parameters by i) adding storage potential as deposits of fine ash and burnt soil (Bodí *et al.* 2012; Woods and Balfour 2008; Woods and Balfour 2010), ii) reducing soil structure and macropore flow (Nyman *et al.* 2010; Onda *et al.* 2008) and iii) reducing pore-space availability and wetting potential due to water repellent soils (Doerr and Moody 2004; Moody and Ebel 2012; Nyman *et al.* 2010). Soil profiles on fire affected hillslopes typically consist of heated and burnt soil that is sandwiched between surface ash and a non-

heated soil matrix. The layered soil profile means that there is often strong variability with depth for hydrological properties such as porosity, particle size distribution and water repellency (Bodí *et al.* 2012; MacDonald and Huffman 2004; Moody and Ebel 2012; Moody *et al.* 2009; Woods *et al.* 2007). Characterizing soil hydrological properties and their effects on the infiltration process in these systems is challenging because it requires simultaneous examination of flow processes in soil layers with different media properties.

The link between impacts on properties and subsequent changes in processes is poorly understood and not well represented in current infiltration models. The properties that dominate infiltration change depending on the spatial and temporal scales at which processes are measured. Water repellency for instance can be quantified as a spatial distribution of a point-based measurement of water drop penetration times (Doerr *et al.* 1998; Robichaud *et al.* 2008a; Woods *et al.* 2007). The water repellency has strong effect on the behaviour of water drops reducing the ability of the soil to absorb water (Doerr *et al.* 2000). However, the strength or persistence of water repellency at points may not translate to large impacts on infiltration if water bypasses the matrix as preferential flow through wettable patches, cracks, and macropores and along roots and rocks (Burch *et al.* 1989; Doerr and Moody 2004; Granged *et al.* 2011; Imeson *et al.* 1992; Nyman *et al.* 2010; Shakesby and Doerr 2006; Urbanek and Shakesby 2009). Similarly the temporal scale of measurement is important. Moisture induced changes in water repellency for instance, may be important when infiltration is modelled across different seasons, but it may be negligible within a single storm-event since the time scale of wetting may be in the order of several hours or days (Crockford *et al.* 1991; Ebel *et al.* 2012; Moody and Ebel 2012).

Representing the interactions between macropore flow, matrix flow and soil wetting is important for understanding and predicting fire-impacts on infiltration processes. Most traditional infiltration models however are based on theory and data from systems where the dominant processes and key properties are different to what is typically observed in fire-affected soils, particularly with regards to wetting behaviour (imbibition) and macropore flow (Ebel and Moody 2013; Nyman *et al.* 2010). In this paper we therefore aim to develop a model for hydraulic conductivity which incorporates moisture dependent water repellency and which accounts for changes in macropore flow during recovery from wildfire. The study is situated in southeast Australia, where both macropore flow and water

repellency are important controls on infiltration rates in forest soils (Burch *et al.* 1989; Crockford *et al.* 1991; Lane *et al.* 2006a; Nyman *et al.* 2010).

This study combines measurements from intact cores and field campaigns to;

- i. Model the interactions between absorption processes (imbibition rate) and hydraulic conductivity in water repellent and intact soil cores.
- ii. Quantify the effects of dryness, water repellency, surface storage and macropore flow on infiltration in headwater catchment recovering from wildfire.

4.2 Methods

4.2.1 Infiltration model

A large proportion of post-fire erosion tends to occur in response to high intensity rainfall events (Ebel *et al.* 2012; Kean *et al.* 2011; Moody 2012; Nyman *et al.* 2011; Smith *et al.* 2011a). The surface runoff generated during rainfall events is therefore assumed to depend on storage of water in surface material and the flow of water out of this storage water and into the soil matrix. Once storage is depleted, the maximum infiltration capacity (K_p) occurs under ponded conditions and is either controlled by i) supply rate of water (R), ii) the hydraulic conductivity of ash/burnt soil mixture (K_{ash}) or iii) the infiltration capacity of the water repellent soil (K_p) which is the sum of steady state infiltration into macropores (K_{mac}) and the matrix (K_{mat}) (Figure 4.1)

Field and laboratory based infiltration measurements were used to parameterize and analyse a storage based infiltration model which represents infiltration, $f(t)$, as a three stage process;

$$\begin{cases} f(t) = H\theta_d/t + K_{mat} & \text{for } (t < t_p) \text{ and } (K_{ash} > K_{mat}) \\ f(t) = K_{mat} + K_{mac} & \text{for } (t > t_p) \text{ and } (K_{ash} > K_{mat}) \end{cases} \quad 4.1$$

where t is time, t_p is time to ponding, H is the surface storage potential (mm), θ_d is the soil moisture deficit, K_{mat} is the flow potential of the soil matrix (mm h^{-1}), K_{mac} is the flow potential through macropores (mm h^{-1}) (Figure 4.1a). The soil moisture deficit is the difference between soil moisture at saturation (θ_s) and the initial soil moisture relative (θ_i) to θ_s , $\theta_d = (\theta_s - \theta_i)/\theta_s$.

The overall flux is restricted by K_{ash} if $K_{ash} < K_{mat}$. The macropore flow K_{mac} is the difference in steady state infiltration between $h = -15$ mm and $h = 5$ mm.

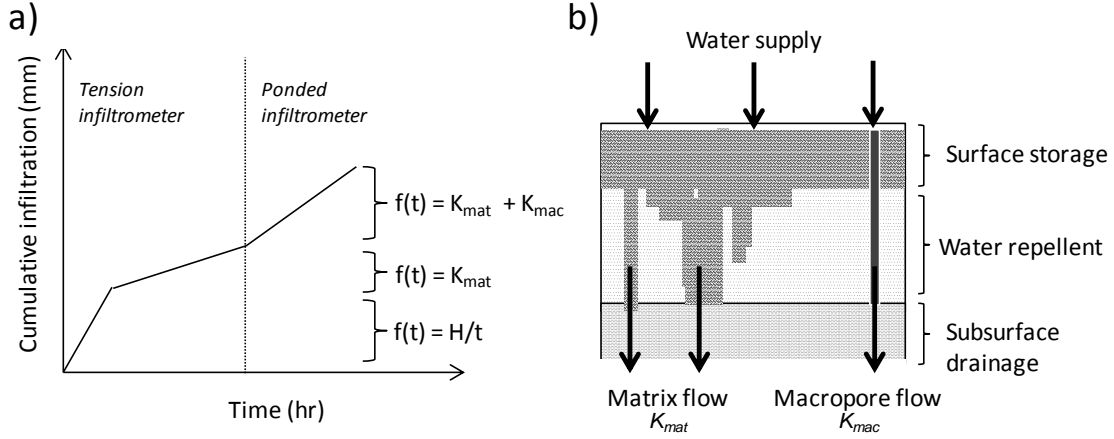


Figure 4.1 a) Storage (H), matrix flow (K_{mat}), and macropore flow (K_{mac}) as three parameters in the infiltration processes. b) A schematic representation of infiltration parameters in a water repellent soil.

The surface storage (V , $\text{cm}^3 \text{cm}^{-3}$) above the water repellent layer could be estimated from

$$V = \frac{RH\theta_d}{R - K_{mat}} * A \quad 4.2$$

Where R is the supply rate of water (mm h^{-1}) to the soil surface and A is the area under infiltration. The potential supply from infiltrometers is high relative to K_{mat} ($R \gg K_{mat}$), hence $V \rightarrow AH\theta_d$ (Kirkby 1975; Scoging 1979).

Water repellency can vary with changes in soil moisture. We used a separate model to represent the infiltration into this layer since wetting processes are slow compared to non-repellent soil. Water repellency was represented as a distribution of critical surface tension (CST , dyn cm^{-1}) at soils depths (d_s) between 0 and 10 cm using the function;

$$CST(d_s) = 72.7 + vd_s * u^{d_s} \quad 4.3$$

Where d_s is soil depth and v and u are fitted parameters. The parameters v and u determine the maximum strength and the distribution of water repellency (CST) in the soil profile. The equation (4.3) represents surface soil as wettable (i.e. $CST = 72.7 \text{ dyn cm}^{-2}$ when $d_s = 0$), an assumption that was supported by data from field based measurements on burnt soil. Using

equation (4.3) to minimize the error in the spatially distributed CST measurements means that both vertical and planar variability are captured in a single function. The maximum strength of water repellency within the soil profile (the ‘bottleneck’ if ash is not limiting) was obtained by calculating CST_{min} at the depth of maximum repellency (d_{max}) which obtained by setting the first derivative of $CST(d_s)$ (4.3) to 0;

$$d_{max} = -1/\log(v) \quad 4.4$$

The slow wetting process in water repellent soils means that the interaction between soil moisture and CST are dependent on weather conditions spanning over days to weeks. For field conditions we use an empirical Keetch-Byram Drought Index ($KBDI$; Keetch and Byram 1968) as a predictor of soil moisture status and CST_{min} ;

$$KBDI_t = KBDI_{t-1} - 10P + \frac{(2000 - KBDI_{t-1})(0.967e^{(0.088T_{max}+1.556)} - 0.83)}{(1 + 1088e^{-0.0017P_{yrs}})1000} \quad 4.5$$

Where P is the daily precipitation (mm), T_{max} is the daily maximum temperature (°C) and P_{yrs} is the annual precipitation at the site (mm). The temporal variability in hydraulic conductivity, K_{mat} , was measured and represented as an empirical function of CST_{min} and $KBDI$.

In the following section we outline a set of laboratory and field experiments that were designed to;

- i) Evaluate the assumption that hydraulic conductivity is restricted by water repellent layer (Figure 4.1) and,
- ii) Quantify the relation between regional weather conditions, soil moisture status, water repellency, macropore availability and hydraulic conductivity of soils recovering from wildfire.

4.2.2 Laboratory and field measurements: overview of methods

Laboratory- and field- based experiments were used to measure infiltration at three fire affected hillslopes in Victoria, southeast Australia (Figure 4.2). The primary study sites

were Stony Creek and Sunday Creek which were burnt by high severity wildfire in February 2009. A third site, Ella Creek, was burnt in January 2007 and was included to represent similar forest environments in a later stage of recovery (Table 4.1). All sites are located in the eastern uplands of Victoria. The climate is Mediterranean with hot and dry summer and cool and wet winters. There is large variability in ecosystem properties across the study area, but the three sites used in this study were all characterized by dry eucalyptus forest and were similar in terms of rainfall, aspect and solar exposure.

Intact soil cores were sampled from each site in April 2010 and used for laboratory-based infiltration measurements. The soil cores were used to quantify the relation between imbibition rate and the hydraulic conductivity of the soil. Laboratory experiments were best suited for this type of study because soil moisture conditions could easily be controlled. Infiltration rates were sampled in the field during several campaigns aimed at identifying key controls on infiltration rate on soils that were recovering from wildfire impacts. The initial soil moisture and the water repellency were measured alongside measurements of surface storage potential, H (mm^3), matrix flow, K_{mat} (mm h^{-1}) and macropore flow K_{mac} (mm h^{-1}). The field measurements were made in headwater catchments (< 2 ha) during a three-year recovery period from wildfire.

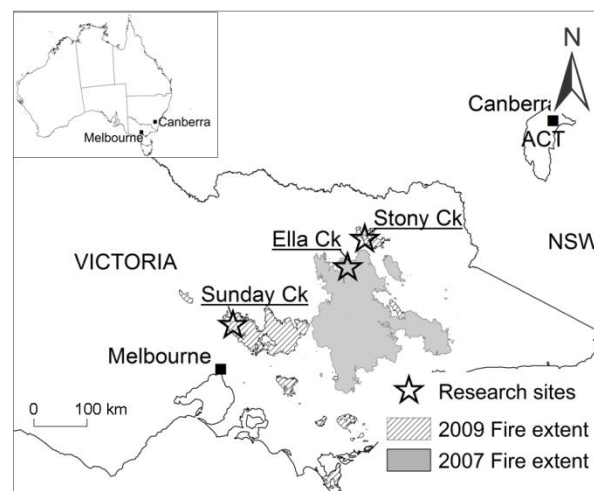


Figure 4.2 The infiltration measurements were made on soils from three sites in uplands of eastern Victoria, southeast Australia.

Table 4.1 The three main study sites and some their key features.

Site	Aspect & Elevation	Burn impact	Annual Rainfall	Forest Type and dominant vegetation	Geology	Soil texture
Ella Creek,	North	Moderate to high severity Jan-2007	1200-1400	Dry Eucalyptus, Broad-leaved peppermint (<i>E. Radiata</i>) Narrow-leaved peppermint (<i>E. Dives</i>)	Shale, Marine Sedimentary	Stony and gravelly clay loam
Sunday Creek	North	High to very high severity Feb-2009	1000-1200	Dry Eucalyptus, Broad-leaved peppermint (<i>E. Radiata</i>)	Siltstone, Marine Sedimentary	Stony and gravelly clay loam
Stony Creek	Northwest	High to very high severity Feb-2009	1000-1200	Dry Eucalyptus, Broad-leaved peppermint (<i>E. Radiata</i>)	Phyllite & Gneiss Metamorphic	Gravelly clay loam

4.2.3 Laboratory study: Flow and re-wetting in water repellent soil

Intact cores were collected from Ella Creek, Sunday Creek and Stony Creek and used to measure hydraulic conductivity and matrix uptake at different stages of imbibition on a tension table. Nine cores (~8 cm deep and 5.3 cm in diameter) were sampled from each site at upper, mid and lower hillslope positions in April 2010. The soil cores were first left to air dry in the laboratory (4 weeks in the lab at 20 degrees), then weighed before the first set of infiltration measurements. The infiltration rate was measured at 15 mm tension ($h = -15$ mm) using Mini-disc (MD) infiltrometer (Decagon) (Moody *et al.* 2009; Robichaud *et al.* 2008a) and a lab procedure for measuring unsaturated hydraulic conductivity described in (Cook 2007). The infiltration measurements in the laboratory were concerned with matrix flow (K_{mat} , $h = -15$ mm), thus excluding the effects of rapid gravity driven flow in macropores which can obscure the effect of water repellency on flow patterns within the matrix.

The cores and the infiltrometer were held in place using clamp and stands during infiltration. Cheesecloth and a shallow layer of pre-wetted contact sand (300 $\mu\text{m} <$ grain size $<$ 600 μm and $K_s > 1000 \text{ mm h}^{-1}$) was placed on the soil surface to ensure good contact between the disc and the soil. In the early stages of infiltration, the rate was usually high,

and then declined towards some low steady state, usually within 5 minutes. The water level was read from the reservoir every 30 seconds for 35 min and only recorded if there was a change from the previous reading. The intervals were longer for cores where the infiltration rate was very low or zero. The core was reweighed at 35 min and replaced in the clamp for another 15 minutes of infiltration measurements if the wetting front had not appeared at the bottom of the core. The core was placed on a buchner funnel set to a tension of -15 mm (same as the mini-disc tension chamber) if the wetting front reached the bottom of the core at 35min. The negative tension at the bottom and top of the core ensured a uniform hydraulic gradient throughout the core and allowed for direct estimation of hydraulic conductivity. This last 15 min of infiltration was used as a measure of the 2D flow potential (K_{mat}) for the initial moisture conditions (θ_i). See Appendix D (Figure 1) for photo of the experimental setup.

After the first set of infiltration experiments, the cores were immediately placed onto a tension table with the tension set so that the average water pressure h for the cores was equal to -15 mm. The tension table was set up with large reservoir of water and constant head burette to maintain constant tension and accommodate any water that was lost due to the water uptake by the cores. Each core was re-weighed after 36hrs on the tension table and a new set of infiltration measurements were carried out, then replaced onto the tension table and reweighed at 60, 100, 148, 268 and 316 hrs. The multiple time steps at which the mass was obtained helped indicate how moisture content changed with time and helped determine a suitable point at which to run a new set of infiltration measurements. A new set of infiltration measurements required a new soil moisture status of the cores. However, after the 268 hrs of wetting at -15 mm tension it was evident that some cores were still dry on the surface. After this time step the water level in the tension table was therefore raised to the midpoint of the core (mean $h = 0$ mm) in attempts to reach a higher moisture levels and ultimately soil saturation.

A third and fourth set of infiltration measurements were carried out after 374 hrs and 681 hrs of wetting. After the final infiltration all cores appeared to be saturated and there was no further increase in mass of cores from this point onwards. The final set of infiltration measurements was taken to represent the saturated hydraulic conductivity at $h = -15$ mm. The cores were finally replaced onto the tension table and drained at fixed tension intervals

(-2.5 < h < -50 cm) in order to characterize the size distribution of pores in the meso-macropore domain.

The porosity of the soil at each site was estimated from the saturated volumetric water content θ_s (cm³ cm⁻³) of the 9 cores that were used in the laboratory infiltration experiment. The macroporosity was estimated from the change in water content (θ) at 5 pressure increments (h) between 0 and -50 cm and using the capillary equation to relate h to pore radius (r , mm);

$$r = \frac{2\rho gh}{\cos(\alpha)} \quad 4.6$$

Where ρ is the density of water, g is gravity and α is the contact angle. A cumulative distribution function was then used to quantify the proportion of pore-space occupied by macropores ($r > 0.5$ mm) (Nyman *et al.* 2010).

4.2.4 Infiltration properties headwater catchments during recovery from wildfire

Infiltration was measured in the field under both ponded ($h = 5$ mm) and tension ($h = -5$ mm), using the min-disc tension infiltrometer (Decagon) and a custom designed ponded infiltrometers with same specifications as that used in the laboratory experiments described above. The measurements were made in three headwater catchments in 4 separate field campaigns, each taken to represent burnt systems in different stages of recovery and in different seasons (Figure 4.3). Infiltration in each headwater catchment was measured at 4 points in 3 quadrats (1 m x 1 m) along three 80 m long transects running perpendicular to the contour ($n = 36$). Quadrats were positioned at upper- (0 m), mid- (40 m) and lower (80 m) sections of the transects. Each sampling campaign was conducted on allocated strips 2 m to the side of the previous campaign to avoid interference from past disturbance effects. A small retention ring (5.3 cm in diameter) was inserted 2-3 cm into the soil in order to prevent lateral flow through wet table surface material which often covered the hillslope. The soil surface was relatively smooth and the infiltrometer disc was small so no contact material was required to achieve contact between the soil and the disc of the tension infiltrometer. The depth of infiltrated water at $h = -15$ mm was measured at 30 s intervals for 8-12 min. The tension infiltrometer was then removed and replaced with the ponded infiltrometer. The soil within the retaining cylinder was flooded so that 5 mm of ponding

was achieved and then the infiltration rate was measured at 15 s intervals for 5-10 minutes. Some photos from field measurements are provided in Appendix D (Figure 2 to 4).

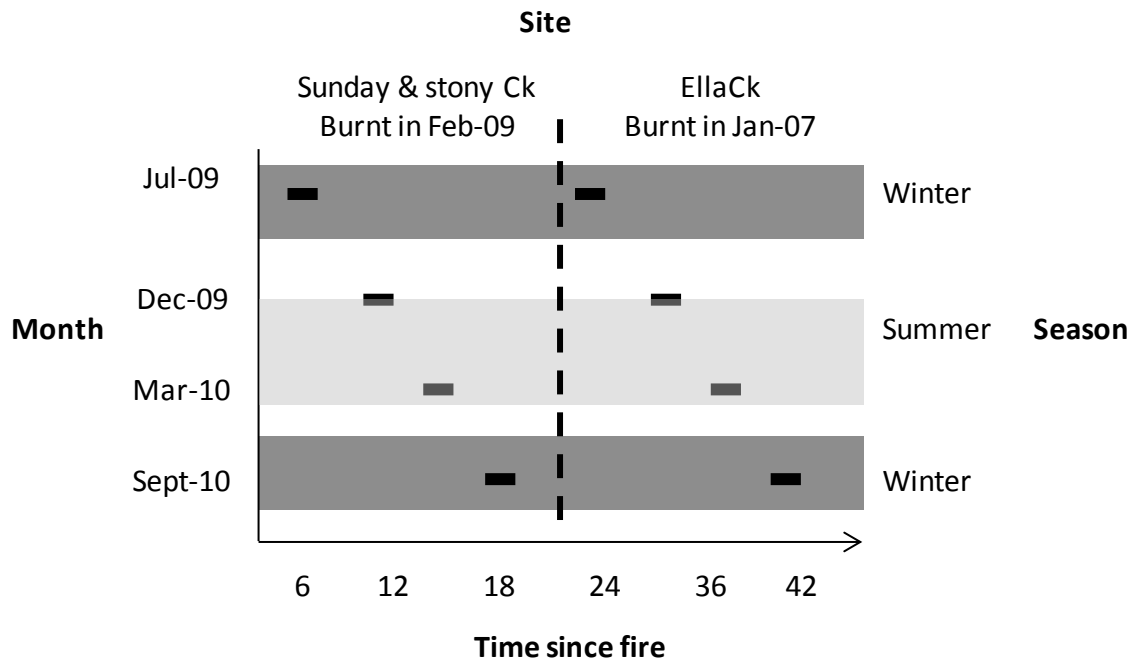


Figure 4.3 The date, time since fire and season for three sites sampled for infiltration rates, water repellency and soil moisture during four measurement campaigns to small headwater catchment in upland areas of eastern Victoria, southeast Australia. The solid black bold horizontal lines represent different sampling campaigns.

Soil samples were collected at 5 depth intervals (0-1, 1-3, 3-5, 5-7.5, 7.5-10 cm) at 10 m intervals along each of the three transects. The samples were a composite of cores (10 cm x 5.5 cm) collected at two points within the 1m quadrat in which the infiltration measurements (above) were performed. In many cases, the soil was too rocky in the vicinity of the infiltration experiments, in which case an area (not above) adjacent to the main transect was sampled instead. The samples were placed in sealed bags and transported back to the laboratory for measuring gravimetric water content and strength of water repellency at field moist conditions. Water repellency was measured on samples in the laboratory using ethanol solutions of different concentrations (0 - 6 M; 0.4 M intervals) and calculating the critical surface tension (*CST*) once three drops of solution penetrated the soil in 3 s (*CST* test) (King 1981; MacDonald and Huffman 2004).

The soil was mixed inside the sealed sampling bag before extracting a subsample which was placed on a petri-dish. Gravel and pebbles were removed from the sample in the petri-dish. Drops of ethanol solutions were then placed on the soil surface and the CST was established once three drops of the same surface tension solution penetrated in 3 s. The remaining soil from the original sample was oven dried at 105 degrees for 48 hrs in order to calculate the gravimetric water content (GWC). For samples collected in March, the soil was left to air-dry first in order to measure the air-dry *CST*. The soils were lightly sieved (< 2 mm) before the *CST* measurement were made on air dry soil samples. The water repellency was often high for soil in the 0-1 cm depth interval. However, the soil surface always seemed to be wet table and absorbed some water during infiltration. Measurements of *CST* were therefore carried on the soil surface during each sampling campaign in order to determine *CST* at $d_s = 0$. Litter was removed while ensuring that the soil was not disturbed prior to the test. The surface material was usually a mix of mineral soil, ash and organic material and was non-repellent in 95-100 % of sampled locations at each site.

4.2.5 Linking point and plot scale infiltration processes

Infiltration was measured in March 2010 at plots (2m x 1.5m) during 3 replicate rainfall simulations at a hillslope near Sunday Creek, southeast Australia (Figure 4.2). The plots were located on steep hillslopes (28°) in dry Eucalypt forest with clay loam soil that was burnt by wildfire in February 2009. The rainfall simulation design and procedure has been described in (Sheridan *et al.* 2007a) and also shown in Appendix D (Figure 5). The rainfall rate (target 100 mm h⁻¹) was first calibrated with steady state runoff from a plastic sheet covering the plot. The sheet was removed and discharge was measured in 0.5 l containers at regular intervals during the entire runoff period from rainfall which was applied at a constant rate for 30 min. An adjacent 1m x 1m plot was used as a test area for measuring infiltration at 4 points per rainfall simulation plot.

4.3 Results

4.3.1 Laboratory study: Flow and absorption in water repellent soil

The soils were water repellent at all sites (Figure 4.2). The measurements were obtained on air-dry soil samples (n = 36) which were collected in March 2010 as part of the broader sampling regime in the headwater catchments (Figure 4.3). The critical surface tension

(*CST*) was highly variable at each sampling depth apart from the lowest depth interval (7.5-10) where the *CST* was usually close to 72 (i.e. non-repellent). The spatial variability in *CST* within the most hydrophobic region of the soil was more skewed at Ella Creek than at the other two sites (Figure 4.3c). The different patterns of variability essentially show that water repellency was more homogenous in the recently burnt sites.

The $CST(d_s)$ function (4.3) explained 31, 17 and 24 % of variability in water repellency at Sunday Creek, Stony Creek and Ella Creek respectively when fitted across all sampling points ($n = 36$) and the parameter optimization was highly significant ($p < 0.01$) for all sites. When fitted to the mean *CST*, the function consistently explained more than 80 % of the variability in *CST* with depth, indicating that spatial variability was the main source of error when the function was fitted across all sampling points. The depth of minimum *CST* (i.e. maximum water repellency) was estimated from equation (4.4) to be 1.2, 1.8 and 1.3 cm for Sunday Creek, Stony Creek and Ella Creek respectively. The corresponding minimum value for *CST* (CST_{min}) was 40.1, 46.5 and 52.4 dyn cm^{-1} .

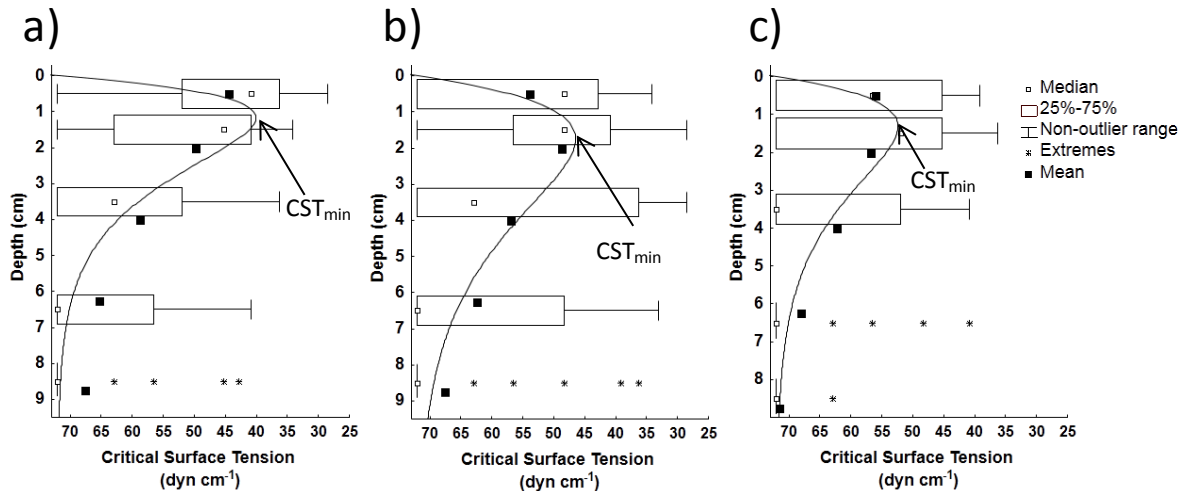


Figure 4.4 The strength of water repellency (critical surface tension) at different depths at a) Sunday Creek, b) Stony Creek and c) Ella Creek in Victoria southeast Australia. Ella Creek was burnt by wildfire in January 2007 and Stony Creek and Sunday Creek were burnt in February 2009.

A summary of soil physical and hydrological properties for the intact cores is provided for each study site in Table 4.2. The porosity and pore-size distribution values were obtained

from the intact cores once the infiltration experiments were completed and the cores were completely saturated ($h = 0$ mm). The porosity at Sunday Creek and Stony Creek was 0.34 and $0.41 \text{ cm}^3 \text{ cm}^{-3}$, respectively. A higher proportion of macropores ($r > 0.5$ mm = 4.7 % of θ_s) at Sunday Creek resulted in higher matrix flow potential (K_{mat} at saturation) at Sunday Creek (66 mm h^{-1}) than at Stony Creek (52 mm h^{-1}) despite Stony Creek having higher overall porosity. The porosity at Ella was higher (0.55) and the matrix flow potential at saturation was ~4 times higher than the two other sites. Porosity was inversely related to gravel content. The values are reported in Table 4.2 are provided as background to the interpretation of infiltration experiments in Figure 4.5. The hydraulic conductivity of repacked cores with wettable surface material (ash, gravel and soil) was 41 mm h^{-1} and 21 mm h^{-1} for Sunday Creek and Stony Creek respectively (Table 4.2). At saturation the mixture had a water holding capacity of $0.40 \text{ cm}^3 \text{ cm}^{-3}$.

Table 4.2 Soil hydrological properties measured on intact cores (~8 cm deep and 5.3 cm in diameter) from Sunday Creek, Stony Creek and Ella Creek in Victoria, southeast Australia

Site	Bulk Density	Gravel $D > 2\text{mm}$	Total Porosity θ_s	Macro-porosity ($r > 0.5\text{mm}$)	Macro-porosity ($r > 0.5$ mm)	Air-dry CST_{min}	K_s^a ($h = -15\text{mm}$)	K_{ash}^b ($h = -15\text{mm}$)
	n = 9	n = 9	n = 9	n = 9	n = 9	n = 24	n = 9	n = 5
	g cm^{-3}	% mass	$\text{cm}^3 \text{ cm}^{-3}$	%	$\text{cm}^3 \text{ cm}^{-3}$	dyn cm^{-1}	mm h^{-1}	mm h^{-1}
Sunday Creek	1.29	62	0.34	4.7	1.6×10^{-2}	40.1	66 (18)	41 (4.0)
Stony Creek	1.31	36	0.41	1.7	0.7×10^{-2}	46.5	52 (41)	21 (4.9)
Ella Creek	0.97	27	0.55	2.6	1.4×10^{-2}	52.4	240 (81)	n/a

^a This is the hydraulic conductivity of the cores when completely wetted at $h = -15$ mm.

^b Repacked cores contained a mixture of gravel, burnt soil and ash.

The initial soil moisture of all cores was equal after air drying. In subsequent measurements the soil moisture was consistently higher at Stony Creek than Sunday Creek but highest at Ella Creek (Figure 4.5a), reflecting an increasing trend in porosity. The effective hydraulic

conductivity K_{mat} was low relative to the true saturated conductivity (K_s) for all sites in the three first three sets of infiltration measurements (Figure 4.5b). The largest change in K_{mat} occurred between the third and the fourth set of infiltration experiments with cores from Ella Creek displaying a larger increase than the two other sites (Figure 4.5b).

The volumetric uptake ($\Delta\theta$) represents the change in mass between the initial and final content conditions for each 35 infiltration, without the storage ($\Delta\theta = \theta_i - \theta_f - V$). Surface storage volume (V) ($0.01-0.03 \text{ cm}^3 \text{ cm}^{-3}$) during early (non-steady) stage of infiltration was obtained from H , a fitted infiltration parameter from equation (4.1). The change in water content of cores before and after 35 min infiltration was relatively large ($0.08 < \Delta\theta < 0.15$) for first set of infiltration experiments (Figure 4.5c). The water uptake $\Delta\theta$ during infiltration was similar for the second and third set of measurements ($0.04 < \Delta\theta < 0.07$) (Figure 4.5c). In the fourth and last set of infiltration the pore space within the cores was completely saturated and there was a very small and $\Delta\theta \rightarrow 0$ (Figure 4.5c). At the last stage of wetting the K_{mat} was considered to represent the true K_s of the soil matrix ($h = -15\text{mm}$) (Table 2).

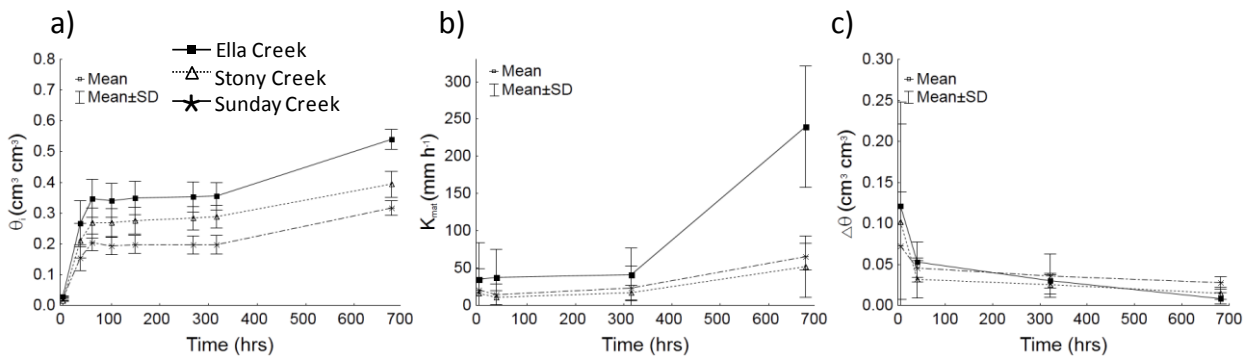


Figure 4.5 a) Initial soil moisture (θ_i) b) matrix flow potential (K_{mat}) and c) change in soil moisture ($\Delta\theta$) during infiltration into intact soil cores from Ella Creek, Stony Creek and Sunday Creek ($n = 9$) at different stages of wetting on a tension table. All values are for $h = -15 \text{ mm}$. The water uptake in c) was obtained from the mass of soil cores measured before and after each 35 minute infiltration.

The relationship between initial soil moisture (θ_i), effective conductivity (K_{mat}) and wetting rate ($\Delta\theta/t_{hrs}$) during different stages of imbibitions were combined across the three study sites by normalizing K_{mat} by saturated conductivity, K_s , and $\Delta\theta$ and θ_i by total porosity, θ_s (Figure 4.6). The normalized variables K_{mat}/K_s and $(\Delta\theta/\theta_s t_{hrs})$ were plotted as a function of

normalized initial moisture content θ_i/θ_s (the proportion of pore space that was active at the start of the infiltration measurement).

The wetting rate, $(\Delta\theta/\theta_s)/t_{hrs}$, declined linearly with increasing initial soil moisture θ_i/θ_s . This decline represents the effects of i) decreasing pore-space availability due to water repellent soil and ii) an overall decline in moisture deficit. The linear relation means that the wetting rate is proportional to initial soil moisture ($\Delta\theta/\Delta t = -\lambda\theta_i$), thus giving rise to an exponential relation between soil moisture and the duration of infiltration. However, the hydraulic conductivity remained relatively low ($K_{mat}/K_s < 0.4$) and constant while $\theta_i/\theta_s < 0.6$, indicating that some sections of the soil remained dry and hence inactive in the overall flow process. The hydraulic conductivity K_{mat} increased exponentially with increasing soil moisture when $\theta_i/\theta_s > 0.6$. The change in hydraulic conductivity with θ_i/θ_s could be represented by an exponential function which asymptoted at some minimum flow potential in dry and repellent soils. In summary the patterns of flow and absorption shows that the hydraulic conductivity was dependent on the rate at which pore space was activated and introduced to the infiltration process. The rate at which the soil matrix was activated was strongly dependent on initial soil moisture conditions. The data support the assumptions underlying the conceptual model of restricted flow in Figure 4.1

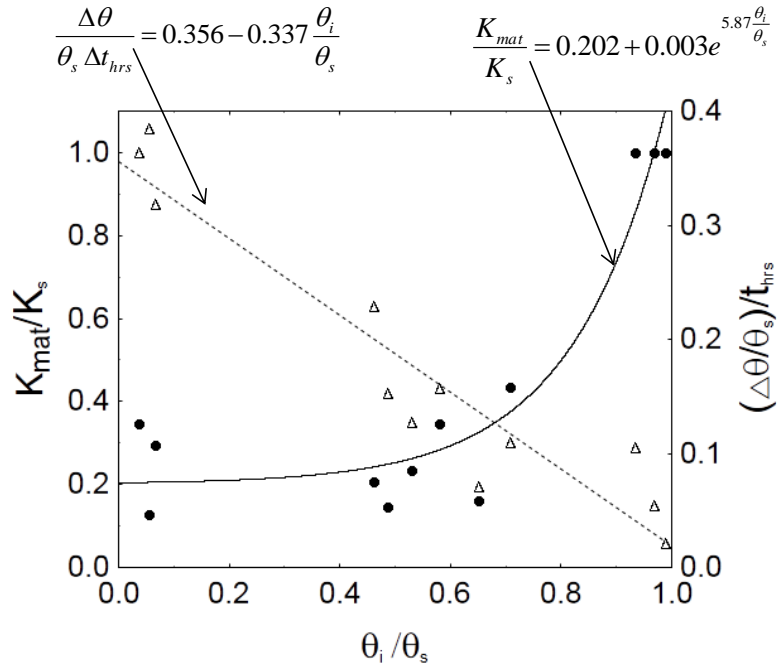


Figure 4.6 The normalized hydraulic conductivity (K_{mat}/K_s) and absorption rate $(\Delta\theta/\theta_s)/t_{hrs}$ as a function of initial soil moisture. The data was obtained from infiltration measurements on intact cores that were sampled from Ella, Stony Creek and Sunday Creek ($n = 9$) at 4 different stages of wetting (Figure 4.5). The normalized flow potential was fitted with an exponential function. Once this function equals 1, the matrix flow potential K_{mat} is equal to the full flow potential of the soil K_s and there can be no further increase in K .

4.3.2 Infiltration in burnt headwater catchments

The storage parameter (H) was obtained by fitting equation (4.1) to the mini-disc infiltration measurements (mm h^{-1}) at 1 min intervals. The steady state infiltration K_{mat} ($t > 6$ min) was retained as a fixed parameter in the regression. The soil hydraulic parameters obtained from four measurement campaign at Sunday Creek, Stony Creek and Ella Creek are given in Table 3. Soil moisture was highest in September 2010 after a relatively wet spring period. The normalized soil moisture decreased linearly ($R^2 = 0.61$) with increasing $KBDI$. Overall, the moisture deficit remained relatively high (> 0.5) despite $KBDI$ approaching 0 (Figure 4.7a) and the range of soil moisture contents ($0.10 < \theta_i/\theta_s < 0.43$) was low compared to the range achieved under laboratory conditions. There was no relationship between initial soil moisture and the matrix flow K_{mat} (Figure 4.7b). This may have been expected given that laboratory measurements (Figure 4.6) showed that K_{mat} is invariant with θ_i when $\theta_i/\theta_s < 0.6$.

The CST_{min} (dyn cm^{-1}) ranged from 24.8 – 43.1, 42.3 - 63.8 and 29.2 - 58.2 for Sunday Creek, Stony Creek and Ella Creek respectively (Table 4.3). The relation between CST_{min} with $KBDI$ was scattered which sites were combined without adjusting for the different background repellency. The aim however was to generalize the relation between $KBDI$, CST_{min} and hydraulic conductivity across dry eucalypt forest recovery from wildfire. The CST_{min} was therefore normalized by the lowest CST_{min} value (i.e. strongest water repellency) measured under field conditions, that way producing a relative measure (CST_{min}^+) which could be represented as a function of $KBDI$ (Figure 4.7c). Water repellency increased with increasing $KBDI$ although the soil remained repellent even when $KBDI$ was close to 0, indicating the water repellency is likely to be present during most weather conditions for these forest systems during recovery from wildfire. In terms of infiltration the persistence of water repellency meant that flow was always restricted by water repellent soil, and that the true saturated hydraulic conductivity (K_s) could not be measured under field conditions.

The strong relation between K_{mat} and CST_{min} indicate that water repellency was an important source of variability when soil moisture levels were lower than water repellency thresholds (Figure 4.7d). The matrix flow K_{mat} was most sensitive to changes in water repellency status for $CST_{min} > 40$. The potential flow under non-repellent conditions (K_s) was estimated to be $\sim 50 \text{ mm h}^{-1}$ by extrapolating a value for K_{mat} at $CST_{min} = 72.7 \text{ dyn cm}^{-1}$ (Figure 4.7d). The extrapolated value corresponds well with laboratory measurements of K_s for Stony Creek and Sunday Creek (Table 4.2) but is much smaller than the K_s measured on soil cores from Ella Creek.

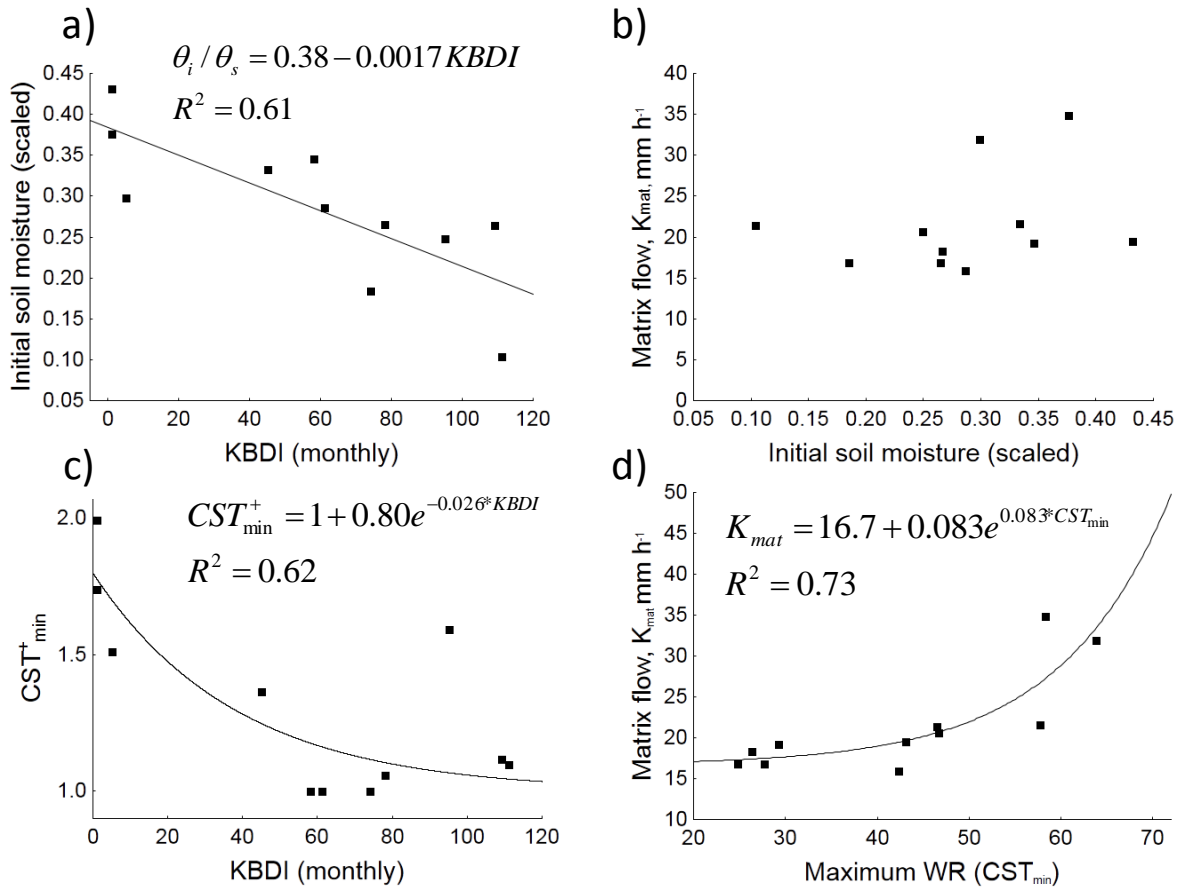


Figure 4.7 Soil hydrological properties of headwater catchments in dry Eucalypt forests during recovery from wildfire. a) Initial soil moisture versus KBDI. b) Matrix flow K_{mat} and soil moisture c) Normalised water repellency (CST_{min}^+) versus KBDI. d) The change in matrix flow K_{mat} with changing water repellency (CST_{min}). Each soil moisture and water repellency (CST) data point represents the average of 27 measurements made on composite samples collected from two points ($d_s = 0-10$ cm) at 9 locations along 3 transects (80 m) at Sunday Creek, Stony Creek and Ella Creek ($n = 27$). Each matrix flow K_{mat} data point is the average of 4 mini-disc measurement point in quadrats (1 x 1 m) at 3 locations along each of three sampling transects (total $n = 36$).

Table 4.3 Summary of soil hydrological properties and initial conditions for four separate measurement campaigns to headwater catchments in southeast Australia which were recovering from wildfire impacts.

Date	Sunday Creek							Stony Creek							Ella Creek						
	t_{sf}	$KBDI$	θ_i	CST_{min}	H	K_{mat}	K_p	t_{sf}	$KBDI$	θ_i	CST_{min}	H	K_{mat}	K_p	t_{sf}	$KBDI$	θ_i	CST_{min}	H	K_{mat}	K_p
	mo	-	$\text{cm}^3 \text{cm}^{-3}$	dyn cm^{-1}	mm	mm h^{-1}	mm h^{-1}	mo	-	$\text{cm}^3 \text{cm}^{-3}$	dyn cm^{-1}	mm	mm h^{-1}	mm h^{-1}	mo	-	$\text{cm}^3 \text{cm}^{-3}$	dyn cm^{-1}	mm	mm h^{-1}	mm h^{-1}
	-	-	n=27	n=27	n=36	n=36	n=36	-	-	n=27	n=27	n=36	n=36	n=36	-	-	n=27	n=27	n=36	n=36	n=36
Jul-09	6	89	0.09	27.6	1.9	16.7 (22.1)	56 (93)	6	26	0.14	57.7	3.6	21.7 (32.4)	32 (61)	30	1	0.21	58.2	1.2	34.9 (30.6)	371 (419)
Dec-09	10	66	0.06	24.8	1.6	16.9 (24.6)	63 (134)	10	62	0.12	42.3	2.9	16.0 (17.4)	40 (96)	34	54	0.19	29.2	1.2	19.3 (19.4)	162 (174)
Mar-10	13	32	0.09	26.3	1.8	18.3 (27.8)	83 (188)	13	151	0.04	46.5	3.7	21.5 (26.9)	27 (39)	37	86	0.14	46.6	1.3	20.7 (26.4)	306 (444)
Sept-10	19	0	0.15	43.1	1.2	19.6 (16.3)	142 (163)	19	16	0.12	63.8	1.0	31.9 (27.7)	70 (54)	43	0	0.28	45.1	1.8	10.3 (12.0)	109 (196)

Macropores can contribute to a high proportion of flow in forest soil when given abundant supply of water. Macropore flow was quantified by subtracting matrix flow (K_{mat} ; $h = -15$ mm) from ponded flow (K_p ; $h = 5$ mm) (Table 4.3). The difference in flow was then expressed relative to K_{mat} ($\Delta K/K_{mat}$), and scaled by macroporosity ($r > 0.5$ mm) (Table 4.3) in order to provide a scaled measure of macropore flow (K_{mac}^+) which was independent of site and water repellency status. The normalized macropore flow was also calculated for a south-facing headwater at Sunday Creek ($n = 24$ at each time step) and a wet Eucalyptus forest using infiltration data from Nyman et al. (2010).

The data from all the sites were plotted as a function of time since fire (Figure 4.8a). In general there was a linear increasing in the scaled macropore flow during recovery of burnt catchments, indicating that the fire has a large impact on macropore availability. The variable cluster of points at 2-3.5 yrs after fire is from Ella Creek which was the site that had recovered the most. The macropore flow at Stony Creek was lower than expected at two time-steps. This site had the lowest overall macroporosity (Table 4.2) and was the only site located on a metamorphic geology.

The storage potential (H) was normalized by the moisture deficit (θ_d) and the overall pore-space availability (θ_s) at each site to produce a scaled storage variable, H^+ , shown as a function of time since fire in Figure 4.8b. Storage declined exponentially with time since fire. The initial storage after the burn was not measured and some material had been lost through wind and water erosion prior to the first field campaign. An extrapolated value at $t = 0$ would yield an H^+ of 11.1 which is equal to 4.4 mm of actual storage (H) given an average volumetric storage potential (θ_s) in surface material of $0.40 \text{ cm}^3 \text{ cm}^{-3}$. At Ella Creek (> 30 months after fire) the storage potential (H) was on average ~ 1 mm.

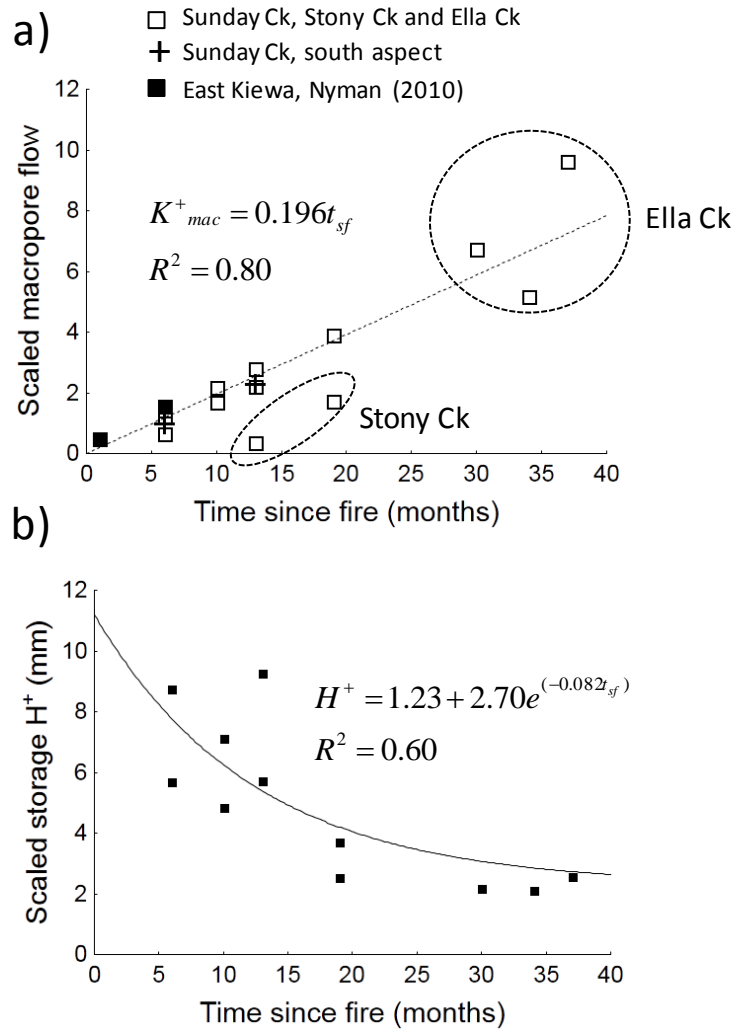


Figure 4.8 a) Scaled a) macropore flow and b) storage as a function of time since fire. The changes in macropore flow during recovery was analysed using infiltration data from Sunday Creek South ($n = 24$) and East Kiewa (Nyman *et al.* 2010) in addition to data from the three main study site at Ella Creek, Sunday Creek and Stony Creek.

4.3.3 Point to plot scale infiltration

The infiltration parameters derived from the mini-disc infiltration measurements at Sunday Creek were evaluated against runoff data from rainfall simulation plots. The aim was to determine how point scale infiltration measurements compare with infiltration rates measured in large plots (3 m^2) under simulated rainfall. The average steady state infiltration was higher and more variable for the mini-disc infiltrometer ($K_{mat} = 10.1 \text{ mm h}^{-1} \pm 10.1$) than under the rainfall simulation plot (steady state infiltration = $7.9 \text{ mm h}^{-1} \pm 3.65 \text{ SD}$) (Figure 4.9a). The time to ponding t_p for a steady state rainfall input R was estimated from tension infiltrometer data as;

$$t_p = H/(R - K_{mat}) \quad 4.7$$

The time to ponding was then combined with steady state infiltration model and kinematic wave equations in order to model the hydrograph from steady state rainfall (Figure 4.9b) (Brutsaert 2005p. 201). The infiltration excess was routed assuming a relationship between water depth (h_w , mm), friction slope (S_f) and average velocity (v , mm h⁻¹);

$$u = C_r h^2 S_f^{-1} \quad 4.8$$

where C_r is a resistance factor (Brutsaert 2005 p. 172). The time to equilibrium, the buildup-phase and the decay-phase were modelled through approximate solutions to the kinematic wave equation under steady lateral rainfall input (R). The hydrograph modelled using mini-disc parameters (H and K_{mat}) corresponded well with the runoff measurements from plot-scale rainfall simulations (Figure 4.9b). The ponded infiltration (25 mm h⁻¹) reflects the maximum infiltration potential of the soil and was ~2.5 time higher than the steady infiltration rate under simulated rainfall. The actual areal infiltration rate for rainfall events on hillslopes where $R \gg K_{mat}$ is likely to be somewhere between K_{mat} and $K_{mat} + K_{mac}$ (e.g. Smith and Goodrich 2000). Overall, the rainfall simulations showed that centimetre-scale infiltration measurements can be an effective way to parameterize infiltration models for plot-scale runoff.

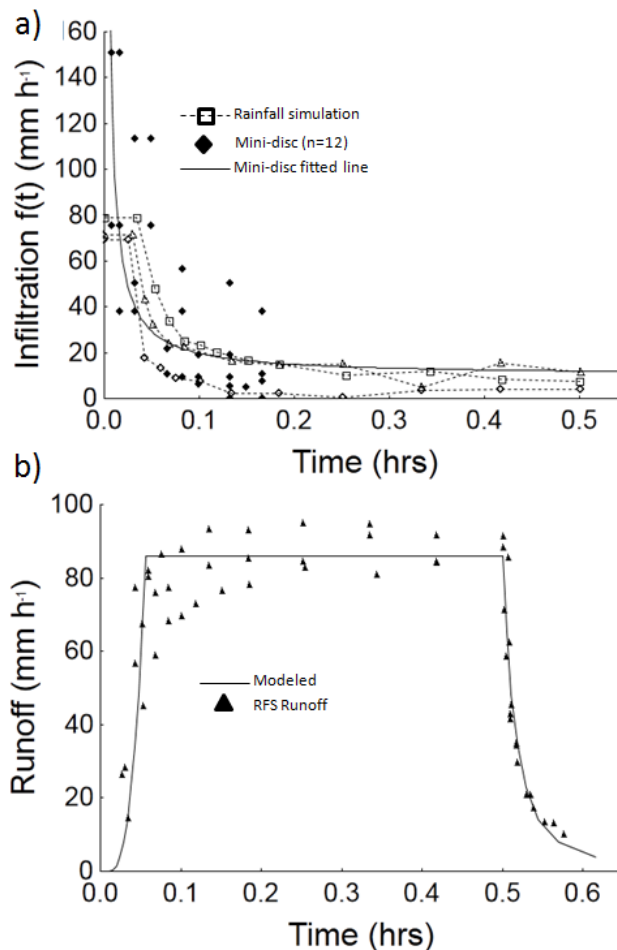


Figure 4.9 a) The infiltration rate for tension infiltrometer measurements ($n = 12$) and rainfall simulation plots ($2 \times 1.5 \text{ m}$; $n = 3$) at Sunday Creek in March 2010. A storage based infiltration equation (4.1) was fitted to all 12 replicate tension infiltrometer measurements and shown as a single function representing the average infiltration for the three plots. b) The runoff from rainfall simulation plots (data points) and the modelled hydrograph using the parameters from the fitted function in a).

4.4 Discussion

The effects of surface storage, water repellency and macropores on infiltration in burnt soils were quantified using infiltrometers and a storage-based infiltration model. The model was used to quantify the interaction between storage (H), water repellency (CST_{min}), soil moisture (θ_i), hydraulic conductivity (K_{mat}) and macropore flow (K_{mac}) during infiltration in soils that were burnt by wildfire. Both laboratory and field measurements showed that strength of water repellency was driving weather dependent changes in hydraulic conductivity (K_{mat}) of the soil matrix. The slow wetting rate in

repellent soils meant that the soil required long exposure to wet conditions before reaching full flow potential (K_s). On recently burnt hillslopes the soil surface was generally non-repellent and capable of storing up to 4 mm of water, thereby buffering subsurface soils from participating in the infiltration process in a similar way to what has been described for burnt systems elsewhere (e.g. Ebel *et al.* 2012; Woods and Balfour 2008). The surface material contained ash, but was actually a mixture of ash, gravel, burnt soil and charred organics that eroded or was incorporated back into the soil profile during recovery.

Water repellency at the study sites in southeast Australia displayed consistent trends with depth, peaking at soil depths of 1 - 3 cm, and largely non-repellent at the soil surface and at depths > 8 cm. Similar patterns of variability with depth has been observed in water repellent forest soils elsewhere (Benavides-Solorio and MacDonald 2001; DeBano 2000; Doerr *et al.* 1996; Doerr *et al.* 2000; MacDonald and Huffman 2004; Miyata *et al.* 2007; Nyman *et al.* 2011). This means that the water repellency function, $CST(d_s)$ in equation (4.3), could be useful for characterizing repellency in other burnt systems. Overall the sites displayed moderate to extreme repellency with air-dry soils on the most recently burnt sites (0.5 years after fire) being more repellent than air-dry soils from Ella Creek. Variability in water repellency status (CST_{min}) with degree of dryness is consistent with other studies of water repellent soils (Burch *et al.* 1989; Crockford *et al.* 1991; Leighton-Boyce *et al.* 2005; Sheridan *et al.* 2007a).

Moisture induced changes to water repellency (CST_{min}) took place over long timescales and the wetting rate was therefore considered to be a 'dryness' related process and represented as a separate process to infiltration during storms. Separating between the two processes is consistent with concepts presented in Moody and Ebel (2012) which show that infiltration into water repellent and dry soils may be controlled diffusion-adsorption processes (timescale: days to weeks) rather than capillary and gravity driven processes (timescale: minutes to hours). The system contrasts however with common infiltration models that assume that hydraulic conductivity changes as a function of matrix potential and a wetting front that advances uniformly into the soil. The hydraulic conductivity K_{mat} was strongly dependent on the availability of actively conducting pore-space. Laboratory experiments showed that K_{mat} remained at $< 40\%$ of K_s while the relative soil moisture (θ_i/θ_s) was < 0.80 . The magnitude of the water repellency

effect on hydraulic conductivity (K_{mat}/K_s) is similar to the 60-70 % reduction in wet Eucalypt forest (Nyman *et al.* 2010; Sheridan *et al.* 2007a) and the range of impacts reported for forest soils in some other places (Imeson *et al.* 1992; Leighton-Boyce *et al.* 2007). Hydraulic conductivity (K_{mat}) increased exponentially with θ_i when $\theta_i/\theta_s > 0.8$ which means that the last 20 % of pore-space within the core was contributing disproportionately to the overall hydraulic conductivity of the soil matrix. The slow wetting rate for $\theta_i/\theta_s > 0.8$ and the exponential dependency between K_{mat} and θ_i for $\theta_i/\theta_s > 0.8$ suggests that the hydraulic conductivity was restricted by a water repellent layer that acted as a cross-sectional ‘throttle’ for flow.

The slow wetting rate of the water repellent layer meant that the matrix never reached full potential (K_s) under field conditions, and that water repellency was restricting flow even under relatively wet conditions. Temporal variability in hydraulic conductivity due to weather dependent water repellency dynamics was modelled at inter-storm timescales by linking CST_{min} with the Keech-Byram Drought Index ($KBDI$) which varies over time as function of rainfall and temperature. Both soil moisture and CST_{min} declined with increasing $KBDI$. The CST_{min} displayed consistent trends with $KBDI$ and was driving variability in K_{mat} . There was considerable scatter caused by different background conditions at the three study sites so the model of $KBDI$ -dependent changes in water repellency was improved by normalizing CST_{min} values by CST_{min} for the most severe water repellency conditions at the site (e.g. Karunarathna *et al.* 2010). Soil moisture (θ_i/θ_s) declined linearly with increasing $KBDI$, but the range of soil moisture conditions was too low to drive temporal variability in K_{mat} .

Initially after fire, the soil surface was capable of storing ~4 mm of rainfall which is in the lower range of values from recently burnt hillslopes in Colorado (3.6 - 5.5 mm) (Ebel *et al.* 2012). The wettable surface material was on average of 1 cm deep and had a water holding capacity of $0.40 \text{ cm}^3 \text{ cm}^{-3}$ which was low compared to the range of values (0.58 – 0.95) reported for ash in the literature (Cerdà and Doerr 2008; Ebel *et al.* 2012; Leighton-Boyce *et al.* 2007; Woods and Balfour 2008). This may be explained partly by the high gravel content of 36 and 62 % (by mass) at Stony and Sunday Creek, respectively. Under field conditions the surface storage (H) declined exponentially with time since fire and asymptoted towards a background storage capacity of ~1.2 mm. The decline in storage was primarily caused by erosion.

The hydraulic conductivity of surface material at Stony Creek and Sunday Creek was high compared to a K_s of 8.6 mm h^{-1} for ash reported in Colorado (Ebel *et al.* 2012), lower than 51 mm h^{-1} in Montana (Woods and Balfour 2008) and much lower than values for other laboratory measurements ($138 - 600 \text{ mm h}^{-1}$) on repacked cores (Bodí *et al.* 2012; Woods and Balfour 2010). Without gravel the K_s of ash/surface material ($< 2 \text{ mm}$) at Stony Creek became much lower (6.8 mm h^{-1}) while it remained high at Sunday Creek (36.4 mm h^{-1}). At Stony Creek the hydraulic conductivity in the field ($16.0 - 21.5 \text{ mm h}^{-1}$) was equal to the hydraulic conductivity of surface material ($K_{ash} = 21 \text{ mm h}^{-1}$) on two occasions during the sampling campaign within the first year of the fire (Table 2), suggesting the K_{ash} may be restricting flow while hillslopes were mantled by burnt soil/ash. The effect of water repellency was stronger however, under really dry conditions when the $K_{mat} < K_{ash}$. At Sunday Creek the matrix flux (K_{mat} : $16.7 - 19.6 \text{ mm h}^{-1}$) was always less than the saturated hydraulic conductivity of ash/surface material ($K_s = 41 \text{ mm h}^{-1}$).

The linear increase in macropore availability during recovery shows that the surface of ash and burnt soil limits gravity driven flow through structural components of the soil. The exact mechanism underlying the effect was not established but previous studies have shown that ash/burnt soil lacks structure and can limit flow by acting as a restricting layer and/or by clogging of exiting macropores within the soil profile (Ebel *et al.* 2012; Mallik *et al.* 1984; Nyman *et al.* 2010; Onda *et al.* 2008; Woods and Balfour 2010). The role of macropore flow (K_{mac}) on infiltration during storm events is dependent on the scale and rainfall intensity. The rainfall simulation shows that macropores were largely inactive and that K_{mat} was a better predictor of infiltration than the overall infiltration capacity (K_p) which is the sum of matrix and macropore flow ($K_{mat} + K_{mac}$). The effect of K_{mac} on infiltration is likely to increase with increasing rainfall intensity and increasing spatial scale. This is because large scale measurements increase supply of water to macropores through ponding and increase the probability of activating macropores due to a larger proportion of the hillslope being inundated (Davis *et al.* 1999; Leonard *et al.* 2004; Sheridan *et al.* 2007a).

The results from infiltration measurements in headwater catchments were used to model the spatial and temporal variability in infiltration processes as a function of time since fire (t_{sf}) and the degree of dryness ($KBDI$) as determined by monthly weather patterns.

The relations underlying the model can be summarised as follows. Water repellency was represented by the minimum critical surface tension (CST_{min}) in the soil profile which increased exponentially with decreasing $KBDI$ (i.e. the strength of water repellency decreased exponentially as the monthly $KBDI$ approached wet conditions). The matrix flow (K_{mat}) in turn, increased exponentially with increasing CST_{min} . The storage potential (H) declined exponentially with t_{sf} , due to the loss of a discrete layer of wettable surface soil. At the same time, the macropore flow increased linearly with t_{sf} due to increased macropore availability during recovery from the fire impact. The relations are given as empirical equations in Figures 4.7 and 4.8. In future work we will aim to model infiltration during actual storm events and test these relations against observed runoff responses from burnt hillslopes

4.5 Conclusion

The overall objective of the study was to identify key properties contributing to variability in infiltration during recovery from wildfire and to quantify their effect. A storage base infiltration model was used as framework for analysing infiltration data which was obtained in the laboratory on intact cores and in the field. The model fitted the data well and could be used effectively to partition the infiltration process into its key components of storage, matrix flow and macropore flow. Infiltration on intact cores showed that a water repellent layer acted as a throttle on flow and that the soil moisture status of the soil therefore could have large effects on the overall flow potential of the soil matrix. The slow wetting process in the water repellent layer meant that only after prolonged exposure to saturated conditions did the soil become fully saturated and able to conduct water at its full potential. In headwater catchments that were recovering from wildfire ($t_{sf} < 3.5$ years) the soils always displayed some degree of water repellency resulting in incomplete saturation, which meant that the maximum flow potential of the soil (K_s) could not be measured in the field. The variability in the infiltration capacity (K_p) was driven primarily by changes in macropore availability but also by temporal variability in water repellency due to monthly weather patterns. The storage potential in of the surface soil was initially high after wildfire but declined exponentially during recovery. The results could be organised into a series of equations which link variability in infiltration parameters to recovery processes and the moisture conditions of the soil.

Chapter 5: Sediment availability on burnt hillslopes

Paper currently in review with *Journal of Geophysical Research – Earth Surface*:

Nyman, P., G. J. Sheridan, J. A. Moody, H. G. Smith, and P. N. J. Lane (2011), Sediment availability on burnt hillslopes. *Submitted in December 2012*

Abstract

In general, erosion has been modelled as being proportional to some form of energy or force (such as shear stress or stream power) with the proportionality constant being erodibility, which is a characterization of sediment availability. Erosion models typically consider this property as constant with soil depth. However, observations of erosion following fire indicate that erosion often occurs predominately through the removal of shallow and highly erodible layers of ash, charged organics and mineral soil. We hypothesise that the depth of this highly erodible layer is a primary control on post-fire erosion. This study used both field- and laboratory based experiments to quantify sediment availability as a depth-dependent parameter on burnt hillslopes. Results from flume experiments on intact cores showed that erodibility of fire-affected soil was highest at the soil surface and then declined dramatically within the top 2 cm of the soil profile. Fine roots (< 2 mm diameter) were found to provide cohesion and reduce the erodibility of surface soils. The soil depth and root density accounted for ~60 % of variation in the erodibility at soil depths < 2 cm. At greater depths the root effect diminished and other soil properties (% silt and clay in particular) became more important as predictors of erodibility. In field measurements, the fire-effect on sediment availability was captured by assuming that burning produces a non-cohesive soil layer of variable depth. This depth was characterized as a probability density function with a single parameter that changed during recovery (0-3 years) as the available soil was depleted. Measurements in southeast Australia found that initially after a wildfire, the hillslope had a layer (0.75-0.91 cm in depth) of non-cohesive soil, which represented 97-117 t ha⁻¹ of transport limited sediment. The thickness of this layer decreased exponentially with time since the wildfire, to 0.04 cm (< 5 t ha⁻¹) after 3 years of recovery. The results are organized into a conceptual framework for modelling fire-effects on sediment availability for systems with low and high pre-fire erodibility. The fire-effect produces an equal depth of non-cohesive soil for both systems but this represents a greater perturbation for systems with low pre-fire erodibility than for those systems with a high pre-fire erodibility.

5.1 Introduction

The interaction between sediment availability and transport ultimately determines how hillslopes respond to erosive rainfall events during the recovery from fire impacts (Cannon *et al.* 2001b; Lane *et al.* 2006b; Moody and Martin 2001a; Sheridan *et al.* 2007a). Wildfire and prescribed fire impacts sediment availability through soil heating and combustion of aboveground vegetation, litter and organic material within the soil (Hungerford *et al.* 1991). The heat pulse into the near-surface soil can result in the lethal heating and combustion of organic binding agents including roots, hyphae and humus, thereby reducing soil structure and cohesion (DeBano *et al.* 2005; Giovannini and Lucchesi 1983; Hart *et al.* 2005; Moody *et al.* 2005; Neary *et al.* 1999). Vegetative ash acts as an additional source of material which is initially deposited as non-cohesive and easily eroded material (Gabet and Sternberg 2008).

Erodibility is a term used to characterize sediment availability and is generally defined as the ease with which material is detached by flow. It is the inverse of soil resistance to erosion and determines how much sediment is detached per unit energy or force applied by overland flow. It is applied as a parameter in commonly used erosion models (eg. WEPP and EURSEM; Laflen *et al.* 1997; Morgan *et al.* 1998; Nearing *et al.* 1989). Erodibility is a function of the physical, chemical and biological factors that contribute to the formation of a cohesive and structured soil matrix (Grabowski *et al.* 2011; Jenny 1994; Tisdall and Tisdall 2006). It is a site specific parameter which can be estimated from empirical studies of sediment detachment in flumes and hillslope erosion experiments in different landscapes at different stages of disturbance (Elliot *et al.* 1989; Robichaud *et al.* 2010; Sheridan *et al.* 2007a).

The effect of ash input and burning on soil properties is usually restricted to near surface soils with soil heating rarely extending more than 5 cm into the soil profile (DeBano *et al.* 2005; Hungerford *et al.* 1991). This results in a layered soil profile with strong anisotropic variability in soil structure near the surface. The fire-effect on sediment availability in this layered system can be conceptualized as change in the depth of soil that displays low or no cohesion (i.e. no detachment required prior to transport) (Figure 5.1). The initial production of non-cohesive soil, the recovery of the soil-vegetation system, and depletion of the finite pool of erodible soil are poorly understood and not represented explicitly in post-fire erosion models.

Measuring the erodibility of burnt soils in overland flow experiments is problematic due to large changes in sediment availability during the experimental period over which the parameter is determined (Moffet *et al.* 2007; Robichaud *et al.* 2010; Sheridan *et al.* 2007a). By measuring erosion under steady-state conditions the erodibility parameter represents a time-averaged constant, which may lead to underestimation of the true erodibility of the soil surface. This is because the sediment availability within the test area is depleted and shifts towards a detachment limited domain within the experimental period. A time averaged parameter may therefore lead to underestimation of sediment loads for individual high-magnitude erosion events on recently burnt hillslopes. The role of initial sediment availability and depletion are likely to be particularly important when the aim is to estimate magnitude of loads generated by a few storm events when both the initial supply and rate of depletion can affect the sediment flux at the end of a hillslope. Such events often occur in response to short and high intensity rainfall and can account for a large proportion of the overall sediment that is generated from burnt areas (Cannon *et al.* 2001a; Lane *et al.* 2011; Moody and Martin 2001a; Smith *et al.* 2011a).

The aim of the studies described in this chapter was to develop a new framework for explicitly representing spatial changes in sediment availability as a result of wildfire disturbance. The hypotheses were that i) erodibility of fire-affected soils varies with root density and the depth below the surface, that ii) this variability results in a dependency between sediment flux and soil loss, and that iii) this dependency is captured by using the depth of non-cohesive material as a measure of wildfire effect. These hypotheses were tested with data from three experiments. The specific objectives of these experiments were to:

- i) measure detachment rates as a function of depth in controlled laboratory experiments, and to evaluate the effect of roots and soil physical properties on detachment rates,
- ii) evaluate the temporal changes in sediment availability in the field by simulating overland flow in bounded erosion plots, and
- iii) link spatial and temporal variations in soil shear strength to the availability of non-cohesive material on hillslopes that were recovering from wildfire.

The results from the experiments were combined into a framework for quantifying wildfire effects on sediment availability in systems with different background (or intrinsic) soil properties. The framework was developed to provide a basis for explicitly linking sediment availability to measures of fire severity, soil heating and sediment depletion.

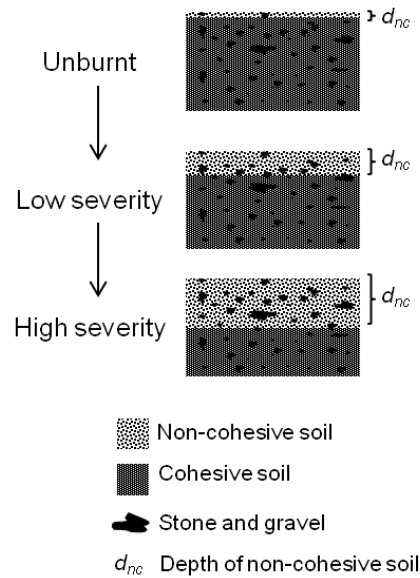


Figure 5.1 A conceptual representation of fire-effects on sediment availability in forest soils.

5.2 Methods

5.2.1 Overview

The method was set out to determine the factors controlling sediment availability on burnt hillslopes using both field and laboratory based approaches. A laboratory study was conducted using a tilting flume and intact soil cores collected from three contrasting sites in western USA, representing different ecosystems and geological settings. These experiments were designed as an in-depth study of the factors that drive variations in erodibility with depth. In the field-based experiments we used flume measurements on hillslopes in southeast Australia to determine the depth of transport limited erosion (i.e. depth of non-cohesive soil). This non-cohesive soil depth was linked to a critical shear strength determined by shear vane measurements in areas adjacent to the flume beds. This critical shear strength provided a method of using simple shear vane measurements to determine the depth of non-cohesive soil in burnt headwater catchments of southeast Australia. The measurement technique allows for

extensive sampling of spatially variable soils and is simpler and less resource intensive to carry out than flume experiments. Table 5.1 provides a summary of site characteristics and the location study sites are shown in Figure 5.2.

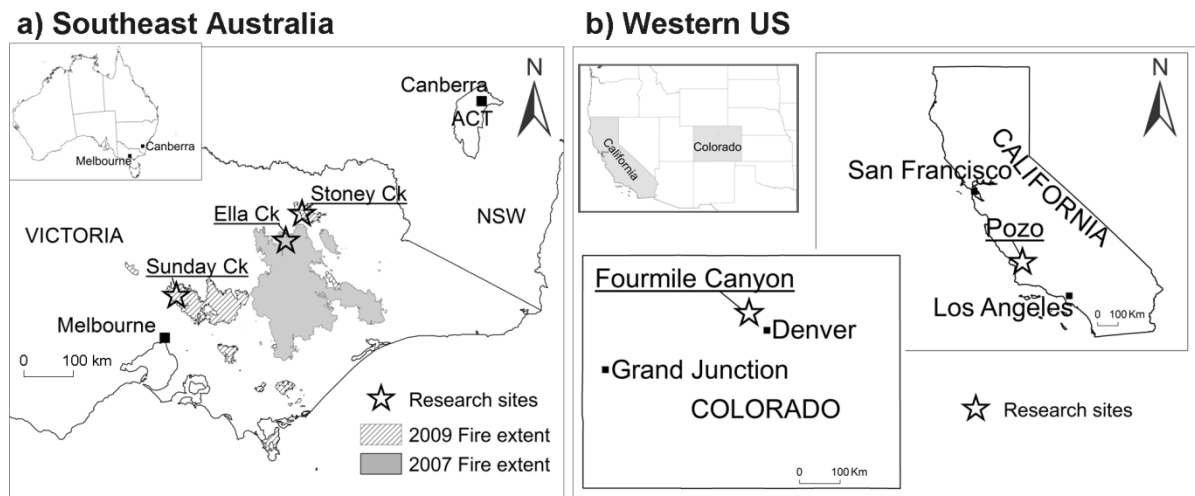


Figure 5.2 Map showing the location of research sites in a) southeast Australia (Sunday Creek, Stony Creek and Ella Creek) and b) western US (Fourmile Canyon in Colorado and Pozo in California).

Table 5.1 List of research sites used in different components of the study.

Site	Aspect ^a	Burn impact	Annual Rainfall mm	Forest Type and dominant vegetation	Geology	Soil texture / Bulk density, BD (0-5 cm) (g cm ⁻³)
<u>Laboratory Study – Western United States</u>						
Fourmile Canyon	South	Oct-2010	500-600	Coniferous Ponderosa Pine (<i>Pinus ponderosa</i>)	Granite	Stony and gravelly sandy loams BD =1.34
Fourmile Canyon	North	Oct-2010	500-600	Coniferous, Douglas Fir (<i>Pseudotsuga menziesii</i> subspecies <i>glauca</i>)	Granodiorite	Coarse to fine stony sandy loams BD =1.21
Pozo	South	Aug-2010	500-600	Chaparral, Manzanita (<i>Arctostaphylos sp.</i>), Chamise (<i>Adenostoma sp.</i>),	Marine sedimentary	Fine clay loam BD =1.27
<u>Field Study - southeast Australia</u>						
Ella Creek,	North	Jan-2007	1200-1400	Dry Eucalyptus, Broad-leaved peppermint (<i>E. radiata</i>) Narrow-leaved peppermint (<i>E. dives</i>)	Shale, Marine Sedimentary	Stony and gravelly clay loam BD = 0.94
Sunday Creek	North	Feb-2009	1000-1200	Dry Eucalyptus, Broad-leaved peppermint (<i>E. radiata</i>)	Siltstone, Marine Sedimentary	Stony and gravelly clay loam BD = 0.97
Stony Creek	North-west	Feb-2009	1000-1100	Dry Eucalyptus, Broad-leaved peppermint (<i>E. radiata</i>)	Phyllite & Gneiss Metamorphic	Gravelly clay loam BD =1.14

^aAspect effects are reversed in terms of solar radiation in southeast Australia versus Western US

5.2.2 Effects of roots on erodibility (laboratory study)

5.2.2.1 Sampling of intact cores and depth-stratified soil segments

The sampling strategy was designed to provide i) intact cores for quantifying detachment rates at different soil depths in a laboratory flume and ii) soil samples for measuring soil properties (roots density, root length density, loss on ignition, bulk density and % silt and clay) at 5 depth increments between 1-10 cm. Soils were sampled from the Fourmile Canyon Fire, Colorado and the Pozo Fire, central California (see Table 5.1 and Figure 5.2 for site details on site location and attributes). Further information on sampling protocol and site characteristics are provided in Moody and Nyman (2012). Three sets of soil samples were collected at each site in three clusters (sampling areas approximately 4 m²), each randomly located along a transect running parallel to the flow line (Figure 5.3). Each set of soil samples was comprised of:

- i) Five intact soil cores (length = 7.5 cm, diameter = 4.7 cm), used for the flume experiments.
- ii) Three soil samples collected in cylindrical cores (length = 10 cm, diameter 4.7 cm) from 5 depth intervals (0-1, 1-3, 3-5, 5-7.5, 7.5-10 cm) for measuring bulk density, organic matter (loss on ignition) and particle-size distribution.
- iii) Three soil samples from 5 depth intervals (same as above) for measuring root properties.

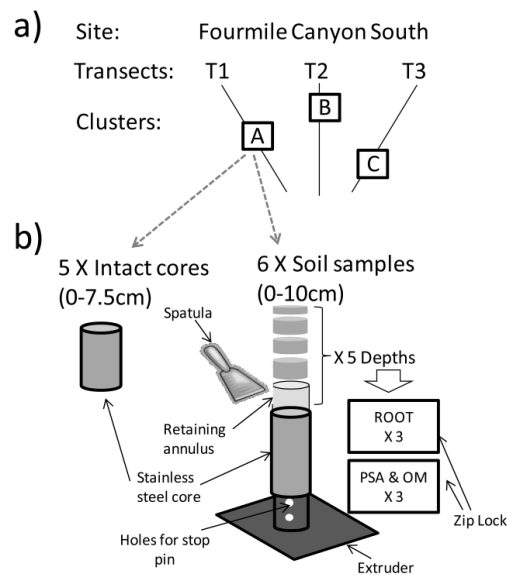


Figure 5.3 Upper section a) shows the location for collecting cluster samples (A, B, and C) along transects (T1, T2, and T3) from one site called Fourmile Canyon South. b) Lower section shows the details of the method of collecting subsamples of the soil core. See Appendix E (Figure 1) for photo of sampling technique.

5.2.2.2 Tilting flume – variations in erodibility with depth

The depth dependent detachment rates is difficult to quantify in the field due to depletion effects and the transport limited erosion that can occur during the initial stages of flow experiments. Therefore a laboratory flume was used to quantify the change in erodibility with depth in similar manner to Nachtergaele and Poesen (2002) (Figure 5.4). The detachment rate was measured based on the material delivered from intact cores at five target depths (0, 1-2, 2-3, 4 and 5-6 cm) at four levels of shear stress (2.2, 6.3, 14.4, and 42.1 Pa). The shear stress was calculated using equation 1 with additional acceleration terms added to account for non-uniform flow across the test area. The measurements were recorded during the experiments in units of dynes, cm and grams to be consistent with the scale of measurement (Moody and Nyman 2012). However, in this paper we report the shear stress (τ_f) and erodibility(k_d) in SI units (Pa and $s\ m^{-1}$, respectively) to be consistent with measurements presented elsewhere.

The shear stress was obtained through four combinations of slope and flow depth: i) 0.053, 0.3 cm; ii) 0.053, 0.60 cm; iii) 0.088, 1.10 cm; and iv) 0.177, 1.05 cm. The slope of the flume bed was adjusted using a tilting device built into the base of the flume. The flow was adjusted to the required depth using a manual flow valve. The shear stress, τ_f (Pa), was calculated as the product of slope, S , and water depth, h_w ,

$$\tau_f = \rho g h_w S \quad 5.1$$

where ρ is density of water ($1.0\ kg\ m^{-3}$), and g is acceleration of gravity ($9.8\ m\ s^{-2}$).

Detachment rates were calculated based on the total mass of material ($>0.063\ mm$) eroded after 12 L of flow. In some cases at the third depth interval (2-3cm), the soil core had to be sliced in order to expose a new surface after extruding the soil (see extruder in Figure 5.4b). On these surfaces the material was collected over a longer time-interval in order to reduce the impact of disturbance effects due to slicing. Further details on flume specification and data collection are provided in Moody and Nyman (2012). A photo of the flume is provided in Appendix E (Figure 2).

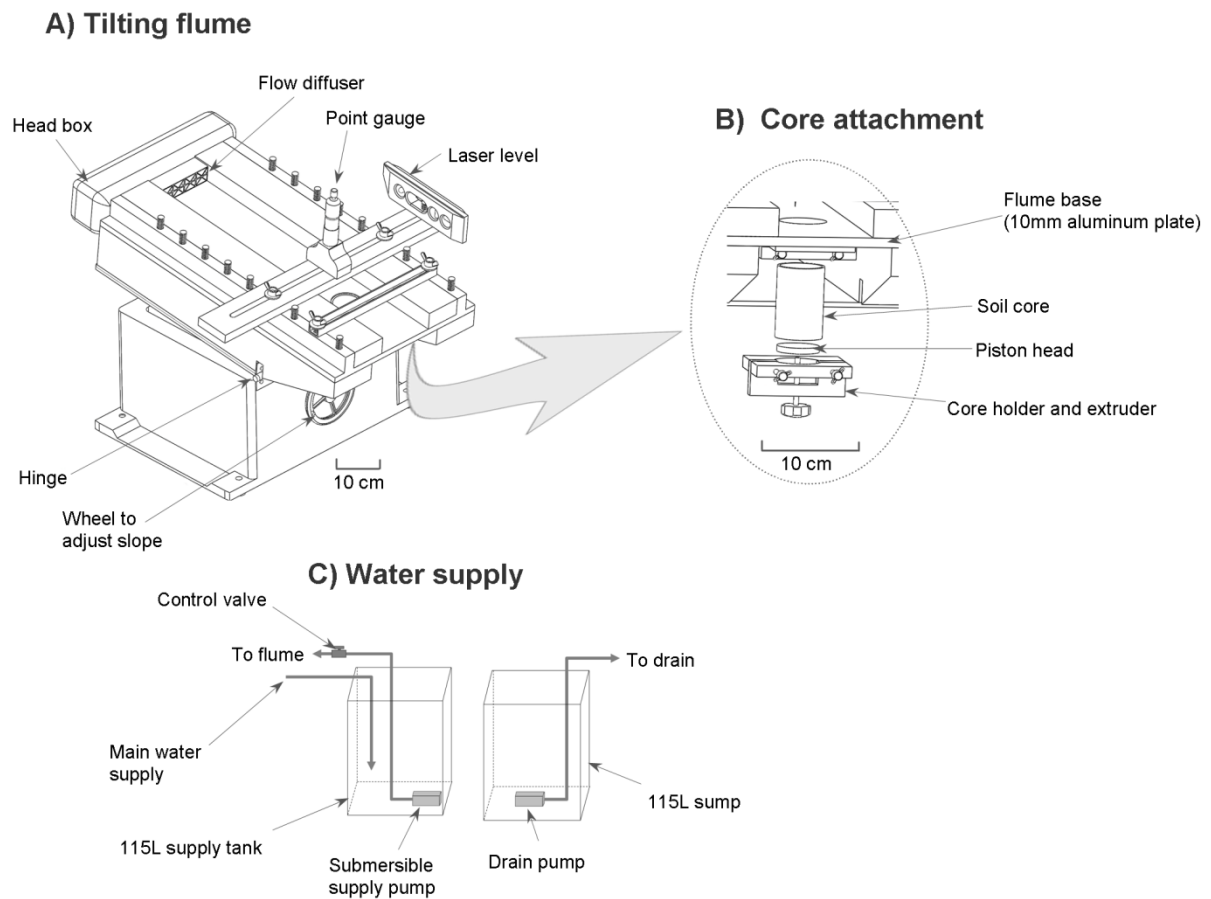


Figure 5.4 The components of the a) tilting flume, b) the core attachment and extruding device and the c) water supply system. Additional flume specification available in (Moody and Nyman 2012).

5.2.2.3 Soil analysis - variation in soil and root properties with depth

The 15 soil samples from each site were processed for particle size by using standard sieve methods (Guy 1977). The sample was dried at 105°C for 24 hours, weighed to determine the total mass, and split into 2 parts: one part was used for particle size analysis and one part was used for soil organic content analysis. Bulk density was computed from the total oven dry mass, the thickness (depth interval) and diameter of the core (4.7 cm). Samples were measured for loss on ignition (LOI) at 500°C for 2 hours (Heiri *et al.* 2001).

Root density (*RD*) and root length density (*RLD*) were measured from soil samples which were first air dried, then weighed and poured gently onto a 2 mm sieve. Roots which were easily detected were collected before sieving in order to avoid unnecessary fragmentation. The sieved soil and roots were washed into a white enamel tray with a

gridded base (5 cm grid squares) filled with water to an approximate depth of 10 mm, then systematically collected at each grid under a 10 x magnification. In cases where roots were highly abundant and where there was little other floating material, the roots could be extracted using a suction pipette. This method was more time efficient but not suitable for samples with abundant organic material which would contaminate the root sample and lead to bias in the root mass measurements.

Live and dead roots could not be distinguished. However charred roots disintegrate when disturbed leaving behind a sooty residue. These could be distinguished and were not extracted. All other roots (length > 1mm and diameter < 2 mm) were extracted. Root length was measured using the line-intersect method (Tennant 1975). The root-grid line intersections were counted for each individual sample from photographs. For a subset of samples we validated the line intersect method by estimating root length using manual length measurements, direct intersect counts and counts from photographs (examples provided in Appendix E, Figure 3). Root mass was measured to nearest 0.001 g, after drying at 65 °C for 48 hrs.

5.2.3 Depth of transport limited erosion on burnt hillslopes (field study)

5.2.3.1 Field flumes– the flux and availability of sediment

Field flume experiments measured sediment flux from confined test areas at multiple time steps from the onset of erosion until the system reached a steady-state flux, and hence constant erodibility. Three field flumes (4 m long and 0.15 m wide test area) were installed at Sunday Creek (southeast Australia) on a planar slope close to a ridge-top in an area that had not been affected by overland flow. The experiments were conducted one year after wildfire so there was some evidence of rainsplash erosion from post-fire rainfall events. The slope angle was determined from measurements at the top, mid and bottom section of the test area. Steel edging (1m segments) were carefully driven into the soil and stabilized using steel pegs inserted along the outer edge. Sharpened erosion pins (150 mm long and 4 mm in diameter) were inserted at 8 points spaced at regular intervals inside the test area. These were used to measure depth of erosion at the end of the experiment. Experimental setup is shown in Appendix E (Figure 4).

The experiments were run as a sequence of successively increasing flow rates, q (0.2, 0.5, 1.0, 1.5 L s⁻¹). Water was pumped from a tank (2000 L) filled by water from a nearby creek and carried to the research site on a trailer. At each flow rate, the water was delivered into a small reservoir at the top the flume using a pump, a ball valve and a rotameter to control the flow rate. Once full, the water in the reservoir flowed into the confined test area. At the bottom of the flume, water and sediment was diverted through a 1 x 0.15 m diameter pipe to a collection point. The flow was sampled in 500 mL containers at 6 time intervals during each 60 s sampling period for each flow rate, starting with the initial surge, then every 10 s. The first sample was collected once water and sediment reached the collection point at the end of the flume. The flow was sampled by sweeping the 500ml container through the flow three times. At 60 s, the samples consisted of relatively clear water, and sampling was terminated since the system was approaching a steady state at his point. Data from similar experiments in these type of systems indicate that after 60 s the sediment flux remains constant (Sheridan *et al.* 2007a).

The non-sampled sediment was continuously collected in an overflowing 20 L bucket at the collection point. The material in the bucket was kept along with all the 6 x 500 ml samples. The flow depth (h_w) during the each flow rate in each experiment was measured at each erosion pin and used to calculate the shear stress (τ_f) as per equation (5.1). Flow velocity was measured using a dye tracer that was injected at the top of the test area and timed until the dye front had reached the collection point at 4 m. The discharge rate from the plot was measured three times at the end of the flume using a 10 L bucket and a stopwatch. Once all measurements were collected, the protocol was repeated for a next flow rate. The final erosion depth was measured at each erosion pin after the final flow experiment.

The particle size distribution of eroded material was determined for individual samples collected from the flume. Each oven dried sample was gently disaggregated and placed in a nest of sieves to separate between gravel (2 - 11 and 11 - 16mm), coarse sand (0.6-2mm) fine and medium sand (0.063 - 0.6 mm) and silt and clay (<0.063 mm). The measurements were then combined across each of the three replicate experiments based on the time intervals 0-1 s, 1-15 s, 16-35 s and 36-55 s to produce an average particle size distribution as a function of time.

5.2.3.2 Non-cohesive soil linked to variations in soil shear strength with depth

Each flume experiments was coupled with shear strength measurements, τ_v (kPa), using a HM-504A Pocket Shear Vane Set (total range = 0-250 kPa), at 10 points along a transect on a non-eroded section of soil adjacent to each of the three field flumes at Sunday Creek. The vane shear strength of a soil is the maximum internal resistance of a soil to the movement of its particles and provides an effective measure of cohesiveness. The measurements were repeated at 5 depths (0, 10, 30, 60 and 95 mm) at each sampling point by carefully excavating a small trench using the end of a metal ruler to expose an area (51 mm vane diameter) for each new depth increment. The vane blades were 5 mm high so each measurement integrates a small volume of soil and the actual measurement therefore occurs over a small 5 mm depth interval.

5.2.3.3 Availability of non-cohesive soils (extensive sampling)

An extensive survey of soil shear strength was carried out in headwater (zero order) catchments at Ella Creek, Sunday Creek and Stony Creek in the eastern uplands of Victoria, southeast Australia (see Figure 5.2a and Table 5.1). The measurements were obtained in order to capture the temporal changes in non-cohesive properties of near-surface soil during a 0-3 year post-fire period. Stony Creek and Sunday Creek were both burnt in February 2009 and measurements were made in September 2009 and March 2010, 0.5 and 1 year after the wildfire, respectively. Ella Creek was burnt in January 2007 and the same measurement campaigns in September 2009 and March 2010 represent conditions at 2.5 and 3 years after wildfire. The inclusion of Ella Creek in the sampling campaigns means that the measurements spanned across a longer recovery window. This space for time substitution assumes that spatial and temporal variation is equivalent. Ella Creek was considered to be suitable site in this respect given its similarities to Stony Creek and Sunday Creek in terms of soil, vegetation and fire impact (see Table 5.1 for site characteristics).

Each headwater catchment was sampled at 0m (near ridge top), 40 m and 80 m along three evenly distributed transects running perpendicular to the contours. Three replicate measurements were conducted at random points in a 2 m² quadrat at each sampling location. At each point the shear strength was measured at 5 depths using the same protocol as the measurements taken as part of the field flume experiment (above). One

headwater (3 transects) was sampled at Ella Creek and Stony Creek. At Sunday Creek, the shear strength was measured in two replicate headwaters (6 transects).

Some sections of the hillslopes had been affected by surface runoff in the 6 months prior to when the measurements were obtained in September 2009. The aim of this first sampling campaign was to characterize the fire-affected material which covered the soil surface and the measurements were therefore representative of the conditions immediately following the fire. The 2 m² quadrat was therefore positioned outside of the areas where surface runoff paths had obviously eroded the surface soil. The repeat measures in March 2010 were made in quadrats placed on the opposite side of the sampling transect in order to avoid potential disturbance effects from the first round of sampling. The majority of the hillslopes had experienced some erosion prior to this sampling campaign. At this time step, the measurements were sampled randomly from eroded and non-eroded surfaces. Soil moisture was measured gravimetrically on soil samples collected at each sampling quadrat (composited by hillslope position) and at depth intervals that corresponded with the depth of shear vane measurements.

5.3. Results

5.3.1 Effects of roots on variations in erodibility with depth (laboratory study)

In this section we report results from the laboratory flume experiments. The aim was to quantify changes in erodibility with depth and to evaluate the effects of soil and root properties. This chapter is mainly concerned with the erodibility of near-surface soils that had been impacted by the fire. The analysis is therefore restricted to measurements in at soil depths less than 5 cm. The erodibility parameter k_d (s m⁻¹) was obtained for each detachment measurement by assuming a linear relation between soil detachment capacity, D_c (kg m⁻² s⁻¹) and shear stress, τ_f (Pa):

$$k_d = \frac{D_c}{\tau_f} \quad 5.2$$

The detachment capacity D_c , at different depth intervals of intact soil in cores was estimated from the combined mass of all eroded sediment ($D > 0.45$ mm) from each depth interval. The critical shear stress term was assumed to be negligible because the critical shear stress for typical particles (0.063-1.0 mm) is 0.2-0.8 Pa (Moody *et al.* 2005; Wiberg and Smith 1987), which is smaller than the shear stress used in the experiments (2.2-42.1 Pa). A cluster-average was calculated from four erodibility

estimates at each depth interval within each cluster. Each of the four erodibility values was measured at a unique depth which fell within some predefined depth interval. An average depth of the four measurements was therefore calculated and used as the depth value which corresponded to each cluster-average erodibility value. The raw data is provided in (Moody and Nyman 2012).

The erodibility of burnt soils decreased exponentially with d_s between the soil surface and $d_s = 2$ cm (Figure 5.5). The relatively low value of k at 2 cm was therefore assumed to represent a constant once surface material was depleted. This assumption does not consider potential changes in erodibility for $d_s > 2$ cm. The average erodibility at ~2cm depth for Fourmile Canyon (FMC) North, FMC South and Pozo, respectively, was 1.48×10^{-4} , 2.03×10^{-4} and $1.47 \times 10^{-4} \text{ s m}^{-1}$, with similar levels of variability for all sites (coefficient of variation, CV = 95-100 %). Unburnt clusters consistently displayed the lowest erodibility on the soil surface although at the Pozo site the difference between unburnt and burnt was very small in 2 out of 3 clusters.

The variability in erodibility of burnt surface soils within sites was almost identical for all the three sites with coefficient of variation (CV) ranging from 81 to 82 %.

Interestingly, this variability is higher than the variability in erodibility of surface soils between the three sites (CV = 59 %). This means that the variable surface properties at scales $< 1 \text{ m}^2$ within sites are more important than site factors in explaining sediment availability in near surface soils. Further analysis of variability shows that the ratio of CV between clusters to CV between sites ($CV_{\text{cluster}}/CV_{\text{site}}$) decrease with soil depth, which suggests that the influence of site factors on erodibility increase with depth. This finding supports the notion that surface soil following fire is non-cohesive and therefore independent of the site specific geological and pedological factors which contribute to cohesion.

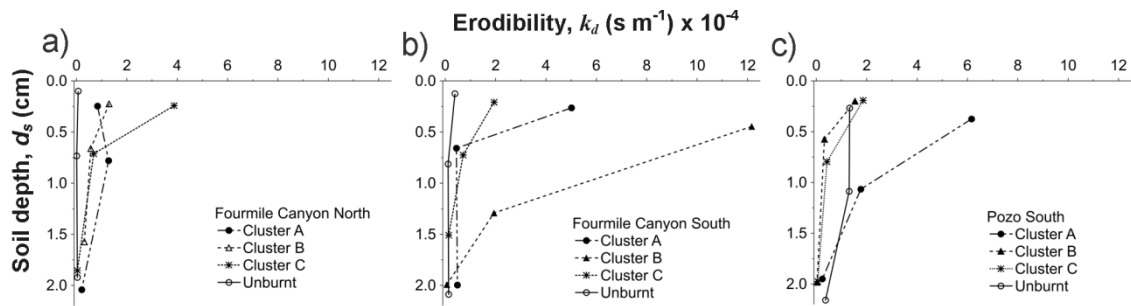


Figure 5.5 Changes in mean erodibility of burnt near surface soil at a) Fourmile Canyon North, b) Fourmile Canyon South and c) Pozo South. Three burnt clusters and one unburnt cluster are plotted for each site. Each point is the average erodibility obtained from four detachment experiments on four different cores in each cluster. The surface erodibility of four burnt soil cores at FMC North ranged from 8.37×10^{-4} to 38.8×10^{-4} . At FMC South the corresponding values were 19.4×10^{-4} and 122×10^{-4} and at Pozo they were 15.3×10^{-4} and 61.6×10^{-4} .

The influence of soil, root density (*RD*) and root length density (*RLD*) on erodibility was initially explored by simple correlations split by soil depth (Table 5.2). Root properties are the most important predictor of erodibility at the soil surface (0-1cm). The percentage silt and clay and the bulk density were the most influential variables at depths 3-5 cm. These were also the soil variables which displayed the largest differences between sites at this depth (Moody and Nyman 2012). These correlations should be interpreted in context of the negative correlation between bulk density and % silt and clay. At depths of 1-3cm, none of the variables were significantly correlated with erodibility. This could indicate a transitional zone where the variability between cores meant that no single variable emerged as dominant predictor. All data on soil properties are reported in more detail in Moody and Nyman (2012).

Table 5.2 Correlations between soil properties and erodibility at different depths. Significant correlations are in typed in bold font.

Depth	Statistics	Bulk Density (g cm ⁻³)	LOI (%)	Root density, RD (g cm ⁻³)	Root length density, RLD (cm cm ⁻³)	silt&clay (%)
0-1cm	R	-0.25	-0.37	-0.58	-0.37	0.12
	p-value	0.167	0.84	0.001	0.04	0.52
1-3cm	R	0.29	-0.5	-0.26	0.03	-0.42
	p-value	0.37	0.87	0.42	0.93	0.17
3-5cm	R	0.54	-0.46	-0.127	0.07	-0.53
	p-value	0.07	0.13	0.97	0.82	0.07

The variability in erodibility for $d_s < 3$ cm was analysed further using a general linear mixed model with site, soil and root variables as predictors. The analysis was restricted to measurements in the depth interval, $0 < d_s < 3$ cm, (i.e. the three uppermost erodibility measurements) because we were interested in soils that may have been impacted by the fire. Linear interpolation was used to determine soil and root properties for the exact depth at which erodibility was measured. For the first erodibility estimate, the depth was less than the midpoint of the uppermost soil sampling interval. The corresponding soil and root properties were estimated by extrapolation at 1cm and 3cm. The variable was given a value of zero if extrapolated values would be negative. Predictor variables were not log transformed.

Initially the model was defined so that site represented random effects with d_s , RD , and RLD modelled as fixed effects. Other soil properties were initially included but were subsequently removed from the analysis since they were non-significant and provided no additional improvement to the overall fit. Also there were no site-effects so the model was reduced to include d_s and either RD or RLD as predictors. The best fit was obtained using root density and soil depth as predictor variables in the linear model; $\log_{10}(k_d) = \beta_1 + \beta_2 d_s + \beta_3 RD + \beta_4 d_s RD + \varepsilon$. All coefficients were significant ($p < 0.01$) and the overall model explained ~ 60 % of variability in the log transformed k ($R^2 = 0.63$, $F_{3, 32} = 17.8$, $MSE = 0.22$ $p < 0.001$) (Figure 5.6). The positive interaction effect between soil depth and RD indicates the erodibility-reducing effect of roots decrease with depth. This is consistent with the correlation coefficients listed in Table

5.2. A similar but weaker ($R^2 = 0.56$) relation was obtained when RLD was used as predictor instead of RD .

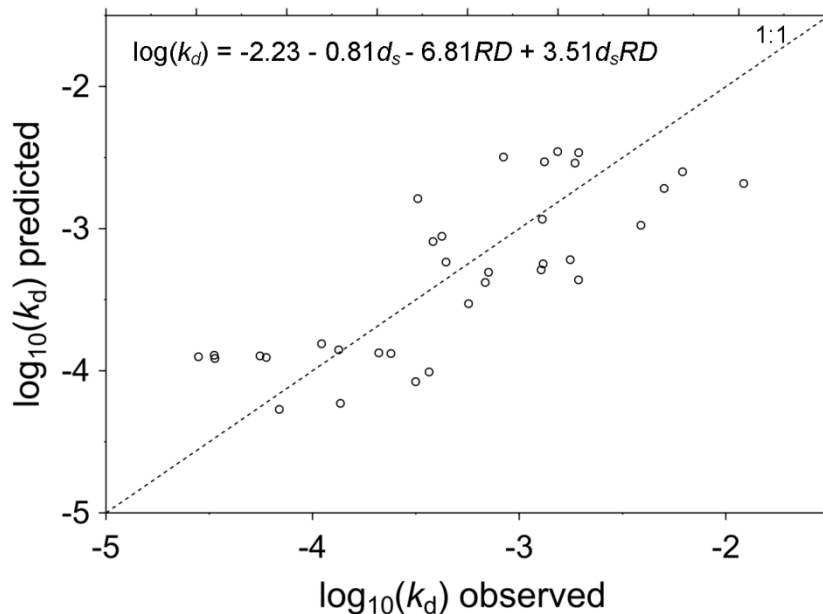


Figure 5.6 The observed and predicted erodibility, k_d ($s\ m^{-1}$), from a general linear model with depth, d_s (cm), and root density, RD ($g\ cm^{-3}$), as fixed effects. The analysis was performed on \log_{10} transformed erodibility values.

Results from the analysis above show that surface erodibility varies exponentially with d_s and RD . This analysis of k_d as a parameter which varies with depth and root density was possible because the laboratory flume provides the controlled conditions required for measuring detachment rates at specific depths within the soil profile. Field experiments that simulate rill erosion are unable to explicitly capture this variation in k_d with depth. The exponential change in k_d for $d_s < 0.02$ m can be expected to produce an exponential dependency between sediment flux and soil loss, which would be apparent as a change in sediment flux with time. The next result section is concerned with how variation in surface erodibility affects sediment flux during the erosion plot experiments

5.3.2 Depth of transport limited erosion on burnt hillslopes (field study)

5.3.2.1 Field flumes – the flux and availability of sediment

The intensive laboratory measurements showed that erodibility was highly variable with depth. In this section we carry out field flume experiments which were designed to capture how variations in erodibility with depth may influence sediment flux during

runoff events on hillslopes. The values measured for slope (S), water depths (h_w) and flow velocity in the field flume are provided in Table 5.3 along with the range of shear stress (τ_f) values estimated for each flow rate applied during the experiments.

Sediment flux measured in the erosion plot experiments at Sunday Creek decreased rapidly with time. For all flow rates, the sediment flux, q_s ($\text{kg m}^{-1} \text{s}^{-1}$) from the flume decreased rapidly (by up to two orders of magnitude) during the first 20-30 s of erosion (Figure 5.7). The detachment capacity, D_c ($\text{kg m}^{-2} \text{s}^{-1}$), towards the end of the experiment ($t > 45$ s) was used to calculate a steady-state erodibility, k_d (s m^{-1}), from D_c/τ_f as per equation (5.2). The erodibility values beyond this time ($t > 45$ s, $n = 9$) asymptoted towards a single value and produced an average steady-state erodibility, k_d , of $1.2 \times 10^{-4} \text{ s m}^{-1} \pm 0.5 \times 10^{-4}$ (SD).

Table 5.3 Flow properties measured in the field flume and the associated estimates of shear stress and sediment flux parameters.

Flow rate	Mean flow depth	Flow Velocity	Shear stress ^a	Fitted Parameters ^b		Steady flux
q (L s^{-1})	h_w (cm)	(m s^{-1})	τ_f (Pa)	a	b -	q_{smin} ($\text{kg s}^{-1} \text{m}^{-1}$)
0.2	0.6 – 0.7	0.52-0.71	21.3- 26.9	0.987	0.0047	0.017
0.5	0.9 – 1.1	0.63-0.89	33.5 – 41.0	0.989	0.0042	0.027
1.0	1.0 – 1.3	1.04-1.05	37.0 – 47.4	0.984	0.0059	0.031
1.5	1.3 – 1.5	1.05-1.26	49.6 – 57.7	0.971	0.0431	0.039

^a Slope ranged from 36 to 40 percent

^b Parameter values from equation (5.3) and fitted functions in Figure 5.7.

The changes in sediment flux, q_s , with time within each flow rate was fitted with a two parameter function:

$$q_s(t) = \frac{q_{smin}}{1.0 - ae^{-bt}} \quad 5.3$$

where a and b are fitted and the asymptote (q_{smin}) was determined by the steady-state sediment flux per unit flow width, w :

$$q_{smin} = \frac{k_d * \tau_f}{w} \quad 5.4$$

The denominator in the sediment flux equation (5.3) contains an exponential term which captures the temporary effects of a finite supply of near-surface soil which is transported more easily than the underlying matrix in which q_s approaches q_{smin} . The parameters a and b , respectively, determine q_s at $t = 0$ and $\delta_v q_s / \delta t$ for $q_s > q_{smin}$. When fitted to data within replicate flow rates the function accounted for 61 – 80 % of variability in q_s for $0 < t < 60$ s. Parameter values are provided in Table 2.3. Within flow rates the q_s function (5.3) represent two stages of the erosion process. Initially the change in flux with change in time is proportional to the soil loss rate ($\delta q_s \delta t = -b q_s$), hence an exponential dependence between q_s and t , but the available soil is limited and then exhausted so $\delta q_s \delta t$ approaches 0 (i.e q_s is constant) at some minimum values for q_s . Given unlimited sediment, the initial sediment flux at $t = 0$ could be constrained by the transport capacity of the flow, T_c ($\text{kg m}^{-1} \text{s}^{-1}$) (the limiting rate at which sediment can be transported for a given shear stress). However, the data did not indicate that transport capacity was limiting flux for any period of time during the experiments.

If flux was limited by transport capacity over time, then the rate of change with time ($\delta q_s \delta t$) would be low (close to 0) prior to the onset of depletion. The inverse sigmoid form of equation (5.3) means that the function can represent such a phase; however the sediment flux would need to be modelled as an inverse function of time, $q_s^{-1}(t)$, with an asymptote ($1/q_{smin}$) reflecting the maximum resistance of the soil to erosion. It is noteworthy for three samples (all from the initial surge from the flume) the sediment flux (or concentration, $\text{m}^3 \text{m}^{-3}$) exceeded T_c by up to 1.9 times when T_c was estimated from transport equations by Govers (1990) and Foster and Meyer, (1972), and for a single sample (1.4 times) when T_c was estimated for steep slopes from the relations provided by Zhang et al. (2011; Equation 8).

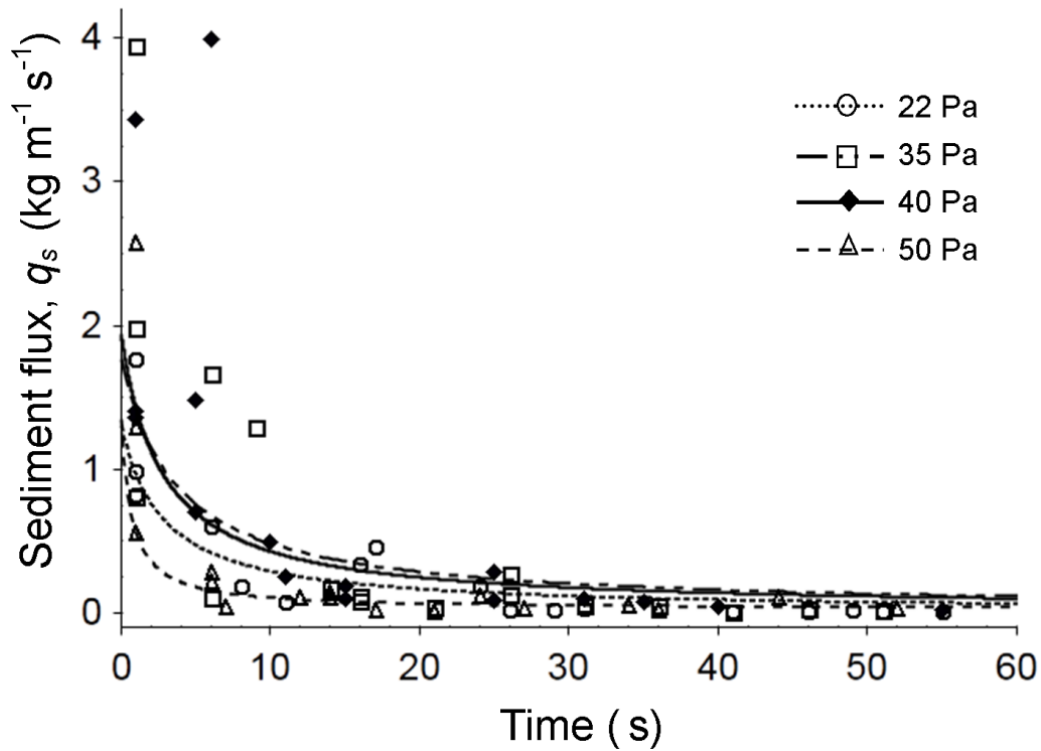


Figure 5.7 The mean change in sediment flux (q_s) with time (t) for sequentially increasing levels of shear stress (τ_f) in field flumes (4m long and 0.15 m wide) on a burnt hillslope at Sunday Creek (southeast Australia)

Within individual flow rates (particle size distribution averaged for bins at different time steps), the particle size of eroding sediment decreased with time (Figure 5.8a). Initially the eroded soil contained a large proportion of gravel sized particles with an overall median particle size, D_{50} , of 9.6, 6.7, 9.4 and 12 mm for 22, 35, 40 and 50 Pa respectively. The particle size declined more gradually for the intermediate flow rates ($\tau_f = 35$ and 40 Pa) than the first and last set of flow rates ($\tau_f = 22$ and 50 Pa, respectively). Between flow rates (particle size distribution averaged for the full 60 s experimental period), there was an overall coarsening in the eroded sediment with increasing shear stress for all $\tau_f < 40$ Pa, with D_{50} increasing from 3.07 to 7.26 mm between 22 and 40 Pa (Figure 5.8b). The lower quartile of distribution (D_{25}) displayed the strongest trend in relative terms (log scale), indicating that fine material was preferential eroded from the flume bed at the lower τ_f .

The results in Figure 5.8 shows that for the given range of shear stress values ($22 \text{ Pa} \leq \tau_f \leq 50 \text{ Pa}$) the particle size of transported sediment was primarily affected by a depletion

process which acted uniformly across the particle-size distribution within the available soil. The depletion resulted in a temporal shift in the composition of the soil that was available for transport, and this shift corresponded with a strong reduction in q_s (Figure 5.7). The relatively small shift in particle size distribution with increasing shear stress reflected preferential depletion of fine material at low flow rates rather than increased capacity of the flow to transport the larger particles on the flume bed. This was expected given that the critical shear stress of the largest particles (15 mm = 12 Pa for uniform non-cohesive sediments) is well below the minimum τ_f (20 Pa) applied in the flume experiments.

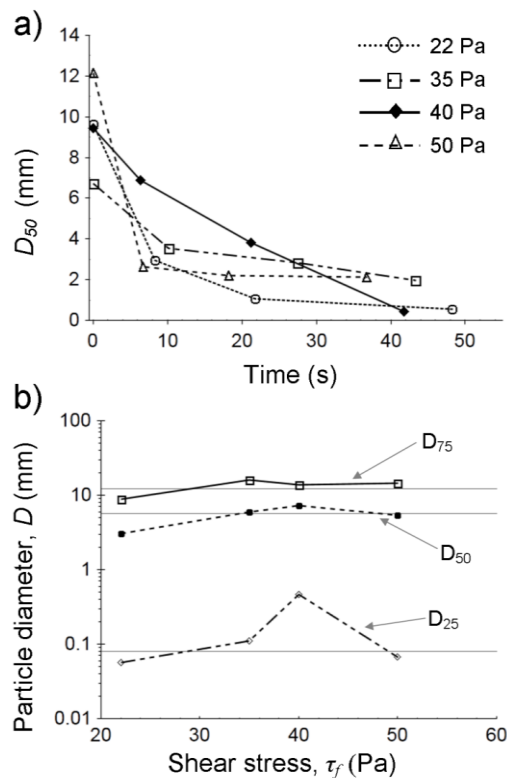


Figure 5.8 a) Median particle diameter (D_{50}) of eroded sediment for different flow rates applied sequentially to a confined test area on steep slopes (36-38 %) burnt at high severity. b) The particle size distribution as a function of sequentially increasing shear stress (τ_f) shown using the median (D_{50}), upper (D_{75}), and lower (D_{25}) quartiles of the distribution.

At low flow rates ($q = 0.2$ and 0.5 l s^{-1}), some of the flume bed did not erode in the initial surge of sediment, thus creating flow paths between elevated sections of intact surface material. Once established the flow paths were relatively stable with no lateral spread and q_s was limited by the detachment capacity at the bed of the flume. New

material was accessed and flow paths widened once the flow rate was increased. This resulted in a return to high q_s , followed by rapid depletion once the system reached a new equilibrium state. This meant that the initial spike in q_s with each new flow rate could be interpreted as the effect of increased access to a finite pool of readily available soil. The pattern was repeated for each level of τ_f up to 50 Pa where all material had probably been removed, thus exposing a resistant soil matrix across the entire flume bed. At each new τ_f , an increasing proportion of the overall available sediment was transported off the flume bed.

This depletion effect was estimated from equation (5.3) by first estimating the total flux as the integral of equation (2) between 0 and 60 s for each τ_f . The total flux in excess of the steady state rate (q_{smin}) was then obtained by subtracting $q_s(t) = q_{smin}$ from $q_s(t)$. This quantity was estimated to be 3.0, 4.9, 3.9, and 0.8 kg m⁻² for τ_f of 22, 35, 40 and 50 Pa, respectively. For erosion under constant erodibility ($k_d = 1.2 \times 10^{-4} \text{ s m}^{-1}$, $q_s = q_{smin}$), the total erosion over 60 s would have been 1.6 kg m⁻², approximately 10 times less than the sediment actually generated. The average depth of erosion (measured from erosion pins within the three flumes) was 1.1 cm \pm 0.2 (n = 30). The analysis above indicate that only 8 % of this depth consist of erosion where $q_s = q_{smin}$. The estimated depth of non-steady erosion is therefore estimated to be 1.1 cm minus 8 % which is \sim 1.0 cm. This value is defined as the depth on non-cohesive soil d_{nc} .

The sum of modelled erosion for all flow rates (total = 12.6 kg m⁻²) is 11 % higher than the estimate obtained from the average total mass of sediment (11.3 kg m⁻² \pm 3.0) captured in the bucket and rill bottles at the bottom of the flumes (3.1, 3.5, 3.6 and 1.1 kg m⁻² for τ_f of 22, 35, 40 and 50 Pa, respectively). Sources of error leading to discrepancy between measurement and the estimates from equation (5.2) could include i) fine sediment escaping from the overflowing bucket, ii) relatively few data points in the regression relative to the large variability in q_s and iii) a gradual asymptote in equation (2) which consistently over-predicted q_s for $t > 30$ s.

The depletion of soil which was non-cohesive (d_{nc}) was presented as a cumulative function of τ_f , using measured and modelled values for erosion (Figure 5.9), both of which displayed similar trends. The relation between cumulative sediment availability and τ_f shows that the majority (\sim 70 %) of the material was eroded for τ_f between 20 and

40 Pa, with only residual soil left for $\tau_f > 40$ Pa. However, if the depth of non-cohesive soil (d_{nc}) was lower, then it is possible that a lower τ_f would be required for all the soil to be effectively submerged and transported away from the flume bed. The cumulative availability was therefore also plotted as a function of flow depth (h_w) relative to the depth of non-cohesive soil ($d_{nc} = 1.0$ cm). The sediment availability increased sharply when h_w/d_{nc} was close to 1. Less than 10 % of soil remained on the flume bed when $h_w/d_{nc} > 1$ ($\tau_f = 40$ Pa). The pattern indicates that the non-dimensional ratio, h_w/d_{nc} , could be a more meaningful and transferrable variable than τ_f when determining the proportion of soil within d_{nc} that is available for a given flow rate.

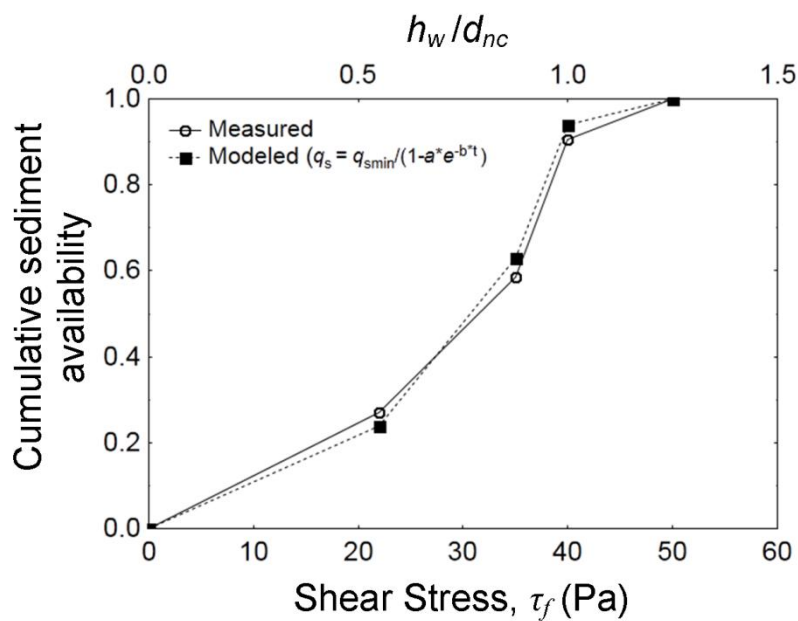


Figure 5.9 The cumulative availability of sediment as a function of shear stress (τ_f) and the non-dimensional ratio, h_w/d_{nc} (i.e. flow depth relative to the depth of available material). The plots are generated from i) measurements of total erosion (kg m^{-1}) and ii) modelled erosion from the fitted sediment flux functions (Equation 2; Figure 5.7).

5.3.2.2 Non-cohesive soil linked to variations in soil shear strength with depth

This section aims to link variations in soil shear vane strength (τ_v) with depth (d_s) with the depth of soil (d_{nc}) which was non-cohesive and transported from the flume bed under condition where $q_s > q_{smin}$. The average of five τ_v measurements from outside of each flume bed at Sunday Ck ($n = 15$) were plotted as a function of soil depth, d_s , (Figure 5.10) and represented by the function,

$$\tau_v(d_s) = \frac{\tau_{vmax}}{1.0 + f e^{-pd_s}} \quad 5.5$$

This function is analogous to the sediment flux function (5.2), the only difference being that the dependent variable (τ_v) is inversely related to sediment availability and increases rather than decreases with the explanatory variable (d_s). Hence a positive sign on the exponential effect-term in the denominator. The parameter $\tau_{v(max)}$ is the constant value which τ_v approaches at depth, whereas f and p , determine τ_v at $d_s = 0$ and $\delta_v\tau/\delta d_s$. The function accounted for 99 % of variability in mean τ_v with d_s for the depth-averaged data of τ_v . The strong gradient in τ_v between d_s of 1.25 and 3.25 cm and the sigmoid relation shows that surface and subsurface soil display different properties, with a strong gradient of change between them. In this analysis we use the depth of non cohesive soil (d_{nc}) from the previous section to determine a shear strength value above which the soil is easily eroded by overland flow. The aim to characterise the soil as two discrete layers; a non-cohesive surface layer with low strength overlying a cohesive and resistant subsurface layer. The value of τ_v at the transition from non-cohesive to cohesive soil was obtained by solving $\tau_v(d_s)$ (equation 4) for $d_s = d_{nc} = 1.0$ cm (i.e. the depth of non-cohesive soil in the adjacent flume). In this way, the τ_v threshold for non-cohesive soil was estimated to be 5 kPa (Figure 5.10).

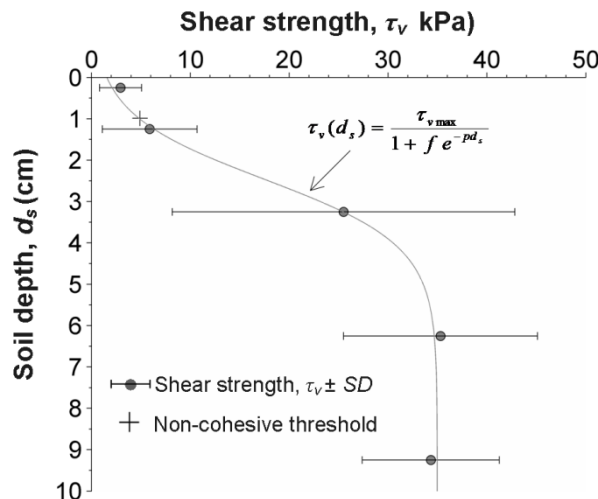


Figure 5.10 Mean vane shear strength (τ_v) and standard deviation (SD) as a function of soil depth (d_s) for 15 sample points along the outside edge of the flume experiment test area at Sunday Creek. The depth of highly erodible soil, d_{nc} , was used to define the point (+) of transition from non-cohesive to cohesive material.

5.3.2.3 Availability of non-cohesive soils (extensive sampling)

In the following section the aim of the analysis is to i) quantify changes in the vane shear strength distribution with depth, $\tau_v(d_s)$, as per equation (5.5), during recovery from wildfire and ii) characterize the depth of non-cohesive soil, d_{nc} , on hillslopes in burnt headwaters (Ella Creek, Sunday Creek and Stony Creek) as a function of time since fire, t_{sf} (years). The τ_v values obtained in September had to be adjusted for the effect of 24 to 33 % higher soil moisture at $d_s \geq 3$ cm at this measurement campaign, compared to the measurements obtained in March. The adjustment ensured that $\tau_v(d_s)$ was interpreted independently from the temporal variation caused by soil moisture fluctuations. A linear correction function ($\tau_{v, \text{March}} = 0.9\tau_{v, \text{Sept}} + 0.15$; $n = 9$; R-square = 0.97) was obtained by plotting September measurements ($d_s \geq 3$ cm) for all three sites with the corresponding measurement in March. The variability in the depth-averaged τ_v with d_s was well represented by equation (5.5) ($R^2 = 0.94 - 0.99$), although the variability within depths within sites was often high as shown by the large standard deviation (Figure 5.11).

At the two sites which burnt in February 2009 (Stony Creek and Sunday Creek) the τ_v at the soil surface in September (0.5 years after fire) was very low ($\tau_v = 1.7\text{-}2.4$ kPa), homogenous (SD < 1.0 kPa) and similar in the two burnt headwaters (Figure 5.11a and b). The shear strength increased to between 3 - 4 kPa at $d_s = 1.25$ cm and became more variable (SD ranging from 2.9 - 3.2 kPa). The shear strength of surface soils increased markedly in the 0.5-year period between September and March. At Stony Creek in March (1 year after fire), there was no discrete surface layer of erodible soil, the shear strength on the soil surface was higher (12.2 ± 5.6 kPa) and there was a linear (as opposed to sigmoid) increase in τ_v with d_s between the soil surface and $d_s = 3$ cm. Sunday Creek displayed a more modest increase in surface τ_v from September ($\tau_v = 2.4$ kPa) to March ($\tau_v = 7.1 \pm 6.5$ kPa). At Ella Creek (burnt 2007) the soil remained more or less unchanged between September (2.5 years since fire) and March (3 years since fire) so that a single function was used to represent both sets of measurements (Figure 5.11c). The average τ_v at the soil surface for both measurement campaigns at Ella Creek was 11.4 ± 9.1 kPa and there was a linear increase in τ_v for d_s between 0 and 3 cm. At $d_s > 3$ cm, the shear strength approached a constant value of $\tau_{v, \text{max}} = 55$ kPa.

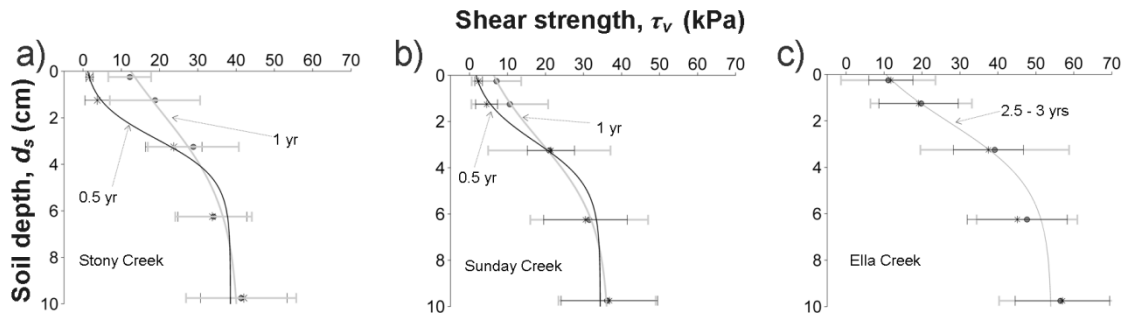


Figure 5.11 Changes in shear strength (τ_v) with depth (d_s) at two time steps (September 2009 and March 2009) at a) Stony Creek ($n = 27$) b) Sunday Creek ($n = 50$) and c) Ella Creek ($n = 27$), systems in different stages of recovery from wildfire. The shear strength at 0.5 yrs since fire was measured on non-eroded sections of the hillslope and therefore represents the surface properties without depletion effects that may have taken place between the initial fire impact and the sampling campaign (i.e. taken to represent conditions immediately following the burn). At Stony Creek and Sunday Creek the number of sampling points was about 10 % lower for d_s at 6.5 and 10 cm, due to the rock and gravel encountered during sampling.

The high spatial variability in τ_v of near-surface soil in the sampled headwaters ($n = 36$) meant that the τ_v at each depth was a distribution which included cohesive and non-cohesive soil even if the average τ_v was greater than the average non-cohesive threshold of 5 kPa (determined in section 3.1.2). The d_{nc} (where erosion requires little or no detachment prior to transport) was therefore quantified at each sampling depth as the proportion of sampling points (reflective of the proportional area) where $\tau_v < 5\text{kPa}$ (Figure 5.12a). At Sunday Creek and Stony Creek all the sampled points (100 %) at the surface were non-cohesive on non-eroded surfaces 6 months after fire. At 1 year after the fire the proportion on non-cohesive points across the headwaters reduced to 54 % and 7 % for Sunday Creek and Stony Creek, respectively. Less than 20 % of surface soil was non-cohesive at Ella, 2.5 to 3 yrs after fire.

An exponential cumulative distribution function ($cdf = 1 - e^{-\lambda d_s}$) was fitted to the cumulative proportion of non-cohesive soil with increasing d_s ($R^2 = 0.84-0.98$) and plotted as a probability density function (pdf) (Figure 5.12b). All soil particles at $d_s = 0$ were assumed to be non-cohesive in the fitting procedure. The expected value of the

pdf, $E[d_s] = 1/\lambda$, is the average depth of non-cohesive soil (d_{nc}) across the sampled headwaters and could be represented as an exponential decay function of time since fire ($R^2 = 0.96$) (Figure 5.12c). The measurements collected 0.5 yrs after fire were obtained from non-eroded sections and assumed to represent a maximum depth immediately following the fire. The two parameter exponential function represented both the initial production (by wildfire) of non-cohesive soil and the decline in availability over time.

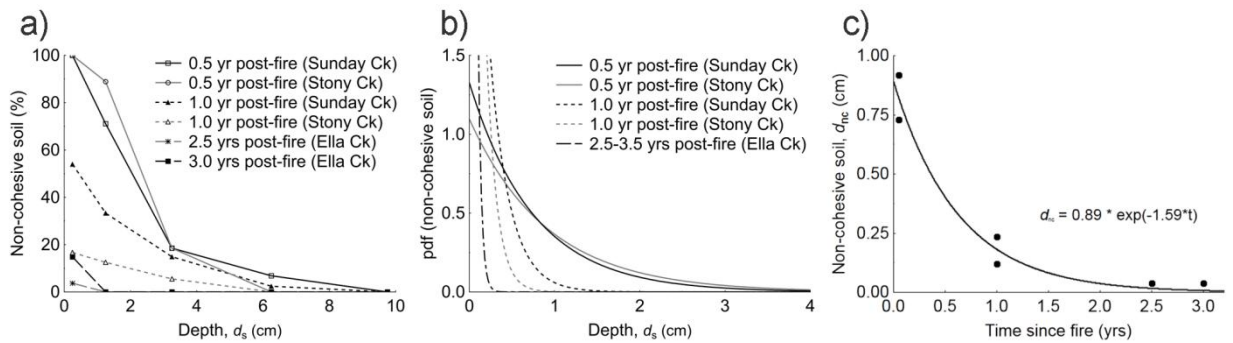


Figure 5.12 a) The percentage non-cohesive soil plotted as function of depth (d_s) by applying a vane shear strength (τ_v) threshold of 5 kPa. The threshold was defined based on the average depth of soil removed from the flume bed in sediment flux experiments at Sunday Creek (Figure 5.10). b) A cumulative density function was fitted to the data in a) and presented as a probability density function (pdf). c) The expected depth $E[d_s]$ of the pdf in b) as a measure of the average depth of non-cohesive soil, d_{nc} , (cm) as function time (years) since fire (t_{sf}).

In the preceding sections we combined flume experiments with shear vane measurements to characterize variability in sediment availability as function of soil depth. The analysis showed that sediment availability changed due to a shift from non-cohesive to cohesive soil near the surface. Over short time-scales within flow experiments (seconds to minutes), the sediment availability decreased exponentially with time due to depletion and exhaustion of the available soil on the flume bed. Between flow rates, the proportion of sediment that was available increased with sequentially increasing shear stress. Over time during recovery (months to years), the availability of non-cohesive soil, decreased exponentially between the fire and 2.5 years into recovery.

5.5. Discussion

5.5.1 Transport limited erosion on burnt hillslopes

Flume experiments in the laboratory and in the field showed that burnt hillslopes erode initially, in a layer of highly erodible surface soil. This highly erodible soil lacks structure and has been shown to consist of ash, partially combusted organics, gravel and mineral soil (Badia and Marti 2003; Moody and Ebel 2012; Woods and Balfour 2010). The largely non-cohesive properties meant that no detachment was required to initiate erosion, therefore resulting in transport-limited case (Hairsine and Rose 1992; Zhang *et al.* 2009). Once depleted however, the erosion process shifted towards a detachment-limited case where the detachment rates and sediment flux was determined by flow properties and the erodibility of the cohesive soil-matrix. At Sunday Creek, the shift from the transport limited erosion to detachment limited erosion corresponded with a threefold shift in shear strength within the 1-3 cm depth interval of the soil profile. The strong anisotropic variability in soil strength within 1-3 cm of the soil surface contrasts with undisturbed forests and agricultural systems where most erosion models were originally developed, parameterized, and tested. Traditional methods for characterizing erodibility and erosion processes may therefore prove ineffective at capturing the fire-effect.

In this study we considered the soil as a two-layered system where the availability of non-cohesive surface soil was represented in general as a decay function of time or soil depth which approached a constant value that reflected a cohesive subsurface soil matrix. The non-cohesive surface soils and the cohesive soil matrix were distinguished by coupling field-based flume experiments with shear vane measurements to define a shear-strength threshold below which the soil was transport limited. The measurement focus then shifted to the spatial distribution and depth of transport-limited material. The proportion of non-cohesive soil could be represented as a cumulative distribution (cdf) of non-cohesive soil as a function of d_s . The cdf was parameterized using shear vane measurements at multiple depths and at several time steps following the burn impact. A spatially distributed sampling regime ensured that the distribution was representative of an entire converging headwater unit (~1 hectare), and provided a simple, yet effective representation of fire-effects. The measure incorporates spatial variability in the depth of transport limited soil through the single parameter, λ , in the exponential distribution.

The parameter can be determined for large areas at different stages of recovery (time since fire) using a relatively simple measurement technique.

The exponential decline of non-cohesive soil depth, d_{nc} , during recovery (Figure 5.12c), indicates that the d_{nc} parameter was responsive to fire-related impacts on sediment availability and recovery of soil system. Initially after the burn, the entire surface consisted of non-cohesive soil that was readily available for transport. The average depth of non-cohesive soil was estimated to be between 0.7 and 0.9 cm. With an average bulk density of 1.3 g cm^{-3} (measured for soils 0-3 cm), this non-cohesive soil equates to $97 - 117 \text{ t ha}^{-1}$ of transport limited soil on the recently burnt hillslopes. Failing to incorporate this non-cohesive soil as a part of the overall sediment availability could be an important source of error in existing models that are used to predict post-fire erosion. The depth, d_{nc} , diminished exponentially with time in response to depletion, redistribution and recovery of the soil profile. At 2.5 - 3 years since fire the d_{nc} was reduced to reflect a thin ($< 0.04 \text{ cm}$, $< 5 \text{ t ha}^{-1}$) layer of non-cohesive soil, essentially corresponding to a single-particle layer.

The initial depth of non-cohesive soil and the change with time during recovery could be represented across three sites by a two parameter exponential function with one parameter reflecting the initial production of material and the other describing the decline with time (Figure 5.11c). The initial magnitude of d_{nc} can be seen as a function the fire severity in relation to intrinsic properties of the soil-vegetation system while the rate of decline with time depends on the depletion of soil and the recovery of the soil profile. Depletion is a function of erosive rainfall inputs relative to the initial depth of non-cohesive soil that was made available through burn impacts on the soil and inputs of vegetative ash. Recovery would tend to operate as a deterministic process through the re-establishment of fine root networks and through cycles of wetting and drying, both acting to increase cohesiveness by increasing aggregating and consolidating loose soil and ash (Bryan 2000; De Baets and Poesen 2010; Kemper *et al.* 1987; Nearing *et al.* 1988).

5.5.2 Effect of roots on sediment availability

The depth of burn impacts in the soil can be linked to fire severity (DeBano *et al.* 2005; Hungerford *et al.* 1991; Parsons *et al.* 2010). However, no explicit link has previously

been drawn between burn impacts on the soil systems and the erodibility of the soil. In this study, we coupled measured soil properties with measurements of erodibility and show that fine (< 2 mm diameter) roots play an important role in limiting detachment rates in fire-affected soils. The averaged surface erodibility of burnt soils ranged from 20×10^{-4} - $63 \times 10^{-4} \text{ s m}^{-1}$. These values are very high resulting in high detachment capacity relative to transport capacity and hence a under field condition producing transport limited conditions where $q_s \rightarrow T_c$ (Zhang *et al.* 2005). The erodibility declined by 1 to 2 orders of magnitude between the surface and a depth of 2 cm. As such, the results are consistent with the two layered system described earlier. Below the highly erodible surface soil the erodibility across the three sites ranged from 1.5×10^{-4} - $2.0 \times 10^{-4} \text{ cm s}^{-1}$. These values are slightly higher but similar in magnitude to the steady state erodibility measured in the field flume at Sunday Creek ($1.08 \times 10^{-4} \text{ s m}^{-1}$) and similar to steady-state erodibility reported for burnt forest soils elsewhere (Wagenbrenner *et al.* 2010).

Roots reinforce the soil matrix by introducing extra cohesion in addition to the intrinsic cohesion of the soil (De Baets and Poesen 2010; Fattet *et al.* 2011; Gyssels *et al.* 2005). In burnt soils the effect of root density on erodibility was strongest at the soil surface, thus supporting past observations that root can act to reduce erosion after fire (Gould 1998). A linear model with soil depth and root density (and their interaction) as predictors accounted for 62 % of the variability in log transformed erodibility, indicating that fire-induced changes to erodibility can be predicted using a variable such as root properties that is directly related to heat impacts on the soil (Parsons *et al.* 2010). The results show that effect of roots on erodibility diminished with depth. It therefore seems that for the intact soil cores used in the flume experiments there was a relatively shallow critical zone where the roots provided the main source of cohesion and where the absence of roots is associated with large increase in erodibility.

In higher severity burns with larger impacts on the soil this zone may extend deeper than what was observed in this study. The reduced importance of roots with depth may be due to the increasing importance of other soil properties such as the percentage silt and clay which was the only explanatory variable which significantly explained variability in erodibility at $d_s > 3 \text{ cm}$. This pattern is consistent with observations by DeBano *et al.*, (2005) that at greater soil depths the amount of organic matter decreases

and inter-particle bonds become increasingly important as sources of soil structure and cohesion. The inorganic binding agents associated with clays provide cohesion and is an important predictor of soil erodibility (Sheridan *et al.* 2000; Tisdall and Tisdall 2006; Wischmeier and Mannering 1968)

5.5.3 Large scale implication – a conceptual model

The strong anisotropic variability in soil strength (cohesion) with soil depth after forest fire translates into a transient effect of burning on sediment availability. This effect is in some ways analogous to other disturbed soil systems such as road fills and freshly tilled agricultural soil which initially display a of low soil resistance to erosion and hence high sediment availability (Kemper *et al.* 1987; Megahan 1974; Nearing *et al.* 1988). The initial conditions following these soil perturbations can be viewed in relation to the soil system under undisturbed conditions (Figure 5.13). There is an initial production of non-cohesive soil with a corresponding increase in erodibility. The subsequent return to pre-fire conditions can take different trajectories depending on the initial production of non-cohesive soil by fire (related to fire severity and pre-fire soil conditions) and the local factors that contribute to depletion and soil recovery. High burn severity may result in deeper burn impacts, deeper layer of non-cohesive soil, and delayed onset of depletion and recovery. In systems with low background erodibility the fire effect on sediment availability represent a larger perturbation than in system with high background erodibility (Figure 5.13 a and b). In highly erodible systems (Figure 5.13b) the transition from the non-cohesive soil produced during burning to the underlying soil matrix is poorly defined and erosion is likely to be dominated by detachment and sediment entrainment at the base of rills. This represents a different process to the lateral migration of shallow rills within a non-cohesive surface layer and above a soil matrix where the erosion rate at the base of the flow is restricted by low erodibility and high critical shear stress (Figure 5.13a).

The interplay between background erodibility and influence of fire on sediment availability can have important implication for the type and magnitude of post-fire erosion responses. For instance *Larsen* (2006) showed that the frequency of debris flows were insensitive to fire-effects on weathering-limiting systems with low sediment availability on hillslopes. Similarly, *Nyman et al.* (2011) found that weathering-limited catchments in plutonic granite terrain in north-east Victoria (southeast Australia) were

less susceptible to runoff generated debris flows after fire than the adjacent sedimentary catchment, where the soil mantled hillslopes provided a major source of fine sediment to post-fire debris flows (Smith *et al.* 2012). Cannon *et al.* (2003) observed a similar pattern where the presence of non-cohesive soil on hillslopes resulted in earlier initiation of debris flows than on hillslopes with less available sediment. These studies therefore suggest that explicit representation of fire effects on sediment availability is important for predicting both type and magnitude of erosion responses on burnt hillslopes. The relation between fire-effects and background erodibility ultimately determines the sensitivity of geomorphic systems to fire in terms of the sediment availability.

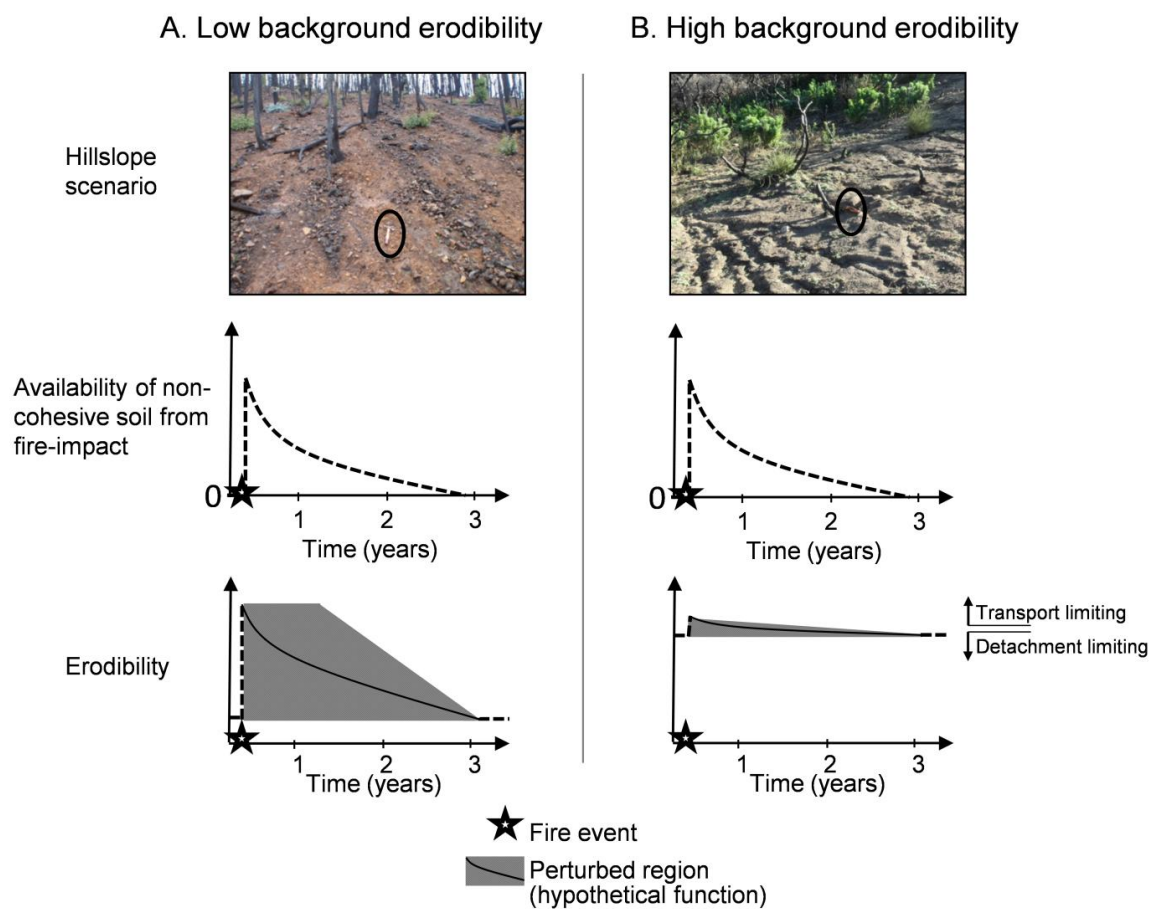


Figure 5.13 Conceptual models of sediment availability on burnt hillslopes in systems with a) low and b) high background erodibility. The low and high background erodibility scenarios represent hillslopes from Sunday Creek, southeast Australia (clay loam soil) and Arroyo Seco, California (sandy soil) (see Kean *et al.* 2011). The fire-effect in the conceptual models is equal for both systems in terms of the depth of non-cohesive soil produced during burning. The impact on sediment availability however is different due to contrasting background (fire-independent) soil properties.

5.6 Conclusion

In burnt soils there is an upper layer of non-cohesive soil which can provide an important source of available sediment during the post-fire period, particularly for events shortly after the initial burn impact. Instead of measuring steady state erodibility parameters of burnt hillslopes, we should therefore focus on quantifying fire-effects as the amount of non-cohesive soil produced by the fire through burn impacts and ash deposition. The non-cohesive properties of burnt surface soils mean that transport is initially a direct function of transport capacity, and independent of the background erodibility of the forest soil. During recovery, the availability of non-cohesive soil is depleted or incorporated back into the soil matrix and the system trends back towards a cohesive state. This shift could be represented spatially and temporally as a probability distribution of non-cohesive soil depth with a mean that decreases exponentially with time since fire.

Background variability in sediment availability can be predicted using information on soil texture, bulk density and soil organic matter. However, in unburnt states the erosion rates in forests are usually low due to stable and highly structured soils. When burnt, the soil system shifts to a different state and new variables may drive the variability in erodibility within and between systems. The study shows that root properties represent an important variable that can be used to predict erodibility of burnt soil. This means that an explicit link can be made between sediment availability and a property which is directly impacted by burning. Linking root distribution in near surface soils with burn severity and the depth distribution of non-cohesive material is a particularly interesting avenue for future studies and something which may provide useful insight into the quantitative link between soil burn severity and sediment availability on hillslopes.

A conceptual model of sediment availability was presented and provides a new framework for quantifying changes in sediment availability due to fire-effects in different soil-vegetation systems. The explicit representation of fire-effects means that sediment availability can be explored in context of burn severity and its interaction with intrinsic catchment properties such as soil, geology and vegetation. The model can also be coupled with information on fire-effects on runoff to assess the relative importance of sediment availability versus runoff generation mechanisms as fire-sensitive components which determine how different geomorphic systems respond to fire.

Chapter 6: Sediment availability and infiltration as controls on the initiation and magnitude of runoff-generated debris flows – a synthesis

6.1 Introduction

Post-fire erosion responses in southeast Australia and elsewhere are variable and exhibit distinct differences in the types of processes operating in different ecosystems and geological settings. Geology, topography, vegetation and local climate vary across landscapes and cause variability in the properties that control the post-fire hydrologic or geomorphic responses. Variability in soil properties within catchments at small scales is often considered to be random (Elliot *et al.* 2001; Robichaud *et al.* 2007) while at large spatial scales the systematic changes in for instance climate, vegetation and geology means that the proportion of variability that is systematic and predictable increases while the proportion of random variability decreases (Lane *et al.* 2011; Larsen *et al.* 2006; Moody *et al.* 2008a; Robichaud *et al.* 2007; Shakesby and Doerr 2006; Wondzell and King 2003). Systematic variability can be predicted by linking response parameters (properties) to the local climate, geology and biogeography, and thus providing a basis on which to explore the synergy between extrinsic sources (fire and rainfall regimes) and intrinsic sources (e.g. geology, vegetation) of variability in post-fire erosion processes and responses (Larsen *et al.* 2006; Moody *et al.* 2008a).

In Chapter 2 we showed that post-fire debris flows in burnt forests of southeast Australia are produced from progressive sediment bulking on hillslopes and in channels. This was an important finding in that it provided new insights into the processes that dominate sediment delivery to streams following wildfire. In the past, the post-fire erosion research in the southeast Australian regions was largely confined to instrumented catchments and the role of extreme events as a geomorphic agent and as a source of hazard was therefore poorly understood. The underlying processes, the landscape controls, and the magnitude of events had not been documented previously. Forest 'dryness' was found to be a driver of heterogeneity in terms of how burnt catchments in eastern uplands of Victoria generate runoff after. The forest ecosystems (or ecological vegetation class, EVC) of the region vary over short geographic distances due to strong moisture gradients which form in response to variable rainfall (orography, shading and climatology) and variable incoming solar energy (cloud and slope orientation). Differences in EVC can have large implications for how systems respond

to wildfire and storms. Hillslopes in wet EVCs (annual rainfall usually > 1600 mm) for instance, recover quickly; they have porous, aggregated and structured soils, high infiltration rates and hence relatively low erosion rates (Lane *et al.* 2006b; Nyman *et al.* 2011; Sheridan *et al.* 2007a; Smith *et al.* 2011b). These wet ecosystems (typically dominated by *Eucalyptus regnans* and *E. deligatensis*) appear to be resilient in terms of erosion (Lane *et al.* 2011), when compared to the dry mixed-species EVC (typically containing a combination of peppermints and box species such as *E. dives*, *E. dives*, *E. albens*) (Nyman *et al.* 2011; Smith *et al.* 2011a).

Chapter 2 also showed that the geology and its effects on sediment availability was a source of variability in the response of burnt catchments to intense storms. At the Mt Buffalo intrusion in northeast Victoria for instance, the granitic outcrops and the large sections of exposed bedrock on hillslopes meant that sediment was limited and that the debris flow initiation from surface runoff and sediment bulking was less likely when compared to the surrounding catchments in soil mantled terrain (sedimentary and metamorphic geologies). Geologic controls on debris flow and other post-fire erosion processes have also been documented in the intermountain western US (Larsen *et al.* 2006; Moody *et al.* 2008a). When combined with research findings from other regions in southeast Australia, the results from Chapter 2 highlight that the response of burnt catchment to storms is highly variable within this landscape and that it is therefore problematic (and potentially misleading) to evaluate the distinctiveness of this region (southeast Australia) as a single geomorphic unit.

In Chapter 3 the aim was to i) measure debris flow magnitude, ii) quantify the potential delivery of water quality constituents to rivers, and to iii) parameterize an erosion model for runoff generated debris flows. A total of 10 debris flows were surveyed and used to generate a dataset of event magnitude as function of the erosion depth on hillslopes and in channels. The rainfall underlying the debris flow events was quantified for each site using a combination of ground-based rainfall measurements and radar data. The depth of channel erosion (E_{ch}) was highly variable within catchments but could be represented as a linear function of slope (S) and rainfall excess (Q_{30}) in the transport equation, $S^m Q_{30}^n$ (Chapter 3; Equation (3.2), where m and n were fitted using channel survey data. The rainfall excess (Q_{30}) was calculated as the difference between rainfall (I_{30} , mm h⁻¹) and steady state infiltration capacity (K_p , mm h⁻¹) using ponded infiltration

measurements from Chapter 2. Channel initiation by debris flows was assumed to be determined by the same erosion processes operating during channel erosion and modelled as a threshold function of S^m and Q_{30}^n . Hillslope erosion was modelled in a similar way, although using rainfall intensity at 15-minute time steps (I_{15}) since this produced a better fit and was considered to be more representative of the timescales of peak runoff on hillslopes in upper catchments (typical slope lengths: 150-250 m).

Wildfire results in temporal changes to infiltration and erodibility, which may have implications for sediment availability and transport parameters in the erosion equations. In Chapter 4 and 5 the aim was therefore to measure and model temporal changes in erodibility and infiltration during recovery from wildfire. In Chapter 4 the infiltration experiments showed that the sensitivity of infiltration to macropore flow (K_{mac}) meant that the availability of macropores contributed to large differences in infiltration rates between forest ecosystems (dry and wet) with different soil structure. The flow potential of the soil matrix (K_{mat}) was found to be related to dryness (the monthly weather pattern) and degree of water repellency. In *Eucalypt* forests the soil was naturally repellent and the fire had no detectable impact on this soil property. Presumably the fire would cause more widespread and uniform water repellency due to the initial drying during soil heating and the subsequent increases in soil evaporation due to high exposure to wind and radiation on burnt hillslopes. Chapter 5 showed that hillslope erosion occurred primarily in a layer of non-cohesive, and thus highly erodible soil. The depth of this non-cohesive soil, d_{nc} , on hillslopes decreased exponentially during the first year of recovery from wildfire.

Landscape variability in infiltration and sediment availability can contribute to differences in debris flow susceptibility after fire. Ultimately it is the interplay between these two factors which determined how hillslopes and catchments respond to wildfire. The effects of these properties on debris flow initiation are represented conceptually in Figure 6.1. The diagram draws on observations from Chapter 2. The burnt catchments at Mt Buffalo were sediment limited and produced flash floods in response to intense storms. At East Kiewa in the wet forest environments there was insufficient runoff to trigger major erosion events, despite large storm events. In dry forest (e.g. Rose River and Myrtle Creek) there was sufficient runoff and sufficient sediment availability for debris flow initiation during intense rainfall.

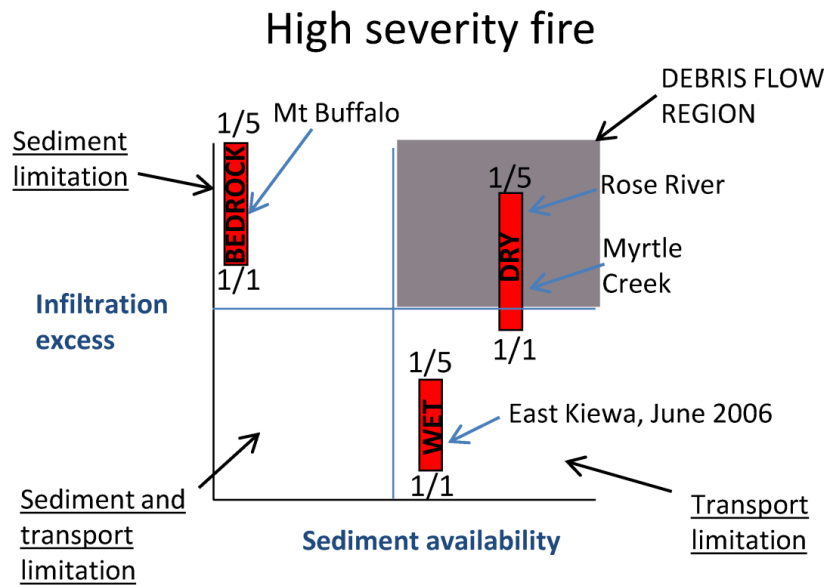


Figure 6.1 Conceptual representation of hillslope controls on debris flow initiation after a high severity fire. The responses at different sites are based on observation and data from Chapter 2. Sediment availability and infiltration excess are affected by fire but differ in different landscape units resulting in debris flows susceptibility which varies depending on geology and forest ecosystems. Landscape units such as exposed bedrock, shallow soil (dry forest) and deep soils (wet forest) are represented as red bars positioned in hypothetical locations along the two axes. The fractions above and below each bar are hypothetical storm return intervals. The bars shift around on the two depending on the severity of the fire and subsequent recovery. The site names are from post-fire erosion surveys in Chapter 2.

In the following sections we revisit the infiltration and sediment availability parameters from Chapter 4 and 5 respectively, and develop a framework for representing how these parameters may vary in space and time. The section provides a summary and a synthesis of the concepts developed in Chapters 2 to 5. A broad distinction is made between the ‘dry’ and ‘wet’ forest types (see detailed description of these categories and their geomorphic and hydrological significance in section “2.2 Regional Setting” in Chapter 2). The aim is to analyse how spatial and temporal variability in infiltration and sediment availability may influence hillslope erosion and debris flow initiation in burnt catchments in the eastern uplands of Victoria (southeast Australia).

6.2 Spatial and temporal variability in infiltration and sediment availability

6.2.1 Infiltration

The steady-state infiltration capacity (K_p) in the transport equations in Chapter 3 were parameterised from a limited set of measurements and assume that the proportion of exposed rock was the only source of variability in infiltration between catchments. Clearly there are other sources of variability in infiltration rates due to surface storage, water repellency and macroporosity being highly variable in space and time. In the following section, the infiltration equations in Chapter 4 (see Figure 4.6 and 4.7) are used to model the temporal dynamics in infiltration capacity (K_p) of dry and wet forests types (EVCs) of eastern uplands of Victoria (Figure 6.2). The aim is to explore how differences between the two systems are captured by the model and what this may mean in terms of debris flow processes. The equations represent a synthesis of the infiltration model and the data from Sunday Creek, Stony Creek and Ella Creek (Chapter 4) and the previous data collected in the East Kiewa Catchments (Nyman *et al.* 2010).

The maximum steady state infiltration capacity or ponded hydraulic conductivity (K_p) is the sum of matrix flow, K_{mat} (mm h^{-1}), and macropore flow, K_{mac} (mm h^{-1}).

$$K_p = K_{mat} + K_{mac} \quad 6.1$$

Matrix flow varies temporally due to changes in water repellency status, CST_{min} (dyn cm^{-1}):

$$K_{mat} = K_{mat(i)} + 0.083 e^{-0.083 * CST_{min}} \quad 6.2$$

The initial matrix flow parameter ($K_{mat(i)}$) is the matrix flow potential (K_{mat}) under highly water repellent conditions. The water repellency, CST_{min} , in the eucalypt forest was independent of the fire event but varied with changes in monthly weather patterns ($KBDI$):

$$CST_{min} = CST_{min(i)} (1 + 0.80 e^{-0.026 * KBDI}) \quad 6.3$$

The initial water repellency, $CST_{min(i)}$, is the CST_{min} for dry field conditions (monthly $KBDI > 100$) and corresponds with the matrix flow potential (K_i) in equation (6.2).

Macropore flow (K_{mac}) increases linearly with time since fire t_{sf} (yrs), and is proportional to macroporosity (θ_{mac}) and the soil matrix which is active and not water repellent (K_{mat}). Macroporosity (θ_{mac}) is the total volume of pores with radius > 0.5 mm and was determined by from the water holding capacity ($\text{cm}^3 \text{cm}^{-3}$) between pressure heads (h) of -15 and 0 mm (Figure 4.8, Chapter 4);

$$K_{mac} = 235 * K_{mat} \theta_{mac} t_{sf} \quad 6.4$$

The matrix flow (K_{mat}) is obtained from the matrix flow equation (6.2) above. In this equation (6.4), the macropore flow (K_{mac}) increases indefinitely with t_{sf} . This is not realistic since the effect of recovery should be diminishing with time where K_{mac} approaches some value representative of undisturbed conditions. The data used to derive the ratios in equation (6.4), however, did not provide sufficient evidence to characterise the asymptote. The interpretation of the function is therefore restricted to a single year following the fire impacts.

The parameter values for $K_{min(i)}$, $CST_{min(i)}$ and θ_{mac} in dry forest ecosystems (EVC) were 1.57 cm h^{-1} , 30.0 dyn cm^{-1} and $1.2 \times 10^{-2} \text{ cm}^3 \text{ cm}^{-3}$, respectively (these are the average values from Stony Creek, Sunday Creek and Ella Creek reported in Chapter 4.).

Corresponding values for wet EVC at Spring Creek (East Kiewa) were 2.13 cm h^{-1} , 30.0 dyn cm^{-2} , $6.0 \times 10^{-2} \text{ cm}^3 \text{ cm}^{-3}$ (from Nyman *et al.* 2010). All parameters were obtained from sites burned at high severity. The modelled changes infiltration capacity during recovery is presented in Figure 6.2. The change in surface storage potential (H) with t_{sf} (Figure 4.8b) is not presented here in this chapter, because the comparison between wet and dry EVCs is focused infiltration under steady state conditions.

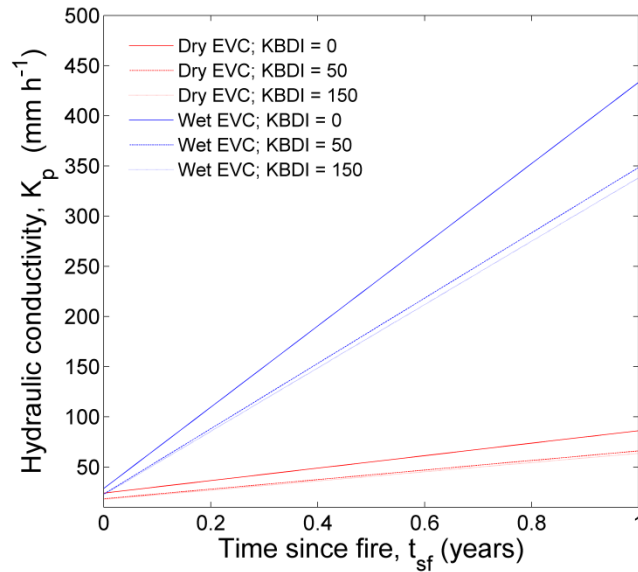


Figure 6.2 Model of infiltration capacity, K_p , as a function of time since fire (t_{sf}) in wet and dry forest ecosystems (EVC) at different levels of dryness ($KBDI$) in eastern uplands of Victoria, southeast Australia. The infiltration capacity is a function of macropore availability (θ_{mac}), matrix flow potential (K_{mat}) and its dependency on temporal dynamics in water repellency (CST_{min}). The model is restricted to conditions where $t_{sf} \leq 1$ yr, because there not sufficient data to support the model for wet and dry EVCs beyond this point.

The model captures changes in infiltration capacity (K_p) due to increased macropore availability with times since fire (t_{sf}) and temporal dynamics due to weather induced changes to water repellency (CST_{min}). The data in Chapter 4 did not indicate that the fire itself impacted on CST_{min} , so this property did not vary with t_{sf} . The model indicates that initially after the fire, there is only a slight difference between infiltration in dry and wet EVCs. This effect suggest that the soil surface after fire is homogenised through heat impacts and ash deposition, consistent with the notion that fire can act to reduce landscape variability (Ebel 2012). More data is required, however, to determine how K_p varies between systems at $t_{sf} = 0$. The infiltration capacity (K_p) of soils in dry and wet EVCs diverge rapidly with t_{sf} in the model. This divergence can be interpreted to be a result of highly contrasting background soil properties. The relatively high levels of macroporosity in wet EVCs ($\theta_{mac} = 6.0 \times 10^{-2} \text{ cm}^3 \text{ cm}^{-3}$) and the dominant role of macropore flow in determining K_p means the changes in K_p in wet forest is more sensitive to the recovery of the heat impacted surface soil. In other words, the wet

forests display a much large change in K_p for every unit of t_{sf} when compared to dry EVCs where background macroporosity is relatively low ($\theta_{mac} = 1.2 \times 10^{-2} \text{ cm}^3 \text{ cm}^{-3}$).

The model of infiltration capacity has obvious limitations in its current form. There is only limited data set to support the different behaviour of soil in wet and dry ecosystems and the relations have been parameterised using small scale infiltration measurements which have yet to be linked to large scale runoff behaviour on hillslopes. The role of macropores is clearly important, but the strong sensitivity of K_p to macropore flow (K_{mac}) means that more work may be required to get refine the infiltration parameters in the highly variable uplands of eastern Victoria. The application of the model in this section should therefore only be seen as an example of how the infiltration parameters from Chapter 4 can be used to represent recovery processes in spatially variable landscapes. As such the model provides a first step towards developing a validated model of runoff generation in a landscape with high spatial-temporal variability.

6.2.2 Sediment availability

In Chapter 5 the sediment availability on burnt hillslopes was modelled as the depth of non-cohesive soil, d_{nc} (cm), and quantified in headwater catchments during a 3 year recovery window. The depth of non-cohesive soil (d_{nc}) was initially 0.9 cm, and then decayed exponentially:

$$d_{nc} = 0.9 * e^{-1.6t_{sf}} \quad 6.5$$

The measurements of sediment availability in Chapter 5 were restricted to dry EVCs. In wet EVCs the parameter for initial d_{nc} after fire was obtained using rill erosion experiments from the East Kiewa Catchments reported in Sheridan et al. (2007a). The parameter was calculated using the method developed in Chapter 4 when analysing of sediment flux from flumes at Sunday Creek (see: 5.3.2.1 Field flumes: the flux and availability of sediment). The initial depth of non-cohesive soil (d_{nc}) for the wet EVCs 1 months after the burn was 1.0 cm, similar to dry forest, indicating perhaps that the heat effect from wildfire is restricted to some maximum depth. The bulk density of surface soils in wet and dry EVC were 0.6 and 1.3 kg m^{-3} , respectively, which means that the mass of available soil was much higher in dry forest systems (Figure 6.3). The large difference in bulk density between the two systems may attributed to the much higher

gravel content in soils of dry EVCs (31-54 %: see Table 3.1) than wet EVCs (3-11 %: Rowe 1972), a feature most likely linked to the different moisture regimes and its effects on site productivity.

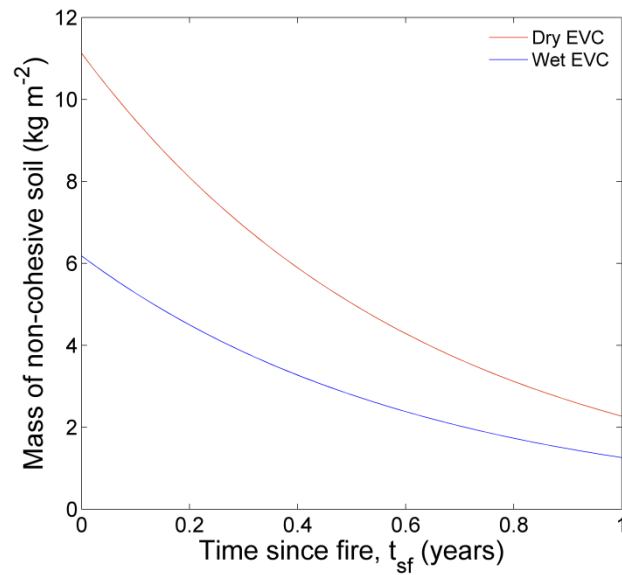


Figure 6.3 Mass of non-cohesive soils on burnt hillslopes in of wet and dry forest ecosystems (EVCs) in Eastern Uplands of Victoria, southeast Australia.

6.3 Modelling response during recovery: transport equations revisited

6.3.1 Rainfall excess

This section revisits the transport equations (3.3) in Chapter 3 and incorporates the new parameter information on spatial variability and recovery on burnt hillslope in dry and wet *Eucalypt* forests in the uplands of eastern Victorian. In Chapter 3 the rainfall excess (Q) was calculated by subtracting steady state infiltration capacity (K_p) from rainfall intensity (I). The infiltration capacity was based on a limited number of samples ($n = 15$) and the geometric mean was taken to represent the average infiltration rate (assuming a log-normal distribution). The data from intensive sampling of ponded infiltration rates in Chapter 5, however, indicate that the steady state infiltration capacity K_p is exponentially distributed (Figure 6.4a).

In this section the rainfall excess (Q) was calculated using the analytical framework presented for steady-state conditions in (Hawkins and Cundy 1987) (Figure 6.4d). The apparent infiltration rate was then estimated as the minimum infiltration rate in the envelope curves presented in (equation 3: Hawkins and Cundy 1987), assuming that

each point on the hillslopes drain independently to the outlet (i.e. no run-on infiltration). This assumption is acceptable during debris flow initiation since the rainfall rates are high relative to K_p (Nahar 2003). The mean infiltration capacity (K_p) at each debris flow sites was adjusted for the percentage of exposed rock on the soil surface (from Table 3.1).

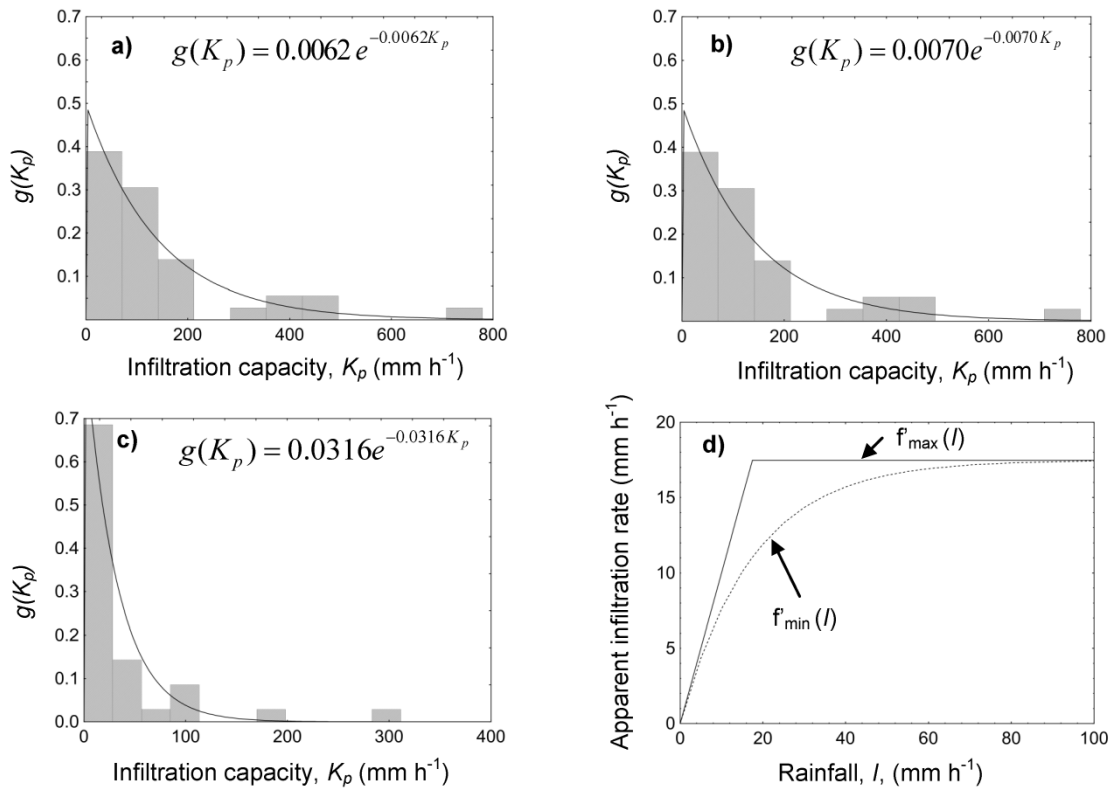


Figure 6.4 Exponential probability distribution function, $g(K_p)$, of infiltration capacity (K_p) measured at a) Ella Creek in July 2009 ($K_p = 161 \text{ mm h}^{-1}$), b) Sunday Creek in Sept 2010 (mean $K_p = 143 \text{ mm h}^{-1}$), and c) Stony Creek in December 2009 (mean $K_p = 31 \text{ mm h}^{-1}$). The distributions were exponential for all time-steps at all other sites. d) The envelope curves for the apparent infiltration rate as a function of rainfall intensity. In this example the mean infiltration capacity (K_p) is 17.5 mm h^{-1} , representative of hillslopes in dry *Eucalypt* with 15% rock content two months after fire.

6.3.2 Debris flows initiation and erosion

The rainfall excess was estimated from 30 and 15-minute rainfall intensities (I_{30} and I_{15}) and steady state infiltration rate, $f_{\min}(I)$, taking into account the changes in infiltration capacity (K_p) with time since fire. See Chapter 3 for details regarding the erosion data and fitting procedure and the used parameterise the parameters in this section. The results from the fitting are shown in Figure 6.5 and Figure 6.6.

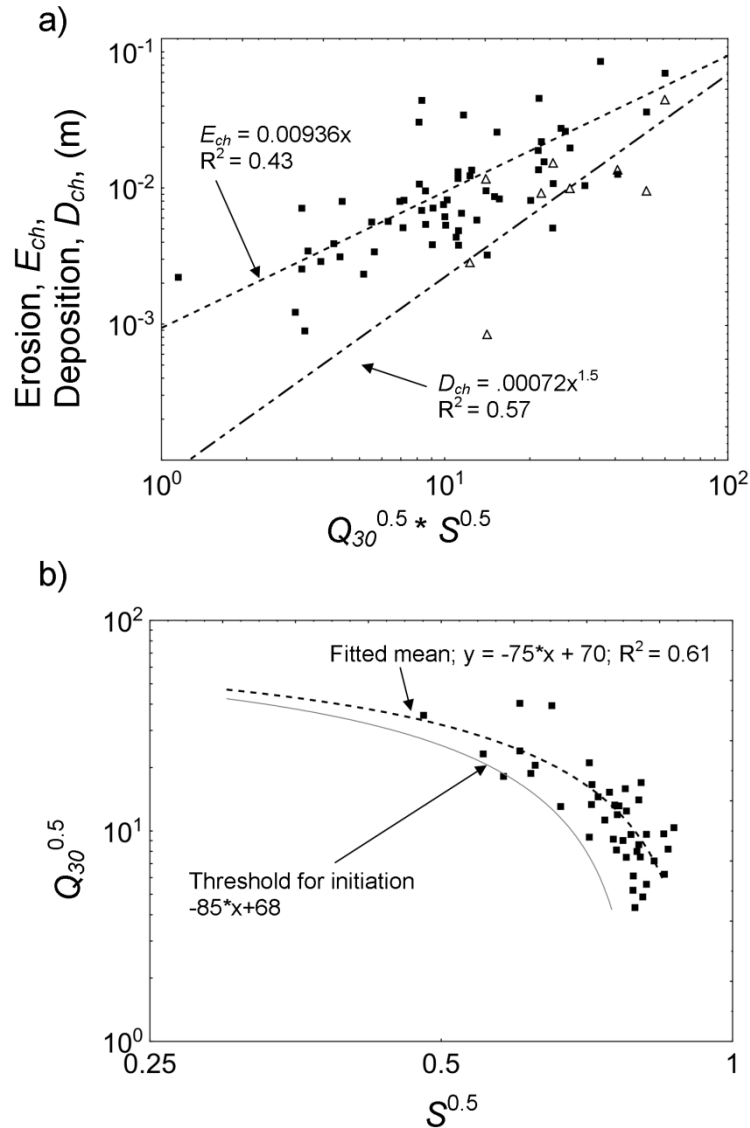


Figure 6.5 a) Depth of channel erosion and deposition and b) channel initiation as a function of contributing infiltration excess and local slope.

The erosion depth on hillslopes was initially fitted using the data from Target Creek and Mt Tamboritha. The debris flows at these sites occurred within one month of the fire events and were therefore considered to be representative of sediment availability immediately following the burn. The parameters m and n from this fitting were retained while fitting the sediment availability parameter, k_e , using the data from the other sites where the debris flows occurred at some point within the first year of the fire (Figure 6.4a). Interestingly the sediment availability parameter decays exponentially at the similar rate (decay constant = -1.5, $R^2 = 0.49$) (Figure 6.4b) as the decay in depth of non cohesive soil, d_{nc} , in see Chapter 5 (decay constant = -1.6) (Figure 5.12c).

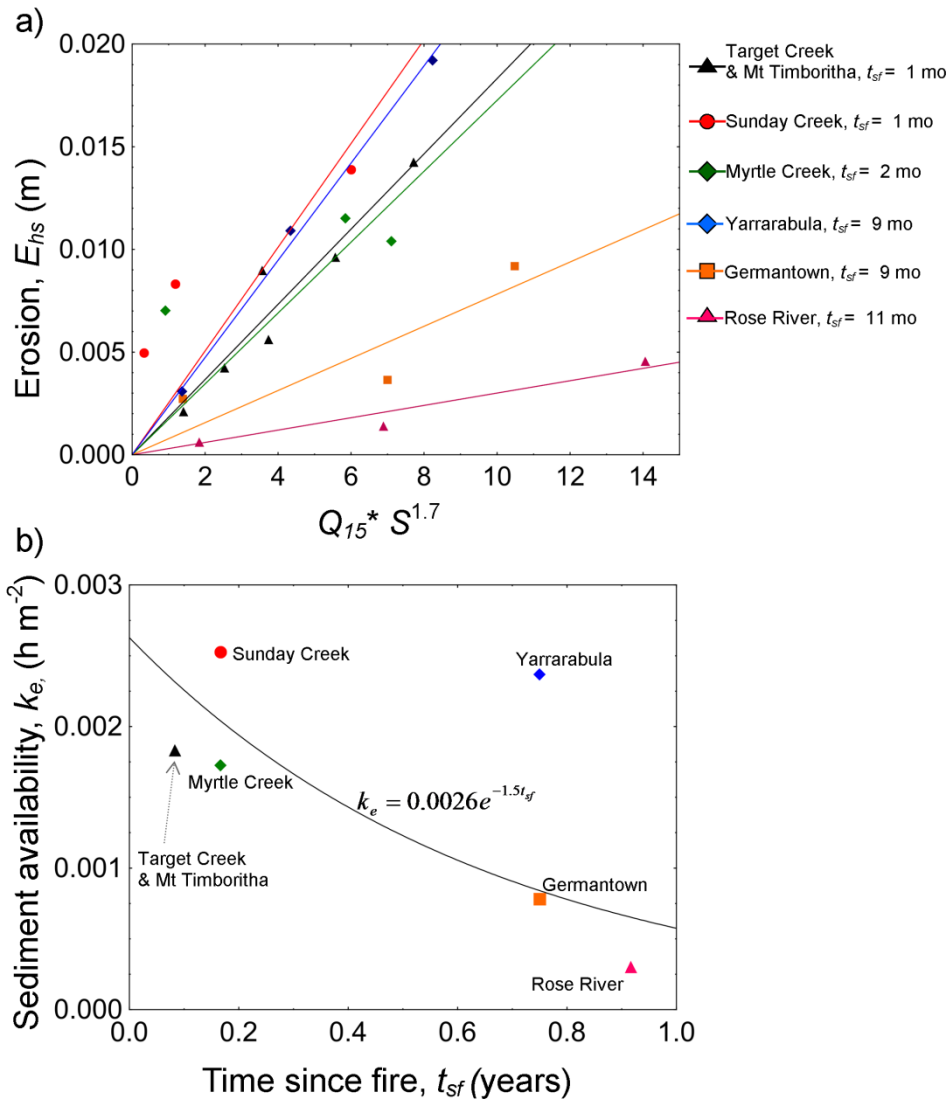


Figure 6.6. a) Hillslope erosion as function of rainfall excess (Q_{15}) and local slope (S). Each site represents erosion at different stages of recovery so the sediment availability parameter k_b varies from site to site. b) Changes in sediment availability, k_e , with time since fire, t_{sf} .

6.3.2 Model applications

The empirical relations in Figure 6.5 and 6.6 link rainfall excess (Q) and local slope (S) to channel initiation and local erosion rates. This type of model can be used to explore the effects of topography and landscape-scale variability in infiltration properties on catchment response. One obvious application is the opportunity to determine the probability of debris flow initiation. Channel initiation by debris flows is a threshold driven process which can be expressed in terms of rainfall excess and local slope

(Figure 6.5b). Spatial and temporal variability in infiltration properties and variable topography means that the rainfall events required for channel initiation varies depending on location of events and their timing in relation to recovery. The probability of exceeding this threshold can be obtained by linking the 30-minute storm intensity to rainfall probabilities from design storm parameters. This approach can be used to evaluate the changes in debris flow probability due to changes in infiltration capacity as a result of recovery or spatial variability between forest ecosystems. This type of output can help inform land managers about variation in hazard across burnt landscapes. The model also provides estimates of the actual probability of debris flow initiation given local catchment conditions (topography and infiltration capacity) and local rainfall regime.

Another application is the prediction of channel and hillslope erosion once the initiation threshold has been exceeded (see Chapter 3). Sediment loads from hillslopes and channels can be modelled separately, something which is important when predicting water quality impacts, given the different properties of the two source contributions (see Chapter 3). In channels, the effects of soil properties on response magnitude is driven by variability in infiltration capacity which impacts on infiltration excess and hence erosion rates. On hillslopes, both infiltration capacity and sediment availability change during recovery, thus influencing the rate of erosion for a given rainfall event. The rate of deposition in channels was represented as a function of the same variables and parameters which determine erosion. The rate of sediment deposition by debris flows varies depending on the magnitude of the debris flow as well as the catchment and channel configuration. This modelling approach provides estimates of debris flow magnitude which take into account the reduced sediment delivery once deposition starts dominating the debris flow process. This means that the catchment outlet does not need to be defined a priori to make predictions of event magnitude. In summary, the equations for hillslope erosion, channel initiation, channel erosion and channel deposition can be combined to predict the initiation and magnitude of post-fire debris flows. In future research we will aim to build a data set which can be used to test the how well the model is able to predict debris flow response in landscapes with properties which vary in space and time.

6.4 Conclusions and future research priorities

Sediment delivery from headwaters to stream networks in upland catchments is often dominated by events such as landslides and debris flow which are patchy and episodic in space and time (Kirchner *et al.* 2001; Meyer *et al.* 2001; Meyer *et al.* 1992; Miller *et al.* 2003a). Most of the time the forested headwaters experience local redistribution of sediment which means that the headwater systems behave as temporal sediment stores (Benda *et al.* 2005; Gomi *et al.* 2002). It is the interplay between rates of sediment accumulation and the frequency of evacuation which determines how headwaters contribute to the overall sediment dynamics at larger scales. Understanding this interplay between storage and delivery of sediment provides is necessary in order to determine the effects of forest disturbance on catchment processes and aquatic ecosystems.

The overall objective of the thesis was to improve the capacity to predict hydrological responses leading to water quality impacts after fire in forested catchments, focusing in particular on high magnitude events, since these were documented to represent a considerable risk to water supply systems in the southeast Australian region (Sheridan *et al.* 2007b; Smith *et al.* 2011c). The large fires in 2003, 2007 and 2009 were used as an opportunity to explore in detail the linkages between debris flow responses, rainfall and landscape controls. Chapter 2 provided a regional context and documented the dominant processes underlying high-magnitude events that resulted in water quality impacts. Chapter 3 quantified the event magnitude, sediment source contributions and triggering rainfall. The results from this chapter formed the basis for developing a set of parameters which could be used to predict initiation and magnitude of debris flows.

Chapter 4 and 5, respectively, were concerned with infiltration and sediment availability as controls post-fire erosion response. The aim of these chapters was to develop new ways of characterising soil properties of burnt systems which incorporated the effects of recovery and variable ecosystem properties. These two chapters provide improved predictive capacity as well as new knowledge relating to fire-effects and the factors which drive spatial and temporal variability in soil properties after fire. In this last chapter (Chapter 6) we have shown how these new insights could be combined to predict the initiation and magnitude of post-fire debris flows in a modelling approach

that allows for more direct representation of soil parameters, fire-effects and recovery than existing statistical models of debris flow initiation and magnitude.

The thesis has improved our understanding of how fire impacts on hydrologic and geomorphic properties and has enhanced the capacity to predict where, when and how debris flows occur in burnt catchments of southeast Australia. The key contributions can be summarised as follows;

- The study first identified the dominant erosion processes underlying post-fire debris flows in the study regions and quantified the magnitude of debris flows, sediment source contributions and triggering rainfall events. Post-fire debris flows were previously not documented in the southeast Australian region and there was a paucity of information relating to processes, controls and magnitude of events.
- Models were then developed in order to represent sediment availability and infiltration capacity as parameters which respond to the effects of fire and subsequent recovery. The layered soil profile in burnt systems means that many of the traditional methods for measuring and modelling sediment availability and infiltration are often unsuitable. This meant that the properties required new conceptual representations and new types of measurements in order to capture the key elements of the system.
- Infiltration capacity and sediment availability were finally incorporated into a model of debris flow initiation and magnitude. The modelling approach means that the debris flow response can be modelled as a function of the temporal and spatial variability in the hillslope parameters which are affected differently by fire in different systems. The data produced during the field surveys was used in the calibration of the model, and in future work we aim to generate additional data sets which can be used to test the ability of the model to capture the effects of topography and variable soil properties on initiation and magnitude of debris flows.

There is scope for building further on the model. First, in its current form, the model represents transport through a combination of topography and a simple expression for rainfall excess. The conversion of rainfall excess to runoff is not represented and the effect of surface roughness is therefore not included in the model. Future improvements

would be to model runoff more comprehensively using either a geomorphic approach or a more parameter intensive dynamic and distributed approach. This leads to a second topic for further research: modelling the transition from surface runoff to debris flow conditions. This process involves complex feedback between runoff generation, sediment entrainment and changes to viscosity, fluid density and subsequent effects on rheology. This modelling challenge is important in terms of understanding the processes. However this type of research may not enhance predictive capacity, given the dominance of surface runoff in terms of initiation mechanism.

The model of infiltration and sediment availability in burnt soils were developed and parameterized for a limited set of sites and burn conditions. There is scope for building on these models and incorporating new data sets from other regions and from fires with different levels of severity. In this context it would also be useful to explore how water availability in the landscape interacts with ecosystem processes, soil development and ultimately how it impacts in the hydro-geomorphic response to wildfire. The categories of 'wet' and 'dry' ecological vegetation classes reflect differences in climate and dryness. A more meaningful approach to characterising this effect would be to develop a dryness variable that responds to spatial variability in solar exposure, temperature and precipitation. This would allow for better linkage between the climatic drivers, topography and fire-effects as controls on erosion rates in the region.

References

- Alexander LV, Hope P, Collins D, Trewin B, Lynch A, Nicholls N (2007) Trends in Australia's climate means and extremes: a global context. *Australian Meteorological Magazine* **56**(1), 1-18.
- Badia D, Marti C (2003) Plant Ash and Heat Intensity Effects on Chemical and Physical Properties of Two Contrasting Soils. *Arid Land Research and Management* **17**(1), 23-41.
- Benavides-Solorio J, MacDonald LH (2001) Post-fire runoff and erosion from simulated rainfall on small plots, Colorado Front Range. *Hydrological Processes* **15**(15), 2931-2952.
- Benda L, Dunne T (1997) Stochastic forcing of sediment supply to channel networks from landsliding and debris flow. *Water Resources Research* **33**(12), 2849-2863.
- Benda L, Hassan MA, Church M, May CL (2005) Geomorphology of steepland headwaters: the transition from hillslopes to channels *JAWRA Journal of the American Water Resources Association* **41**(4), 835-851.
- Benda L, Miller D, Bigelow P, Andras K (2003) Effects of post-wildfire erosion on channel environments, Boise River, Idaho. *Forest Ecology and Management* **178**(1-2), 105-119.
- Berry J, Bradley S (2003) Cruel irony claims firefighter. In 'The Age. ' (FairfaxDigital: Melbourne)
- Bisson PA, Rieman BE, Luce C, Hessburg PF, Lee DC, Kershner JL, Reeves GH, Gresswell RE (2003) Fire and aquatic ecosystems of the western USA: current knowledge and key questions. *Forest Ecology and Management* **178**(1-2), 213-229.
- Blake WH, Wallbrink PJ, Wilkinson SN, Humphreys GS, Doerr SH, Shakesby RA, Tomkins KM (2009) Deriving hillslope sediment budgets in wildfire-affected forests using fallout radionuclide tracers. *Geomorphology* **104**(3-4), 105-116.
- Bodí MB, Doerr SH, Cerdà A, Mataix-Solera J (2012) Hydrological effects of a layer of vegetation ash on underlying wettable and water repellent soil. *Geoderma*(0).

Bowman G, Hutka J (2002) Particel Size Analysis. In 'Soil Physical Measurement and Interpretation for Land Evaluation.' (Eds K Coughlan, H Cresswell and N McKenzie). (CSIRO PUBLISHING: Melbourne)

Bradstock RA (2008) Effects of large fires on biodiversity in south-eastern Australia: disaster or template for diversity? *International Journal of Wildland Fire* **17**(6), 809-822.

Bradstock RA, Hammill KA, Collins L, Price O (2010) Effects of weather, fuel and terrain on fire severity in topographically diverse landscapes of south-eastern Australia. *Landscape Ecology* **25**(4), 607-619. [In English]

Bray RH, Kurtz L (1945) Determination of total, organic, and available forms of phosphorus in soils. *Soil Science* **59**(1), 39-46.

Brown JAH (1972) Hydrologic effects of a bushfire in a catchment in south-eastern New South Wales. *Journal of Hydrology* **15**(1), 77-96.

Brutsaert W (2005) 'Hydrology: an introduction.'

Bryan RB (2000) Soil erodibility and processes of water erosion on hillslope. *Geomorphology* **32**(3-4), 385-415.

Burch GJ, Moore ID, Burns J (1989) Soil hydrophobic effects on infiltration and catchment runoff. *Hydrological Processes* **3**(3), 211-222. [In English]

Cai W, Cowan T, Raupach M (2009) Positive Indian Ocean Dipole events precondition southeast Australia bushfires. *Geophys. Res. Lett.* **36**.

Cannon S, Gartner JE, Parrett C, Parise M Wildfire-related debris-flow generation through episodic pregrssive sediment-bulking processes, western USA. In 'Debris-Flow Hazards Mitigation - Mechanics, Prediction, and Assessment, Proceedings of the Third International Conference on Debris-Flow Hazards Mitigation', 2003, Davos, Switzerland. (Eds. D Rickenmann and CL Chen), pp. 71-82

- Cannon SH (2001) Debris-flow generation from recently burned watersheds. *Environmental & Engineering Geoscience* **7**(4), 321-341.
- Cannon SH, Bigio ER, Mine E (2001a) A process for fire-related debris flow initiation, Cerro Grande fire, New Mexico. *Hydrological Processes* **15**(15), 3011-3023.
- Cannon SH, Gartner JE (2005) Wildfire-related debris flow from a hazards perspective. In 'Debris-flow Hazards and Related Phenomena.' (Eds M Jakob and O Hungr) pp. 363-385. (Springer Berlin Heidelberg)
- Cannon SH, Gartner JE, Rupert MG, Michael JA, Rea AH, Parrett C (2010) Predicting the probability and volume of postwildfire debris flows in the intermountain western United States. *Geological Society of America Bulletin* **122**(1-2), 127-144.
- Cannon SH, Gartner JE, Wilson RC, Bowers JC, Laber JL (2008) Storm rainfall conditions for floods and debris flows from recently burned areas in southwestern Colorado and southern California. *Geomorphology* **96**(3-4), 250-269.
- Cannon SH, Kirkham RM, Parise M (2001b) Wildfire-related debris-flow initiation processes, Storm King Mountain, Colorado. *Geomorphology* **39**(3-4), 171-188.
- Carmichael RS (1989) Practical handbook of physical properties of rocks and minerals. In ' ' Ed. RS Carmichael) pp. 741. (CRC Press: Boca Raton, Florida)
- Cawson JG, Sheridan GJ, Smith HG, Lane PNJ (2012) Surface runoff and erosion after prescribed burning and the effect of different fire regimes in forests and shrublands: a review. *International Journal of Wildland Fire*, -.
- Cecil M (1981) Investigation of a slope mantle. Monash University, Melbourne.
- Cerdà A, Doerr SH (2008) The effect of ash and needle cover on surface runoff and erosion in the immediate post-fire period. *CATENA* **74**(3), 256-263.
- Chafer CJ (2008) A comparison of fire severity measures: An Australian example and implications for predicting major areas of soil erosion. *Catena* **74**(3), 235-245. [In English]

- Chessman BC (1986) Impact of the 1983 wildfires on river water quality in East Gippsland, Victoria. *Marine and Freshwater Research* **37**(3), 399-420.
- Cook F (2007) Unsaturated hydraulic conductivity: Laboratory tension infiltrometer. In 'Soil Sampling and Methods of Analysis.' (Eds M Carter and E Gregorich). (CRC. Retrieved July 27, 2012, from Ebook Library.)
- Costa JE (1988) Rheologic, geomorphic, and sedimentologic differentiation of water floods, hyperconcentrated flows, and debris flows. In 'Flood Geomorphology.' (Eds VR Baker, RC Kochel and PC Patten) pp. 113-122. (Wiley-Intersciences: New York)
- Crockford H, Topalidis S, Richardson DP (1991) Water repellency in a dry sclerophyll eucalypt forest - measurements and processes. *Hydrological Processes* **5**(4), 405-420.
- Davis SH, Vertessy RA, Silberstein RP (1999) The sensitivity of a catchment model to soil hydraulic properties obtained by using different measurement techniques. *Hydrological Processes* **13**(5), 677-688.
- De Baets S, Poesen J (2010) Empirical models for predicting the erosion-reducing effects of plant roots during concentrated flow erosion. *Geomorphology* **118**(3-4), 425-432.
- DeBano LF (2000) The role of fire and soil heating on water repellency in wildland environments: a review. *Journal of Hydrology* **231-232**, 195-206.
- DeBano LF, Neary DG, Folliott PF (2005) Chapter 2: Soil Physical Properties. In 'Wildland fire in ecosystems: effects of fire on soils and water.' (Eds Neary DG, Ryan KC and D LF). (U.S. Department of Agriculture, Forest Service, Rocky Mountain Research Station, : Ogden, UT.)
- Department of Primary Industries (2009) Fisheries Note: Effect of bushfire on trout in Victoria. Fisheries Victoria, Melbourne.
- Department of Sustainability and Environment (2009) Remote Sensing Guideline for Assessing Landscape Scale Fire Severity in Victoria's Forest Estate: Guideline - Reference manual for SOP No.4. Melbourne.

Doerr SH, Blake WH, Shakesby RA, Stagnitti F, Vuurens SH, Humphreys GS, Wallbrink P (2004) Heating effects on water repellency in Australian eucalypt forest soils and their value in estimating wildfire soil temperatures. *International Journal of Wildland Fire* **13**(2), 157-163. [In English]

Doerr SH, Moody JA (2004) Hydrological effects of soil water repellency: on spatial and temporal uncertainties. *Hydrological Processes* **18**(4), 829-832. [In English]

Doerr SH, Shakesby RA, Blake WH, Chafer CJ, Humphreys GS, Wallbrink PJ (2006) Effects of differing wildfire severities on soil wettability and implications for hydrological response. *Journal of Hydrology* **319**(1-4), 295-311.

Doerr SH, Shakesby RA, Walsh RPD (1996) Soil hydrophobicity variations with depth and particle size fraction in burned and unburned Eucalyptus globulus and Pinus pinaster forest terrain in the Águeda Basin, Portugal. *CATENA* **27**(1), 25-47.

Doerr SH, Shakesby RA, Walsh RPD (1998) Spatial variability of soil hydrophobicity in fire-prone eucalyptus and pine forests, Portugal. *Soil Science* **163**(4), 313-324. [In English]

Doerr SH, Shakesby RA, Walsh RPD (2000) Soil water repellency: its causes, characteristics and hydro-geomorphological significance. *Earth-Science Reviews* **51**(1-4), 33-65.

Dulhunty K (2009) Road left covered in sludge. In 'The Border Mail.' (FairfaxDigital: Wodonga)

Ebel BA (2012) Wildfire impacts on soil-water retention in the Colorado Front Range, United States. *Water Resources Research* **48**(12), W12515.

Ebel BA, Moody JA (2013) Rethinking infiltration in wildfire-affected soils. *Hydrological Processes*, n/a-n/a.

Ebel BA, Moody JA, Martin DA (2012) Hydrologic conditions controlling runoff generation immediately after wildfire. *Water Resour. Res.* **48**(3), W03529.

Elliot WJ, Liebenow AM, Laflen JM, Kohl KD (1989) A compendium of soil erodibility data from WEPP cropland soil field erodibility experiments 1987 & 1988. Natl. Soil Erosion Res. Lab., West Lafayette, Indiana.

Elliot WJ, Robichaud. PR, Hall DE, Cuhaciyen. CO, Pierson. FB, Wohlgemuth. PM (2001) A Probabilistic Approach To Modeling Erosion for Spatially-Varied Conditions. In '2001 ASAE Annual Meeting. '

Elliott JG, Smith ME, *et al.* (2004) Analysis and mapping of post-fire hydrologic hazards for the 2002 Hayman, Coal Seam, and Missionary Ridge wildfires. USGS, Colorado, US.

Emelko MB (2011) Implications of land disturbance on drinking water treatability in a changing climate: Demonstrating the need for “source water supply and protection” strategies. *Water Research* **45**(2), 461.

Evans R, Joyce E (1974) Landslides in Victoria. *Victorian Naturalist* **49**, 241-243.

Fattet M, Fu Y, Ghestem M, Ma W, Foulonneau M, Nespoulous J, Le Bissonnais Y, Stokes A (2011) Effects of vegetation type on soil resistance to erosion: Relationship between aggregate stability and shear strength. *CATENA* **87**(1), 60-69.

Ferguson R, Dwyer C, Loffler T, Hardie R (2004) Northeast Catchment Management Authority fire recovery pilot study: Buckland River and Omeo district catchments Earth Tech Engineering Pty Ltd, Wangaratta.

Fernández C, Vega JA, Vieira DCS (2010) Assessing soil erosion after fire and rehabilitation treatments in NW Spain: Performance of rusle and revised Morgan–Morgan–Finney models. *Land Degradation & Development* **21**(1), 58-67.

Flanagan DC, Gilley JE, Franti TG (2007) Water Erosion Prediction Project(WEPP): Development history, model capabilities, and future enhancements. *Transactions of the Asabe* **50**(5), 1603-1612.

Foster GR, Meyer LD (1972) A closed-form soil erosion equation for upland areas. In 'Sedimentation: Symp. to Honor Prof. H.A. Einstein.' Ed. H Shen) pp. 2.1–12.17: Fort Collins, CO)

- Gabet EJ (2003) Post-fire thin debris flows: sediment transport and numerical modelling. *Earth Surface Processes and Landforms* **28**(12), 1341-1348.
- Gabet EJ, Bookter A (2008) A morphometric analysis of gullies scoured by post-fire progressively bulked debris flows in southwest Montana, USA. *Geomorphology* **96**(3-4), 298-309.
- Gabet EJ, Sternberg P (2008) The effects of vegetative ash on infiltration capacity, sediment transport, and the generation of progressively bulked debris flows. *Geomorphology* **101**(4), 666-673.
- García-Ruiz JM, Arnáez J, Gómez-Villar A, Ortigosa L, Lana-Renault N (2012) Fire-related debris flows in the Iberian Range, Spain. *Geomorphology*(0).
- Gartner JE, Cannon SH, Santi PM, Dewolfe VG (2008) Empirical models to predict the volumes of debris flows generated by recently burned basins in the western U.S. *Geomorphology* **96**(3-4), 339-354.
- Giovannini G, Lucchesi S (1983) Effect of fire on hydrophobic and cementing substances of soil aggregates *Soil Science* **136**(4), 231-236. [In English]
- Gomi T, Sidle RC, Richardson JS (2002) Understanding processes and downstream linkages of headwater systems. *Bioscience* **52**(10), 905-916.
- Gould J, WL M, Cheney N, Ellis P, Knight I, Sullivan A (2007) Fire in dry eucalypt forest: Fuel structure, fuel dynamics and fire behavior. CSIRO.
- Gould SF (1998) Proteoid root mats bind surface materials in Hawkesbury Sandstone biomantles. *Soil Research* **36**(6), 1019-1032.
- Govers G (1990) Empirical relationships on the transporting capacity of overland flow. *International Association of Hydrological Sciences* **189**, 45-63.
- Grabowski RC, Droppo IG, Wharton G (2011) Erodibility of cohesive sediment: The importance of sediment properties. *Earth-Science Reviews* **105**(3-4), 101-120.

Granged AJP, Jordán A, Zavala LM, Bárcenas G (2011) Fire-induced changes in soil water repellency increased fingered flow and runoff rates following the 2004 Huelva wildfire. *Hydrological Processes* **25**(10), 1614-1629.

Green WH, Ampt GA (1911) Studies on soil physics, 1. The flow of air and water through soils. *Journal of agricultural science* **4**(1), 1.

Guy HP (1977) Laboratory theory and methods for sediment analysis.

Gyssels G, Poesen J, Bochet E, Li Y (2005) Impact of plant roots on the resistance of soils to erosion by water: a review. *Progress in Physical Geography* **29**(2), 189-217.

Hairsine PB, Rose CW (1992) Modeling water erosion due to overland flow using physical principles: 1. Sheet flow. *Water Resour. Res.* **28**(1), 237-243.

Hancock G, Wilkinson S, Read A (2007) Sources of sediment and nutrients to the Gippsland Lakes assessed using catchment modelling and sediment tracers. Canberra.

Harman C, Stewardson M (2007) Post-fire coarse sediment yield in the Upper Tambo River Basin: Results and Analysis of a Preliminary Field Survey and Literature Review. University of Melbourne.

Hart SC, DeLuca TH, Newman GS, MacKenzie MD, Boyle SI (2005) Post-fire vegetative dynamics as drivers of microbial community structure and function in forest soils. *Forest Ecology and Management* **220**(1-3), 166-184.

Hawkins RH, Cundy TW (1987) Steady-state analysis of infiltration and overland-flow for spatially-varied hillslopes. *Water Resources Bulletin* **23**(2), 251-256. [In English]

Heiri O, Lotter AF, Lemcke G (2001) Loss on ignition as a method for estimating organic and carbonate content in sediments: reproducibility and comparability of results. *Journal of Paleolimnology* **25**(1), 101-110.

Hennessy K, Lucas C, Nicholls N, J Bathols, Suppiah R, Ricketts J (2005) Climate change impacts on fire-weather in south-east Australia. CSIRO Marine and Atmospheric Research.

Houghton J (2007) Never rains, but it pours as town finds itself caught between fire and flood. In 'The Sunday Age. ' (FairfaxDigital: Melbourne)

Hungerford RD, Harrington MG, Frandsen WH, Ryan KC, Niehoff GJ (1991) Influence of fire on factors that affect site productivity *Proceedings - Management and Productivity of Western-Montane Forest Soils* **280**, 32-50.

Hungr O, Evans SG, Bovis MJ, Hutchinson JN (2001) A review of the classification of landslides of the flow type. *Environmental & Engineering Geoscience* **7**(3), 221-238.

Hungr O, Morgan GC, Kellerhals R (1984) Quantitative-analysis of debris flow torrent hazards for design of remedial measures *Canadian Geotechnical Journal* **21**(4), 663-677.

Hyde K, Woods SW, Donahue J (2007) Predicting gully rejuvenation after wildfire using remotely sensed burn severity data. *Geomorphology* **86**(3-4), 496-511. [In English]

Ice GG, Neary DG, Adams PW (2004) Effects of wildfire on soils and watershed processes. *Journal of Forestry* **102**(6), 16-20.

Imeson AC, Verstraten JM, Vanmulligen EJ, Sevink J (1992) The effects of fires and water repellency on infiltration and runoff under Mediterranean type forest. *CATENA* **19**(3-4), 345-361.

Isbell RF (1996) 'The Australian soil classification.' (CSIRO Australia: Collingwood)

Istanbulluoglu E, Tarboton DG, Pack RT, Luce C (2003) A sediment transport model for incision of gullies on steep topography. *Water Resour. Res.* **39**(4), 1103.

Istanbulluoglu E, Tarboton DG, Pack RT, Luce CH (2004) Modeling of the interactions between forest vegetation, disturbances, and sediment yields. *Journal of Geophysical Research* **109**(F01009).

Iverson RM (1997) The physics of debris flows. *Reviews of Geophysics* **35**(3), 245-296.

Jackson M, Roering JJ (2009) Post-fire geomorphic response in steep, forested landscapes: Oregon Coast Range, USA. *Quaternary Science Reviews* **28**(11-12), 1131-1146.

Jenkins JJ (1991) Geomorphology. In 'Introducing Victoria's Geology.' (Eds G Cochrane, G Quick and S-J D.). (Geological Society of Australia (Victorian Division): Melbourne)

Jenny H (1994) 'Factors of soil formation : a system of quantitative pedology.' (New York McGraw-Hill 1941.)

Johansen MP, Hakonson TE, Breshears DD (2001) Post-fire runoff and erosion from rainfall simulation: contrasting forests with shrublands and grasslands. *Hydrological Processes* **15**(15), 2953-2965.

Jordan P, Curran M, Nicol D (2004) Debris flows caused by water repellent soils in recent burns in the Kootenays. *Aspect* **9**(3), 4-9.

Julien PY, Lan Y (1991) Rheology of Hyperconcentrations. *Journal of Hydraulic Engineering* **117**(3), 346-353.

Kantz H, Altmann E, Hallerberg S, Holstein D, Riegert A (2006) 'Extreme events in nature and society / S.Albeverio, V.Jentsch, H.Kantz (eds.).' (Springer: Berlin :)

Karunaratna AK, Kawamoto K, Moldrup P, de Jonge LW, Komatsu T (2010) A Simple Beta-Function Model for Soil-Water Repellency as a Function of Water and Organic Carbon Contents. *Soil Science* **175**(10), 461-468.

Kean JW, Staley DM, Cannon SH (2011) In situ measurements of post-fire debris flows in southern California: Comparisons of the timing and magnitude of 24 debris-flow events with rainfall and soil moisture conditions. *Journal of Geophysical Research-Earth Surface* **116**.

Keetch JJ, Byram GM (1968) 'A drought index for forest fire control.' (US Department of Agriculture, Forest Service, Southeastern Forest Experiment Station)

Kemper WD, Rosenau RC, Dexter AR (1987) Cohesion Development in Disrupted Soils as Affected by Clay and Organic Matter Content and Temperature. *Soil Science Society of America Journal* **51**(4), 860-867.

Kennedy A, Jamieson D Ecological Fire Management in North East Victoria. In 'The Joint AFAC/Bushfire CRC Conference', 2007, Hobart, Tasmania,

Kernshaw A, Clark J, Gill A, D'Costa D (2002) 'A history of fire in Australia ' (Cambridge University Press: Cambridge)

King PM (1981) Comparison of methods for measuring severity of water repellence of sandy soils and assessment of some factors that affect its measurement. *Australian Journal of Soil Research* **19**(4), 275-285.

Kirchner JW, Finkel RC, Riebe CS, Granger DE, Clayton JL, King JG, Megahan WF (2001) Mountain erosion over 10 yr, 10 k.y., and 10 m.y. time scales. *Geology* **29**(7), 591-594. [In English]

Kirkby MJ (1975) Hydrograph Modelling Strategies. In 'Process in Physical and Human Geography B2 - Process in Physical and Human Geography. ' pp. 69-90

Laflen JM, Elliot WJ, Flanagan DC, Meyer CR, Nearing MA (1997) WEPP-predicting water erosion using a process-based model. (computer model for predicting soil erosion). *Journal of Soil and Water Conservation* **v52**(n2), p96(7).

Lane P, Sheridan G, Noske P, Sherwin C, Costenaro J, Nyman P, Smith H Fire effects on forest hydrology: lessons from a multi-scale catchment experiment in SE Australia. In 'In Revisiting Experimental Catchment Studies in Forest Hydrology, Proceedings of a Workshop held during the XXV IUGG General Assembly', July 2011 2011, Melbourne,

Lane PNJ, Feikema PM, Sherwin CB, Peel MC, Freebairn AC (2010) Modelling the long term water yield impact of wildfire and other forest disturbance in Eucalypt forests. *Environmental Modelling & Software* **25**(4), 467-478.

Lane PNJ, Hairsine PB, Croke JC, Takken I (2006a) Quantifying diffuse pathways for overland flow between the roads and streams of the Mountain Ash forests of central Victoria Australia. *Hydrological Processes* **20**(9), 1875-1884. [In English]

Lane PNJ, Sheridan GJ, Noske PJ (2006b) Changes in sediment loads and discharge from small mountain catchments following wildfire in south Eastern Australia. *Journal of Hydrology*(331), 495-510.

Lane PNJ, Sheridan GJ, Noske PJ, Sherwin CB (2008) Phosphorus and nitrogen exports from SE Australian forests following wildfire. *Journal of Hydrology* **361**(1-2), 186-198.

Larsen IJ, MacDonald LH (2007) Predicting postfire sediment yields at the hillslope scale: Testing RUSLE and Disturbed WEPP. *Water Resources Research* **43**(11), 18. [In English]

Larsen IJ, MacDonald LH, Brown E, Rough D, Welsh MJ, Pietraszek JH, Libohova Z, de Dios Benavides-Solorio J, Schaffrath K (2009) Causes of Post-Fire Runoff and Erosion: Water Repellency, Cover, or Soil Sealing? *Soil Science Society of America Journal* **73**(4), 1393-1407.

Larsen IJ, Pederson JL, Schmidt JC (2006) Geologic versus wildfire controls on hillslope processes and debris flow initiation in the Green River canyons of Dinosaur National Monument. *Geomorphology* **81**(1-2), 114-127.

Lavee H, Kutiel P, Segev M, Benyamini Y (1995) Effect of surface-roughness on runoff and erosion in a mediterranean ecosystem - the role of fire *Geomorphology* **11**(3), 227-234.

Leavesley GH, Lusby GC, Litchy RW (1989) Infiltration and erosion characteristics of selected tephra deposits from the 1980 eruption of Mount St Helens, Washington, USA. *Hydrological Sciences Journal* **34**(3).

Lee D, Elrick D, Reynolds W, Clothier B (1985) A comparison of three field methods for measuring saturated hydraulic conductivity. *Canadian journal of soil science* **65**(3), 563-573.

Leighton-Boyce G, Doerr SH, Shakesby RA, Walsh RPD (2007) Quantifying the impact of soil water repellency on overland flow generation and erosion: a new approach using rainfall simulation and wetting agent on <I>in situ</I> soil. *Hydrological Processes* **21**(17), 2337-2345.

- Leighton-Boyce G, Doerr SH, Shakesby RA, Walsh RPD, Ferreira AJD, Boulet A, Coelho COA (2005) Temporal dynamics of water repellency and soil moisture in eucalypt plantations, Portugal. *Australian Journal of Soil Research* **43**(3), 269-280.
- Leitch C, Flinn D, van de Graaff R (1984) Erosion and nutrient loss resulting from Ash Wednesday (February 1983) wildfires: a case study. *Australian Forestry* **46**(3), 173-180.
- Leonard J, Perrier E, Rajot JL (2004) Biological macropores effect on runoff and infiltration: a combined experimental and modelling approach. *Agriculture Ecosystems & Environment* **104**(2), 277-285.
- Letey J Measurement of contact angle, water drop penetration time, and critical surface tension. In 'Symposium of Water-Repellent Soils', May 1969, Riverside, pp. 43-47
- Loughran RJ, Elliott GL, McFarlane DJ, Campbell BL (2004) A Survey of Soil Erosion in Australia using Caesium-137. *Australian Geographical Studies* **42**(2), 221-233.
- Lu H, Moran ChJ, Prosser IP, Raupach MR, Olley J, Petheram C (2003) Sheet and rill erosion and sediment delivery to streams: A basin wide estimation at hillslope to medium catchment scale. CSIRO, Canberra.
- Lyon JP, O'Connor JP (2008) Smoke on the water: Can riverine fish populations recover following a catastrophic fire-related sediment slug? *Austral Ecology* **33**(6), 794-806.
- MacDonald LH, Huffman EL (2004) Post-fire soil water repellency: Persistence and soil moisture thresholds. *Soil Science Society of America Journal* **68**(5), 1729-1734. [In English]
- MacDonald RC, Isbell RF, Speight JG, Walker J, Hopkins MS (1990) 'Australian Soil and Land Survey Field Handbook.' (Inkata Press: Melbourne)
- Mallik AU, Gimingham CH, Rahman AA (1984) Ecological effects of heather burning 1. Water infiltration, moisture retention and porosity of surface soil *Journal of Ecology* **72**(3), 767-776.

- Martin DA, Moody JA (2001) Comparison of soil infiltration rates in burned and unburned mountainous watersheds. *Hydrological Processes* **15**(15), 2893-2903.
- McCarthy MA, Malcolm Gill A, Lindenmayer DB (1999) Fire regimes in mountain ash forest: evidence from forest age structure, extinction models and wildlife habitat. *Forest Ecology and Management* **124**(2-3), 193-203.
- McGeehan SL, Naylor DV (1988) Automated instrumental analysis of carbon and nitrogen in plant and soil samples 1. *Communications in Soil Science and Plant Analysis* **19**(4), 493-505.
- Megahan WF (1974) Erosion over time on severely disturbed granitic soils: a model. Intermountain forest and range experiment station, Ogden, Utah.
- Meyer GA, Pierce JL, Wood SH, Jull AJT (2001) Fire, storms, and erosional events in the Idaho batholith. *Hydrological Processes* **15**(15), 3025-3038.
- Meyer GA, Wells SG (1997) Fire-related sedimentation events on alluvial fans, Yellowstone National Park, USA. *Journal of Sedimentary Research* **67**(5), 776-791.
- Meyer GA, Wells SG, Balling RC, Jull AJT (1992) Response of alluvial systems to fire and climate change in Yellowstone National Park. *Nature* **357**(6374), 147-150.
- Miller D, Luce C, Benda L (2003a) Time, space, and episodicity of physical disturbance in streams. *Forest Ecology and Management* **178**(1-2), 121-140.
- Miller DJ, Burnett KM (2008) A probabilistic model of debris-flow delivery to stream channels, demonstrated for the Coast Range of Oregon, USA. *Geomorphology* **94**(1-2), 184-205.
- Miller JD, Nyhan JW, R. Yool S (2003b) Modeling potential erosion due to the Cerro Grande Fire with a GIS-based implementation of the Revised Universal Soil Loss Equation. *International Journal of Wildland Fire* **12**(1), 85-100.
- Miyata S, Kosugi Ki, Gomi T, Onda Y, Takahisa M (2007) Surface runoff as affected by soil water repellency in a Japanese cypress forest. *Hydrological Processes* **21**(17), 2365-2376.

Moffet CA, Pierson FB, Robichaud PR, Spaeth KE, Hardegree SP (2007) Modeling soil erosion on steep sagebrush rangeland before and after prescribed fire. *CATENA* **71**(2), 218-228.

Moody JA (2012) An Analytical Method for Predicting Postwildfire Peak Discharges. US Geological Survey.

Moody JA, Ebel BA (2012) Hyper-dry conditions provide new insights into the cause of extreme floods after wildfire. *CATENA* **93**(0), 58-63.

Moody JA, Kinner DA, Úbeda X (2009) Linking hydraulic properties of fire-affected soils to infiltration and water repellency. *Journal of Hydrology* **379**(3-4), 291-303.

Moody JA, Martin D (2009a) Synthesis of sediment yields after wildland fire in different rainfall regimes in the western United States. *International Journal of Wildland Fire* **18**, 96-115.

Moody JA, Martin DA (2001a) Initial hydrologic and geomorphic response following a wildfire in the Colorado Front Range. *Earth Surface Processes and Landforms* **26**(10), 1049-1070.

Moody JA, Martin DA (2001b) Post-fire, rainfall intensity–peak discharge relations for three mountainous watersheds in the western USA. *Hydrological Processes* **15**(15), 2981-2993.

Moody JA, Martin DA (2009b) Forest fire effects on geomorphic processes. In 'Fire effects on soils and restoration strategies.' (Eds A Cerda and PR Robichaud) pp. 41-79. (Science Publisher: Enfield, New Hampshire)

Moody JA, Martin DA, Cannon SH (2008a) Post-wildfire erosion response in two geologic terrains in the western USA. *Geomorphology* **95**(3-4), 103-118.

Moody JA, Martin DA, Haire SL, Kinner DA (2008b) Linking runoff response to burn severity after a wildfire. *Hydrological Processes* **22**(13), 2063-2074.

Moody JA, Nyman P (2012) Variations in soil detachment rates after wildfire as a function of soil depth, flow and root properties. Scientific investigations Report 2012-5233. US Geological Survey, Virginia.

Moody JA, Smith JD, Ragan BW (2005) Critical shear stress for erosion of cohesive soils subjected to temperatures typical of wildfires. *Journal of Geophysical Research-Earth Surface* **110**(F1).

Morgan RPC, Quinton JN, Smith RE, Govers G, Poesen JWA, Auerswald K, Chisci G, Torri D, Styczen ME (1998) The European Soil Erosion Model (EUROSEM): a dynamic approach for predicting sediment transport from fields and small catchments. *Earth Surface Processes and Landforms* **23**(6), 527-544.

Myronidis D, Emmanouloudis D, Mitsopoulos I, Riggos E (2010) Soil Erosion Potential after Fire and Rehabilitation Treatments in Greece. *Environmental Modeling & Assessment* **15**(4), 239-250.

Nachtergaele J, Poesen J (2002) Spatial and temporal variations in resistance of loess-derived soils to ephemeral gully erosion. *European Journal of Soil Science* **53**(3), 449-463.

Nahar N (2003) Influence of the runoff process on water and solute movement over heterogeneous hillslopes. Purdue University, Purdue

Nearing MA, Foster GR, Lane LJ, Finkner SC (1989) A process-based soil-erosion model for USDA water erosion prediction project technology. *Transactions of the Asae* **32**(5), 1587-1593.

Nearing MA, West LT, Brown LC (1988) A consolidation model for estimating changes in rill erodibility. *Transactions of the ASAE* **31**(3), 696-400.

Neary DG, Klopatek CC, DeBano LF, Ffolliott PF (1999) Fire effects on belowground sustainability: a review and synthesis. *Forest Ecology and Management* **122**(1-2), 51-71.

Nicholls N (1995) Long-term climate monitoring and extreme events. *Climatic Change* **31**(2), 231-245.

Noske PJ, Lane PNJ, Sheridan GJ (2010) Stream exports of coarse matter and phosphorus following wildfire in NE Victoria, Australia. *Hydrological Processes* **24**(11), 1514-1529.

- Nyman P, Sheridan G, Lane PNJ (2010) Synergistic effects of water repellency and macropore flow on the hydraulic conductivity of a burned forest soil, south-east Australia. *Hydrological Processes* **24**(20), 2871-2887.
- Nyman P, Sheridan GJ, Smith HG, Lane PNJ (2011) Evidence of debris flow occurrence after wildfire in upland catchments of south-east Australia. *Geomorphology* **125**(3), 383-401.
- O'Brien JS, Julien PY, Fullerton WT (1993) Two-Dimensional Water Flood and Mudflow Simulation. *Journal of Hydraulic Engineering* **119**(2), 244-261.
- Onda Y, Dietrich WE, Booker F (2008) Evolution of overland flow after a severe forest fire, Point Reyes, California. *CATENA* **72**(1), 13-20.
- Pak JH, Lee J-J (2008) A Statistical Sediment Yield Prediction Model Incorporating the Effect of Fires and Subsequent Storm Events1. *Journal of the American Water Resources Association* **44**(3), 689-699.
- Parsons AJ, Robichaud PR, Lewis SA, Napper C, Clark JT (2010) Field guide for mapping post-fire soil burn severity. USDA, Rocky Mountain Research Station.
- Perroux KM, White I (1988) Design for disk permeameters. *Soil Science Society of America Journal* **52**(5), 1205-1215. [In English]
- Philip JR (1957) The theory of infiltration: 1. The infiltration equation and its solution. *Soil Science* **83**(5), 345.
- Pierce JL, Meyer GA, Jull AJT (2004) Fire-induced erosion and millennial-scale climate change in northern ponderosa pine forests. *Nature* **432**(7013), 87-90.
- Pierson TC (2005) Distinguishing between debris flows and floods from field evidence in small watersheds In 'USGS Fact sheet 2004-3142.' (U.S. Department of the Interior)
- Pitman A, Narisma G, McAneney J (2007) The impact of climate change on the risk of forest and grassland fires in Australia. *Climatic Change* **84**(3), 383-401.

Prochaska A, Santi P, Higgins J, Cannon S (2008) Debris-flow runout predictions based on the average channel slope (ACS). *Engineering Geology* **98**(1), 29-40.

Prosser IP, Williams L (1998) The effect of wildfire on runoff and erosion in native Eucalyptus forest. *Hydrological Processes* **12**(2), 251-265.

Rawls W, Brakensiek D, Miller N (1983) Green-ampt Infiltration Parameters from Soils Data. *Journal of Hydraulic Engineering* **109**(1), 62-70.

Rees D (1982) A study of soils in the Reefton experimental area; with particular reference to hydrological properties. Soil Conservation Authority, Melbourne.

Renard KG, Foster GR, Weesies GA, Porter JP (1991) RUSLE - Revised Universal Soil Loss Equation. *Journal of Soil and Water Conservation* **46**(1), 30-33.

Reneau SL, Katzman D, Kuyumjian GA, Lavine A, Malmon DV (2007) Sediment delivery after a wildfire. *Geology* **35**(2), 151-154.

Reynolds WD (1993) Saturated Hydraulic Conductivity: Field Measurements. In 'Soil Sampling and Methods of Analysis.' Ed. MR Carter) pp. 599-613. (Lewis Publisher: Florida)

Reynolds WD, Bowman BT, Brunke RR, Drury CF, Tan CS (2000) Comparison of Tension Infiltrometer, Pressure Infiltrometer, and Soil Core Estimates of Saturated Hydraulic Conductivity. *Soil Science Society of America Journal* **64**(2), 478-484.

Rhoades CC, Entwistle D, Butler D (2011) The influence of wildfire extent and severity on streamwater chemistry, sediment and temperature following the Hayman Fire, ColoradoA. *International Journal of Wildland Fire* **20**(3), 430-442.

Risse LM, Nearing MA, Savabi MR (1994) Determining the Green-Ampt effective hydraulic conductivity from rainfall-runoff data for the WEPP model. *American Society of Agricultural Engineers* **37**(2). [In 0001-2351]

Ritchie R (2009) District Officer. In. ' Forest Commission of Victoria edn.: Wangaratta)

Robichaud P, Lewis S, Ashmun L (2008a) New procedure for sampling infiltration to assess post-fire soil water repellency. United States Department of Agriculture Forest Service, Fort Collins.

Robichaud P, Wagenbrenner J, Brown R, Wohlgemuth P, Beyers J (2008b) Evaluating the effectiveness of contour-felled log erosion barriers as a post-fire runoff and erosion mitigation treatment in the western United States. *International Journal of Wildland Fire* **17**(2), 255-273.

Robichaud PR (2000) Fire effects on infiltration rates after prescribed fire in Northern Rocky Mountain forests, USA. *Journal of Hydrology* **231-232**, 220-229.

Robichaud PR, Ashmun LE (2012) Tools to aid post-wildfire assessment and erosion-mitigation treatment decisions. *International Journal of Wildland Fire*, -.

Robichaud PR, Elliot WJ, Pierson FB, Hall DE, Moffet CA (2007) Predicting postfire erosion and mitigation effectiveness with a web-based probabilistic erosion model. *CATENA* **71**(2), 229-241.

Robichaud PR, Wagenbrenner JW, Brown RE (2010) Rill erosion in natural and disturbed forests: 1. Measurements. *Water Resour. Res.* **46**(10), W10506.

Rowe RK (1972) A study of the land in the catchment of the Kiewa river. Soil Conservation Authority, Victoria, Australia.

Rutherford ID, Bishop P, Loffler T Debris flows in northeastern Victoria, Australia: occurrence and affects on the fluvial system. In 'Variability in stream and sediment transport', 1994, Canberra. (Eds. LJ Olive, RJ Loughran and JA Kesby),

Santi PM, deWolfe VG, Higgins JD, Cannon SH, Gartner JE (2008) Sources of debris flow material in burned areas. *Geomorphology* **96**(3-4), 310-321.

Scoging HM (1979) Infiltration characteristics in a semiarid environment The hydrology of areas of low precipitation. Proc. Canberra Symp., Canberra, Australia. December 1979. *The hydrology of areas of low precipitation. Proc. Canberra Symp., Canberra, Australia. December 1979*, 159.

Shakesby RA, Doerr SH (2006) Wildfire as a hydrological and geomorphological agent. *Earth-Science Reviews* **74**(3-4), 269-307.

Sharma ML, Gander GA, Hunt CG (1980) Spatial variability of infiltration in a watershed. *Journal of Hydrology* **45**(1-2), 101-122.

Sharples JJ (2009) An overview of mountain meteorological effects relevant to fire behaviour and bushfire risk. *International Journal of Wildland Fire* **18**(7), 737-754.

Sheridan G, Lane P, Smith H, Nyman P (2009) A rapid risk assessment procedure for post-fire hydrologic hazards: 2009/10 fire season. . Victorian Department of Sustainability and Environment (DSE), Report ISBN 9780734041470, Melbourne.

Sheridan GJ, Lane PNJ, Noske PJ (2007a) Quantification of hillslope runoff and erosion processes before and after wildfire in a wet Eucalyptus forest. *Journal of Hydrology* **343**(1-2), 12-28.

Sheridan GJ, Lane PNJ, Noske PJ, Feikema P, Sherwin CB (2007b) Impact of the 2003 Alpine Bushfires on Streamflow: Estimated changes in stream exports of sediment, phosphorus and nitrogen following the 2003 bushfires in Eastern Victoria. Murray-Darling Basin Commission, Canberra.

Sheridan GJ, So HB, Loch RJ, Walker CM (2000) Estimation of erosion model erodibility parameters from media properties. *Soil Research* **38**(2), 265-284.

Smith HG, Dragovich D (2008) Post-fire hillslope erosion response in a sub-alpine environment, south-eastern Australia. *CATENA* **73**(3), 274-285.

Smith HG, Sheridan GJ, Lane PNJ, Bren LJ (2011a) Wildfire and salvage harvesting effects on runoff generation and sediment exports from radiata pine and eucalypt forest catchments, south-eastern Australia. *Forest Ecology and Management* **261**(3), 570-581.

Smith HG, Sheridan GJ, Lane PNJ, Noske PJ, Heijnis H (2011b) Changes to sediment sources following wildfire in a forested upland catchment, southeastern Australia. *Hydrological Processes* **25**(18), 2878-2889.

Smith HG, Sheridan GJ, Lane PNJ, Nyman P, Haydon S (2011c) Wildfire effects on water quality in forest catchments: A review with implications for water supply. *Journal of Hydrology* **396**(1-2), 170-192.

Smith HG, Sheridan GJ, Nyman P, Child DP, Lane PNJ, Hotchkis MAC, Jacobsen GE (2012) Quantifying sources of fine sediment supplied to post-fire debris flows using fallout radionuclide tracers. *Geomorphology* **139–140**(0), 403-415.

Smith HG, Sheridan GJ, Nyman P, Lane PNJ, Haydon S (2009) A framework for modelling suspended sediment flux following wildfire in forested water supply catchments, south-eastern Australia. In '8th World IMACS Congress and MODSIM09 International Congress on Modelling and Simulation. ' (Eds RS Anderssen, RD Braddock and LTH Newham) pp. 3549-3555: Cairns)

Smith R (2002) 'Infiltration theory for hydrologic applications.'

Smith RE, Goodrich DC (2000) Model For Rainfall Excess Patterns on Randomly Heterogeneous Areas. *Journal of Hydrologic Engineering* **5**(4), 355-362.

Specht RL (1972) 'The vegetation of South Australia: handbook of the flora and fauna of South Australia.' 2nd ed. edn. (Govt. Pr.: Adelaide)

Stone M, Collins A, Thoms MC (2012) 'Wildfire and water quality : processes, impacts and challenges / edited by Mike Stone, Adrian Collins & Martin Thoms.' (Wallingford, OX : IAHS Press, 2012.)

Strahler AN (1957) Quantitative analysis of watershed geomorphology. *Transactions of the American Geophysical Union* **38**(6), 913-920.

Teague B, Mcleod R, Pascoe S (2010) 2009 Victorian Bushfire Royal Commission. Parliament of Victoria, Melbourne.

Tennant D (1975) A Test of a Modified Line Intersect Method of Estimating Root Length. *The Journal of Ecology* **63**(3), 995-1001. [In English]

Tennant W, Turner M (2009) Upper Goulburn turbidity investigation. In. ' (Goulburn-Broken Catchment Management Authority: Victoria)

Tisdall JM, Tisdall (2006) Organic matter and water-stable aggregates in soils. *The Journal of soil science* **33**(2), 141.

Tolhurst KG, Kelly N (2003) Ecological effects of repeated low-intensity fire - summary report (1984-1999): Chapter 2 - Fuel dynamics. Victorian Department of Sustainability, Victoria.

Tomkins KM, Humphreys GS, Gero AF, Shakesby RA, Doerr SH, Wallbrink PJ, Blake WH (2008) Postwildfire hydrological response in an El Niño-Southern Oscillation-dominated environment. *Journal of Geophysical Research-Earth Surface* **113**(F2).

Tomkins KM, Humphreys GS, Wilkinson MT, Fink D, Hesse PP, Doerr SH, Shakesby RA, Wallbrink PJ, Blake WH (2007) Contemporary versus long-term denudation along a passive plate margin: the role of extreme events. *Earth Surface Processes and Landforms* **32**(7), 1013-1031.

Tryhorn L, Lynch A, Abramson R, Parkyn K (2008) On the meteorological mechanisms driving postfire flash floods: A case study. *Monthly Weather Review* **136**(5), 1778-1791.

Turner MG, Romme WH (1994) Landscape dynamics in crown fire ecosystems. *Landscape Ecology* **9**(1), 59-77.

Urbanek E, Shakesby RA (2009) Impact of stone content on water movement in water-repellent sand. *European Journal of Soil Science* **60**(3), 412-419.

Vafeidis AT, Drake NA, Wainwright J (2007) A proposed method for modelling the hydrologic response of catchments to burning with the use of remote sensing and GIS. *CATENA* **70**(3), 396-409.

VanDine DF, Rodman RF, Jordan P, Dupas J (2005) Kuskonook Creek, an example of a debris flow analysis. *Landslides* **2**(4), 257-265.

Wagenbrenner JW, Robichaud PR, Elliot WJ (2010) Rill erosion in natural and disturbed forests: 2. Modeling Approaches. *Water Resour. Res.* **46**(10), W10507.

Wasson R, Croke B, McCulloch M, Mueller N, Olley J, Starr B, Wade A, White I, Whiteway T (2003) Sediment, particulate and dissolved organic carbon, iron and manganese input to corin reservoir ActewAGL, Canberra.

- Welcker C (2011) Bulking debris flow initiation and impacts. University of Idaho,
- Wells G (1987) The effects of fire on the generation of debris flows in southern California. *Reviews in engineering geology* **7**, 105-114.
- Whetton PH, Fowler AM, Haylock MR, Pittock AB (1993) Implications of climate change due to the enhanced greenhouse effect on floods and droughts in Australia. *Climatic Change* **25**(3), 289-317.
- White I, Wade A, Worthy M, Mueller N, Daniell T, Wasson R (2006) The vulnerability of water supply catchments to bushfires: Impacts of the January 2003 wildfires on the Australian Capital Territory. *Australian journal of water resources* **10**(2), 1-16.
- Wiberg PL, Smith JD (1987) Calculations of the critical shear stress for motion of uniform and heterogeneous sediments. *Water Resour. Res.* **23**(8), 1471-1480.
- Wilkinson S, Peter Wallbrink, Shakesby R, Blake W, Doerr S (2007) Impacts on water quality by sediments and nutrients released during extreme bushfires: Summary of findings. CSIRO Land and Water Science Report 38/07.
- Wischmeier WH, Mannering JV (1968) Relation of Soil Properties to its Erodibility. *Soil Science Society of America Journal* **33**(1), 131-137.
- Wohl EE, Pearthree PP (1991) Debris flows as geomorphic agents in the Huachuca Mountains of southeastern Arizona. *Geomorphology* **4**(3-4), 273-292.
- Wondzell SM, King JG (2003) Postfire erosional processes in the Pacific Northwest and Rocky Mountain regions. *Forest Ecology and Management* **178**(1-2), 75-87.
- Woods SW, Balfour VN (2008) The effect of ash on runoff and erosion after a severe forest wildfire, Montana, USA. *International Journal of Wildland Fire* **17**(5), 535-548.
- Woods SW, Balfour VN (2010) The effects of soil texture and ash thickness on the post-fire hydrological response from ash-covered soils. *Journal of Hydrology* **393**(3-4), 274-286.

Woods SW, Birkas A, Ahl R (2007) Spatial variability of soil hydrophobicity after wildfires in Montana and Colorado. *Geomorphology* **86**(3-4), 465-479.

Worthy M (2006) Major erosion events and past fires in the Cotter River Catchment. Centre for resource and environmental studies, Australian National University, Canberra.

Worthy M, Wasson R (2004) Fire as an agent of geomorphic change in southeastern Australia: implications for water quality in the Australian Capital Territory. CRC Landscape Environments and Mineral Exploration.

Zhang G-h, Liu Y-m, Han Y-f, Zhang XC (2009) Sediment Transport and Soil Detachment on Steep Slopes: II. Sediment Feedback Relationship. *Soil Science Society of America Journal* **73**(4), 1298-1304.

Zhang GH, Wang LL, Li G, Tang KM, Cao Y (2011) Relationship between Sediment Particle Size and Transport Coefficient on Steep Slopes. **54**(3), 869-874.

Zhang X-C, Li Z-B, Ding W-F (2005) Validation of WEPP Sediment Feedback Relationships using Spatially Distributed Rill Erosion Data. *Soil Science Society of America Journal* **69**(5), 1440-1447.

Appendices

Appendix A



Figure 1. The Wellington River near Licola (Victoria, southeast Australia) after multiple debris flow events in headwater catchments. *Photo: Adrian Murphy, Melbourne Water.*



Figure 2. Sunday Creek near Kinglake (Victoria, southeast Australia) after debris flow events 1-2 months after wildfire. Sunday Creek flows into the Sunday Creek Reservoir which feeds into the Goulburn Murray Water supply systems



Figure 3. The confluence of the Goulburn River and the Jamieson River above Lake Eildon. The local Catchment Management Authorities (CMA) experienced water quality issues in the Goulburn River due to the large volumes of sediment that had been deposited by debris flows in the Goulburn River after wildfires in 2007. The Jamieson catchment was burned at lower severity the river did not experience similar sediment concentrations; hence the strong contrast in colour. *Photo: Wayne Tennant, Goulburn Murray CMA.*



Figure 4. Debris flow deposit in Rose River, in 2009, three years after wildfires in 2007. *Photo: Hugh Smith*

Appendix B



Figure 1. Channel scour after a debris flow event at Dingo Creek in the upper Buckland River, 2003. A fire fighter died after being caught at a road crossing. *Photo: Gary Sheridan*



Figure 2. Debris flow event across Mt Tamboritha Road, near Licola in 2007. The town was closed off due to the road damage caused by the debris flow. *Photo: Adrian Murphy*



Figure 3. Debris flow processes in the headwaters of Target Creek impacted directly on the downstream township of Licola after wildfires in 2007. *Photo: Jodi Halliwell*



Figure 4. A damaged shack near Harrietville after debris flows in wildfire-affected areas of the Upper Owens River in 2013. *Photo Gary Weston*



Figure 5. Scour on trees, and the channel eroded to bedrock; two key indicators of debris flow processes. Photo from Rose River headwaters in 2008.



Figure 6. A large debris flow events in the headwater of the Wellington River, 2007. Scour on trees, large boulder deposits supported by a matrix of fine material and channel eroded to bedrock are key indicators of debris flow processes.



Figure 7. Measuring channel cross sections in headwaters of Rose River that were scoured by debris flows in December 2007



Figure 8. A channel initiation point in headwaters at Yarrarabula.



Figure 9. Intact pedestals used to obtain a measure of erosion depth on hillslopes. Photo is from Yarrarabula in November 2007.



Figure 10. Survey work in wet and bleak conditions with Hugh Smith in the background and Petter Nyman in front.

Appendix C



Figure 1. Wide and shallow rills forming in response to stripping of surface soil on hillslope near Sunday Creek, April 2009.



Figure 2. No surface soil left after widespread sheet erosion on hillslope at Myrtle Creek, June 2009.



Figure 3. Convergence zone (or hollow) above the channel initiation point, Myrtle Creek, 2009. The Stanley-Myrtleford road is visible in the background.



Figure 4. Channel initiation, Sunday Creek, 2009.



Figure 5. Deposits in three distinct levees reflecting multiple debris flow surges. Sunday Creek, 2009.



Figure 5. Terminal deposit at intersection with Sunday Creek. The debris flow supply large volumes of coarse material to streams and can create large pools as a result.



Figure 1. Mini-disc infiltrimeters and soil cores held in place using a clamp and stand. A buchner funnel was used to create a negative pressure at the bottom of the core (this can be seen in the clamp and stand positioned to the left of the basin). The cores were placed in the tension table (far right hand side) between infiltration experiments in order to (eventually) obtain saturated soil cores.



Figure 2. Using min-disc infiltrometers from Decagon to measure infiltration rates at Ella Creek, 3 years after wildfire. Peter Mercurio is carefully taking a reading.



Figure 3. Infiltrometers require little water and are easily carried around headwaters enabling widespread sampling of infiltration properties. Water was carried in a 15 L bladder inside the backpack.



Figure 4. Evidence of preferential flow at Stony Creek (March 2010) after 15 minutes of infiltration under ponded conditions. The soils were highly repellent during this measurement campaign.



Figure 5. Rainfall simulation setup on steep slopes (25°) at Sunday Creek. With help from Sina Moshirvaziri, Craig Mason and Gary Sheridan.

Appendix E



Figure 1. Depth stratified soil sampling on a burnt hillslope near Pozo, California, January 2011.

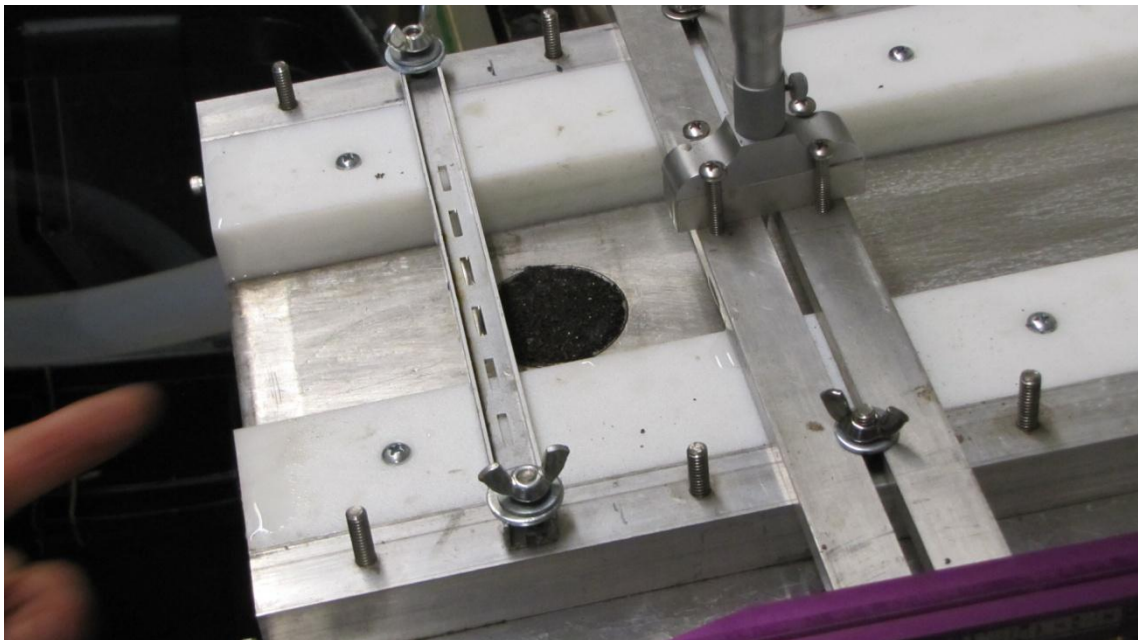


Figure 2. A laboratory flume used to measure detachment rates from intact cores. The core (diameter 5.1 cm) is located at the centre of the flume bed. The flow depth was measured using point gauges at the centre the rails above and below the core.

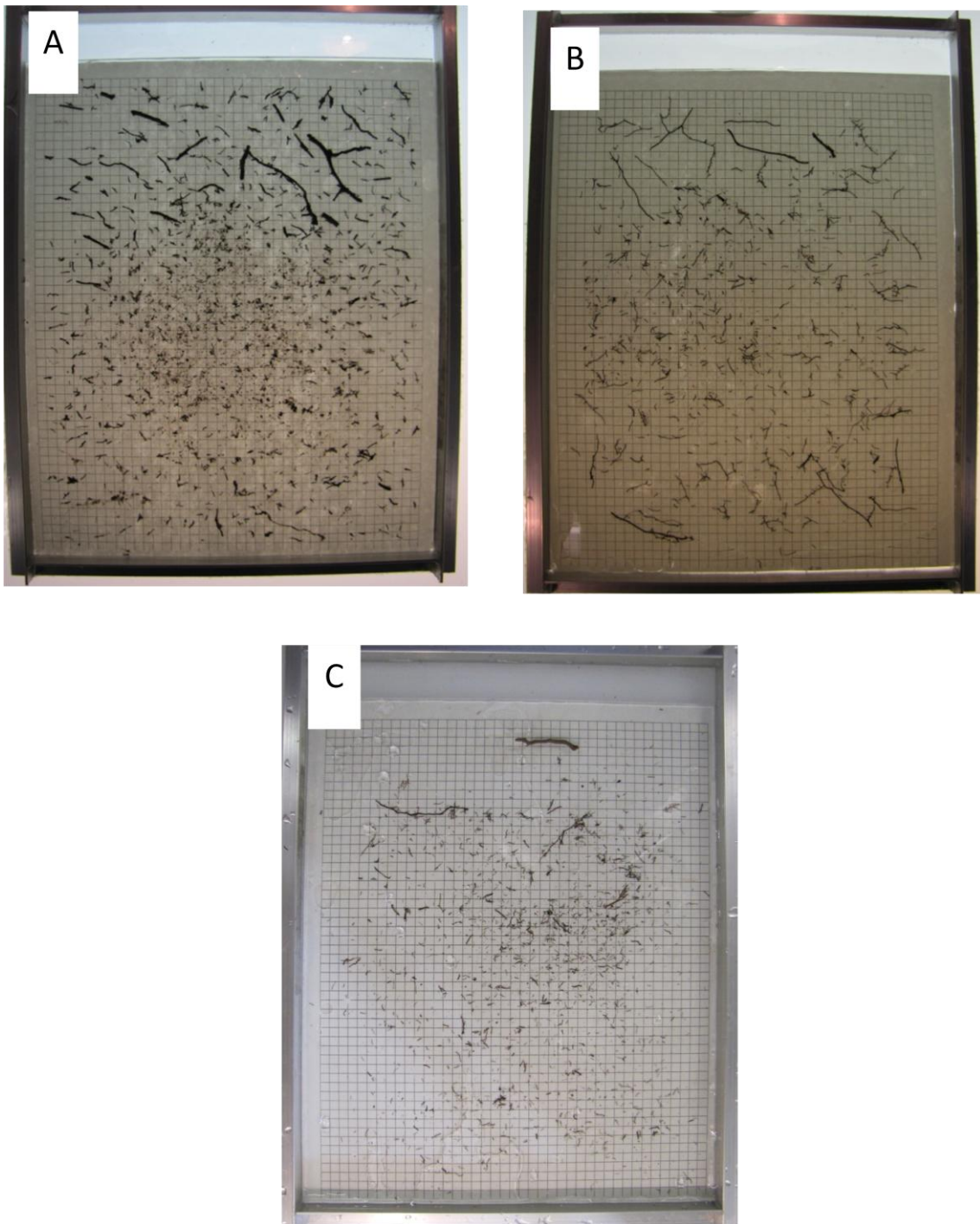


Figure 3. Extracted roots from 3-5 cm below the soil surface from burned sites. A. Fourmile Canyon-North. B. Fourmile Canyon-South and C. Pozo. The tray is 22 cm wide by 30 cm long and each grid cell is 5 mm x 5 mm.



Figure 4. Flume experiments on hillslopes at Sunday Creek. Water was pumped through a rotameter and introduced to the test area from a small retention basin at the top of the flume. The test area is 4 m long and 0.15 m wide. Sediment was collected at the pipe outlet in 0.5 L containers at set time intervals. Philip Noske is walking off to start the pump.



Minerva Access is the Institutional Repository of The University of Melbourne

Author/s:

NYMAN, PETTER

Title:

Post-fire debris flows in southeast Australia: initiation, magnitude and landscape controls

Date:

2013

Citation:

Nyman, P. (2013). Post-fire debris flows in southeast Australia: initiation, magnitude and landscape controls. PhD thesis, Melbourne School of Land and Environment, The University of Melbourne.

Persistent Link:

<http://hdl.handle.net/11343/38350>

File Description:

Post-fire debris flows in southeast Australia: initiation, magnitude and landscape controls